

Novel and colourful flavonoids - characterisation, secondary structures and properties

Helge Berland

Thesis for the degree of Philosophiae Doctor (PhD)
University of Bergen, Norway
2021

UNIVERSITY OF BERGEN



Novel and colourful flavonoids - characterisation, secondary structures and properties

Helge Berland



Thesis for the degree of Philosophiae Doctor (PhD)
at the University of Bergen

Date of defense: 03.06.2021

© Copyright Helge Berland

The material in this publication is covered by the provisions of the Copyright Act.

Year: 2021

Title: Novel and colourful flavonoids - characterisation, secondary structures and properties

Name: Helge Berland

Print: Skipnes Kommunikasjon / University of Bergen

Table of contents

Table of contents	iii
Preface	v
Acknowledgements	vi
Abstract	vii
List of abbreviations	ix
List of publications	x
1 INTRODUCTION	1
1.1 Flavonoids	1
1.1.1 Structures	1
1.2 Anthocyanins	2
1.2.1 Primary structures	2
1.2.2 Secondary structures	5
1.2.3 Colour	7
1.2.4 Stability	8
1.2.5 Anthocyanins in plants	9
1.2.6 Human applications	12
1.3 Aurones	15
1.3.1 Structures	15
1.3.2 Aurones in plants	15
1.3.3 Human utility	16
2 EXPERIMENTAL METHODS	19
2.1 Extraction and purification methods	19
2.1.1 Extraction from plant material	19
2.1.2 Liquid-liquid extraction	20
2.1.3 Amberlite XAD-7 adsorption chromatography	20
2.2 Separation and isolation methods	20
2.2.1 Size exclusion chromatography	21
2.2.2 Semi-preparative high-performance liquid chromatography	21
2.3 Analytical methods	22
2.3.1 Analytical high-performance liquid chromatography	22

2.3.2 Nuclear magnetic resonance spectroscopy	24
2.3.3 Mass spectrometry	26
2.3.4 Ultraviolet/Visible light absorption spectroscopy	26
2.3.5 Thin layer chromatography	27
3 RESULTS AND DISCUSSION	29
3.1 Pigments of <i>Marchantia polymorpha</i> (Paper I)	29
3.1.1 Auronidins – A new class of flavonoids	30
3.1.2 Pigments from transgenic material of <i>Marchantia polymorpha</i>	30
3.1.3 Chemical properties of auronidin 4- <i>O</i> -neohesperidoside (1)	34
3.1.4 Biosynthesis of auronidins	38
3.2 Cell wall pigment of <i>Sphagnum</i> sp. (Paper II)	39
3.2.1 Isolation of Sphagnorubin C (5)	39
3.2.2 Structure elucidation of secondary structures of 5	40
3.2.3 The network of anthocyanin forms of 5	44
3.2.4 Influence of solvent on ¹ H NMR shift values	48
3.3 New anthocyanin sources	51
3.3.1 New anthocyanins from flowers of <i>Erlangea tomentosa</i> (Paper III)	51
3.3.2 Anthocyanins from blue potatoes	57
3.3.3 Anthocyanins from ‘Sun black’™ tomato (Papers IV and V)	58
4 CONCLUSIONS AND FUTURE PROSPECTS	61
REFERENCES	63
APPENDIX A: TABLES OF ¹H AND ¹³C NMR DATA	81
Appendix A-1: Pigments 1 and 2	81
Appendix A-2: Pigment 5	83
Appendix A-3: Pigments 6 and 7	85
APPENDIX B: FIGURES OF NMR SPECTRA	87
Appendix B-1: Pigment 1	87
Appendix B-2: Pigment 2	91
APPENDIX C: FIGURES OF MS SPECTRA	93
Appendix C-1: Pigment 1	93
Appendix C-2: Pigment 2	94

Preface

This thesis is submitted for the degree of Philosophiae Doctor (PhD) in chemistry at the University of Bergen, Norway. The experimental work in this thesis was carried out at the Department of Chemistry, University of Bergen, during the period 2013-2017. The thesis consists of five papers preceded by a summary of the results.

The main aim of this thesis was to study the colourful flavonoid pigments found in two basal land plants: liverworts (*Marchantia polymorpha*) and peat moss (*Sphagnum* sp.). These red pigments possess some distinct structural differences to the anthocyanins found in vascular plants. Studying how the structure of these pigments change in different solvent compositions may give a deeper insight of how the first land plants might have stabilised these colourful functional compounds.

Another aim was to isolate and identify new anthocyanins. These can expand the diversity of structures, and new structures might display other chemical properties than previously known.

A third aim was to identify new anthocyanin sources. Anthocyanins from new sources might give more diverse options for dietary intake of anthocyanins, and provide broader nutraceutical applications than we know of today.

Chapter 1 introduces the field of study, chapter 2 presents the experimental methods used in the thesis, chapter 3 gives the results of the papers this thesis is based on, with some discussion of the results, and chapter 4 concludes the thesis and presents some future prospects.

Acknowledgements

I would first like to thank my two supervisors: Professor Øyvind M. Andersen and Associate Professor Monica Jordheim for excellent supervision during my work. You both have deep knowledge of our field and wisdom in discussions about the problems at hand. Especially I want to thank my main supervisor Øyvind for all the understanding, encouragement and patience, and for the constant reminder that it will work out in the end.

I want to thank for the support of Bjarte Holmelid for recording MS data, Olav-Audun Bjørkelund for technical support on the 600 MHz instrument, and Unni Hauge for general technical support. Financial support was provided by the Research Council of Norway through the Norwegian NMR Platform (NNP-226244/F50), which opened a space for recording spectra on the 850 MHz NMR instrument, and I want to thank Jarl Underhaug and José C. R. Guerrero for help with recording for recording these spectra.

I also want to thank all my colleagues at the institute: Irene Skaar, who provided help and insight throughout my master and start of doctoral work, Ingrid Kyrkjebø for providing several samples of isolated anthocyanins, and especially Anne Stavland for excellent work on the *Marchantia* project.

I also want to thank my professional collaborators in New Zealand, Kevin Davies, Nick Albert and colleagues, for the great work the *Marchantia* project that got published in PNAS in 2019.

I want to thank my good friends and colleagues Camilla and Audun for all the great lunch breaks and wonderful conversations over the years. I do not know how I would cope without your friendship. Also, I want to thank Christer for all the good times together and for all the encouragement you have given me.

Lastly, I want to thank my dear and wonderful wife, Ingvild, for always supporting me and always loving me.

Bergen, February 2021

Helge Berland

Abstract

This dissertation focuses on isolation and structural elucidation of flavonoid pigments. The properties of these pigments have been explored, in terms of their chemical properties, especially regarding secondary structures in neutral solvents.

Liverworts (Marchantiophyta) are basal land plants considered the probable most recent common ancestor of land plants and algae. The liverwort *Marchantia polymorpha* produces red flavonoid pigmentation in response abiotic stress, bound to the cell wall, that is proposed to be early evolved anthocyanidin forms. Taking advantage of transgenic marchantia plants overexpressing flavonoid production, two red pigments were isolated and their structure elucidated to be 2,3,6,8-tetrahydroxybenzofuro[3,2-*b*]chromen-5-ium-6-*O*-(2-*O*- α -rhamnopyranosyl- β -glucopyranoside (**1**), and its aglycone (**2**). In this work we show that these pigments represent a previously unreported flavonoid class named auronidins, for their similarities in structure to anthocyanidins and to aurones. Chemically, auronidins are capable of expressing a wide range of colours depending on the pH similar to anthocyanins. They also express strong fluorescence under UV light, in contrast to the majority of known anthocyanins. The chemical properties of **1** have been compared to both an aurone (aureusidin 4-*O*-glucoside, **4**) and an anthocyanin (cyanidin 3-*O*-glucoside, **3**). We have also shown that auronidins comes from the flavonoid biosynthetic pathway, which is a part of the larger phenylpropanoid pathway, but from a path distinct from that leading to anthocyanins. A summary of their work is presented here.

Peat moss (*Sphagnum*) is another basal land plant that are more evolutionary advanced than liverwort. Several species of peat moss produce red pigmentation bound to the cell walls in response to abiotic stress. These pigments have been isolated from *Sphagnum* sp. and Sphagnorubin C (**5**) have been structurally elucidated. This anthocyanin lacks glycosidic substitution, have an extended aromatic skeleton, and lacks the characteristic hydroxyl group in 3-position (3-deoxyanthocyanidin) featured in the vast majority of anthocyanins. In addition to the flavylium cation form, the *trans*-chalcone form

of **5** have been elucidated, which in pure DMSO is stable and is fully reversible to the flavylum cation form by the addition of acid. No signs of neither hemiketal forms nor the *cis*-chalcone form was observed. This was the first full structural elucidation of a *trans*-chalcone form of a naturally occurring anthocyanin.

In addition to the pigments isolated from basal land plants, several new sources of anthocyanins have been discovered. Isolation and structural elucidation of anthocyanins from the mauve flowers of *Erlangea tomentosa* provided this thesis with two new anthocyanins, based on the novel anthocyanidin erlangidin, the first reported natural anthocyanidin having C-ring methoxylation (erlangidin 5-*O*-(4-(*E*-caffeoyl)-6-(malonyl)- β -glucopyranoside)-3'-*O*-(6-(3-(β -glucopyranosyl)-*E*-caffeoyl)- β -glucopyranoside), **6**, and erlangidin 5-*O*-(6-(malonyl)- β -glucopyranoside)-3'-*O*-(6-(3-(β -glucopyranosyl)-*E*-caffeoyl)- β -glucopyranoside), **7**). Additionally, new sources of petanin (**8**) and negretein (**9**) were discovered, including 'Sun black' tomato (*Solanum lycopersicum*), a tomato cultivar bred to produce deep purple to black anthocyanin-rich skin, and several cultivars of blue potato (*Solanum tuberosum*).

List of abbreviations

AVI	Anthocyanic Vacuolar Inclusion
DAD	Diode-Array Detection
DMSO	DiMethyl SulfOxide
DQF-COSY	Double Quantum Filtered COrrrelation SpectroscopY
ESI	ElectroSpray Ionisation
HMBC	Heteronuclear Multiple Bond Correlation
HPLC	High Performance Liquid Chromatography
HSQC	Heteronuclear Single Quantum Coherence
LC-MS	Liquid Chromatography Mass Spectrometry
LLE	Liquid-Liquid Extraction
(HR)-MS	(High Resolution) Mass Spectrometry
NMR	Nuclear Magnetic Resonance
PVC	PreVacuolar Compartment
R_f	Retardation factor (TLC)
ROESY	Rotating frame Overhauser Effect SpectroscopY
SEC	Size Exclusion Chromatography
t_R	Retention time (HPLC)
TFA	TriFluoroacetic Acid
TLC	Thin Layer Chromatography
TOCSY	TOTAL Correlation SpectroscopY
UV/Vis	Ultraviolet/Visible light

List of publications

- I. Berland, H., Albert, N. W., Stavland A., Jordheim M., McGhie T. K., Zhang H., Deroles S. C., Jordan B. R., Davis K. M. & Andersen Ø. M. (2019) Auronidins are a previously unreported class of flavonoid pigments that challenges when anthocyanin biosynthesis evolved in plants. *Proceedings of the National Academy of Sciences of the United States of America*, 116 (40), p. 20232-20239 <https://doi.org/10.1073/pnas.1912741116>
- II. Berland H., Andersen Ø. M. (2021) Characterization of a natural, stable, reversible and colourful anthocyanidin network from *Sphagnum* moss based mainly on the yellow trans-chalcone and red flavylum cation forms. *Molecules*, 26 (3), p. 709 <https://dx.doi.org/10.3390%2Fmolecules26030709>
- III. Adaku C., Skaar I., Berland H., Byamukama R., Jordheim M., Andersen Ø. M. (2019) Anthocyanins from mauve flowers of *Erlangea tomentosa* (*Bothriocline longipes*) based on erlangidin – The first reported natural anthocyanidin with C-ring methoxylation. *Phytochemistry Letters*, 29, p. 225-230 <https://doi.org/10.1016/j.phytol.2018.12.016>
- IV. Blando F., Berland H., Maiorano G., Durante M., Mazzucato A., Picarella M. E., Nicoletti I., Gerardi C., Mita G., Andersen Ø. M. (2019) Nutraceutical characterization of anthocyanin-rich fruits produced by ‘Sun Black’ tomato line. *Frontiers in Nutrition*, 6 (133), p. 133 <https://doi.org/10.3389/fnut.2019.00133>
- V. Blando F., Calabriso N., Berland H., Maiorano G., Gerardi C., Carluccio M. A., Andersen Ø. M. (2018) Radical scavenging and anti-inflammatory activities of representative anthocyanin groupings from pigment-rich fruits and vegetables. *International Journal of Molecular Sciences*, 19 (1), p. 169 <https://dx.doi.org/10.3390%2Fijms19010169>

Paper I is published under PNAS licence. Papers II, IV and V are published under Creative commons CC-BY licence. Paper III is © 2018 Phytochemical Society of Europe, published by Elsevier Ltd. and reprinted with permission.

1 Introduction

1.1 FLAVONOIDS

Flavonoids are one of the four main classes of plant pigments, together with chlorophylls, carotenoids and betalains. They are a major group of polyphenolic compounds found in plants, with more than 8150 reported different structures (Andersen and Markham, 2006). They have a range of functions in plants, including antioxidants, antimicrobials, photoreceptors, visual attractors, feeding repellents and for light screening (Pietta, 2000, Harborne and Williams, 2000).

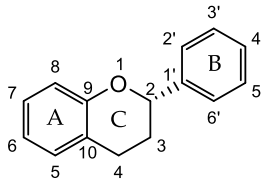


Figure 1: The structure of the basic flavonoid structure, flavan, with numbering system and ring designation, on which most flavonoids are based.

1.1.1 Structures

The basic flavonoid structure has a 15-carbon skeletal backbone (Figure 1) and there are at least 20 classes of flavonoids, with differences in the size, oxidation state and substitution pattern on the C-ring (Figure 2) (Buckingham and Munasinghe, 2015).

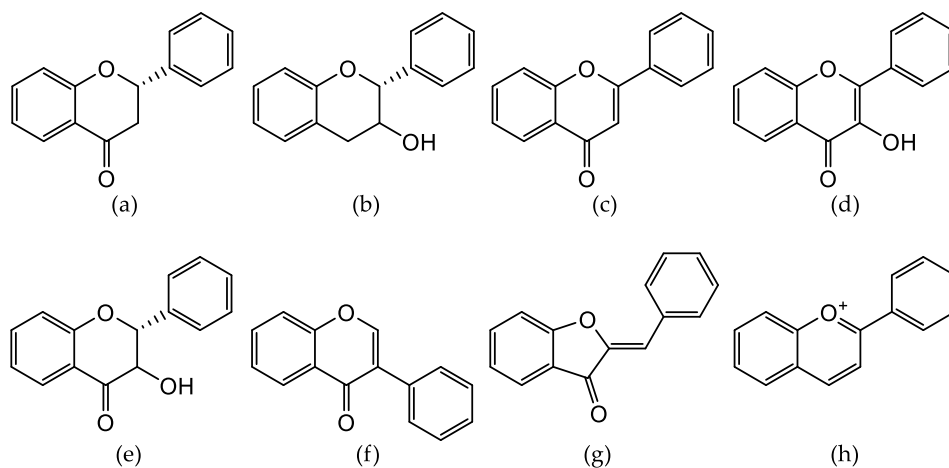


Figure 2: Basic skeletal backbone of some flavonoid structures: (a) flavanone, (b): flavanol, (c): flavone, (d): flavonol, (e): flavanonol, (f): isoflavone, (g): aurone, (h): flavylium cation.

1.2 ANTHOCYANINS

Anthocyanins are a major group of flavonoids, best known for their red to blue colours in fruit, vegetables, flowers and leaves. The word *anthocyanin* comes from the Greek words *anthos* (άνθος), meaning flower, and *kyanos* (κυανός), meaning blue, and was used originally to describe the pigments of blue cornflower, *Centaurea cyanus* (Marquardt, 1835). They are polyphenolic, water-soluble pigments found throughout the plant kingdom (Strack and Wray, 1994). There has been a tremendous increase in reports of new anthocyanins for the last quarter decade (Andersen and Jordheim, 2006), due to both improvements in analytical techniques for structural elucidation of these complex structures, for instance nuclear magnetic resonance (NMR) spectroscopy, and in the increased interest in anthocyanins for their potential health benefits (see section 1.2.6). It is to date identified around 800 unique anthocyanin structures isolated from plants.

1.2.1 Primary structures

The structure of anthocyanins is centred around an aglycone called anthocyanidin, which is based on the flavylium cation skeletal backbone. Substitutions on this skeleton give rise to a very diverse group of pigments, that enables them to exhibit a wide range of colours and properties.

Aglycones

Around 92 % of all anthocyanins occurring in nature is based on just six anthocyanidins: pelargonidin, cyanidin, peonidin, delphinidin, petunidin and malvidin (Figure 3), which only differ in the hydroxylation and methoxylation of the B-ring (Francis, 1989, Andersen and Jordheim, 2010). Other anthocyanidins include methylation in position 5 and/or 7 (Iwashina, 2000, Toki et al., 2008, Skaar et al., 2012).

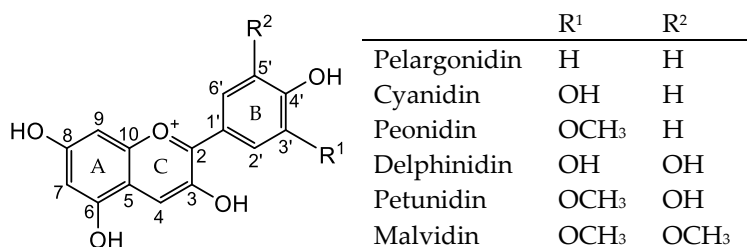


Figure 3: The structure with substitution pattern of the six most common anthocyanidins found in nature, including the numbering system.

3-Deoxyanthocyanidins is a subgroup of anthocyanidins that lacks the hydroxylation in 3-position, and were the only anthocyanidins found in their non-glycosylated form in nature (Andersen and Jordheim, 2006) until cyanidin, peonidin and pelargonidin were indicated as present in a non-glycosylated form in black beans (Macz-Pop et al., 2006). Examples of 3-deoxyanthocyanidins are several pigments from *Sorghum* sp. (Awika et al., 2005, Shih et al., 2007), carajuron and derivatives from *Arrabidaea chica* (Zorn et al., 2001, Devia et al., 2002), several pigments from Dragon's blood resin (Sousa et al., 2008) , and simple 3-deoxyanthocyanidins from ferns (Crowden and Jarman, 1974).

Just a small handful of anthocyanidins have been identified with an extended carbon skeleton, namely the Sphagnorubins from peat moss (*Sphagnum* sp.) (Vowinkel, 1975), and the rosacyanins from rose petals (Fukui et al., 2002, Fukui et al., 2006). Pyranoanthocyanidins also have an extended skeleton, with an extra C₃ unit making a fourth ring (D-ring) interconnecting the A and C rings. They have been found to occur naturally in red onions (Fossen and Andersen, 2003) and strawberries (Andersen et al., 2004), but are mostly associated with a number of processed food sources, especially wine (Bakker and Timberlake, 1997, Bakker et al., 1997, Schwarz et al., 2004).

Sugar moieties

Glucose is the most common glycosylation of anthocyanins, found in 90 % of the identified structures, followed by rhamnose, galactose, xylose and arabinose, and

glucuronic acid (Andersen and Jordheim, 2006) (Figure 4). There is also one report of apiose as a moiety in a disaccharide linked to an anthocyanin (Andersen et al., 2010).

Most anthocyanins are substituted with one or several sugar moieties, mainly as *O*-glycosylations at position 3, in the form of mono-, di- or trisaccharides. Glycosylations also occur in positions 5, 7, 3' and 5' (Brouillard, 1988, Fossen et al., 2003a), and is even reported in the 4' position, as for ternatin A1 isolated from *Clitoria ternatea* (Terahara et al., 1990) and cyanodelphin isolated from *Delphinium hybridum* (Kondo et al., 1991). In addition there are some reports where the sugar is attached via a *C*-linkage (Saito et al., 2003, Tatsuzawa et al., 2004).

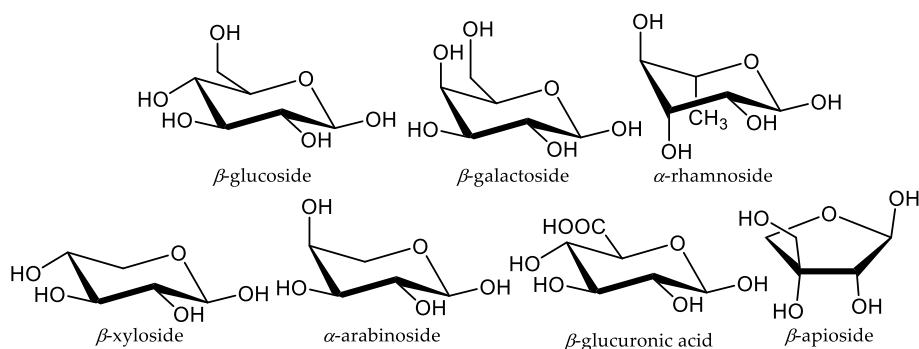


Figure 4: The structures of the most common monosaccharide moieties found in anthocyanins (Andersen and Jordheim, 2013).

Acyl moieties

More than 69 % of all anthocyanins contain one or more acylations of the sugar moieties (Andersen and Jordheim, 2013). The addition of acylation to the structure, depending on the nature, number and linkage position, can greatly change the properties of the anthocyanin with respect to colour (section 1.2.3) and stability (section 1.2.4). The most frequently observed acylation is with malonic acid, identified in 27 % of all anthocyanins (Andersen and Jordheim, 2013) (Figure 5). Acylated anthocyanins are prone to losing the acylation due to hydrolysis of the ester bond during the workup procedure, because of storage at elevated temperatures or with elevated amounts of acid in the solvent. Dicarboxylic acids linked to anthocyanins are also prone to esterification by the solvent (i.e. methanol) in the presence of small amounts of acid (Fossen et al., 2001). The type and number of acylations found in anthocyanins have been linked to which plant family of species the anthocyanins come from, and it has been shown that anthocyanins from fruits have on average 0.1

aromatic acyl groups, whilst anthocyanins from vegetables have on average 0.9 aromatic acyl groups (Andersen and Jordheim, 2013).

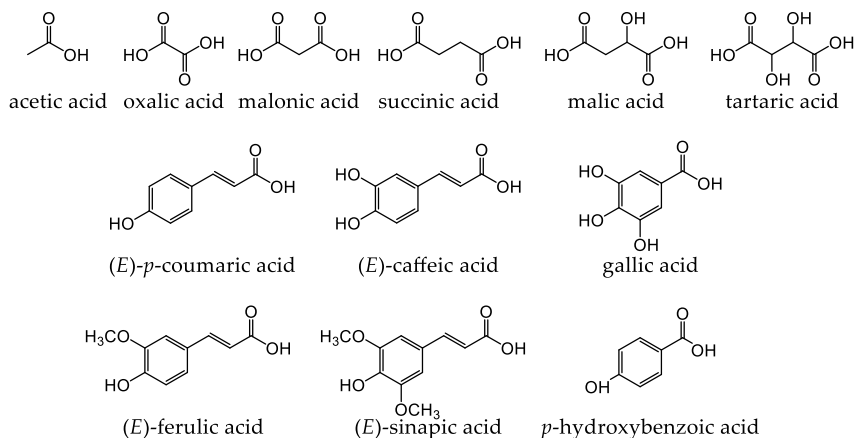


Figure 5: Structures of the most common aromatic and aliphatic acyl moieties found linked to glycosylic moieties in anthocyanins (Andersen and Jordheim, 2013).

1.2.2 Secondary structures

Anthocyanidins are known to occur in several different forms (secondary structures) in equilibrium, which contribute to several properties of anthocyanins, including colour (section 1.2.3) and stability (section 1.2.4). Thermodynamic and kinetic studies of anthocyanins and anthocyanidins have contributed to a generally accepted equilibrium scheme, presented in Figure 6, where certain transformations (proton transfer, hydration, tautomerisation and isomerisation) of the flavylium cation form, depending on a number of factors, including the substitutions of the anthocyanidin, the pH of the solvent and the presence or absence of light, give rise to the secondary structures (Sondheimer, 1953, Jurd, 1963, Jurd and Geissman, 1963, Jurd, 1969, Brouillard and Delaporte, 1977, Brouillard and Dubois, 1977, McClelland and Gedge, 1980, Pina, 1998, Pina et al., 2012). In strongly acidic conditions (below pH 2), anthocyanidins predominantly occur on the flavylium cation form (AH^+). In slightly acidic or neutral conditions, deprotonation of the flavylium cation gives rise to quinoidal forms (**A**), and, depending on the substitutions of the anthocyanidin, several forms are possible based on the position of the keto group (**A₅**, **A₇**, **A₄**). At even higher pH values, these forms can be further deprotonated and give quinoidal bases (**A₅⁻**, **A₇⁻**, **A₄⁻**), and additional deprotonations may be possible in certain structures. In weakly acidic solutions in the presence of water, the flavylium cation form can be hydrated,

giving rise to the hemiketal forms (*R* or *S*), also known as hemiacetals and, historically, carbinol pseudobases. Hydration mainly occur in the 2-position (**B₂**), but hydration in 4-position (**B₄**) have also been observed. The hemiketal forms **B₂** can undergo tautomerisation and ring opening to form the *cis*-chalcone (**cC**), which further can isomerise and give the *trans*-chalcone (**tC**).

The deprotonation of the flavylum cation form to the quinoidal form (**AH⁺**→**A**) is a faster and kinetically driven equilibrium, but the hydration (**AH⁺**→**B**) and the consequent formation of the chalcone forms (**B₂**→**cC**→**tC**) is possibly more stable, driving towards thermodynamic equilibrium.

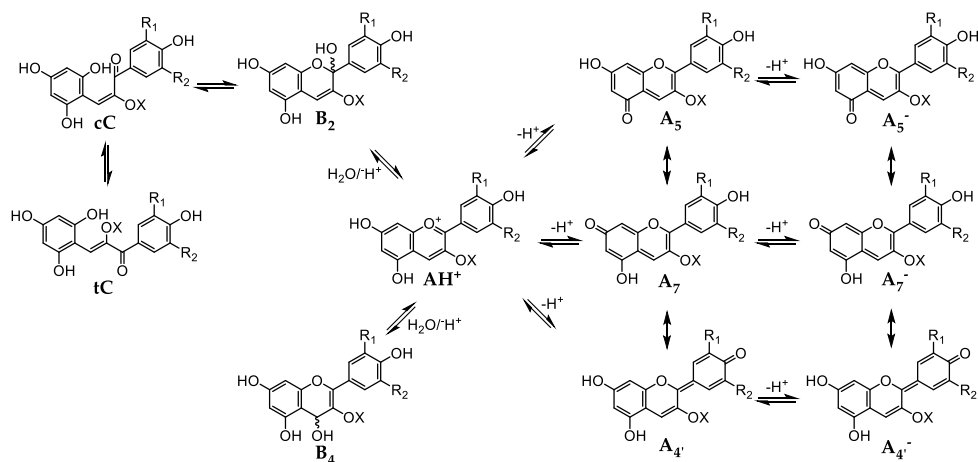


Figure 6: The generally accepted scheme showing the secondary structures of anthocyanins and transformations between them, in aqueous solutions. X: usual site for glycosylation, R₁ and R₂: hydroxyl or methoxyl, depending on the identity of aglycone.

This generally accepted scheme is proposed by a variety of methods, including pH-jump method and UV/Vis absorption spectroscopy. Because of the various transformations possible in similar pH regimes (pH 3-7), structural investigation of the secondary structures by nuclear magnetic resonance (NMR) spectroscopy and mass spectrometry (MS) have generally been of limited value. The flavylium cation form of the anthocyanidins is by far the best understood form, as it is the predominant form in acidic solvents (below pH 2). The ¹H NMR shifts of seven secondary structures of malvidin 3-*O*-glucoside were tentatively assigned by dissolving the pigment in *d*₄-methanol/*d*₂-water (1:4, v/v) and varying the temperature and the pH of the solvent (Cheminat and Brouillard, 1986). Two epimeric hemiketals (**a** and **b**) of 3-*O*-glucosides of delphinidin, petunidin, and malvidin and cyanidin 3-*O*-galactoside have been

structurally elucidated using 1D and 2D NMR techniques, when the pigments were dissolved in pure deuterated methanol (Jordheim et al., 2006a). Only the **B₂** hemiketal form was observed, and the molar fraction of the flavylium form and the two hemiketal forms were observed to be very similar across the studied pigments, even after storage for weeks.

Chalcone forms were first properly described with spectroscopic data by Brouillard et al. (1979). The chalcone forms of malvidin 3,5-*O*-diglucoside and malvidin 3-*O*-glucoside were observed by UV/Vis absorption detection in a HPLC system after the chalcone forms were generated in solvents of pH 3.5 stored in the dark over night at room temperature (Preston and Timberlake, 1981). The solvent at the time of elution from the HPLC was 0.6 % perchloric acid and methanol (3:1, v/v) at pH 1.5, and within 1 hour stored in the dark, the flavylium cation were regenerated, without any sign of degradation. In another study, the chalcone forms of cyanidin 3-*O*-sambubioside-5-*O*-glucoside, cyanidin 3,5-*O*-diglucoside, cyanidin 3-*O*-sambubioside and cyanidin 3-*O*-glucoside were reported in 0.1 M hydrochloric acid extracts from elderberry, after adjusting the pH to 4.5 and the solvent heated to the boiling point followed by immediate cooling (Brønnum-Hansen and Hansen, 1983). Both the *cis*- and *trans*-chalcone forms were detected, using HPLC and a UV/Vis absorption detector. The assignment of ¹H chemical shift values of chalcone forms is discussed in more detail in chapter 3.2.2.

1.2.3 Colour

The colours that anthocyanins express are affected by many different factors, including the identity of the anthocyanidin, type and position of substitutions (hydroxylation, methylation, glycosylation and acylation) and the secondary structure expressed (based on pH), in addition to the concentration in solution, co-pigmentation, metal complexation and intra- and intermolecular associations (Brouillard, 1988).

Based on the six most common anthocyanidin skeletons alone, when occurring on their flavylium cation form dissolved in acidic solutions, pelargonidin appear red, cyanidin and peonidin as magenta and delphinidin, petunidin and malvidin as purple (Andersen and Jordheim, 2010), which show that the colour is expressed by the level of oxidation on the B-ring. The oxidation level of position 3 on the C-ring contribute to a shift of the absorption maximum towards longer wavelengths (bathochromic shift), which indicate that 3-deoxyanthocyanidins, when compared to the common anthocyanidins, will have a shift towards shorter wavelengths (hypsochromic shift) and express colours that are yellow, orange or bright red (Andersen and Jordheim, 2010).

The different secondary structures, which are affected by the pH of the solvent, are also associated with different colours. The flavylum form is mainly thought of as red, while the quinoidal forms are purple and dissociated quinoidal forms are blue. The hemiketal forms have had their chromophore broken by the addition of water and are therefore colourless, but with ring opening to the chalcone forms, a chromophore is regained, showing a yellow colour.

These secondary structures and their colours cannot fully explain the variety of colours anthocyanins express in nature. There are four main proposed mechanisms for the nuances of colours expressed in plants: self-association, intra- and intermolecular co-pigmentation and metal complexation (Nerdal and Andersen, 1991). Sigurdson et al. (2017) found that cyanidin with metal chelates and aromatic acylation resulted in most blue hues at higher pH values, and that 3,5-*O*-diglycosylation also may play a role in blue hues. A wide variety of colours ranging from purplish-blue, light pink, magenta, brick-red, and intense red were produced by adding varying concentrations of phenolic acids or phenolic extracts to samples of extract from purple sweet potato (*Ipomoea batatas* L.) at different pH values (Gras et al., 2017). The bright blue colours of flowers are mostly explained by co-pigmentation, especially with delphinidin as the anthocyanin and a flavone as the co-pigment (Harborne and Williams, 2000), and metal complexation and co-pigmentation with flavonoids have been shown to give bright blue colours to petals of several species of flowers (Kondo et al., 1992, Takeda et al., 1994, Kondo et al., 1998, Yoshida et al., 2006).

1.2.4 Stability

The stability of anthocyanins are closely related to the colour, secondary structures and co-pigmentation, and degradation can be promoted by a number of factors, like pH, temperature, oxidation, ascorbic acid, light, nucleophilic agents, sulphur dioxide, free sugars and enzymes (Iacobucci and Sweeny, 1983, Jackman et al., 1987). However, several factors contribute to an increased stability. The identity of the anthocyanidin affect the stability of the anthocyanin (Cabrita et al., 2000). The number and positions of both sugar and acyl moieties also affect the stability. It has for instance been shown that aromatically substituted anthocyanins have a higher stability in neutral and alkaline solutions compared to non-acylated anthocyanins (Fossen et al., 1998, Torskangerpoll and Andersen, 2005). Several studies also show a higher colour stability in weakly acidic or neutral conditions for di- or poly-acylated anthocyanins compared to their non-acylated analogues (Yoshida et al., 1992, Saito et al., 1995, Giusti and Wrolstad, 2003, Zhao et al., 2017). Glucuronosylation of anthocyanins have been shown to improve colour stability in response to light compared to non-

glucuronosylated anthocyanins (Osmani et al., 2009). Recently, chlorogenic acid as a co-pigment have been shown to increase the stability of non-acylated cyanidin-based anthocyanins in weakly acidic solutions, more so than for acylated anthocyanins, possibly due to the steric effects and intramolecular co-pigmentation (Gras et al., 2018).

The anthocyanidin may undergo different chemical reactions, some of which is already described as secondary structures (section 1.2.2). The protons in position 6 and 8 of the A-ring is more acidic than the protons on the B-ring, due to a lower proton density and possible keto–enol tautomerisation with the OH-groups in position 5 and 7, which have been studied through a proton-to-deuterium exchange in deuterated methanol (Jordheim et al., 2007). Nucleophilic attack by water at position 2 have been discussed in section 1.2.2 in conjunction with the formation of hemiketal forms. Nucleophilic attack of bisulphite have been shown for malvidin 3-*O*-glucoside, forming a colourless adduct (Berke et al., 1998). The formation of pyranoanthocyanidins have been done both hemisynthetically (Jordheim et al., 2006b), and occurs naturally in winemaking and aging (Fulcrand et al., 2006, de Freitas and Mateus, 2011), and involves both a nucleophilic attack in position 4 and the nucleophilic hydroxyl group in position 5. Thermal degradation is observed when temperatures of 50-150 °C is reached, and the rate depend on other factors like light and pH (Patras et al., 2010). Brownmiller et al. (2008) found that for blueberries, both thermal processing for preservation and storage of preserves had a large impact on the amount of anthocyanins. Anthocyanidins have been shown to degrade in neutral conditions, to form an aldehyde (from the A-ring) and a phenolic acid (from the B-ring), probably due to the unstable α -ketone that can be formed from the chalcone forms (Fleschhut et al., 2006).

1.2.5 Anthocyanins in plants

Function

Anthocyanins are well known in the role of attraction of insects and animals for pollination and seed dispersal purposes. Their presence in young leaves, seedlings, roots and stems is not as well understood. Some evidence points towards the need for protection against environmental factors, i.e. UV-B radiation, cold and draught, nutrient stresses, as protection against pathogens and in association with damage (Chalker-Scott, 1999, Simmonds, 2003, Close and Beadle, 2003, Gould, 2004).

Biosynthesis

The initial step of the biosynthesis of anthocyanins is the condensation of three units of malonyl CoA (shikimate pathway) and one unit of *p*-coumaroyl CoA (polyketide

pathway), to form tetrahydroxychalcone (Figure 7), catalysed by the enzyme chalcone synthase (CHS) (Strack and Wray, 1994). The chalcone is then isomerised by chalcone isomerase (CHI) to form the flavanone naringenin, which is the precursor to several of the flavonoid classes (Cooper-Driver, 2001). For anthocyanins, the flavanone is hydroxylated by flavanone 3-hydroxylase (F3H) to form a dihydroflavonol, and is further added hydroxylation and on the B-ring by appropriate enzymes.

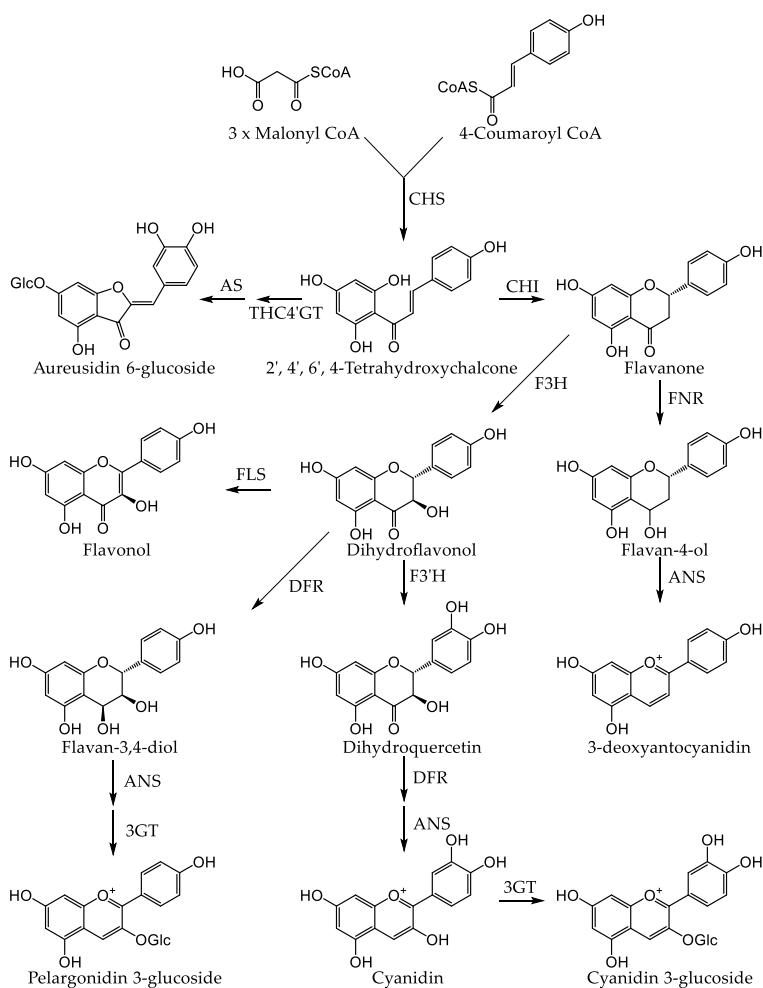


Figure 7: Biosynthesis of anthocyanins and aurones. Adapted from Andersen and Jordheim (2010).

Dihydroflavonols are then reduced by dihydroflavonol 4-reductase (DFH) to form flavan-3,4-diols, that are oxidized to anthocyanidins by the enzyme anthocyanidin synthase (ANS). The anthocyanidins are readily glycosylated by glycosyltransferase

enzymes (GT), can be further acylated by acyltransferase enzymes (AT), and methylated by methyltransferase (MT).

Bioaccumulation

Even though the biosynthetic pathway for anthocyanins have been well studied, the mechanism of which the anthocyanins accumulate in the cells is poorly understood. Most anthocyanins are water-soluble, and are normally found dissolved in the vacuolar solution of the cells. Anthocyanins have also been described as being localised in special organelles called anthocyanoplasts found inside main cell bound to the cell wall (Peckert and Small, 1980). Later anthocyanins were described as localised in anthocyanic vacuolar inclusions (AVIs) (Markham et al., 2000), based on observations in blue-grey carnation (*Dianthus caryophyllus*) and purple lisianthus (*Eustoma grandiflorum*). In these plants, the AVIs occur predominantly in adaxial epidermal cells in the petals where they have a major influence on both intensity and blueness of the colour. They observed that the AVIs did not have a defined membrane boundary and that the anthocyanins were bound to a protein matrix, with specificity to acylated 5,7-*O*-diglycosides. The concentration of anthocyanins in the AVIs were also much higher than what would be possible in vacuolar solution, giving opportunity to have intensified colours. These results have later been confirmed by Zhang et al. (2006), which additionally observed three different forms of AVIs: vesicle-like, rod-like and irregular shaped. Using light and electron microscopy, they observed that the anthocyanins accumulated as vesicle-like bodies in the cytoplasm contained in pre-vacuolar compartments (PVCs), which seemed to be the transport of anthocyanins between the sites of biosynthesis and the AVIs where they accumulate. AVIs have also later been observed in a number of other plants, including sweet potato cells (Nozue et al., 2003), grapevine (Conn et al., 2003), blue roses (Gonnet, 2003) and in the skin of ripe apples (Bae et al., 2006).

Anthocyanins are also known to accumulate in the cell wall. The red pigments in peat moss (*Sphagnum*) is described as cell wall pigments (Rudolph and Vowinkel, 1969), and the pigments found in several species of liverworts (Marchantiophyta) are localised in the cell wall (Kunz et al., 1993). Both these groups of pigments have been found in their non-glycosylated form. Cell wall pigmentation has also been observed in pleurocarpous moss (*Drepanocladus pseudosarmentosus*), and one of the pigments observed showed somewhat similar chemical behaviour as the pigments of *Sphagnum* (Bendz et al., 1962).

1.2.6 Human applications

Food colorants

There is a worldwide interest in the use of natural colorants in food, as the health safety of synthetic dyes (i.e. azo dyes) has been disputed, and as a consequence, a change is seen in consumer preferences (Wrolstad and Culver, 2012). Anthocyanins are utilised as a food colourant, approved by the European Union (Scotter, 2011). Despite the vast number of different anthocyanins found in nature, with varying properties in regard to colour, stability and nutraceutical potential, they have all one common E number (E163). Because of the colour changes and stability at higher pH values, their use in food is limited to acidic foodstuff such as soda and confectionary. The most viable sources for commercially available anthocyanins comes from grapes (*Vitis* spp.), elderberries (*Sambucus nigra*), red cabbage (*Brassica oleracea*) and roselle (*Hibiscus sabdariffa*), but other sources include blood orange, black chokeberry and sweet potato (Bridle and Timberlake, 1997).

Potential health effects

The interest in anthocyanins and their potential health effect have received increased attention the last couple of decades, and is largely related to their antioxidant effect (He and Giusti, 2010, Tsuda, 2012). Anthocyanins are often used as a dietary supplement because of their potential health effects, although their effect is often not well documented. Anthocyanins are potent antioxidants *in vitro*, because of their ability to quench free radicals. The antioxidant activity is mainly measured against equivalents of Trolox, a water-soluble vitamin E analogue. It has for instance been shown that, using oxygen radical absorbance capacity (ORAC), a widely accepted antioxidant assay, cyanidin 3-O-glucoside is 3.5 times more potent than Trolox (Wang et al., 1997).

The ability for anthocyanins to scavenge free radicals is linked to a number of potential health effects, including prevention of cardiovascular diseases (CVD) which is related to the “French paradox” (Wallace, 2011). The paradox observes that there is a lower risk of CVD mortality despite a higher intake of saturated fatty acids in regions where there is a high intake of red wine rich in anthocyanins, especially in France (Renaud and de Lorgeril, 1992). Other potential health effects include proposed anti-carcinogenic effect by a range of different mechanisms (Wang and Stoner, 2008), and anti-inflammatory effect by inhibiting cyclooxygenase-enzymes (COX) equally or more effective than existing COX inhibitors, both *in vitro* and *in vivo* (Wang et al., 1999, Seeram et al., 2001, Rossi et al., 2003). Purified anthocyanins have been shown to

prevent adipose tissue accumulation in rodent models (Tsuda, 2008), and mice fed with purified anthocyanins from blueberries showed lower weight gain than the controls, but mice fed with freeze dried powder of whole fruits actually increased weight gain compared to controls, probably owing to the increased calorie intake (Prior et al., 2008). The possible effect against obesity can contribute to prevention of diabetes type 2 by preventing oxidative stress related to insulin production in the pancreas (Ghosh and Konishi, 2007). Anthocyanins have been reported as improving eye vision, but this effect is disputed (Canter and Ernst, 2004, Nomi et al., 2019). Anthocyanins are also reported to inhibit certain types of viruses, including human immunodeficiency virus type 1 (HIV-1) (Andersen et al., 1997), and to have a protective effect against Parkinson's disease (Ye et al., 2010, Shih et al., 2011).

Bioavailability

The potential health effects of anthocyanins are dependent on their bioavailability, and a considerable amount of work have been gone towards understanding how anthocyanins behave after intake, but our understanding is still vague (McGhie and Walton, 2007, Kay, 2007). It is generally accepted that in order for dietary phytochemicals to be able to influence human health, the compounds must be able to reach target organs, but after ingestion, anthocyanins and predicted metabolites are not always detectable by routine instrumentation (Lila et al., 2016). By using ^{13}C -labelled anthocyanins, both anthocyanins and metabolites can be identified and some information about the bioavailability can be found (Czank et al., 2013), but this is not a viable method for large scale studies because of high production costs of isotope-labelled anthocyanins. Bioavailability studies involving anthocyanins often use detection of metabolites based on a HPLC system equipped with a UV/Vis absorption spectroscopy detector, and is mostly based on the detection of the flavylium cation form (section 1.2.2), which leaves the other forms possibly undetected. Understanding the transformations between the secondary structures of anthocyanins may be integral for understanding their bioavailability, and ultimately, the underlying mechanisms of the potential health effects of anthocyanins. The bioavailability of anthocyanins may also be affected by the different structures of anthocyanins (section 1.2.1), for instance in regard to the nature of the aglycone, as shown by Liu et al. (2014), who subjected anthocyanins from blueberries to a simulated gastrointestinal digestion, and found that fewer hydroxyl groups and more methoxyl groups on the B-ring improved anthocyanin stability. Several studies have shown that anthocyanins are present as intact anthocyanidin glycosides in urine and blood plasma (Matsumoto et al., 2001, Murkovic et al., 2001, Manach et al., 2005, McGhie et al., 2003), while other studies have

shown that anthocyanins is readily metabolised (Kay et al., 2005, Felgines et al., 2003). In addition, most studies of anthocyanin bioavailability are based on animal experiments: rats, rabbits and pigs, and only a handful of studies have been performed on humans (McGhie and Walton, 2007).

During the passage through the gastrointestinal tract (GIT), the anthocyanins are exposed to a range of different pH environments, which alter the chemical structure of anthocyanins, and the form that is absorbed cannot be known with certainty. Considering the low pH environment of the stomach, it is likely that only the flavylium cation form is present there, although some anthocyanins might undergo acid hydrolysis of their sugar or acid groups. Intact anthocyanins might be absorbed through *bilitranslocase* carrier enzyme and transported to the liver, and it is suggested that mono- or oligo-glycosylated anthocyanins are more readily absorbed than aglycones (Passamonti et al., 2002, Talavera et al., 2003, Fernandes et al., 2014b). In the small intestine, glycosides can be hydrolysed by the *lactate phlorizin hydrolase* (LPH) enzyme and the aglycones can be absorbed by passive diffusion (Kay, 2007), or they can be transported to the liver by the SGLT1-transporter. In the colon, anthocyanins are not well absorbed (Fang, 2014), but may undergo fermentation by gut microflora to sugars, aglycones, and phenolic acids (Aura et al., 2005). Some of these metabolites may be absorbed into the liver, while the rest is eliminated through faeces.

In the liver, anthocyanins can undergo Phase II metabolism and be conjugated to methyl, glucuronic acid and sulfate groups, and the methyl conjugates may be transported back into the small intestine (Kay, 2007). The conjugated anthocyanins is transported into the blood stream, where they can be absorbed into various organs and tissue, and seems to be able to pass the blood-brain barrier (BBB), which is necessary for them to have potential health effects in relation to Parkinson's disease (Passamonti et al., 2005). Anthocyanins and conjugates are eliminated through the kidneys, where further conjugation can occur, before being eliminated through urine.

1.3 AURONES

Aurones are a smaller class of flavonoids that have a different skeletal backbone than the flavan structure, and have a 5-ring heterocycle, as shown in Figure 8. Their structure was first elucidated from extracts of flowers of *Coreopsis grandiflora* (Geissman and Heaton, 1943) as a pigment named benzalcoumaranone from a functional aspect, but was later given the less cumbersome name 'aurones', from the Latin word *aurum*, meaning gold, inspired by the golden-yellow colour of the flowers in which they occur (Bate-Smith and Geissman, 1951). Auronols are hydrated derivatives of aurones with a hydroxyl group in position 2.

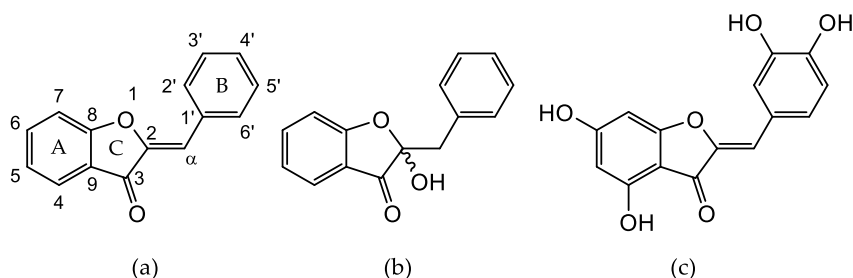


Figure 8: The skeletal backbone of aurones with numbering. (a): basic aurone structure with numbering system and ring designation, (b): basic auronol structure, (c): aureusidin (Boucherle et al., 2017).

1.3.1 Structures

There are to date 122 different aurones identified, including both aurones and auronols, glycosides and dimers of aurones (Boucherle et al., 2017). Aurones share some classical substitution patterns with other flavonoids, with positions 4, 6, 7, 3' and 4' often substituted with hydroxyl, methoxy or glycosylations. The most common aglycones include sulfuretin, maritimetin and leptosidin, and β -glucoside as the most common sugar moiety. Aurones seems to have a much wider diversity in aglycone structure than anthocyanins, as, in addition to substitutions with *O*-linkages, several types of *C*-linkages have been found, including prenylation, fused heterocyclic rings and dimers with other aurones, auronols or flavonoids (Veitch and Grayer, 2006).

1.3.2 Aurones in plants

Aurones are mostly found in the petals of flowers, especially in the family Asteraceae family and in the heartwood of several species of trees, but they have also been found in some seeds and roots, in sedges (Cyperaceae), several species in the Moraceae

family, and even in some bryophytes (i.e. *Marchantia* and *Monocarpus*) (Boucherle et al., 2017).

Function

Aurones possess a bright yellow colour (λ_{\max} of 390-430 nm), unmatched by other flavonoids, often making contrasting patterns, which is important in attraction of pollinators (Penny, 1983, Lunau et al., 1996). Aurones is known to have fluorescent properties (Boucherle et al., 2017), but this have been shown not to be involved in biological processes and pollinator attraction (Iriel and Lagorio, 2010). Aurones have been shown to possess radical scavenging capacity (Okada et al., 2014, Luo et al., 2014), and some aurones have been shown to be produced in conjunction with pathogens (Pare et al., 1991, Farag et al., 2009).

Biosynthesis

The biosynthesis of aurones was early on proposed to stem from the chalcone from the flavonoid biosynthesis (Shimokoriyama and Hattori, 1953). The chalcone from which aurones are proposed to come from have the capacity to spontaneously form a flavanone (see Figure 2), and recent discoveries have identified two distinct biosynthetic strategies producing aurones, one specifically resulting in 4-hydroxy-aurones, the other in 4-deoxyaurones.

The first biosynthetic strategy was reported for the aurones in snapdragon (*Antirrhinum majus*) (Nakayama et al., 2000), in which an aurone synthase (AUS) enzyme was identified. Aurones are produced from 2', 4', 6', 4-tetrahydroxychalcone (THC) or 2', 4', 6', 3, 4-pentahydroxychalcone (PHC) to produce either aureusidin or bracteatin aglycones. AUS also has a higher activity towards the 4-glucosides of THC than PHC (2496 % and 220 % respectively, compared to their non-glycosylated forms), which can indicate that the chalcones may be glycosylated before the aurone structures are made by AUS. The biosynthesis of snapdragon aurones and their regulation have been further analysed by Davies et al. (2006).

A second biosynthetic strategy is reported for the aurones in flowers *Coreopsis grandiflora* (Kaintz et al., 2014), in which another aurone synthase enzyme is identified. The chalcone loses the 6'-hydroxyl group, making it resistant to spontaneous flavonoid formation, before it is transformed to an aurone by AUS.

1.3.3 Human utility

In recent years, aurones have been shown to have potential effect in chemotherapy treatment and chemoprevention, antioxidant activity, antimicrobial, antifungal and antiviral activity, treatment of hyperthyroidism (Auf'mkolk et al., 1986, Boumendjel,

2003, Haudecoeur and Boumendjel, 2012, Sutton et al., 2017). Outside of medical use, the fluorescent property of aurones have been exploited as a stainer in biological applications (Shanker et al., 2011, Espinosa-Bustos et al., 2017), and they have shown useful as a natural dye in dye sensitised solar cells (Kumara et al., 2015).

2 Experimental methods

The process of isolation, purification and structure elucidation of pure plant pigments are relatively time consuming, especially for pigments that are bound to the cell walls, as for those in *Sphagnum* and *Marchantia* species. As discussed in the previous chapter, anthocyanins are relatively unstable and must be handled with care throughout the isolation procedure. Exposure to elevated temperatures, higher pH levels in the solvents and light are all factors that contribute to degradation of the pigments and must be kept to a minimum. Additionally, the isolation procedures remove stabilizing factors like free sugars and acids and other phenolic compounds.

In this chapter, the methods for isolation, purification and identification used in this thesis are presented. The methods are described in general terms, and are based on previously published methods (Andersen and Francis, 2004) and general practices in our lab. See the individual papers for a more detailed description of the exact methods used. The chapter is divided into three sections: extraction and purification methods (2.1), separation and isolation methods (2.2) and analytical methods (2.3).

2.1 EXTRACTION AND PURIFICATION METHODS

A range of techniques for extraction and purification is used to isolate the pigments from the plant material. Between each step, a small sample is usually taken out and analysed by analytical high-performance liquid chromatography (HPLC), to identify the types pigments present in the sample and to survey the effect and status of the purification and isolation steps.

2.1.1 Extraction from plant material

Pigments were extracted from fresh plant material using 0.5 % trifluoroacetic acid (TFA) in methanol (v/v), and from freeze-dried plant material using 0.5 % TFA in 80

% methanol (v/v). Extractions were performed in a refrigerator (4 °C) to keep thermal degradation at a minimum, except for the *Sphagnum* and *Marchantia* plant materials, which were extracted at room temperature (20 °C).

The various plant materials were extracted up to seven times for a maximum of 24 hours each time. The extracts were combined and filtered through glass wool or paper filters, before the solvents were removed using a rotary evaporator under reduced pressure at 27-30 °C.

2.1.2 Liquid-liquid extraction

Extracted non-polar compounds such as fats, chlorophylls, carotenoids, and other fat-soluble compounds were removed from the crude extract dissolved in 0.5 % TFA in water (v/v) by liquid-liquid extraction (LLE) against ethyl acetate. Because the crude extract of *Sphagnum* was not soluble in water, an alternative method for liquid-liquid extraction was used, which is described in more detail in the associated section in Results and discussion (section 3.2.1). LLE was repeated until the ethyl acetate ran mostly clear. The solvents were then removed under reduced pressure.

2.1.3 Amberlite XAD-7 adsorption chromatography

The crude extracts were dissolved in a minimal volume of 0.5 % TFA in water (v/v) and applied to a column filled with Amberlite XAD-7 (Merck, Germany) resin equilibrated with 0.5 % TFA in water (v/v), where anthocyanins and other polyphenolic compounds were adsorbed, while free sugars and acids and other aliphatic compounds were washed out using an excess of water. The pigments were then eluted using 0.5 % TFA in methanol (v/v). The purified crude extracts were evaporated to dryness under reduced pressure, freeze-dried and stored in a deep freezer (-18 °C) until further purification and isolation of pigments. Again, because the extract of *Sphagnum* was not soluble in water, an alternative method for Amberlite purification was used, which is described in more detail in section 3.2.1.

2.2 SEPARATION AND ISOLATION METHODS

The various pigments in the extracts were separated from impurities and isolated using techniques based on different chemical or physical properties of the pigments and the impurities. In this thesis, two main properties of the pigments were used: their size, and their solubility in different solvents.

2.2.1 Size exclusion chromatography

Size exclusion chromatography (SEC) is a chromatographic method that separates compounds based on their size, where the bulkiest compounds (generally highest molecular mass) will eluate first, followed by the smaller compounds. In this thesis, SEC was performed in an open column using two different column materials.

Sephadex LH-20

Sephadex LH-20 column material (Merck, Germany) has been used for separating anthocyanins for a number of years (Lee and Wicker, 1991). The pore size of Sephadex is slightly bigger than that of Toyopearl, and offers a faster solvent flow and pigment migration through the column. In this work, Sephadex columns were used to separate groups of pigments from other aromatic compounds, and separate pigments of similar sizes from each other, i.e., diglycosides from monoglycosides, or acylated from non-acylated pigments, before a further isolation of pigments using a different method.

Toyopearl HW-40F

Toyopearl HW-40F column material (Merck, Germany) is similar to Sephadex LH-20, but offers some advantages and disadvantages over Sephadex (Frøylog et al., 1998). Toyopearl has a smaller pore size than Sephadex, and consequently, the solvent flow is slower, but offers better band retention and better separation of pigments. In this work, Toyopearl columns were used to separate a few pigments from each other, or isolate a pigment from a small amount of impurities.

Typical procedure for SEC: A column of length and diameter to fit the sample size to be applied was prepared and equilibrated with 0.5 % TFA in 20 % methanol (v/v). The sample is dissolved in a minimal volume of eluent and applied to the column. The sample was eluted and the pigments was separated, and if applicable, a stepwise gradient with increasing concentration of methanol in increments of 10 % to a maximum of 40 % methanol. Fractions of the eluate were collected manually based on visual cues from the bands in the column. Each fraction was analysed by analytical HPLC and compared to the profile of the crude extract.

2.2.2 Semi-preparative high-performance liquid chromatography

If the pigments after SEC were not sufficiently pure for structure determination and further analysis, they were further purified using semi-preparative high-performance liquid chromatography (HPLC). The instrument used was a Gilson 321 pump (Gilson, USA) with an Ultimate 3000 variable wavelength detector (Thermo Fisher Scientific, USA). The column was a 22×250 mm 10 µm particle size Econosphere C₁₈ column (Grace, USA). For general samples, the following method was used: A: 0.5 % TFA in

water (v/v), B: 0.5 % TFA in acetonitrile (v/v). For *Sphagnum* samples the following mobile phases was used: A: 0.5 % TFA in water (v/v), mobile phase B: 0.5 % TFA in B: methanol containing 0.5 % TFA (v/v). Table 1 shows the gradients that was used for the two types of samples. The flow rate for both methods were 15 mL/min and the volume of injections was 100-500 μ l of filtered (0.45 μ m) highly concentrated pigment samples.

Table 1: Solvent gradients for semi-preparative HPLC of pigment samples.

General samples		<i>Sphagnum</i> samples	
Time	% B	Time	% B
0 min	10 %	0 min	30 %
10 min	14 %	14 min	40 %
14 min	14 %	20 min	50 %
22 min	18 %	30 min	50 %
31 min	28 %	32 min	80 %
32 min	40 %	38 min	80 %
40 min	40 %		

2.3 ANALYTICAL METHODS

The analytical methods serve mainly three purposes in the isolation and identification process: To assess the purity of a sample, to elucidate or confirm the structure of pigments, and to determine their physical or chemical properties. A combination of these methods usually gives an identity of the pigment in question, but the purity of the samples can only be assessed to the absence of impurities detectable by these methods, not for instance water and inorganic salts.

2.3.1 Analytical high-performance liquid chromatography

Analytical HPLC with diode-array detection (DAD-HPLC) was used in each step of purification and isolation of pigments to monitor the progress. The UV/Vis spectra provided by DAD-HPLC can give useful information as indication of the structure identity based on key features of pigments in these spectra. HPLC is also a robust method for quantification of pigments in a sample (Andersen and Francis, 2004).

The instrument used was a HP Agilent 1100 system equipped with a 1280 diode-array detector and an 1100 Auto sampler. The DAD had a spectral width of 190-900 nm and a 2 nm step length. Depending on the pigments to be analysed, different columns and gradients was used. For most samples, a 4.6 \times 250 mm (5 μ m) Hypersil

ODS C18 column (Thermo Fisher Scientific, USA) was used, but for *Sphagnum* samples, a 4.6×250 mm (5 µm) Supelco Ascentis RP-Amide (Merck, Germany) column was used. The mobile phases were A: 0.5 % TFA in water (v/v) and phase B: 0.5 % TFA in acetonitrile (v/v). Table 2 shows the gradients that were used for the three types of samples that were analysed. The solvent flow rate was 1 mL/min for all gradients and the volume of injections was 20 µl of filtered (0.45 µm) extract. An example of a chromatogram is presented in Figure 9.

Table 2: Solvent gradients for HPLC analysis of pigment samples.

Hypersil ODS C18 column				Ascentis RP-Amide	
General samples		Anthocyanidin samples		<i>Sphagnum</i> samples	
Time	% B	Time	% B	Time	% B
0 min	10 %	0 min	10 %	0 min	30 %
10 min	14 %	10 min	18 %	7 min	40 %
14 min	14 %	20 min	22 %	10 min	50 %
22 min	18 %	35 min	25 %	15 min	50 %
31 min	28 %	36 min	40 %	17 min	80 %
32 min	40 %	41 min	40 %	22 min	80 %
40 min	40 %				

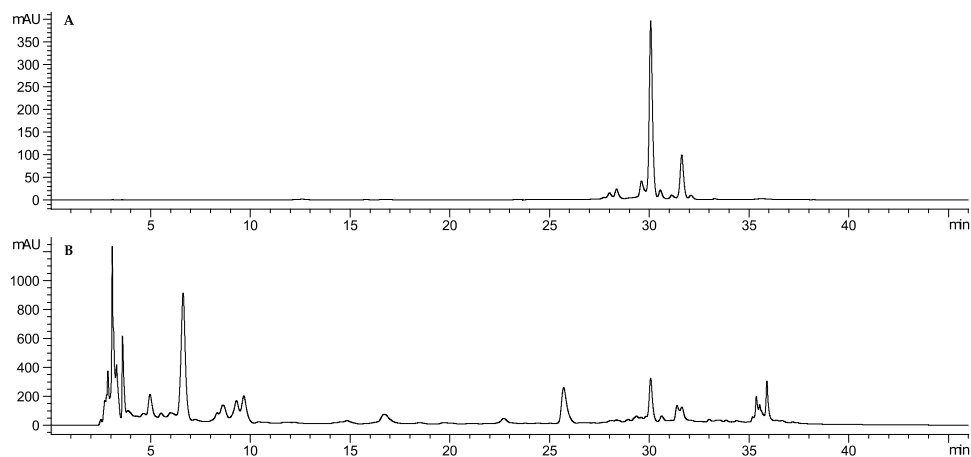


Figure 9: HPLC chromatogram of 'Sun Black' tomato crude extract. A: Detection at 520±20 nm. B: Detection at 280±10 nm.

Quantification of pigments

Quantification of pigments were performed using the analytical DAD-HPLC. A set of calibrators were prepared 5 or more concentration levels with cyanidin 3-*O*-glucoside

(3) as the calibrant, detected at 520 ± 20 nm. A known amount of plant material was extracted in a known volume of solvent (0.5 % TFA in methanol for fresh plant material, 0.5 % TFA in 80 % methanol for freeze dried material). Each calibrator level and each sample were analysed in triplicate and the average of the area under the curve were calculated. The concentrations in the samples were then calculated as equivalents to 3 using the calibrator curve.

2.3.2 Nuclear magnetic resonance spectroscopy

Nuclear magnetic resonance (NMR) spectroscopy is the most powerful analytical tool for structure elucidation. A combination of 1D (^1H) and 2D (^1H - ^1H and ^1H - ^{13}C) techniques are used to elucidate the structure of an unknown pigments, determine secondary structures of pigments, and confirming the structure of known pigments. NMR spectroscopy is also good for detecting tiny amounts of impurities, including water.

The experiments in this thesis were performed using two different instruments: a Bruker Ascend™ 600 MHz spectrometer at 600.17 MHz and 150.91 MHz for ^1H and ^{13}C respectively, equipped with a TCI CryoProbe at 298 K, and a Bruker Ascend™ 850 MHz spectrometer at 850.13 MHz and 213.77 MHz for ^1H and ^{13}C respectively, equipped with a TCI CryoProbe at 298 K. The deuteriomethyl ^{13}C signal and the residual ^1H signal of the solvents, deuterated methanol (*d*-MeOD) and deuterated DMSO (*d*-DMSO), were used as a secondary references at δ 49.15 and δ 3.31 for ^{13}C and ^1H , respectively, for methanol and δ 39.51 and δ 2.50 for ^{13}C and ^1H , respectively, for DMSO (Cambridge Isotope Laboratories Inc., 2010), unless otherwise is stated. Deuterated TFA (*d*-TFA) was used at 5 % (v/v) for acidifying samples. The following spectra were used for structure elucidations in the papers in this thesis,

1D ^1H spectrum

A 1D ^1H NMR spectrum is the most useful of the NMR techniques, as the ^1H isotope has an abundance of 99.98 %, and has a high sensitivity in the magnetic field of the instrument. This makes 1D ^1H spectra fast to record and can give a lot of information for the structure elucidation. The shift values give information about the chemical environment of each proton, coupling constants (J_{HH}) between protons give information about the neighbouring protons, and the integration of the peaks can show the quantitative relationship between the individual protons, as their area is proportional to the number of protons contained in the peak.

1D ¹³C spectrum

Because of the low abundance (1.2 %) of the ¹³C isotope, and the low sensitivity (¼ that of protons), recording useful 1D ¹³C spectra can be very time consuming. In this thesis, these spectra were therefore used exclusively to identify the position of the secondary reference of the deuteriomethyl ¹³C signal from the solvents. All carbon data in this thesis is collected from two-dimensional spectra, namely HSQC and HMBC.

DQF-COSY spectrum

The 2D ¹H-¹H double quantum filtered correlation spectroscopy (DQF-COSY) experiment gives diagonal peaks which is representative of the 1D ¹H spectrum. Cross peaks can be found when protons are J_{HH} -coupled to each other, either to the same carbon (geminal) or to adjacent carbons (vicinal), and in some cases further, especially in aromatic systems. This is very useful to identify neighbouring protons on aromatic rings and on the sugar moieties. It is very useful in combination with TOCSY to identify individual sugar moieties in the structure.

2D TOCSY spectrum

The 2D ¹H-¹H total correlation spectroscopy (TOCSY) experiment gives information about protons that are in the same spin system even if they are not directly J_{HH} -coupled. This is useful when identifying the protons of sugar moieties, as they will be in the same spin system. Together with a DQF-COSY spectrum and the coupling constants of a ¹H spectrum, it is possible to identify the sugar moieties, even if the pigment contains several moieties with overlapping shift values.

2D ROESY spectrum

The 2D ¹H-¹H rotating frame nuclear overhauser effect spectroscopy (ROESY) experiment gives spectra with cross-peaks where there is a relationship between protons though space. The most useful feature is spin-spin relaxation through space, where two protons in close spatial proximity gives a cross-peak. This is useful to identify the linkage points between different structural moieties in the pigments. Conformational changes and chemical exchanges are also possible to detect in a ROESY experiment.

HSQC spectrum

The 2D ¹H-¹³C heteronuclear single quantum coherence (HSQC) experiment gives spectra with correlation peaks where a proton is directly coupled to a carbon. When the chemical shifts of protons are known, the peaks are useful to identify the chemical shifts of carbons with one or more hydrogen directly coupled.

HMBC spectrum

The 2D ^1H - ^{13}C heteronuclear multiple bond correlation (HMBC) experiment gives spectra with correlation peaks where there is a multiple heteronuclear bond coupling between proton and carbon. The most sensitive couplings are $^2J_{\text{CH}}$ and $^3J_{\text{CH}}$, and the coupling can go through heteroatoms (like oxygen), helping the identification of the position of moieties.

2.3.3 Mass spectrometry

In this thesis, high-resolution mass spectrometry (HR-MS) was used to confirm the exact molecular mass of identified pigments, and sometimes fragment ions from the spectra assisted in verifying the structure of pigments.

Liquid Chromatography Mass Spectrometry (LC-MS)

High-resolution LC-MS with electrospray ionisation and time-of-flight separation (ESI/TOF), either in negative or positive ionisation configuration were used. The instrument used was a JEOL AccuTOF JMS-T100LC coupled to an Agilent 1200 series HPLC system. A 2.1×50 mm (1.8 μm) Zorbax SB-C18 column was used, and the gradient from analytical HPLC was adapted to compensate for the difference in column dimensions, and formic acid was used instead of TFA.

Direct Injection (DI)

When a pure pigment sample was analysed, it could be injected directly into the ionisation chamber. The same MS instrument was used, and the sample was dissolved in either methanol or DMSO, sometimes with 0.5 % TFA (v/v) added.

2.3.4 Ultraviolet/Visible light absorption spectroscopy

Ultraviolet/Visible light (UV/Vis) absorption spectra of pigments can be obtained from the on-line analytical HPLC system or from dedicated UV/Vis absorption instruments. Two instruments were used in this thesis: A Biochrom Libra S32PC UV/Vis absorption spectrometer with a spectral width of 190-700 nm and a 1 nm step length, which useful for recording UV/Vis absorption spectra of pure samples, and a HunterLab UltraScan PRO spectrophotometer with a spectral width of 350-1050 nm and a 5 nm step length. The latter instrument has the capability of recording series of spectra at given intervals, useful for looking at changes in samples over time. Some important parameters from UV/Vis absorption spectra include visible light wavelength with maximum absorption ($\lambda_{\text{Vis-max}}$), absorption (A) at $\lambda = 440$ nm (A_{440}) compared to A at $\lambda_{\text{Vis-max}}$ ($A_{440}/A_{\text{Vis-max}}$) and A at $\lambda_{\text{UV-max}}$ compared to $A_{\text{Vis-max}}$ ($A_{\text{UV-max}}/A_{\text{Vis-max}}$).

2.3.5 Thin layer chromatography

Thin layer chromatography (TLC) separates compounds based on their relative solubility in a mobile phase and stationary phase. TLC is a quick analysis that can determine similarities between different pigments. The retardation factor (R_f) is the ratio between the travel distance of the pigments and the travel distance of the solvent, and the R_f value can be compared to published values for specified solvent systems. The R_f value can also give information about the type of aglycone, the number of glycosyl units and the presence or absence of acylation, and is consequently useful in for instance monitoring the acid hydrolysis of pigments. In this thesis, TLC was carried out using microcrystalline cellulose (F5556, Merck, Germany) with two different solvents: FHW (formic acid, hydrochloric acid-conc., water, 54.4:7.2:41:4, v/v) and BAW (*n*-butanol, acetic acid-conc., water, 4:1:5, v/v, upper phase).

Acid hydrolysis

The sample was dissolved in 1 mL water and 1 mL 6 M HCl into a sealed sample vial and subjected to hydrolysis at 90°C for 120 minutes. The reaction was monitored by TLC (every 30 minutes) and HPLC (every 60 minutes).

3 Results and discussion

3.1 PIGMENTS OF *MARCHANTIA POLYMORPHA* (PAPER I)



Picture 1: Microscope image of a longitudinal section of *Marchantia polymorpha*, showing of the red pigmentation in the cell wall. Picture taken by Nick W. Albert.

Liverworts (Marchantiophyta) are non-vascular plants that form, together with mosses and hornworts, the group of basal land plants known as Bryophytes. Liverworts are thought to be the closest living relative to the proposed first land plants (Qiu et al., 1998). Liverworts are known to be able to thrive in even the most inhospitable of environments, as evidenced by liverworts living in the cold and arid landscape of Antarctica (Post, 1990, Snell et al., 2007, Clarke and Robinson, 2008, Snell et al., 2009, Newsham, 2010). The genome of the model species of liverworts *Marchantia polymorpha* (*marchantia*) have recently been sequenced (Bowman et al., 2017), and this study found that its genome was resembling what had been predicted for the ancestral land plant.

Some species of liverworts are known to produce red pigmentation in response to nutritional stress (Nagai, 1915, Kunz and Becker, 1995) that is located in the cell

walls (Picture 1), and recently it has been shown that a R2R3MYB transcription factor, *MpMyb14*, is triggered in response to both light- and nutrient deprivation stresses, activating the production of the red pigmentation (Albert et al., 2018).

3.1.1 Auronidins – A new class of flavonoids

A red pigment have previously been identified in marchantia, called ‘Riccionidin A’ (Kunz et al., 1993), and it was classified as an anthocyanin because of its red colour similar to many anthocyanins, and of its positive heterocyclic ring pyrylium ring found in anthocyanidins. We realised that the hydroxyl substitution pattern of ‘riccionidin A’ did not fit with the A-ring being derived from the shikimate pathway and the B-, C- and D-ring being derived from the polyketide pathway. In **Paper I**, we present results that show that the pigment being an anthocyanin is based on a misunderstanding of the biosynthetic origin, and why it should be a part of a previously unreported class of flavonoids for which we propose the name ‘auronidins’. We show that from a chemical standpoint, auronidins have a pyrylium ring similar to anthocyanidins, enabling the pigment to show a range of colours based on various proportions of the auronidin and its anionic forms in a simple acid-base equilibrium, but they are not able to transform into the typical secondary structures (hemiketal and chalcone forms) of anthocyanins when the pH of the solvent weakly acidic or neutral. We also show that from a biosynthetic standpoint, auronidins are not derived from the same biosynthetic pathway as anthocyanins but are derived from the flavonoid pathway somewhere before the formation of the heterocyclic pyrylium ring of anthocyanins.

3.1.2 Pigments from transgenic material of *Marchantia polymorpha*

The amount of pigmentation in wild type plants is quite low and are dependent on light- or nutritional deprivation stress to be produced (details in section 3.1.4). Transgenic plants of marchantia overexpressing the *MpMyb14* transcription factor, displaying strong activation of the flavonoid pathway, were produced and grown by Dr. Kevin Davies and his research group at New Zealand Institute for Plant & Food Research in Palmerston North, New Zealand. These plants were found to produce two pigments in considerably elevated amounts compared to wild type marchantia: a novel glycoside identified to be auronidin 4-*O*-neohesperidoside (**1**), and its aglycone, auronidin (**2**), previously described as ‘riccionidin A’ (Kunz et al., 1993).

Isolation of 1 and 2

The red pigmentation was isolated from freeze-dried transgenic marchantia material using the methods described in section 2.1. Purification by Amberlite XAD-7 column

chromatography was skipped as the pigmentation tightly bound to the column material. The analytical HPLC (Figure 10) revealed two pigments which were isolated from the extract using Toyopearl column chromatography (pigment **1**) and preparative HPLC (pigment **2**).

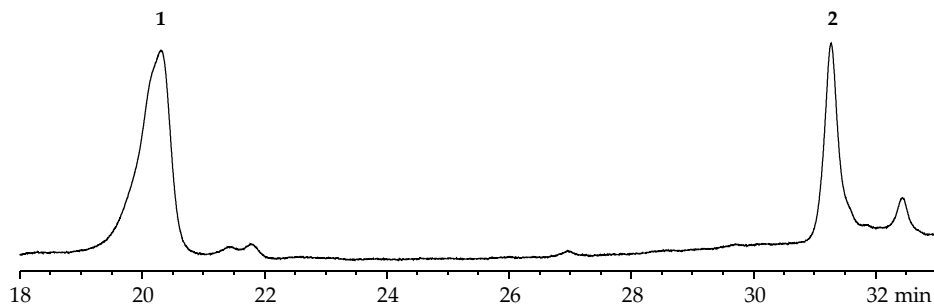


Figure 10: HPLC chromatogram section of the pigments of *Marchantia polymorpha*, detected at 498 nm.

Structure elucidation of **2**

The elucidation of the structures **2** was done using a combination of 850 MHz 1D (^1H) and 2D (HSQC, HMBC, ROESY) NMR spectroscopy and high-resolution MS. A ^1H NMR spectrum of a sample of **2** dissolved in 5 % *d*-TFA in *d*-MeOD (v/v) showed five aromatic proton signals in the downfield region. Two of these at δ 6.64 ppm (*d*, 1.6 Hz, H7) and δ 6.45 ppm (*d*, 1.6 Hz, H5) were identified as protons in meta positions on a six-membered aromatic ring (A-ring), and their carbon shifts found in the HSQC spectrum as cross peaks at δ 6.64/92.43 ppm (H7/C7) and δ 6.45/100.70 ppm (H5/C5), respectively, also have cross peaks to each other respectively at δ 6.64/100.70 ppm (H7/C5) and δ 6.45/92.43 ppm (H5/C7), respectively, in the HMBC spectrum (Figure 11). In the HMBC spectrum they both have common cross peaks to a carbon at δ 6.45/172.43 (H5/C6) and δ 6.64/172.43 ppm (H7/C6), and C6 have an oxygen functional group. H5 also have a cross peak in the HMBC spectrum at δ 6.45/159.51 ppm (H5/C4) to C4 which also has an oxygen function. H7 also have a cross peak in the HMBC spectrum, at δ 6.64/165.79 ppm (H7/C8), to C8 which have a third oxygen function. The last carbon of the aromatic ring at has HMBC cross peaks to both H5 and H7 at δ 6.45/101.34 ppm (H5/C9) and δ 6.64/101.34 ppm (H7/C9) respectively. The last HMBC cross peak of both H5 and H7 is to an aromatic carbon at δ 6.45/159.06 ppm (H5/C3) and δ 6.64/159.06 ppm (H7/C3) respectively, which also have an oxygen function. C3 has a third cross peak in the HMBC spectrum at δ 8.74/159.06 ppm (H α /C3) positioned on a different six-membered aromatic ring placing the third proton

at δ 8.74 (s, H α), which in turn have a cross peak in the HSQC spectrum at δ 8.74/127.65 ppm (H α /C α).

The two last protons at δ 7.55 ppm (*d*, 0.5 Hz, H3') and δ 7.46 ppm (*s(b)*, H6') were identified as protons in para positions on a six-membered aromatic ring (B-ring), and their carbon shifts were found in the HSQC spectrum as cross peaks at δ 7.55/104.06 ppm (H3'/C3') and δ 7.46/112.67 ppm (H6'/C6'), respectively. H3' and H6' have common cross peaks in the HMBC spectrum at δ 7.55/151.37 ppm (H3'/C2') and δ 7.46/151.37 ppm (H6'/C2') to C2', δ 7.55/156.93 ppm (H3'/C4') and δ 7.46/156.93 ppm (H6'/C4') to C4', and δ 7.55/149.19 ppm (H3'/C5') and δ 7.46/149.19 ppm (H6'/C5'), all

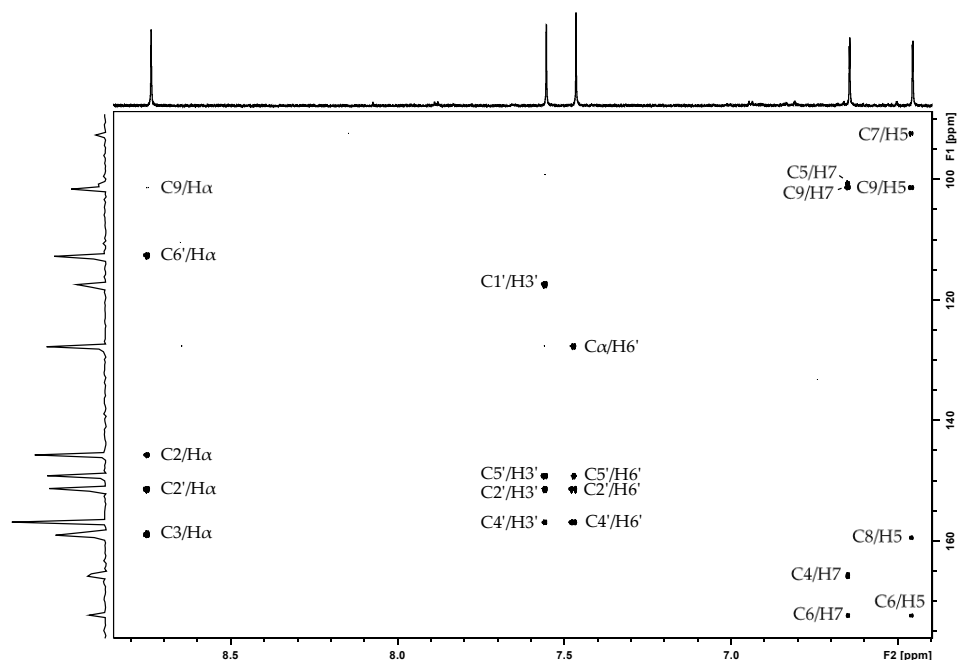


Figure 11: ^1H - ^{13}C HMBC NMR spectrum of the aromatic region of auronidin (**2**) in 5% *d*-TFA in *d*-MeOD (v/v) recorded at 25°C (850 MHz instrument).

three with oxygen functions. Additionally, H6' have a cross peak in the HMBC spectrum to the last carbon of the aromatic ring at δ 7.46/117.30 ppm (H6'/C1'). H6' and H α have cross peaks to each other's carbon in the HMBC spectrum at δ 7.46/127.65 ppm (H6'/C α) and δ 8.74/112.67 ppm (H α /C6'), respectively, in addition to having a cross peak in the ROESY spectrum at δ 7.46/8.74 ppm (H6'/ H α). With all the carbons in the B-ring accounted for, H α must be located on a different aromatic ring (D-ring) fused to the B-ring. The last HMBC cross peak is between H α and the last aromatic carbon at δ 8.74/146.72 ppm (H α /C2), and C2 has an oxygen function. Because

the functional groups of the A-ring are symmetric, but H5 and H7 have different shift values, the A-ring has to be fused to the D-ring giving an aromatic five-ring (C-ring) analogue to that of aurones. This is in correspondence with the aglycone 2,3,6,8-tetrahydroxybenzofuro[3,2-b]chromen-5-ium (auronidin, **2**). Additional NMR spectra used in the structure elucidation is available in Appendix B-2. The HR-MS spectrum of **2** (Appendix C-2) showed a molecular ion with m/z 285.03971 corresponding to the empirical formula $C_{15}H_9O_6^+$ (calc. 285.03991), which confirms the structure of **2** (Figure 12).

When we compared this elucidation of **2** to the identification of 'riccionidin A' done by Kunz et al. (1993), out of the several signals labelled "Assignments may be exchanged", we found that three of these pairs were indeed exchanged. A table with updated 1H and ^{13}C shifts with coupling constants for **2** is presented in Appendix Table A-1.

Structure elucidation of 1

The structure of auronidin 4-neohesperidoside (**1**) were conducted in a similar way to auronidin, but also included 2D DQF-COSY and TOCSY NMR experiment to help resolve the signals from the sugar moieties. A 1H NMR spectrum of **1** dissolved in 5 % *d*-TFA in *d*-MeOD (v/v) was very similar to that of **2**, with H α , H3' and H6' easily identifiable at 8.88 (s), 7.66 (s), and 7.50 (s) ppm, respectively. The exception was the overlapping signals of H5 and H7, that were assigned to δ 6.826 ppm (*d*, 1.6 Hz) and δ 6.832 ppm (*d*, 1.6 Hz) respectively based on the common cross-peaks in the HMBC with the other aromatic proton signals.

A TOCSY spectrum identified the two groups of shift values indicating two glycoside moieties. One anomeric proton of a glycoside at δ 5.49 ppm (*d*, 7.5 Hz, H1'') have a cross peak in the HMBC spectrum at δ 5.49/157.34 ppm (H1''/C4) showing the that the sugar is located in position 4 on the aglycone. In addition, a cross peak in the ROESY spectrum at δ 5.49/6.826 ppm (H1''/H5) confirms the position of a sugar unit. The rest of the glycoside was elucidated by a chain of the proton shifts with common coupling constants and cross peaks in the HMBC spectrum and assisted by a DQF-COSY spectrum. Their carbon shifts were found from the HSQC spectrum, indicating a β -glucopyranosyl moiety.

Another anomeric proton of a glycoside at δ 5.42 ppm (*d*, 1.8 Hz, H1''') have a cross peak in the HMBC spectrum at δ 5.42/81.64 ppm (H1'''/C2'') show that the second sugar unit is located at position 2'' of the β -glucopyranosyl moiety. The rest of the sugar unit was elucidated the same way as the β -glucopyranosyl moiety, and was identified

as a α -rhamnopyranosyl moiety. This identifies the sugar as a neohesperidoside. A table with all ^1H and ^{13}C shifts with coupling constants for **2** is presented in Appendix Table A-1. NMR spectra used in the structure elucidation is available in Appendix B-1.

The HR-MS spectrum of **1** (Appendix C-1) showed a molecular ion at m/z 593.15099 corresponding to the empirical formula $\text{C}_{27}\text{H}_{29}\text{O}_{15}^+$ (calc. 593.15064). This is in agreement with the novel pigment auronidin 4-*O*-(2''-*O*- α -rhamnopyranosyl- β -glucopyranoside) (auronidin 4-*O*-neohesperidoside, **1**). In addition, the HR-MS spectrum of **1** showed a fragment ion with m/z 285.03656 corresponding to the empirical formula $\text{C}_{15}\text{H}_9\text{O}_6^+$ (calc. 285.03991). This is in correspondence with the auronidin (**2**) (Figure 12). This concludes the structure elucidation of auronidin 4-*O*-neohesperidoside (**1**).

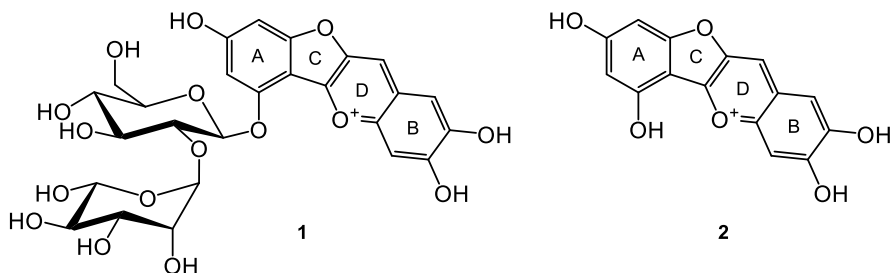


Figure 12: Structures of auronidin 4-*O*-neohesperidoside (**1**) and auronidin (**2**).

3.1.3 Chemical properties of auronidin 4-*O*-neohesperidoside (**1**)

Auronidins are a new class of flavonoid pigment that provide plants colourisation capable of screening in the visible light. The knowledge about the chemical properties of these pigments is very sparse. In this section, the properties of the newly identified auronidin 4-*O*-neohesperidoside (**1**) have been explored using UV/Vis absorption spectroscopy and ^1H NMR spectroscopy.

Colour and pH

As shown in Picture 1 and as described in the literature, the colour of the pigmentation of the plant is red, but when **1** is isolated and dissolved in acidic solvents, a drastic hypsochromic shift is observed. When **1** is dissolved in 0.5 % TFA in methanol (v/v), the colour of the solution is bright yellow ($\lambda_{\text{vis-max}}$ 495 nm) (Figure 13). This is in contrast to anthocyanins which, at this pH level, depending on its substitutions, usually is in the red to purple region. Anthocyanins are represented here with the spectrum of cyanidin 3-*O*-glucoside (**3**), the most common anthocyanin in nature, which is bright pink ($\lambda_{\text{vis-max}}$ 529 nm) when dissolved in 0.5 % TFA in methanol (v/v) (Figure 13). This

is also in contrast to the aurone aureusidin 4-*O*-glucoside (**4**) that is very weakly yellow ($\lambda_{\text{Vis-max}}$ 402 nm) in the same solvent (Figure 13).

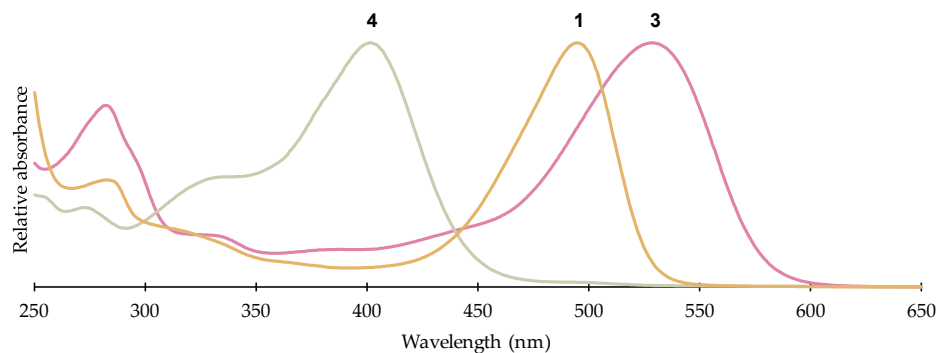


Figure 13: UV/Vis absorption spectroscopy of aureusidin 4-*O*-glucoside (**4**), auronidin 4-*O*-neohesperidoside (**1**) and cyanidin 3-*O*-glucoside (**3**) dissolved in 0.5 % TFA in methanol (v/v), showing the $\lambda_{\text{Vis-max}}$ values of the three pigments. The colour of the line is closely related to the colour displayed by the sample recorded.

The colour displayed by anthocyanins in weakly acidic to neutral conditions have been explored in section 1.2.2, and is mainly based on the hydration of the flavylium cation form to form the colourless hemiketal forms, and further ring-opening to form colourless to weakly yellow chalcone forms. **1** does not show any sign of colourless forms in weakly acidic to neutral conditions. This has been demonstrated using both UV/Vis absorption spectroscopy and 1D ^1H NMR spectroscopy. **1** displays a deep orange colour ($\lambda_{\text{Vis-max}}$ 497 nm) in weakly acidic solutions and a bright pink colour ($\lambda_{\text{Vis-max}}$ 521 nm) in neutral solutions (Figure 14). This colour change is probably based on various proportions of the auronidin and its neutral and possibly anionic forms in a simple acid-base equilibrium, and is probably linked to the pyrylium ring of the structure. These results show that auronidins are capable of displaying a range of colours usually mostly exclusive for anthocyanins. **1** was also dissolved in both acidic, weakly acidic and neutral *d*-MeOH and ^1H NMR spectra was recorded for each solvent (Figure 15). We can see that the proton shifts of all five aromatic signals is shifted upfield when the pH of the solvent is raised towards neutral. This change in chemical shift can be linked to the shift in colour that was seen using UV/Vis absorption spectroscopy. We did not find any evidence in the ^1H NMR spectra for any of the secondary structures (hemiketal or chalcone forms) in the weakly acidic to neutral solvents, in the same way anthocyanins do, as described in section 1.2.2.

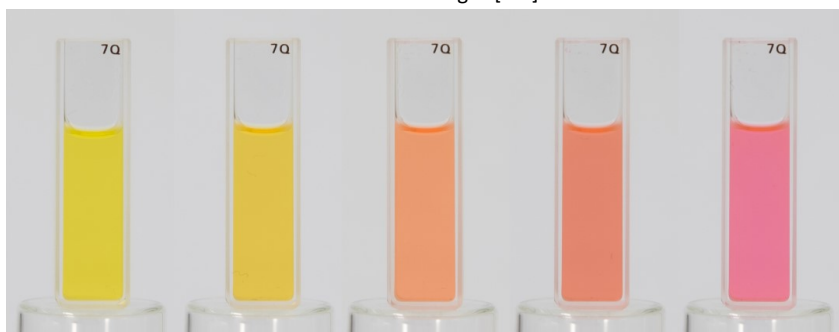
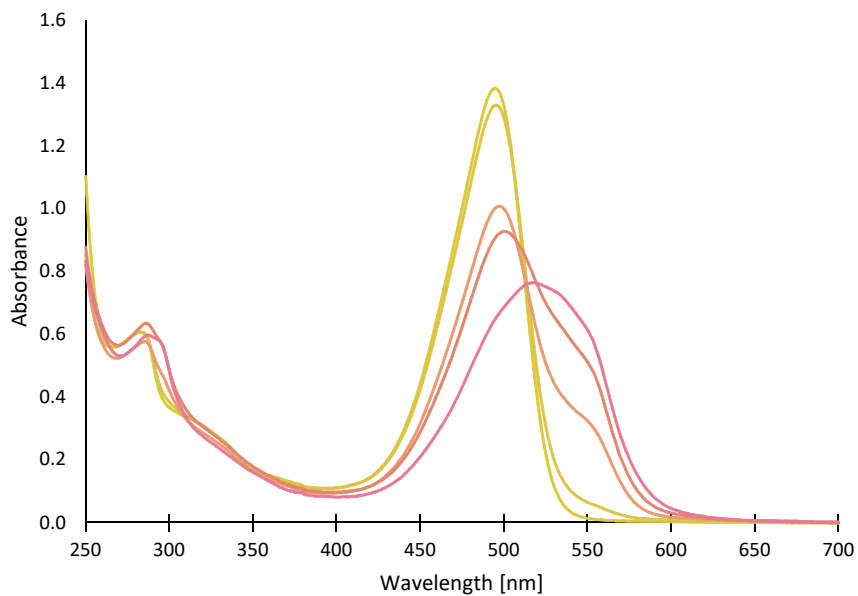


Figure 14: Top: UV/Vis absorption spectra of auronidin 4-neohesperidoside (1) in methanol at five different pH levels, yellow in acidic to pink in neutral. **Bottom:** Photos the cuvettes with the samples yellow in acidic to the left to pink in neutral to the right.

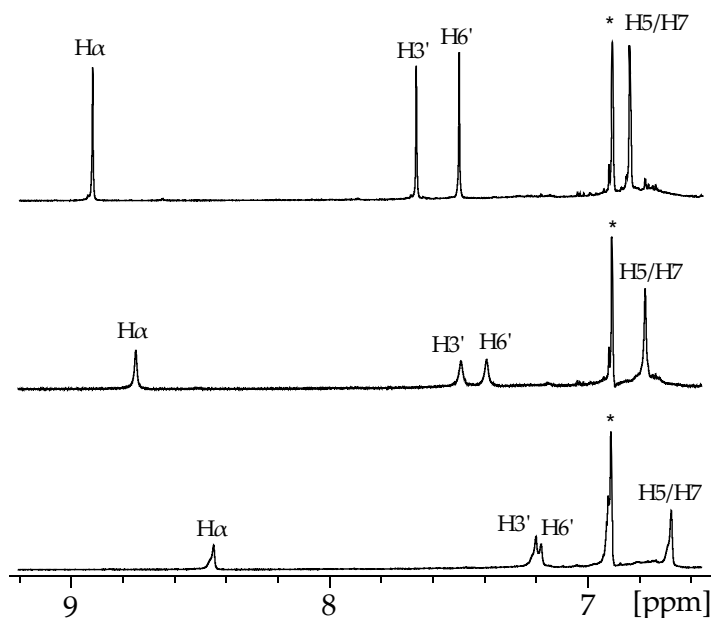


Figure 15: ^1H NMR spectra of auronidin 4-neohesperidoside (**1**) in acidic (top), weakly acidic (middle) and neutral (bottom) deuterated methanol, showing a downfield shift of all protons, but no signs of new peaks that could indicate secondary structures (hemiketal or chalcone forms).

*Impurity

Fluorescence

In addition to showing yellow to red colours that is usually only found in anthocyanins, the auronidins show strong fluorescence under 365 nm UV-light. The colour of the fluorescence is highly dependent on the solvent, as shown in Figure 16.



Figure 16: Fluorescence of auronidin 4-neohesperidoside (**1**) under 365 nm UV radiation showing a range of different fluorescent colours, depending on the solvent. Left: 5 % *d*-TFA in *d*-DMSO (v/v). Middle: 0.5 % TFA in MeOH (v/v). Right: Methanol with a drop of 1M NaOH.

3.1.4 Biosynthesis of auronidins

(This section is adapted from **Paper I** and is based on the work done by Prof. Kevin M. Davies, Dr. Nick W. Albert and colleagues in New Zealand.)

To confirm our hypothesis that the auronidins do not come from the same biosynthetic path as anthocyanins, a series of marchantia plants with mutations in the flavonoid biosynthesis was made. The biosynthesis of flavonoids is described in section 1.2.5. In wild type (WT) plants, both flavone *O*-glycosides and **2** were produced when the plants were put under nutrient stress. Chalcone isomerase (CHI) is responsible for the formation of the heterocyclic 6-ring of flavonoids. In plants with knockout mutations for the *chi* gene, there were no detectable flavones, but the production of auronidin was unaltered. This confirms that auronidin must come from a biosynthetic branch different for that of anthocyanins, which is based on the enzyme CHI.

To confirm that auronidin comes from the flavonoid pathway, similar to aurones (section 1.3.2), another mutant was made, knocking out the enzyme chalcone isomerase-like (CHIL), which is responsible for the efficiency of early biosynthetic steps in the flavonoid pathway (Morita et al., 2014). These plants still produced both flavones and auronidin under nutrient stress, but at significantly lower levels. A *chi/chil* double mutant was also made, which had no detectable flavonoids and barely detectable levels of auronidin. This shows that auronidins does indeed come from the flavonoid pathway.

3.2 CELL WALL PIGMENT OF *SPHAGNUM* SP. (PAPER II)



Figure 2: Red buds of *Sphagnum* sp. Taken by the author.

Peat moss (*Sphagnum*) is a non-vascular basal land plant living in moors and bogs and generally wet environments. Peat moss is capable of storing large amounts of liquid in its porous structure, up to 20 times its own dry weight, and peat moss was for this used as an absorbent in provisional wound dressing during the first world war (Hotson, 1921). Some species of peat moss produce bright red pigments located in the cell walls in response to light, low temperatures and water and nutrient deprivation (Rudolph, 1964). These red pigments were first chemically described by Rudolph and Vowinkel (1969) as pigments displaying some of the same properties as anthocyanidins, and was named ‘Sphagnorubins’. The structure was found to have an extended aromatic system compared to the common anthocyanidins, and additionally it was lacking the hydroxyl group in position 3 making it a 3-deoxyanthocyanidin. In **Paper II** we present a method for isolation and purification of Sphagnorubins, and provide the first full structural elucidations of the flavylium cation form of Sphagnorubin C (**5**) and the *trans*-chalcone form of **5**, the latter also being, as far as we know, the first full structural elucidation of a *trans*-chalcone form of a naturally occurring anthocyanin.

3.2.1 Isolation of Sphagnorubin C (**5**)

Sphagnorubin C (**5**) was isolated from red peat moss (*Sphagnum* sp.) collected in Western Norway (60.2744 N, 5.4974 E) in February 2015. Because of the unusual

extended aromatic ring of the anthocyanidin and the lack of sugar groups, this anthocyanin is insoluble in water. Since the methodology described in section 2 is largely based on anthocyanins' generally good solubility in water, the methods had to be modified to be viable for **5**.

The collected plant material was first air dried and then milled into a powder using a blender. Pigments were extracted using 0.5 % TFA in methanol for 24 hours at room temperature. Because peat moss has such capacity to absorb liquid, a fruit press was used to maximise the output. Extraction with methanol was performed a total of four times, and the methanolic extracts were combined and most of the methanol was removed under reduced pressure. The extract was added 0.5 L of 0.5 % TFA in water, before the rest of methanol was removed under reduced pressure. The now water-based extract was partitioned against ethyl acetate. Three layers formed in the separation funnel: a slightly pigmented water layer on the bottom, a middle layer of thick purple precipitate, and a brown ethyl acetate layer on top. The water and middle layer were removed and partitioned six more times against ethyl acetate. The water and middle layers were evaporated to dryness under reduced pressure and dissolved in a minimal volume of 0.5 % TFA in methanol, which was applied to a column of Amberlite XAD-7 resin (section 2.1.3) equilibrated with water. Some of the pigment was retained in the column, but most was washed out as a precipitate using 0.5 % TFA in water. The water was largely removed under reduced pressure, and the extract was lyophilized to remove all solvents. The lyophilized pigments were recovered using a minimal volume of 0.5 % TFA in methanol, which produced a concentrated crude extract of about 50 mL. Using semi-preparative HPLC (see section 2.2.2 for details), Sphagnorubin C (**5**) was isolated from the concentrated crude extract, each injection of 500 μ L yielding about 1 mg of pure **5**.

3.2.2 Structure elucidation of secondary structures of **5**

Both the flavylum cation and the *trans*-chalcone forms of **5** have been elucidated in this thesis, with full ^1H and ^{13}C chemical shift assignments using a range of 1- and 2D NMR techniques, and HR-MS.

Flavylum cation form

A sample of **5** was dissolved in 5 % *d*-TFA in *d*-DMSO (v/v), and both 1D (^1H) and 2D (DQF-COSY, HSQC, and HMBC) NMR spectroscopy at 600 MHz was recorded for the structure elucidation. There were 10 signals in the aromatic region of the ^1H spectrum. Three of these signals formed an AMX coupling pattern at δ 8.09 ppm (*d*, 2.2 Hz, H2'), δ 7.16 ppm (*d*, 8.6 Hz, H5') and δ 8.26 ppm (*dd*, 2.2, 8.6 Hz, H6'), and together with one

methoxy group at δ 4.03 ppm (MeO-C3') that coupled to C3' in the HMBC spectrum it formed a similar pattern to corresponding signals of the B-ring of anthocyanins with the peonidin aglycone. The aromatic region had a peak at the high chemical shift typical for anthocyanidin H4 protons at δ 10.04 ppm (*d*, 9.1 Hz, H4), but with a J_{HH} -coupling of 9.1 Hz. This coupling suggested that there also was a vicinal proton, which was confirmed from a cross peak at δ 8.74/10.03 ppm in the DQF-COSY spectrum, which places the proton at H3 (δ 8.74 ppm, *d*, 9.0 Hz). Both these protons had common cross peaks in the HMBC spectrum at δ 10.03/168.98 and δ 8.74/168.98 ppm with H2' at δ 8.09/168.98 ppm placing C2 at 168.98 ppm, confirming that the assignment is of a 3-deoxyanthocyanidin. The rest of the carbon atoms of the C-ring was assigned from the HMBC spectrum.

One of the protons at δ 8.13 ppm (*s*, H12) have common cross peaks at δ 8.13/158.35 and δ 8.13/117.81 ppm in the HMBC-spectrum with H4 at δ 158.35 ppm (C12a) and with H3 at δ 8.74/117.81 ppm (C4a) placing C12a and C4a respectively. The H12 proton had also a common cross peak at δ 8.13/168.68 ppm in the HMBC spectrum with a methoxy group δ 4.44/168.68 ppm placing the second methoxy group at C12. The rest of the carbon atoms of the A-ring was assigned from the HMBC spectrum. Another proton at δ 8.72 ppm (*d*, 9.0 Hz, H5) had a cross peak at δ 8.72/117.81 ppm to C4a in the HMBC spectrum, in common with H12 at δ 8.13/117.81 ppm, in addition to a common cross peak to another carbon at δ 8.72/119.70 ppm (C10b). H5 had cross peak in the COSY spectrum at δ 8.72/8.20 ppm, which was used to assign H6 at δ 8.20 ppm (*d*, 8.9 Hz), which also have a common cross peak in the HMBC spectrum with H4 at C4b (δ 8.20/129.43 ppm). A singlet proton at δ 7.47 ppm (H7) have a common cross peak with H6 at C10a (δ 8.20/123.77 ppm) in the HMBC spectrum, and these protons both have cross peaks in the HMBC spectrum to each other's carbon at δ 7.47/131.49 ppm and δ 8.20/111.95 ppm, respectively. The last carbon on the D-ring was assigned by a cross peak at δ 8.72/129.27 ppm in the HMBC spectrum, placing C6a. This carbon also has a cross peak in the HMBC spectrum to H10 of the E-ring (δ 9.05/129.27 ppm), assigning the last proton in the structure. The two remaining carbon atoms was assigned by a cross peak with H10 at δ 9.05/147.68 ppm and a cross peak with H7 at δ 7.47/147.99 ppm in the HMBC spectrum, assigning the shifts of C8 and C9, respectively. With all protons and quaternary carbons assigned, the HSQC spectrum confirmed the shift values of the tertiary carbons, which concludes the NMR structure elucidation of the flavylum cation form of Sphagnorubin C (5). All shift values are tabulated in Appendix A-1. The NMR spectra used in the elucidation is available in **Paper II** and its Supplementary materials.

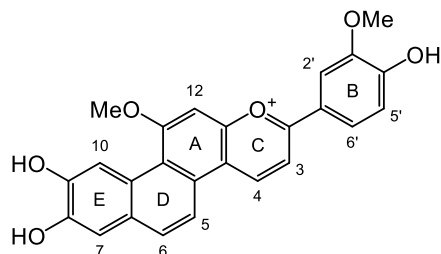


Figure 17: Structure of the flavylium cation of Sphagnorubin C (**5**), with numbering.

A positive mode HR-ESI-MS spectrum of **5** showed a molecular ion at m/z 415.11833 corresponding to the empirical formula $C_{25}H_{19}O_6^+$ (calc. 415.11816), which is in agreement with the structure of **5** in its flavylium cation form Figure 17.

The general structure of Sphagnorubins was first elucidated using acetylation of functional groups and derivatisation of Sphagnorubin A, followed by UV/Vis absorption spectroscopy, IR spectroscopy, mass spectrometry and NMR spectroscopy (1H only) of the acetylated pigments and derivatives (Vowinkel, 1975). The structure of **5** was later elucidated with assignments of 1H NMR (Mentlein and Vowinkel, 1984), but the assignments were in some cases uncertain. A comparison of the assignments of shift values in this thesis resolved the assignments of H2' and H6', and corrected a switch between H12 and H7, which both were determined by 2D NMR techniques. This thesis therefore provides the first full structural characterisation of the flavylium cation form of **5**.

Trans-chalcone form

A sample of **5** was dissolved in pure deuterated DMSO, equilibrated for 24 hours, and both 1D (1H) and 2D (DQF-COSY, NOESY, HSQC and HMBC) NMR spectroscopy at 600 MHz was recorded for the structure elucidation. These spectra showed, in addition to peaks belonging to the flavylium cation, a set of peaks corresponding to another form of **5**. The 1H spectrum had three peaks from protons with a similar AMX coupling pattern as the B-ring of the flavylium cation of **5**, but with slightly different shift values at δ 7.56 ppm (d , 2.0 Hz, H2'), δ 9.93 ppm (d , 8.2 Hz, H5') and δ 7.59 ppm (dd , 2.0, 8.6 Hz, H6'), including the methoxy group at δ 3.87 ppm (s , MeO-C3'). The carbon values of the B-ring of this structure were determined from the HSQC and HMBC spectra. H2' and H6' had both cross peaks in the HMBC spectrum at δ 7.56/187.78 and δ 7.59/187.78 ppm, respectively, to the same carbon with a shift value corresponding to a carbonyl function (δ 187.78 ppm, C=O). This carbonyl

function had further cross peaks in the HMBC spectrum to two protons at δ 7.97/187.78 and δ 8.34/187.78 ppm, with cross peaks to each other in the COSY spectrum at δ 7.97/8.34 ppm, both with a high coupling constant typical for *trans*-alkenes (15.4 Hz). The proton at δ 7.97 ppm (*d*, 15.4 Hz, H α) has cross peaks in the NOESY spectrum to both H2' and H6' at δ 7.97/7.56 and δ 7.97/7.59 ppm, indicating this peak is the closest to the carbonyl function. The other proton is at δ 8.34 ppm (*d*, 15.4 Hz, H β). The coupling patterns for the remaining five proton signals were analogue to that of the flavylium form of **1** and the protons were identified as δ 8.89 ppm (*s*, H5), δ 7.18 ppm (*s*, H8), δ 7.67 ppm (*d*, 9.2 Hz, H9) and δ 7.87 ppm (*d*, 9.2 Hz, H10). The shifts for the rest of the tertiary carbons were found from the HSQC spectrum, by cross-referencing with the HMBC spectrum, the quaternary carbon shifts are found, and the structure is confirmed to be the *trans*-chalcone of **5** (Figure 18). All shift values are tabulated in Appendix A-2. The NMR spectra used in the elucidation is available in **Paper II** and its Supplementary materials. The negative mode HR-ESI-MS spectrum of the *trans*-chalcone of **1** showed a molecular ion at m/z 431.11338 corresponding to the empirical formula C₂₅H₁₉O₇ (calc. 431.11308), which agrees with a deprotonated *trans*-chalcone.

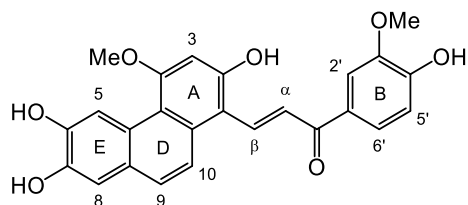


Figure 18: Structure of *trans*-chalcone of **5**, with new numbering.

A tetra-acetate derivative of the *trans*-chalcone form of **1** was inadvertently synthesised and structurally elucidated by Mentlein and Vowinkel (1984), with ¹H NMR data, as a means to identify the positions of the hydroxyl groups. In the same paper, the 3'-OH analogue of **5**, Sphagnorubin B, was made into a penta-acetate derivative, which have been supplied with partial ¹³C NMR data. This thesis therefore provides the first complete structural elucidation of the *trans*-chalcone form of **5**.

Identification of chalcone forms of anthocyanins in general is usually only inferred from the elucidation of the flavylium cation forms, and the presence of characteristic chalcone features in UV/Vis absorption spectra. As far as I know, the first definite spectroscopic data on chalcones formed from natural anthocyanins was recorded by Brouillard et al. (1979) (UV/Vis absorption spectroscopy) using malvidin 3-*O*-glucoside. 2D NMR NOESY spectra were recorded of malvin (malvidin 3,5-*O*-diglucoside) which provided useful information on the structural transformations,

and also provided the first partial assignments of shift values for a natural chalcone anthocyanin form (Santos et al., 1993). Later the ^1H shifts of the chalcone forms of both malvidin 3-*O*-glucoside and cyanidin 3-*O*-glucoside have been fully assigned (Houbiers et al., 1998, Fernandes et al., 2014a). Thus, this structure elucidation of the *trans*-chalcone form of **1** is, as far as I know, the first full structural characterisation with both ^1H and ^{13}C NMR data of a naturally occurring anthocyanin chalcone form.

3.2.3 The network of anthocyanin forms of **5**

The generally accepted scheme of transformations between secondary structures of anthocyanidins (section 1.2.2) dictates that in order to form the *trans*-chalcone form, the flavylium cation form, dissolved in weakly to neutral solvents, first has to be hydrated to form hemiketals, which undergoes tautomerisation to form the *cis*-chalcone, that isomerise to form the *trans*-chalcone form. When **5** was dissolved in 5 % *d*-TFA in *d*-DMSO (*v/v*) for NMR spectroscopy structure elucidation, the sample was red, and only signals from the flavylium cation was present, and the sample was stable for 88 days at -20 °C. When **5** was dissolved in pure *d*-DMSO, the sample was also red, only peaks from the flavylium cation form present in the first ^1H spectrum recorded after 30 minutes. However, regular recordings of ^1H spectra over the next 24 hours revealed another set of peaks belonging to the *trans*-chalcone form. During this period, an equilibrium between the two forms established at a 1:1 ratio had formed, and the sample had turned an orange colour. This equilibrium ratio was stable for 76 days at -20 °C. No other peaks appeared in the NMR spectrum, neither from the hemiketal forms or the *cis*-chalcone form nor any degradation products. After the 76 days, the NMR sample was acidified with 5 % *d*-TFA (*v/v*), which after 1 hour still showed the two forms at a 1:1 equilibrium ratio in the ^1H spectrum, and no signs of peaks of other compounds. After 6 days at -20 °C however, peaks from the flavylium cation form were dominating the ^1H spectrum with just traces of peaks from the *trans*-chalcone form, and after 10 days at -20 °C only peaks from the flavylium cation were present in the ^1H spectrum. This network between the red flavylium cation form and the more orange colour of the flavylium cation/*trans*-chalcone forms 1:1 ratio seems to be both stable without any degradation and fully reversible under the changing pH conditions they were submitted to, and without signs of the intermediate hemiketals or *cis*-chalcone forms.

The colours observed in the NMR samples from the various forms in the network of anthocyanidin structures was more closely studied using visible absorption spectroscopy on a HunterLab spectrophotometer (see section 2.3.4), which

have a much faster sampling time and far less demand for sample per experiment. Visible absorption spectroscopy also records the colours of the samples accurately. Before recording the spectra, a standardised stock sample of **5** was prepared. The process through which **5** was isolated includes many steps where both water and TFA are solvents, and when samples of purified pigments were evaporated to dryness, it contained residuals of these solvents. Pigment from one injection from the semi-preparative HPLC (section 2.2.2) was therefore dissolved in 10 mL 0.5 % TFA in methanol (v/v), divided into aliquots suitable for visible absorption spectroscopy, and evaporated to dryness under nitrogen. Some aliquots were further purified by dissolving it in 1 mL pure methanol, and evaporated to dryness under nitrogen, which removed some of the residual water and/or TFA making a more neutral sample. This process was repeated once to produce an even more neutral sample. Further processing did not significantly alter the properties of the samples.

One aliquot (sample A) was dissolved in 0.5 % TFA in DMSO and showed a red colour and with characteristic spectrum with a λ_{\max} at 540 nm (Figure 19, black line) in the visible absorption spectrum. Three aliquots (samples B-D) were dissolved in pure DMSO after differing degrees of processing. Sample B was dissolved directly in pure

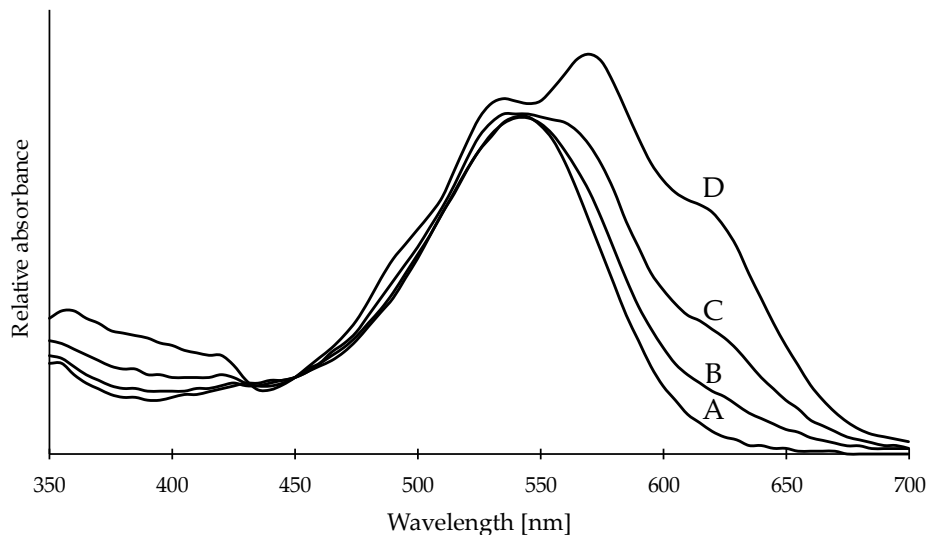


Figure 19: Visible light spectra of four aliquots (Samples A-D) from a standardised batch of purified Sphagnorubin C (**5**). **Sample A:** Dissolved in 5 % TFA in DMSO. **Sample B:** Dissolved in pure DMSO. **Sample C:** Processed once and dissolved in pure DMSO. **Sample D:** Processed twice and dissolved in pure *d*-DMSO. The spectra are normalised to the isosbestic point at 450 nm.

DMSO (Figure 19, red line), sample C was processed once and dissolved in pure DMSO (Figure 19, purple line), and sample D was processed twice and dissolved in deuterated DMSO (Figure 19, blue line). Deuterated DMSO was used in the last sample to maximise the purity of the solvent. The colour of Sample B was very similar to sample A and they showed very similar visible absorption spectra. Sample D had a dark blue/purple colour immediately after dissolving in deuterated DMSO, and its visible absorption spectra showed a λ_{\max} at 570 nm and additional shoulders above 600 nm which was in accordance with quinoidal forms of **5**. Sample C showed both colour and a visible absorption spectrum in accordance with a mixture of the flavylum cation and the quinoidal forms of **5**.

After dissolving sample B in pure DMSO without processing, visible absorption spectra were recorded every 2 hours for 24 hours (Figure 20a), which revealed the transformation from the red flavylum cation form to the yellow *trans*-chalcone form with a λ_{\max} at 420 nm. In contrast to the NMR sample, this sample showed an almost complete transformation to the *trans*-chalcone form, as seen by the low absorbance at 540 nm, which reached equilibrium after about 14 hours. After 24 hours the sample was acidified with 5 % TFA (v/v) and spectra were recorded every 2 hours for another 24 hours (Figure 20b). These spectra showed the transformation of the *trans*-chalcone form back to the flavylum cation form that reached equilibrium after about 16 hours,

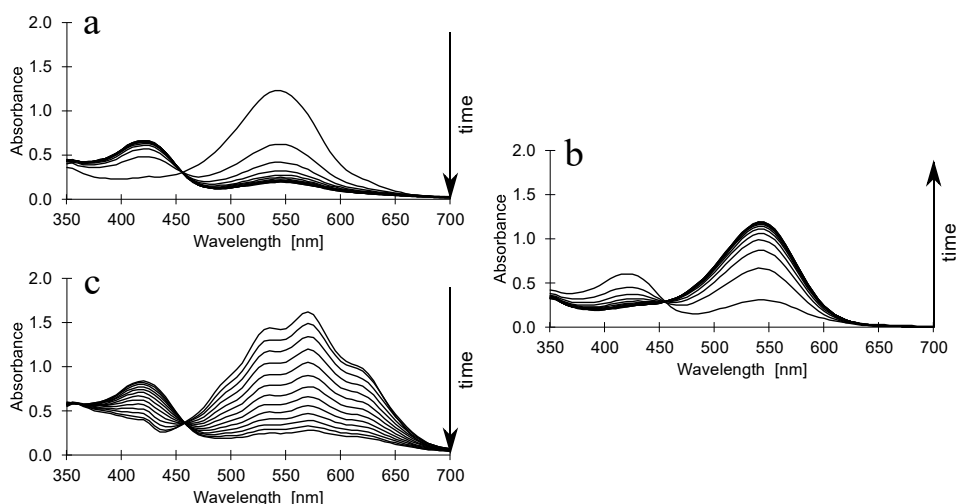


Figure 20: Visible light spectra of samples of **5** recorded at 2-hour intervals for 24 hours, with different pre-treatments of the samples. **a:** Sample B dissolved in pure DMSO. **b:** Sample C twice neutralised and dissolved in pure deuterated DMSO. **c:** Sample B equilibrated for 24 hours, then added 5 % TFA (v/v).

as also observed in the NMR sample that was acidified. After 24 hours the absorbance of the acidified Sample B at 540 nm was at 97 % of its level immediately after initially dissolving in pure DMSO, the missing 3 % can be accounted for by the dilution by addition of the acid. Thus, it seems like the flavylium cation form can be fully regenerated from the *trans*-chalcone form, without signs of degradation detectable by NMR spectroscopy.

Visible absorption spectra of sample D were also recorded every 2 hour for 24 hours (Figure 20c). The blue/purple colour of the sample slowly changed into the same yellow colour of sample B, and the spectra revealed same transformation into the *trans*-chalcone form, but with the quinoidal base as starting point. This sample did not reach full equilibrium even after 24 hours, but most of the quinoidal base had transformed, as seen by the low absorbance in the 530-600 nm range. This sample was also acidified with 5 % TFA (v/v) after 24 hours, and spectra were again recorded every 2

hours for 24 hours. These spectra were identical to the first series of spectra in an acidified sample seen in Figure 20c. These observations showed that the flavylium cation form quickly transforms into quinoidal forms under neutral conditions, but the more thermodynamically stable *trans*-chalcone form eventually dominates. Sphagnorubin C (5) thus seems to have the network of transformations as described generally for anthocyanins in section 1.2.2, and once the flavylium cation form is transformed both into quinoidal forms and the *trans*-chalcone form, can be fully regenerated without any signs of degradation (Figure 22).

For a further in-depth discussion of the implications of this stability in the network of transformations and a comparison to a representative common anthocyanin, please see the Results and discussion section in **Paper II**.

A last interesting note to the series of spectra shown in Figure 20, is that all series of spectra, an isosbestic point at 455 nm is present. This is yet another indication that the transformation between the acidic red flavylium cation form and the neutral yellow *trans*-chalcone and blue quinoidal forms of 5 are based on the same network of transformations as the common anthocyanins.

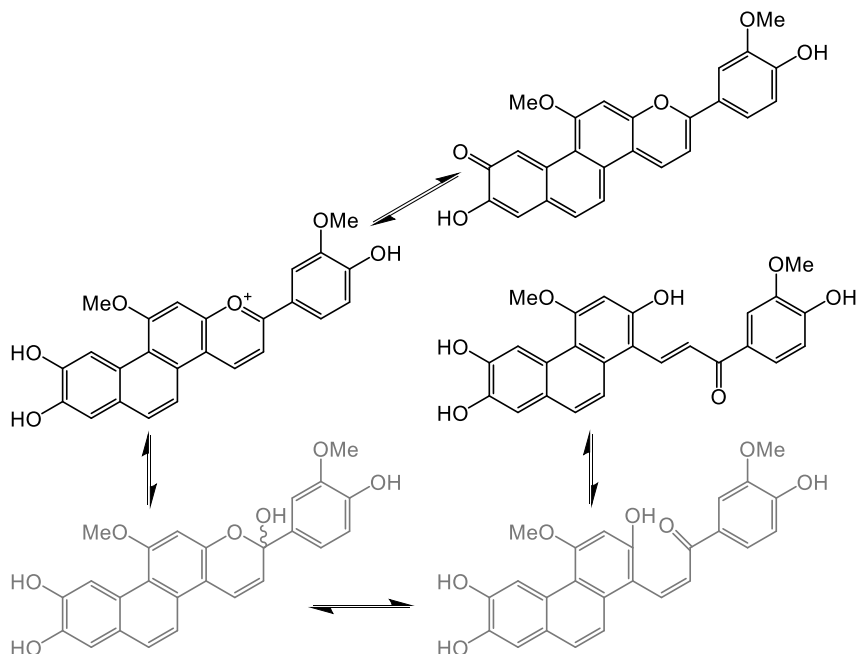


Figure 21: Network of equilibrium forms of Sphagnorubin C (**5**). The hemiketal and *cis*-chalcone forms (grey) were not spectroscopically detected because of rapid transformation between the flavylium cation and *trans*-chalcone forms.

3.2.4 Influence of solvent on ^1H NMR shift values

The chemical shift value of a proton in a structure is related to the electron density at that proton, which in turn can be an indication on the reactivity of the structure at that position. Looking at how different solvents change the chemical shifts of the flavylium cation form may contribute to the understanding of the structural characteristics that is relevant for the transformation to the different equilibrium forms. During the structure elucidation of **5**, ^1H chemical shifts of the flavylium cation form were recorded in different combinations of solvents: *d*-DMSO and *d*-MeOD, both with and without added 5 % *d*-TFA (v/v), which revealed some differences in the shift values depending on the solvent composition.

When **5** is dissolved in MeOD, there is a marked difference whether there is acid present in the solvent or not (Figure 22, circles), and generally showing more downfield shift values without the acid present. However, in DMSO, the shift values are even more downfield than for MeOD, but there is virtually no difference whether there is acid present or not (Figure 22, triangles). A sample dissolved in pure MeOD

and equilibrated for 24 hours did not show any signs of the other forms of **5**, even though there was a larger shift value increase when omitting the acid from MeOD compared to omitting the acid from DMSO. This difference in behaviour is probably due to DMSO being an aprotic solvent, where the acid has no solvent to assist in the dissociation of the acidic proton, rendering the acid in turn unable to affect the structure in the same way as if the solvent was MeOD. Even though it is in pure DMSO that the flavylum cation transforms into the *trans*-chalcone, it is not the chemical shift change of the protons when omitting the acid that enables the transformation, but rather the intrinsically higher shift values of the protons when using DMSO as the solvent. Even though there are minimal shift changes between the pure and acidified DMSO, the acidified solvent has a low enough pH to both hinder the protonation to form the quinoidal base and to minimise the nucleophilic attack by water to form the

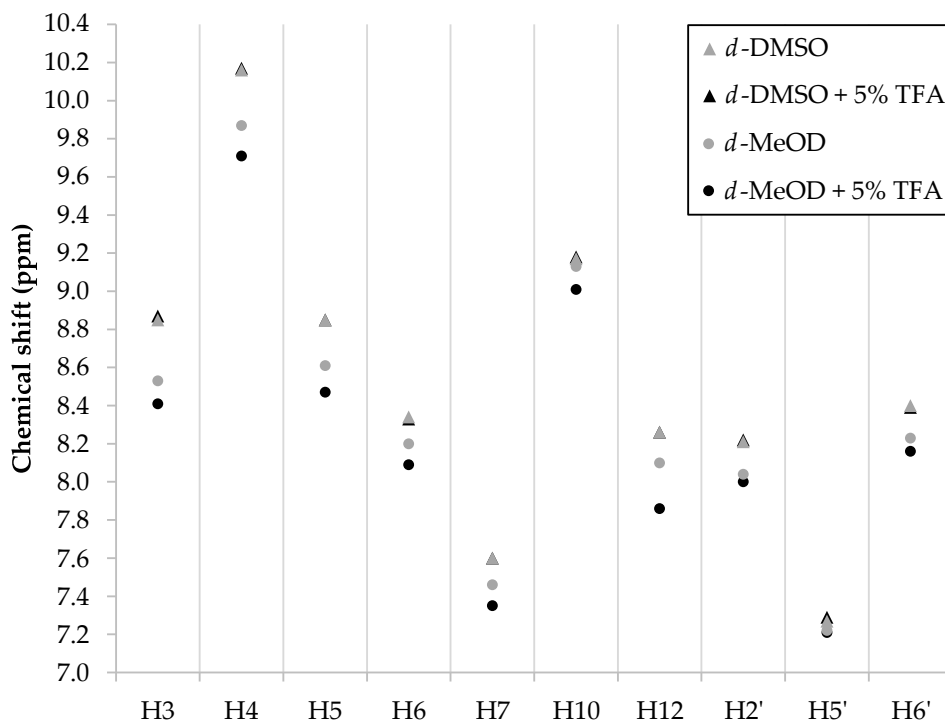


Figure 22: Chemical shifts of the aromatic protons of **5** in different solvents: deuterated methanol (● and ●) and DMSO (▲ and ▲), with and without 5 % TFA (v/v), showing *d*-DMSO having more downfield shift values compared to *d*-methanol, but with little to no change in difference if the acid is present, and showing that the absence of acid in *d*-methanol (●) have more downfield shifts than with the added acid (●).

hemiketals. However, in MeOD, even the large chemical shift increases the protons showed when omitting the acid does not enable the flavylum cation form to transform. It may indicate that it is absolute chemical shift values of the protons that defines whether the structure is able transform or not. Additionally, the presence of acid in DMSO changes the pH of the solvent enough that the structure is unable to transform regardless of the higher absolute chemical shifts.

One additional interesting note is that the biggest chemical shift change was observed for H12 when omitting acid from MeOD. This is the analogue position of H8 in a common anthocyanidin and is known to be prone to hydrogen-deuterium exchange in both acidified and pure MeOD (Jordheim et al., 2007), although their results showed that the rate of exchange was not affected by the amount of acid. We did not observe hydrogen-deuterium exchange for 5.

Because of very poor peak resolution when dissolved in pure *d*-MeOD, it was not possible to record carbon data for the flavylum cation form, and a corresponding study for carbon data unfortunately not possible.

3.3 NEW ANTHOCYANIN SOURCES

3.3.1 New anthocyanins from flowers of *Erlangea tomentosa* (Paper III)



Picture 3: Pink-mauve flowers of *Erlangea tomentosa*. Taken by Christopher Adaku.

Erlangea tomentosa (*Bothrioline longipes*) Oliv. & Hiern S. Moore (family Compositae) is a plant native to tropical Africa, widely distributed in South, Central and East Africa. The plant has by locals been used to treat a range of health conditions including colic pains, stomach ache, syphilis, fever and miscarriage (Asiimwe et al., 2014). The pink-mauve flowers were found to contain two pigments, erlangidin 5-*O*-(4-(*E*-caffeoyl)-6-(malonyl)- β -glucopyranoside)-3'-*O*-(6-(3-(β -glucopyranosyl)-*E*-caffeoyl)- β -glucopyranoside) (**6**) and erlangidin 5-*O*-(6-(malonyl)- β -glucopyranoside)-3'-*O*-(6-(3-(β -glucopyranosyl)-*E*-caffeoyl)- β -glucopyranoside) (**7**) at levels of 1.55 mg/g and 0.60 mg/g fresh weight, respectively. **6** and **7** are based on the aglycone erlangidin, first reported in **paper III**, the first reported natural anthocyanidin with a methoxy-group on the heterocyclic C-ring.

Structure elucidation of 6 and 7

Pigments were extracted and isolated using the method described in chapter 2, using 5 % TFA in methanol (v/v) for extraction, and purification using partition against ethyl acetate and purifying using an Amberlite XAD-7 column, and finally isolation of the pigments using Sephadex LH-20 and preparative HPLC. The pigments were identified using 1- and 2D NMR spectroscopy and HR- MS.

The ^1H NMR spectrum of **6** showed sixteen protons in the aromatic region. Three of these at δ 8.42 ppm (*d*, 2.1 Hz, H2'), δ 8.39 ppm (*dd*, 2.1 Hz, 8.8 Hz, H6') and δ 7.27 ppm (*d*, 8.8 Hz, H5') corresponded with the substitution pattern of the B-ring of cyanidin, and δ 8.64 ppm (*s*, H4), δ 7.09 ppm (*d*, 2.0 Hz, H6) and δ 7.02 ppm (*d* (broad), H8) corresponded to the protons on the A-, and C-rings. The chemical shifts of the corresponding carbons were done using a HSQC spectrum and the remaining carbons of the aglycone were identified from a HMBC spectrum.

The HMBC spectrum also contained a strong cross-peak at δ 4.25/149.19 ppm (C3). The signal at δ 4.25 ppm integrated to three protons in the ^1H spectrum, which is in accordance with a methoxy group located in position 3 of the anthocyanidin. The location of this group is also supported by a cross-peak in a NOESY spectrum, at δ 8.64/4.25 ppm between H4 and the methoxy group. In addition, the HR-MS spectrum showed a fragment ion with *m/z* 301.0853 corresponding to the empirical formula $\text{C}_{16}\text{H}_{13}\text{O}_6^+$ (calc. 301.0707) and was in accordance with a 3-methoxy-5, 7, 3', 4'-tetrahydroxyflavylium cation (3-methoxycyanidin). Since this is the first recording of a natural anthocyanidin with a methoxy group on the C-ring, the anthocyanidin was given the name erlangidin.

Five of the protons in the aromatic region were coupled through HMBC, with coupled aromatic shifts of δ 6.96 ppm (*d*, 1.8 Hz, H2''), δ 6.71 ppm (*d*, 8.2 Hz, H5'') and δ 6.63 ppm (*dd*, 8.2 Hz, 1.9 Hz, H6''), and the coupled olefinic shifts at δ 7.22 ppm (*d*, 15.9 Hz, β'') and δ 6.10 ppm (*d*, 15.9 Hz, α''). These signals, with their corresponding carbon shifts and couplings in the HMBC spectrum to quaternary carbons and an ester carbonyl at δ 168.06 ppm, correspond to a caffeic acid group. Similarly, the remaining five aromatic signals corresponded to a second caffeic acid group.

The sugar region of the ^1H spectrum in combination with a TOCSY spectrum indicated the presence of three sugar units in **6**. Starting from the anomeric proton at δ 5.35 ppm (*d*, 7.8 Hz, H1'''), a cross-peak at δ 5.35/3.92 ppm in the DQF-COSY spectrum supported by the cross-peak in the HSQC spectrum at δ 5.35/102.47 ppm was used to assign H2'''. Similarly, the chain of coupled protons in the sugar moiety was identified, and with their coupling constants assigned, the signals were in accordance with a β -glucopyranosyl moiety. A cross-peak at δ 5.35/156.00 ppm in the HMBC spectrum between H1''' and C5 of the aglycone and the cross-peak at δ 5.35/7.09 in the NOESY spectrum between H1''' and H6 showed that this sugar was connected to the aglycone at position 5.

Similarly, starting with the anomeric proton at δ 5.16 ppm (*d*, 7.6 Hz, H1''''), the second sugar moiety was also identified as a β -glucopyranosyl moiety. Cross-peaks at

δ 5.16/146.89 ppm (H1^{'''}/C3[']) in the HMBC spectrum and δ 5.16/8.42 ppm (H1^{'''}/H2[']) in the NOESY spectrum showed that the second sugar was connected to the aglycone at position 3'. The third and last anomeric proton at δ 4.69 ppm (*d*, 7.6 Hz, H1^{'''}) was also identified as a β -glucopyranosyl moiety, with cross-peaks at δ 4.69/146.89 ppm (H1^{'''}/C3^{''}) in the HMBC spectrum and δ 4.69/6.96 ppm (H1^{'''}/H2^{''}) in the NOESY spectrum showed that this sugar unit was connected to the 3^{''}-position of the second caffeoyl moiety.

The first caffeic acid moiety, with a cross-peak at δ 5.16/168.18 ppm in the HMBC spectrum between H4['] and the carbonyl function at C^I in the HMBC spectrum, is connected to a glucosyl 4[']-position, whilst the second caffeic acid moiety, with cross-peaks at δ 4.94/168.06 ppm and δ 4.32/168.06 ppm in the HMBC spectrum between H6A^{'''} and the carbonyl function at C^{II} and H6B^{'''} and the carbonyl function at C^{II} respectively, is connected to a glucosyl 6^{'''}-position. In addition, an aliphatic acid moiety was found to be connected to a glucosyl 6^{''}-position, with a cross-peak at δ 4.44/168.40 ppm in the HMBC spectrum between H6A^{''}/6B^{''} and the carbonyl function at C1^{III}.

The HR-MS spectrum of **6** showed a molecular ion at m/z 1197.2903 corresponding to the empirical formula C₅₅H₅₇O₃₀⁺ (calc. 1197.2929). This is in agreement with the novel pigment erlangidin 5-*O*-(4-(*E*-caffeoyl)-6-(malonyl)- β -glucopyranoside)-3'-*O*-(6-(3-(β -glucopyranosyl)-*E*-caffeoyl)- β -glucopyranoside) (**6**) (Figure 23).

By comparing UV/Vis absorption spectra of **6** and **7**, both pigments showed a $\lambda_{\text{Vis-max}}$ value around 530 nm, but **6** showed a stronger local $\lambda_{\text{UV-max}}$ value at 325 nm than **7** with a lower intensity local $\lambda_{\text{UV-max}}$ value at 322 nm, indicating that **7** have only one aromatic acyl group. Based on an analogous structure elucidation as for **6**, the structure elucidation of **7** were done mainly based on NMR spectra recorded of **7b**, a methylmalonated analogue (see details below). The HR-MS spectrum of **7** showed a molecular ion at m/z 1035.2709 corresponding to the empirical formula C₄₆H₅₁O₂₇⁺ (calc. 1035.2612). This is in agreement with the novel pigment erlangidin 5-*O*-(6-(malonyl)- β -glucopyranoside)-3'-*O*-(6-(3-(β -glucopyranosyl)-*E*-caffeoyl)- β -glucopyranoside) (**7**) (Figure 23). All shift values are tabulated in Appendix A-3. The NMR spectra used in the elucidation is available in **Paper III** and its Supplementary materials.

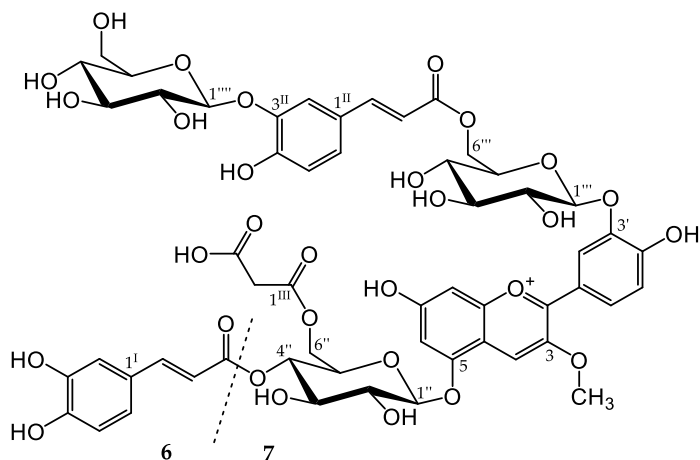


Figure 23: Structure of the two new anthocyanins (**6** and **7**) identified from *Erlangea tomentosa*.

Derivatisation of **6** and **7**

During the extraction, isolation and storage of **6** and **7** in acidified methanol, the pigments were partially derivatised. The chromatograms in Figure 24 show the profile of pigments 1 day after extraction (**A**) and 1 month after extraction (**B**), where **6** and **7** were partially converted into **6a/6b** and **7a/7b**, respectively. Using HR-MS, a difference of 85.9890 Da was found between **6** and **6a**, which is in accordance with the lack of the malonyl group, and in the HR-MS spectrum **6a** showed a molecular ion at m/z 1111.3013, in agreement with erlangidin 5-*O*-(4-(*E*-caffeoyl)- β -glucopyranoside)-3'-*O*-(6-(3-(β -glucopyranosyl)-*E*-caffeoyl)- β -glucopyranoside) (**6a**). A difference of 14.0164 Da was found between **6** and **6b**, and with an extra methoxy signal at δ 3.77 in the ^1H spectrum, a cross-peak at δ 3.77/170.16 ($\text{CH}_3\text{O}/\text{C}3^{\text{m}}$ -carbonyl) in the HMBC spectrum and a cross-peak at δ 3.77/53.3 (CH_3O) in the HSQC spectrum, the structure of **6b** was found to be made by methyl esterification of the free carboxyl group of the malonyl group of **6**. The HR-MS spectrum of **6b** showed a molecular ion at m/z 1211.3086 in agreement with erlangidin 5-*O*-(4-(*E*-caffeoyl)-6-(methylmalonyl)- β -glucopyranoside)-3'-*O*-(6-(3-(β -glucopyranosyl)-*E*-caffeoyl)- β -glucopyranoside).

In a similar way, the structures of **7a** and **7b** was identified to be erlangidin 5-*O*- β -glucopyranoside-3'-*O*-(6-(3-(β -glucopyranosyl)-*E*-caffeoyl)- β -glucopyranoside) (**7a**) and erlangidin 5-*O*-(6-(methylmalonyl)- β -glucopyranoside)-3'-*O*-(6-(3-(β -glucopyranosyl)-*E*-caffeoyl)- β -glucopyranoside) (**7b**), respectively. Table 3 show chromatographic and spectral data for the erlangidin-based pigments.

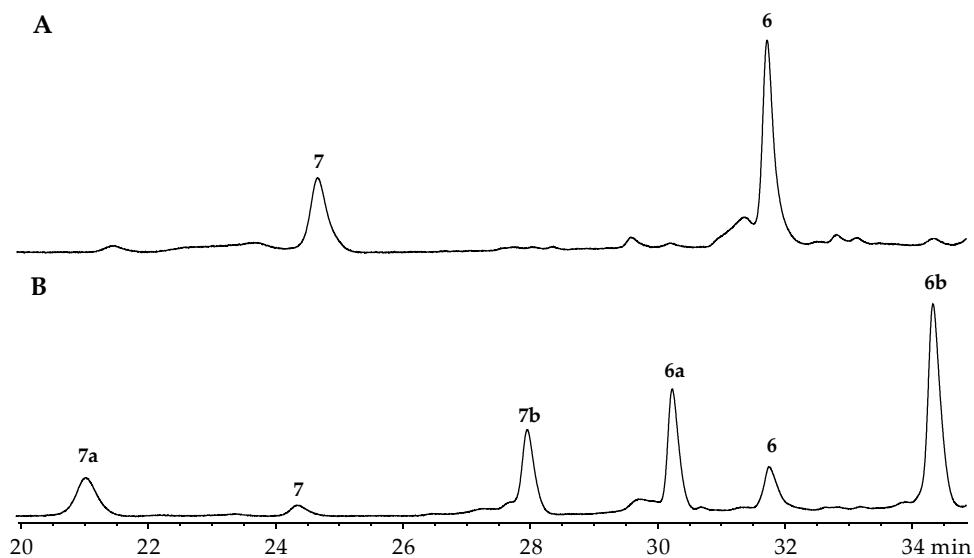


Figure 24: HPLC chromatogram sections of extracts from *Erlangea tomentosa*, extracted with acidified methanol (0.5 % TFA, v/v). **a** denotes the demalonylated pigment, whilst **b** denotes the methoxymalonylated pigment. **A:** Chromatogram 1 day after extraction. **B:** Chromatogram 1 month after extraction. Detected at 520 ± 20 nm

Table 3: Retention times and on-line spectral values on HPLC and high-resolution electrospray ionisation mass spectral data for **6** and **7** isolated from *Erlangea tomentosa* and their demalonylated and methylmalonylated derivatives (**6a/7a** and **6b/7b**, respectively).

	t_R (min)	Vis-max (nm)	Local UV- max (nm)	$A_{440}/A_{vis-max}$ (%)	A_{UV-max} / $A_{vis-max}$ (%)	$[M]^+(obs.)$ (m/z)	$[M]^+(calc.)$ (m/z)	molecular formula
6	31.78	530	282 (sh), 294, 326	18	95	1197.2903	1197.2929	$C_{53}H_{57}O_{30}^+$
6a	30.25	530	280 (sh), 296, 324	19	106	1111.3013	1111.2925	$C_{52}H_{55}O_{27}^+$
6b	34.30	530	282 (sh), 296, 326	18	87	1211.3067	1211.3086	$C_{56}H_{59}O_{30}^+$
7	24.32	530	278, 294 (sh), 322	19	65	1035.2709	1035.2612	$C_{46}H_{51}O_{27}^+$
7a	21.11	528	278, 294 (sh), 320	20	63	949.2653	949.2608	$C_{43}H_{49}O_{24}^+$
7b	27.95	530	278, 294 (sh), 322	19	61	1049.2837	1049.2769	$C_{47}H_{53}O_{27}^+$

(sh): Shoulder

Diagnostic features of erlangidin aglycone

This is the first report of a natural pigment containing a methoxy group in the 3-position, a position most commonly substituted with a glycoside. We examined how this new anthocyanidin compared to some of the common anthocyanidins in regards to several measures.

Aglycones of isolated pigments from blueberries, *Fuchsia* spp. flowers and *E. tomentosa* were made using acid hydrolysis and analysed by TLC and HPLC. On-line UV/Vis absorption spectra were used to find $\lambda_{\text{Vis-max}}$ and $A_{440}/A_{\text{Vis-max}}$ values. From Table 4 we observe that erlangidin has a relatively high R_f value (0.42) compared to peonidin (0.34), despite having the same number of hydroxyl groups and methoxy groups, but in different positions. The $\lambda_{\text{Vis-max}}$ value of erlangidin (525 nm) is not different for that of cyanidin (525 nm) and peonidin (526 nm), both having the same number of substituents on the B-ring.

The NMR signals of the methoxy group on the C-ring of the anthocyanidin have been compared to methoxy groups on the A- and B-rings. The ^{13}C NMR chemical shift values of methoxy groups on the B-ring of anthocyanins are usually observed at 56.7–57.3 ppm in acidified *d*-MeOD, whilst on the A-ring they are observed at 57.7–57.9 ppm. The ^{13}C chemical shift of the methoxy group on the C-ring of **6** and **7** is observed at 58.3 ppm, which is somewhat downfield to the usual shift values on the A- and B-rings. Similarly, the ^1H NMR chemical shift values of methoxy groups on the B-ring of anthocyanins are usually observed at 4.06–4.13 ppm, whilst on the A-ring they are observed at 4.17–4.21 ppm. The proton chemical shift of the methoxy group on the C-ring of **6** and **7** is observed at 4.25 ppm, which is also somewhat downfield to the usual shift values on the A- and B-rings.

Table 4: Retention times (TLC and HPLC) and spectral data (UV/Vis absorption) recorded for five common anthocyanidins compared to erlangidin.

Aglycone	R_f TLC (FHW*)	t_R HPLC (min)	λ_{max} (nm)	$A_{440}/A_{\text{vis-max}}$ (%)
Delphinidin	0.13	18.2	532	25
Cyanidin	0.23	23.7	525	25
Petunidin	0.20	24.9	534	20
Erlangidin	0.42	28.5	525	27
Peonidin	0.34	33.2	526	26
Malvidin	0.30	33.8	533	24

* See section 2.3.5 Thin layer chromatography for description

3.3.2 Anthocyanins from blue potatoes

Potatoes belong to the family *Solanaceae*, containing many species well known to produce anthocyanins, including flowers of *Petunia* (Slimestad et al., 1999, Ando et al., 1999), eggplant and violet peppers (*Solanum melongena* L., *Solanum annuum* L.) (Sadilova et al., 2006) and purple potatoes (*Solanum tuberosum* L.) (Fossen et al., 2003b). The purple anthocyanins found in *Solanaceae* is mostly based on delphinidin, petunidin and malvidin (all substituted in positions 3' and 5' on the B-ring), and have often aromatic acylation on the sugar moieties. These colourful potatoes have been suggested as a potential source for anthocyanins in food colouring (Rodriguez-Saona et al., 1998).

In this thesis, three cultivars of potato have been examined for anthocyanins. 'Blue Congo' is a cultivar used in Scandinavia in the last decades, and the main pigment is petanin, petunidin 3-*O*-[6''-*O*-(4'''-*O*-*E*-*p*-coumaroyl- α -rhamnopyranosyl)- β -glucopyranoside]-5-*O*- β -glucopyranoside (**8**) (Fossen and Andersen, 2000). A Norwegian cultivar was donated by a local enthusiast farmer who called it 'Snertingdal', but this name has not been described as a cultivar in the available literature on Norwegian potato cultivars. The tubers are oblong 5-6 cm long and 1-2 cm in diameter and both its skin and flesh is highly pigmented, and the main pigment is petanin (**8**), identified by on-line UV/Vis absorption spectroscopy from the analytical HPLC, and co-chromatography with **8** isolated from 'Blue Congo' potatoes. The last cultivar is 'Vitelotte', a French cultivar still widely used (Ombra et al., 2015), and the anthocyanins have previously been identified (Eichhorn and Winterhalter, 2005) with the main pigment being negretein, malvidin 3-*O*-[6-*O*-(4-*O*-*E*-*p*-coumaroyl- α -rhamnopyranosyl)- β -glucopyranoside]-5-*O*- β -glucopyranoside (**9**). Figure 25 presents the chromatograms of the three blue potato cultivars. The main pigments of 'Blue Congo' and 'Vitelotte' cultivars, **8** and **9** respectively, were isolated and identified using methods described in chapter 2.

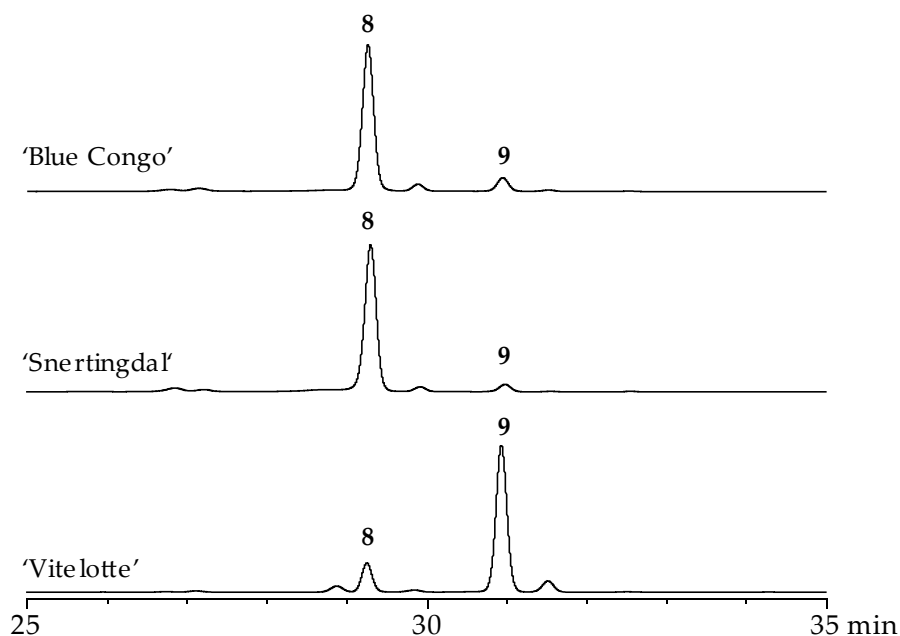
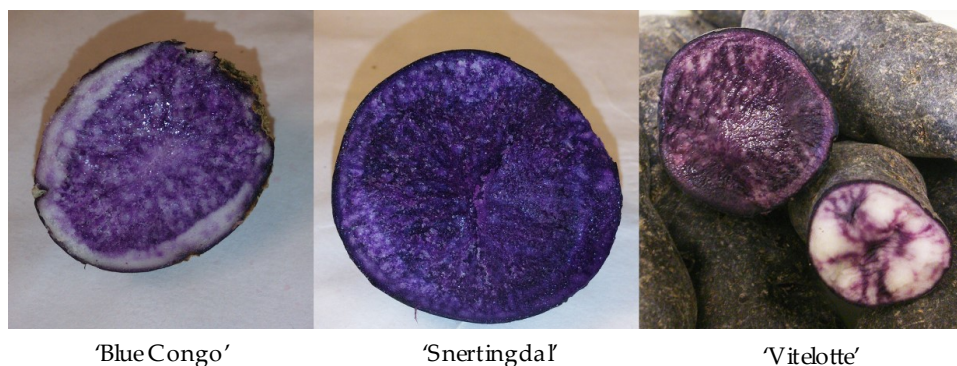


Figure 25: HPLC chromatogram sections of three cultivars of potato (*Solanum tuberosum* L.). Detected at 520 ± 20 nm.



Picture 4: Different cultivars of blue potatoes. Taken by the author.

3.3.3 Anthocyanins from 'Sun black'TM tomato (Papers IV and V)

Tomatoes (*Solanum lycopersicum* L.) also belong to the family *Solanaceae*, but production of anthocyanins is only seen in some cases of wild *Solanum* species (Gonzali et al., 2009). **Paper IV** and **Paper V** describes 'Sun Black', a trademarked tomato line owned by the University of Tuscia (see **Paper V** for details). This line is a new genotype

with a purple to black pigmentation in the epidermis, while the rest of the tomato have no extra pigmentation, and have been commercialised as at least one cultivar, 'Solenero'.

The main pigments of 'Sun Black' were identified as petanin (**8**) and negretein (**9**), using co-chromatography of extracts with pure samples of **8** and **9** isolated from blue potatoes (section 3.3.2). Quantification was done using a standard curve based on cyanidin 3-*O*-glucoside (**3**), calculated on a molar level. This calculation showed that the relative quantities of the identified pigments were 56.6 % and 21.4 % for **8** and **9** respectively (see Figure 27 for chromatogram). The remaining 20.0 % is unidentified at the time of writing.

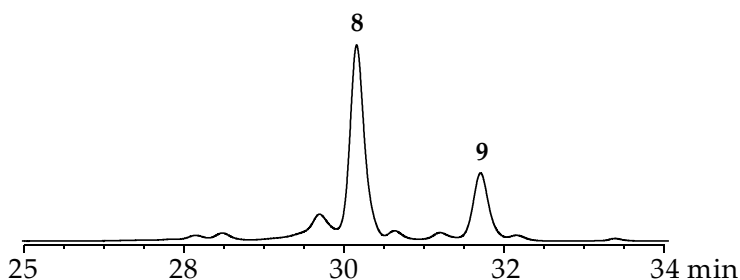


Figure 26: HPLC chromatogram section of 'Sun Black'™ tomato peel extract. Detected at 520 ± 20 nm.

4 Conclusions and future prospects

Two of the most primitive basal land plants living on the globe today is thought to be the closest relatives to the very first land plants. The main focus of this thesis has been to characterise the unique flavonoid pigments these plants produce. The auronidins **1** and **2** isolated from liverworts (*Marchantia polymorpha*) were previously thought to be anthocyanins, but **Paper I** show that their structure is not based on the structure of anthocyanins, but rather on that of aurones. These pigments have a charged aromatic ring similar to that of anthocyanins, which give them similar colour properties. They seem to be stable under weakly to neutral conditions, where anthocyanins are known to lose their colour and often degrade. Their biosynthesis has also been shown to be distinct from that of anthocyanins. In **Paper II**, Sphagnorubin C (**5**) was isolated from peat moss (*Sphagnum* sp.). With its extended aromatic ring system and lack of hydroxyl group in position 3, it seems to follow the network of transformations of anthocyanins. However, with DMSO as the solvent, no sign of the intermediate forms in the transformation between the flavylium cation form and the *trans*-chalcone form were detected. Additionally, the *trans*-chalcone form seems to be fully stable, and reversible back to the flavylium cation form by the addition of acid. This is the first full structural characterisation of a chalcone form of a naturally occurring anthocyanin.

Both these pigments from basal land plants have quite unique structures compared to anthocyanins, and they show stable and vibrant colours under acidic to neutral conditions. It is therefore reasonable to think that these compounds were nature's first attempts at making functional compounds with colour properties, that later in the evolution of land plants became the highly substituted and functional anthocyanins we know from vascular plants. Liverworts are considered the most recent common ancestor of algae and land plants, and its pigments was thought of the first attempt for nature at making anthocyanins. Now that we have shown that

auronidins are a distinct class of flavonoid pigments, Sphagnorubins from peat moss might be the most primitive of the anthocyanins.

This thesis additionally describes several new sources of anthocyanins. Anthocyanins with a unique anthocyanidin (erlangidin), with a 3-methoxyl substitution, was isolated from *Erlangea tomentosa* (**Paper III**). This aglycone show different spectroscopic and chromatographic properties compared to the common anthocyanidins. Additionally, the highly substituted anthocyanins petanin and negretein were isolated from several cultivars of blue potatoes. These pigments were also identified in the 'Sun Black' tomato (**Papers IV and V**), a line of tomatoes producing intense anthocyanin pigmentation in the epidermis, giving us a new nutraceutical source of anthocyanin intake.

Future prospects

There seems to be a great potential in pigments based on auronidin. They change colour from yellow to pink when dissolved in acidic to neutral solvents. Because of the charged pyrylium ring, analogue transformations to the anthocyanidin structure would be possible. This have recently been shown to occur in synthetic auronidin analogues (Alejo-Armijo et al., 2019a, Alejo-Armijo et al., 2019b, Alejo-Armijo et al., 2020). These studies are based on the pH jump method, and it would be interesting to study auronidin in the DMSO based solvent system used in this thesis, as this limits the availability of water.

It would be interesting to expand the DMSO based solvent system by including more anthocyanidin and anthocyanin structures. Sphagnorubin C only showed the flavylium cation and *trans*-chalcone forms in pure DMSO, and the *trans*-chalcone form was fully stable and reversible by the addition of acid. Results from similar studies on different anthocyanins, for instance 3-deoxyanthocyanidins like apigeninidin, common aglycones like peonidin, and highly functionalised anthocyanins like petanin, could help shed light on the exact mechanism for the degradation of anthocyanins.

Another expansion of the DMSO based solvent system would be to push the solvents into basic region using an appropriate base. Sphagnorubin C showed quinoidal forms in a very pure sample dissolved in pure DMSO that still transformed into the *trans*-chalcone form, and it would be interesting to see if a more basic solvent still would produce the *trans*-chalcone form over time. These studies could also include other anthocyanins, to continually further our understanding of the network of transformations of anthocyanins.

References

- Albert, N. W., et al. (2018) Genetic analysis of the liverwort *Marchantia polymorpha* reveals that R2R3MYB activation of flavonoid production in response to abiotic stress is an ancient character in land plants. *New Phytologist*, doi:<https://doi.org/10.1111/nph.15002>.
- Alejo-Armijo, A., et al. (2019a) Ground and excited state properties of furanoflavylium derivatives. *Physical Chemistry Chemical Physics*, 21 (38), p. 21651-21662, doi:<https://doi.org/10.1039/C9CP04917G>.
- Alejo-Armijo, A., et al. (2020) Chemical evolution of the colour systems generated by riccionidin A, 3-deoxyanthocyanidins and anthocyanins. *Phytochemistry*, 174, p. 112339, doi:<https://doi.org/10.1016/j.phytochem.2020.112339>.
- Alejo-Armijo, A., Parola, A. J. & Pina, F. (2019b) pH-Dependent Multistate System Generated by a Synthetic Furanoflavylium Compound: An Ancestor of the Anthocyanin Multistate of Chemical Species. *ACS Omega*, 4 (2), p. 4091-4100, doi:<https://doi.org/10.1021/acsomega.8b03696>.
- Andersen, Ø. M., et al. (2004) Anthocyanin from strawberry (*Fragaria ananassa*) with the novel aglycone, 5-carboxypyranopelargonidin. *Phytochemistry*, 65 (4), p. 405-10, doi:<https://doi.org/10.1016/j.phytochem.2003.10.014>.
- Andersen, Ø. M. & Francis, G. (2004) Techniques of pigment identification. In Davies, K. M. (ed.) *Plant pigments and their manipulation*. Victoria, Australia, Blackwell Publishing Ltd.
- Andersen, Ø. M., Helland, D. E. & Andersen, K. J. 1997. *Anthocyanidin and anthocyanidin derivatives, and their isolation, for treatment of cancer, diseases caused by lesions in connective tissues, and diseases caused by viruses*.

- Andersen, Ø. M. & Jordheim, M. (2006) The anthocyanins. In Andersen, Ø. M. & Markham, K. R. (eds.) *Flavonoids: chemistry, biochemistry and applications*. Boca Raton, USA, CRC Press/Taylor & Francis, p. 471-552.
- Andersen, Ø. M. & Jordheim, M. (2010) Chemistry of flavonoid-based colors in plants. In Andersen, Ø. M. & Markham, Kenneth R (eds.) *Comprehensive natural products II: Chemistry and biology*. Amsterdam, Netherlands, Elsevier Science, p. 547-614.
- Andersen, Ø. M. & Jordheim, M. (2013) Basic Anthocyanin Chemistry and Dietary Sources. In Wallace, T. C. & Giusti, M. M. (eds.) *Anthocyanins in health and disease*. Boca Raton, USA, CRC Press/Taylor & Francis, p. 13-90.
- Andersen, Ø. M., et al. (2010) Anthocyanins with unusual furanose sugar (apiose) from leaves of *Synadenium grantii* (Euphorbiaceae). *Phytochemistry*, 71 (13), p. 1558-63, doi:<https://doi.org/10.1016/j.phytochem.2010.05.025>.
- Andersen, Ø. M. & Markham, K. R. (2006) *Flavonoids: chemistry, biochemistry and applications*, Boca Raton, USA, CRC Press/Taylor & Francis.
- Ando, T., et al. (1999) Floral anthocyanins in wild taxa of *Petunia* (Solanaceae). *Biochemical Systematics and Ecology*, 27 (6), p. 623-650, doi:[https://doi.org/10.1016/S0305-1978\(98\)00080-5](https://doi.org/10.1016/S0305-1978(98)00080-5).
- Asiimwe, S., et al. (2014) Documentation and consensus of indigenous knowledge on medicinal plants used by the local communities of western Uganda. *Journal of Natural Product and Plant Resource*, 4 (1), p. 34-42.
- Auf'mkolk, M., et al. (1986) Inhibition of rat liver iodothyronine deiodinase. Interaction of aurones with the iodothyronine ligand-binding site. *Journal of Biological Chemistry*, 261 (25), p. 11623-30, doi:[https://doi.org/10.1016/S0021-9258\(18\)67288-6](https://doi.org/10.1016/S0021-9258(18)67288-6).
- Aura, A. M., et al. (2005) In vitro metabolism of anthocyanins by human gut microflora. *European Journal of Nutrition*, 44 (3), p. 133-42, doi:<https://doi.org/10.1007/s00394-004-0502-2>.
- Awika, J. M., Rooney, L. W. & Waniska, R. D. (2005) Anthocyanins from black sorghum and their antioxidant properties. *Food Chemistry*, 90 (1-2), p. 293-301, doi:<https://doi.org/10.1016/j.foodchem.2004.03.058>.
- Bae, R. N., et al. (2006) Anatomical observations of anthocyanin rich cells in apple skins. *Hortscience*, 41 (3), p. 733-736, doi:<https://doi.org/10.21273/HORTSCI.41.3.733>.
- Bakker, J., et al. (1997) Identification of an anthocyanin occurring in some red wines. *Phytochemistry*, 44 (7), p. 1375-1382, doi:[https://doi.org/10.1016/S0031-9422\(96\)00707-8](https://doi.org/10.1016/S0031-9422(96)00707-8).

- Bakker, J. & Timberlake, C. F. (1997) Isolation, identification, and characterization of new color-stable anthocyanins occurring in some red wines. *Journal of Agricultural and Food Chemistry*, 45 (1), p. 35-43, doi:<https://doi.org/10.1021/jf960252c>.
- Bate-Smith, E. C. & Geissman, T. A. (1951) Benzalcoumaranones. *Nature*, 167 (4252), p. 688-688, doi:<https://doi.org/10.1038/167688a0>.
- Bendz, G., et al. (1962) Moss Pigments. I. The Anthocyanins of *Bryum cryophilum* O. Mårt. *Acta Chemica Scandinavica*, 16 (5), p. 1183-1190.
- Berke, B., et al. (1998) Bisulfite addition to anthocyanins: revisited structures of colourless adducts. *Tetrahedron Letters*, 39 (32), p. 5771-5774, doi:[https://doi.org/10.1016/S0040-4039\(98\)01205-2](https://doi.org/10.1016/S0040-4039(98)01205-2).
- Boucherle, B., et al. (2017) Occurrences, biosynthesis and properties of auronones as high-end evolutionary products. *Phytochemistry*, 142 (Supplement C), p. 92-111, doi:<https://doi.org/10.1016/j.phytochem.2017.06.017>.
- Boumendjel, A. (2003) Auronones: a subclass of flavones with promising biological potential. *Current Medicinal Chemistry*, 10 (23), p. 2621-30, doi:<https://doi.org/10.2174/0929867033456468>.
- Bowman, J. L., et al. (2017) Insights into land plant evolution garnered from the *Marchantia polymorpha* genome. *Cell*, 171, p. 287-304.
- Bridle, P. & Timberlake, C. F. (1997) Anthocyanins as natural food colours - Selected aspects. *Food Chemistry*, 58 (1-2), p. 103-109, doi:[https://doi.org/10.1016/S0308-8146\(96\)00222-1](https://doi.org/10.1016/S0308-8146(96)00222-1).
- Brouillard, R. (1988) Flavonoids and flower colour. In Harborne, J. B. (ed.) *The Flavonoids*. Boston, USA, Springer US, p. 525-538.
- Brouillard, R. & Delaporte, B. (1977) Chemistry of anthocyanin pigments. 2. Kinetic and thermodynamic study of proton-transfer, hydration, and tautomeric reactions of malvidin 3-glucoside. *Journal of the American Chemical Society*, 99 (26), p. 8461-8468, doi:<https://doi.org/10.1021/ja00468a015>.
- Brouillard, R., et al. (1979) Chemistry of anthocyanin pigments. 4. Absorption spectrum of the chalcone form of malvidin 3-glucoside. *Journal de Chimie Physique*, 76, p. 273-276, doi:<https://doi.org/10.1051/JCP%2F1979760273>.
- Brouillard, R. & Dubois, J. E. (1977) Mechanism of the structural transformations of anthocyanins in acidic media. *Journal of the American Chemical Society*, 99 (5), p. 1359-1364, doi:<https://doi.org/10.1021/ja00447a012>.

- Brownmiller, C., Howard, L. R. & Prior, R. L. (2008) Processing and storage effects on monomeric anthocyanins, percent polymeric color, and antioxidant capacity of processed blueberry products. *Journal of Food Science*, 73 (5), doi:<https://doi.org/10.1111/j.1750-3841.2008.00761.x>.
- Brønnum-Hansen, K. & Hansen, S. H. (1983) High-performance liquid chromatographic separation of anthocyanins of *Sambucus nigra* L. *Journal of Chromatography A*, 262, p. 385-392, doi:[https://doi.org/10.1016/S0021-9673\(01\)88890-Z](https://doi.org/10.1016/S0021-9673(01)88890-Z).
- Buckingham, J. & Munasinghe, V. R. N. (2015) *Dictionary of Flavonoids with CD-ROM*, Boca Raton, USA, CRC Press/Taylor & Francis.
- Cabrita, L., Fossen, T. & Andersen, Ø. M. (2000) Colour and stability of the six common anthocyanidin 3-glucosides in aqueous solutions. *Food Chemistry*, 68 (1), p. 101-107, doi:[https://doi.org/10.1016/S0308-8146\(99\)00170-3](https://doi.org/10.1016/S0308-8146(99)00170-3).
- Cambridge Isotope Laboratories Inc. 2010. *NMR Solvent Data Chart* [Online]. Andover, MA. Available: http://www2.chem.umd.edu/nmr/reference/isotope_solvent.pdf [Accessed 17. oct 2017].
- Canter, P. H. & Ernst, E. (2004) Anthocyanosides of *Vaccinium myrtillus* (bilberry) for night vision—a systematic review of placebo-controlled trials. *Survey of ophthalmology*, 49 (1), p. 38-50, doi:<https://doi.org/10.1016/j.survophthal.2003.10.006>.
- Chalker-Scott, L. (1999) Environmental significance of anthocyanins in plant stress responses. *Photochemistry and Photobiology*, 70 (1), p. 1-9, doi:<https://doi.org/10.1111/j.1751-1097.1999.tb01944.x>.
- Cheminat, A. & Brouillard, R. (1986) PMR investigation of 3-O-(β-d-glucosyl)malvidin structural transformations in aqueous solutions. *Tetrahedron Letters*, 27 (37), p. 4457-4460, doi:[https://doi.org/10.1016/S0040-4039\(00\)84978-3](https://doi.org/10.1016/S0040-4039(00)84978-3).
- Clarke, L. J. & Robinson, S. A. (2008) Cell wall-bound ultraviolet-screening compounds explain the high ultraviolet tolerance of the Antarctic moss, *Ceratodon purpureus*. *New Phytologist*, 179 (3), p. 776-83, doi:<https://doi.org/10.1111/j.1469-8137.2008.02499.x>.
- Close, D. C. & Beadle, C. L. (2003) The ecophysiology of foliar anthocyanin. *Botanical Review*, 69 (2), p. 149-161.
- Conn, Simon, Zhang, Wei & Franco, Christopher (2003) Anthocyanic vacuolar inclusions (AVIs) selectively bind acylated anthocyanins in *Vitis vinifera* L. (grapevine) suspension culture. *Biotechnology Letters*, 25 (11), p. 835-839, doi:<https://doi.org/10.1023/A:1024028603089>.

- Cooper-Driver, G. A. (2001) Contributions of Jeffrey Harborne and co-workers to the study of anthocyanins. *Phytochemistry*, 56 (3), p. 229-36, doi:[https://doi.org/10.1016/S0031-9422\(00\)00455-6](https://doi.org/10.1016/S0031-9422(00)00455-6).
- Crowden, R. K. & Jarman, S. J. (1974) 3-Deoxyanthocyanins from the fern *Blechnum procerum*. *Phytochemistry*, 13 (9), p. 1947-1948, doi:[https://doi.org/10.1016/0031-9422\(74\)85122-8](https://doi.org/10.1016/0031-9422(74)85122-8).
- Czank, C., et al. (2013) Human metabolism and elimination of the anthocyanin, cyanidin-3-glucoside: a ¹³C-tracer study. *The American journal of clinical nutrition*, 97 (5), p. 995-1003, doi:<https://doi.org/10.3945/ajcn.112.049247>.
- Davies, K. M., et al. (2006) Characterisation of aurone biosynthesis in *Antirrhinum majus*. *Physiologia Plantarum*, 128 (4), p. 593-603, doi:<https://doi.org/10.1111/j.1399-3054.2006.00774.x>.
- de Freitas, V. & Mateus, N. (2011) Formation of pyranoanthocyanins in red wines: a new and diverse class of anthocyanin derivatives. *Analytical and Bioanalytical Chemistry*, 401 (5), p. 1463-73, doi:<https://doi.org/10.1007/s00216-010-4479-9>.
- Devia, B., et al. (2002) New 3-deoxyanthocyanidins from leaves of *Arrabidaea chica*. *Phytochemical Analysis*, 13 (2), p. 114-9, doi:<https://doi.org/10.1002/pca.632>.
- Eichhorn, S. & Winterhalter, P. (2005) Anthocyanins from pigmented potato (*Solanum tuberosum* L.) varieties. *Food Research International*, 38 (8), p. 943-948, doi:<https://doi.org/10.1016/j.foodres.2005.03.011>.
- Espinosa-Bustos, C., et al. (2017) Fluorescence properties of aurone derivatives: an experimental and theoretical study with some preliminary biological applications. *Photochemical & Photobiological Sciences*, 16 (8), p. 1268-1276, doi:<https://doi.org/10.1039/c7pp00078b>.
- Fang, J. (2014) Some anthocyanins could be efficiently absorbed across the gastrointestinal mucosa: extensive presystemic metabolism reduces apparent bioavailability. *Journal of Agricultural and Food Chemistry*, 62 (18), p. 3904-3911, doi:<https://doi.org/10.1021/jf405356b>.
- Farag, M. A., et al. (2009) Integrated metabolite and transcript profiling identify a biosynthetic mechanism for hispidol in *Medicago truncatula* cell cultures. *Plant Physiology*, 151 (3), p. 1096-1113, doi:<https://doi.org/10.1104/pp.109.141481>.
- Felgines, C., et al. (2003) Strawberry anthocyanins are recovered in urine as glucuro- and sulfoconjugates in humans. *Journal of Nutrition*, 133 (5), p. 1296-1301, doi:<https://doi.org/10.1093/jn/133.5.1296>.

REFERENCES

- Fernandes, A., et al. (2014a) Structural characterization of inclusion complexes between cyanidin-3-O-glucoside and β -cyclodextrin. *Carbohydrate Polymers*, 102, p. 269-277, doi:<https://doi.org/10.1016/j.carbpol.2013.11.037>.
- Fernandes, I., et al. (2014b) Bioavailability of anthocyanins and derivatives. *Journal of Functional Foods*, 7, p. 54-66, doi:<https://doi.org/10.1016/j.jff.2013.05.010>.
- Fleschhut, J., et al. (2006) Stability and biotransformation of various dietary anthocyanins in vitro. *European Journal of Nutrition*, 45 (1), p. 7-18, doi:<https://doi.org/10.1007/s00394-005-0557-8>.
- Fossen, T. & Andersen, Ø. M. (2000) Anthocyanins from tubers and shoots of the purple potato, *Solanum tuberosum*. *The Journal of Horticultural Science and Biotechnology*, 75 (3), p. 360-363, doi:<https://doi.org/10.1080/14620316.2000.11511251>.
- Fossen, T. & Andersen, Ø. M. (2003) Anthocyanins from red onion, *Allium cepa*, with novel aglycone. *Phytochemistry*, 62 (8), p. 1217-1220, doi:[https://doi.org/10.1016/S0031-9422\(02\)00746-X](https://doi.org/10.1016/S0031-9422(02)00746-X).
- Fossen, T., Cabrita, L. & Andersen, Ø. M. (1998) Colour and stability of pure anthocyanins influenced by pH including the alkaline region. *Food Chemistry*, 63 (4), p. 435-440, doi:[https://doi.org/10.1016/S0308-8146\(98\)00065-X](https://doi.org/10.1016/S0308-8146(98)00065-X).
- Fossen, T., Slimestad, R. & Andersen, Ø. M. (2001) Anthocyanins from maize (*Zea mays*) and reed canarygrass (*Phalaris arundinacea*). *Journal of Agricultural and Food Chemistry*, 49 (5), p. 2318-21, doi:<https://doi.org/10.1021/jf001399d>.
- Fossen, T., Slimestad, R. & Andersen, Ø. M. (2003a) Anthocyanins with 4'-glucosidation from red onion, *Allium cepa*. *Phytochemistry*, 64 (8), p. 1367-74, doi:<https://doi.org/10.1016/j.phytochem.2003.08.019>.
- Fossen, T., et al. (2003b) Anthocyanins from a Norwegian potato cultivar. *Food Chemistry*, 81 (3), p. 433-437, doi:[https://doi.org/10.1016/S0308-8146\(02\)00473-9](https://doi.org/10.1016/S0308-8146(02)00473-9).
- Francis, F. J. (1989) Food colorants: anthocyanins. *Critical Reviews in Food Science and Nutrition*, 28 (4), p. 273-314, doi:<https://doi.org/10.1080/10408398909527503>.
- Frøytlog, C., Slimestad, R. & Andersen, Ø. M. (1998) Combination of chromatographic techniques for the preparative isolation of anthocyanins – applied on blackcurrant (*Ribes nigrum*) fruits. *Journal of Chromatography A*, 825 (1), p. 89-95, doi:[https://doi.org/10.1016/S0021-9673\(98\)00673-6](https://doi.org/10.1016/S0021-9673(98)00673-6).
- Fukui, Y., et al. (2002) Structure of rosacyanin B, a novel pigment from the petals of *Rosa hybrida*. *Tetrahedron Letters*, 43 (14), p. 2637-2639, doi:[https://doi.org/10.1016/S0040-4039\(02\)00305-2](https://doi.org/10.1016/S0040-4039(02)00305-2).

- Fukui, Y., et al. (2006) Two novel blue pigments with ellagitannin moiety, rosacyanins A1 and A2, isolated from the petals of *Rosa hybrida*. *Tetrahedron*, 62 (41), p. 9661-9670, doi:<https://doi.org/10.1016/j.tet.2006.07.068>.
- Fulcrand, H., et al. (2006) Phenolic reactions during winemaking and aging. *American Journal of Enology and Viticulture*, 57 (3), p. 289-297.
- Geissman, T. A. & Heaton, C. D. (1943) Anthochlor Pigments. IV. The Pigments of *Coreopsis grandiflora*, Nutt. I. *Journal of the American Chemical Society*, 65 (4), p. 677-683, doi:<https://doi.org/10.1021/ja01244a050>.
- Ghosh, D. & Konishi, T. (2007) Anthocyanins and anthocyanin-rich extracts: role in diabetes and eye function. *Asia Pacific Journal of Clinical Nutrition*, 16 (2), p. 200-8.
- Giusti, M. M. & Wrolstad, R. E. (2003) Acylated anthocyanins from edible sources and their applications in food systems. *Biochemical Engineering Journal*, 14 (3), p. 217-225, doi:[https://doi.org/10.1016/S1369-703X\(02\)00221-8](https://doi.org/10.1016/S1369-703X(02)00221-8).
- Gonnet, J. F. (2003) Origin of the color of Cv. rhapsody in blue rose and some other so-called "blue" roses. *Journal of Agricultural and Food Chemistry*, 51 (17), p. 4990-4, doi:<https://doi.org/10.1021/jf0343276>.
- Gonzali, S., Mazzucato, A. & Perata, P. (2009) Purple as a tomato: towards high anthocyanin tomatoes. *Trends in Plant Science*, 14 (5), p. 237-241, doi:<https://doi.org/10.1016/j.tplants.2009.02.001>.
- Gould, K. S. (2004) Nature's swiss army knife: The diverse protective roles of anthocyanins in leaves. *Journal of Biomedicine and Biotechnology*, 2004 (5), p. 314-320, doi:<https://doi.org/10.1155/S1110724304406147>.
- Gras, C. C., et al. (2018) Effect of chlorogenic acid on spectral properties and stability of acylated and non-acylated cyanidin-3-O-glycosides. *Food Chemistry*, 240 (Supplement C), p. 940-950, doi:<https://doi.org/10.1016/j.foodchem.2017.07.137>.
- Gras, C. C., et al. (2017) Anthocyanins from purple sweet potato (*Ipomoea batatas* (L.) Lam.) and their color modulation by the addition of phenolic acids and food-grade phenolic plant extracts. *Food Chemistry*, 235 (Supplement C), p. 265-274, doi:<https://doi.org/10.1016/j.foodchem.2017.04.169>.
- Harborne, J. B. & Williams, C. A. (2000) Advances in flavonoid research since 1992. *Phytochemistry*, 55 (6), p. 481-504, doi:[https://doi.org/10.1016/S0031-9422\(00\)00235-1](https://doi.org/10.1016/S0031-9422(00)00235-1).
- Haudecoeur, R. & Boumendjel, A. (2012) Recent advances in the medicinal chemistry of aurones. *Current Medicinal Chemistry*, 19 (18), p. 2861-75, doi:<https://doi.org/10.2174/092986712800672085>.

- He, J. & Giusti, M. M. (2010) Anthocyanins: natural colorants with health-promoting properties. *Annual Review of Food Science and Technology*, 1, p. 163-87, doi:<https://doi.org/10.1146/annurev.food.080708.100754>.
- Hotson, J. W. (1921) Sphagnum used as a surgical dressing in germany during the world war. *The Bryologist*, 24 (5), p. 74-78, doi:<https://doi.org/10.2307/3238003>.
- Houbiers, C., et al. (1998) Color stabilization of malvidin 3-glucoside: self-aggregation of the flavylum cation and copigmentation with the Z-chalcone form. *The Journal of Physical Chemistry B*, 102 (18), p. 3578-3585, doi:<https://doi.org/10.1021/jp972320j>.
- Iacobucci, G. A. & Sweeny, J. G. (1983) The chemistry of anthocyanins, anthocyanidins and related flavylum salts. *Tetrahedron*, 39 (19), p. 3005-3038, doi:[https://doi.org/10.1016/S0040-4020\(01\)91542-X](https://doi.org/10.1016/S0040-4020(01)91542-X).
- Iriel, A. & Lagorio, M. G. (2010) Is the flower fluorescence relevant in biocommunication? *Naturwissenschaften*, 97 (10), p. 915-924, doi:<https://doi.org/10.1007/s00114-010-0709-4>.
- Iwashina, T. (2000) The structure and distribution of the flavonoids in plants. *Journal of Plant Research*, 113 (3), p. 287-299, doi:<https://doi.org/10.1007/PL00013940>.
- Jackman, R. L., et al. (1987) Anthocyanins as food colorants - a review. *Journal of Food Biochemistry*, 11 (3), p. 201-247, doi:<https://doi.org/10.1111/j.1745-4514.1987.tb00123.x>.
- Jordheim, M., Fossen, T. & Andersen, Ø. M. (2006a) Characterization of hemiacetal forms of anthocyanidin 3-O-β-glycopyranosides. *Journal of Agricultural and Food Chemistry*, 54 (25), p. 9340-9346, doi:<https://doi.org/10.1021/jf0619636>.
- Jordheim, M., Fossen, T. & Andersen, Ø. M. (2006b) Preparative isolation and NMR characterization of carboxypyrananthocyanins. *Journal of Agricultural and Food Chemistry*, 54 (10), p. 3572-3577, doi:<https://doi.org/10.1021/jf053240c>.
- Jordheim, M., et al. (2007) Reactivity of anthocyanins and pyrananthocyanins. Studies on aromatic hydrogen-deuterium exchange reactions in methanol. *Journal of Agricultural and Food Chemistry*, 55 (20), p. 8261-8, doi:<https://doi.org/10.1021/jf071132f>.
- Jurd, L. (1963) Anthocyanins and related compounds. I. Structural transformations of flavylum salts in acidic solutions. *The Journal of Organic Chemistry*, 28 (4), p. 987-991, doi:<https://doi.org/10.1021/jo01039a027>.
- Jurd, L. (1969) Anthocyanidins and related compounds—XV: The effects of sunlight on flavylum salt-chalcone equilibrium in acid solutions. *Tetrahedron*, 25 (11), p. 2367-2380, doi:[https://doi.org/10.1016/S0040-4020\(01\)82785-X](https://doi.org/10.1016/S0040-4020(01)82785-X).

- Jurd, L. & Geissman, T. A. (1963) Anthocyanins and related compounds. II. Structural transformations of some anhydro bases. *The Journal of Organic Chemistry*, 28 (9), p. 2394-2397, doi:<https://doi.org/10.1021/jo01044a060>.
- Kaintz, C., et al. (2014) Cloning and functional expression in *E. coli* of a polyphenol oxidase transcript from *Coreopsis grandiflora* involved in aurone formation. *FEBS Letters*, 588 (18), p. 3417-26, doi:<https://doi.org/10.1016/j.febslet.2014.07.034>.
- Kay, C. D. (2007) Aspects of anthocyanin absorption, metabolism and pharmacokinetics in humans. *Nutrition Research Reviews*, 19 (1), p. 137-146, doi:<https://doi.org/10.1079/NRR2005116>.
- Kay, C. D., Mazza, G. & Holub, B. J. (2005) Anthocyanins exist in the circulation primarily as metabolites in adult men. *Journal of Nutrition*, 135 (11), p. 2582-2588, doi:<https://doi.org/10.1093/jn/135.11.2582>.
- Kondo, T., et al. (1991) Structure of cyanodelphin, a tetra-*p*-hydroxybenzoated anthocyanin from blue flower of *Delphinium hybridum*. *Tetrahedron Letters*, 32 (44), p. 6375-6378, doi:[https://doi.org/10.1016/0040-4039\(91\)80173-4](https://doi.org/10.1016/0040-4039(91)80173-4).
- Kondo, T., et al. (1998) A new molecular mechanism of blue color development with protocyanin a supramolecular pigment from cornflower, *Centaurea cyanus*. *Tetrahedron Letters*, 39 (45), p. 8307-8310, doi:[https://doi.org/10.1016/S0040-4039\(98\)01858-9](https://doi.org/10.1016/S0040-4039(98)01858-9).
- Kondo, T., et al. (1992) Structural basis of blue-color development in flower petals from *Commelina communis*. *Nature*, 358 (6386), p. 515-518, doi:<https://doi.org/10.1038/358515a0>.
- Kumara, N. T. R. N., et al. (2015) Efficiency enhancement of Ixora floral dye sensitized solar cell by diminishing the pigments interactions. *Solar Energy*, 117 (Supplement C), p. 36-45, doi:<https://doi.org/10.1016/j.solener.2015.04.019>.
- Kunz, S. & Becker, H. (1995) Cell wall pigment formation of in vitro cultures of the liverwort *Ricciocarpos natans*. *Zeitschrift für Naturforschung C*.
- Kunz, S., Burkhardt, G. & Becker, H. (1993) Riccionidins a and b, anthocyanidins from the cell walls of the liverwort *Ricciocarpos natans*. *Phytochemistry*, 35 (1), p. 233-235, doi:[https://doi.org/10.1016/s0031-9422\(00\)90540-5](https://doi.org/10.1016/s0031-9422(00)90540-5).
- Lee, H. S. & Wicker, L. (1991) Anthocyanin pigments in the skin of lychee fruit. *Journal of Food Science*, 56 (2), p. 466-&, doi:<https://doi.org/10.1111/j.1365-2621.1991.tb05305.x>.

- Lila, M. A., et al. (2016) Unraveling anthocyanin bioavailability for human health. *Annual Review of Food Science and Technology*, 7, p. 375-393, doi:<https://doi.org/10.1146/annurev-food-041715-033346>.
- Liu, Y., et al. (2014) Stability and absorption of anthocyanins from blueberries subjected to a simulated digestion process. *International Journal of Food Sciences and Nutrition*, 65 (4), p. 440-8, doi:<https://doi.org/10.3109/09637486.2013.869798>.
- Lunau, K., Wacht, S. & Chittka, L. (1996) Colour choices of naive bumble bees and their implications for colour perception. *Journal of Comparative Physiology A*, 178 (4), p. 477-489, doi:<https://doi.org/10.1007/BF00190178>.
- Luo, Y., et al. (2014) Isolation, characterisation, and antioxidant activities of flavonoids from chufa (*Eleocharis tuberosa*) peels. *Food Chemistry*, 164, p. 30-5, doi:<https://doi.org/10.1016/j.foodchem.2014.04.103>.
- Macz-Pop, G. A., et al. (2006) Natural occurrence of free anthocyanin aglycones in beans (*Phaseolus vulgaris* L.). *Food Chemistry*, 94 (3), p. 448-456, doi:<https://doi.org/10.1016/j.foodchem.2004.11.038>.
- Manach, C., et al. (2005) Bioavailability and bioefficacy of polyphenols in humans. I. Review of 97 bioavailability studies. *The American Journal of Clinical Nutrition*, 81 (1 Suppl), p. 230S-242S, doi:<https://doi.org/10.1093/ajcn/81.1.230s>.
- Markham, K. R., et al. (2000) Anthocyanic vacuolar inclusions - their nature and significance in flower colouration. *Phytochemistry*, 55 (4), p. 327-336, doi:[https://doi.org/10.1016/S0031-9422\(00\)00246-6](https://doi.org/10.1016/S0031-9422(00)00246-6).
- Marquardt, C. (1835) *Die Farben der Blüten: Eine chemisch-physiolog. Abhandlung*, Bonn, Germany, T. Habicht.
- Matsumoto, H., et al. (2001) Orally administered delphinidin 3-rutinoside and cyanidin 3-rutinoside are directly absorbed in rats and humans and appear in the blood as the intact forms. *Journal of Agricultural and Food Chemistry*, 49 (3), p. 1546-1551, doi:<https://doi.org/10.1021/jf001246q>.
- McClelland, R. A. & Gedge, S. (1980) Hydration of the flavylum ion. *Journal of the American Chemical Society*, 102 (18), p. 5838-5848, doi:<https://doi.org/10.1021/ja00538a024>.
- McGhie, T. K., et al. (2003) Anthocyanin glycosides from berry fruit are absorbed and excreted unmetabolized by both humans and rats. *Journal of Agricultural and Food Chemistry*, 51 (16), p. 4539-4548, doi:<https://doi.org/10.1021/jf026206w>.

- McGhie, T. K. & Walton, M. C. (2007) The bioavailability and absorption of anthocyanins: towards a better understanding. *Molecular Nutrition & Food Research*, 51 (6), p. 702-13, doi:<https://doi.org/10.1002/mnfr.200700092>.
- Mentlein, R. & Vowinkel, E. (1984) Die roten wandfarbstoffe des torfmooses *Sphagnum rubellum*. *Liebigs Annalen der Chemie*, 1984 (5), p. 1024-1035, doi:<https://doi.org/10.1002/jlac.198419840520>.
- Morita, Y., et al. (2014) A chalcone isomerase-like protein enhances flavonoid production and flower pigmentation. *The Plant Journal*, 78 (2), p. 294-304, doi:<https://doi.org/10.1111/tpj.12469>.
- Murkovic, M., et al. (2001) Detection of anthocyanins from elderberry juice in human urine. *Journal of the Science of Food and Agriculture*, 81 (9), p. 934-937, doi:<https://doi.org/10.1002/jsfa.910>.
- Nagai, I. (1915) Ueber roten pigmentbildung bei einigen *Marchantia*-arten. *Shokubutsugaku Zasshi*, 29 (342), p. 90-98, doi:https://doi.org/10.15281/jplantres1887.29.342_90.
- Nakayama, T., et al. (2000) Aureusidin synthase: a polyphenol oxidase homolog responsible for flower coloration. *Science*, 290 (5494), p. 1163-6, doi:<https://doi.org/10.1126/science.290.5494.1163>.
- Nerdal, W. & Andersen, Ø. M. (1991) Evidence for self-association of the anthocyanin petanin in acidified, methanolic solution using two-dimensional nuclear overhauser enhancement NMR experiments and distance geometry calculations. *Phytochemical Analysis*, 2 (6), p. 263-270, doi:<https://doi.org/10.1002/pca.2800020606>.
- Newsham, K. K. (2010) The biology and ecology of the liverwort *Cephaloziella varians* in Antarctica. *Antarctic Science*, 22 (2), p. 131-143, doi:<https://doi.org/10.1017/S0954102009990630>.
- Nomi, Y., Iwasaki-Kurashige, K. & Matsumoto, H. (2019) Therapeutic effects of anthocyanins for vision and eye health. *Molecules*, 24 (18), p. 3311, doi:<https://doi.org/10.3390/molecules24183311>.
- Nozue, M., et al. (2003) VP24 found in anthocyanic vacuolar inclusions (AVIs) of sweet potato cells is a member of a metalloprotease family. *Biochemical Engineering Journal*, 14 (3), p. 199-205, doi:[https://doi.org/10.1016/S1369-703x\(02\)00223-1](https://doi.org/10.1016/S1369-703x(02)00223-1).
- Okada, Y., et al. (2014) Isolation and identification of flavonoids from *Coreopsis lanceolata* L. petals. *Natural Product Research*, 28 (3), p. 201-4, doi:<https://doi.org/10.1080/14786419.2013.856905>.

- Ombra, M. N., et al. (2015) In vitro antioxidant, antimicrobial and anti-proliferative activities of purple potato extracts (*Solanum tuberosum* Cv Vitelotte noire) following simulated gastro-intestinal digestion. *Natural Product Research*, 29 (11), p. 1087-91, doi:<https://doi.org/10.1080/14786419.2014.981183>.
- Osmani, S. A., et al. (2009) Effect of glucuronosylation on anthocyanin color stability. *Journal of Agricultural and Food Chemistry*, 57 (8), p. 3149-55, doi:<https://doi.org/10.1021/jf8034435>.
- Pare, P. W., Dmitrieva, N. & Mabry, T. J. (1991) Phytoalexin aurone Induced in *Cephalocereus senilis* liquid suspension culture. *Phytochemistry*, 30 (4), p. 1133-1135, doi:[https://doi.org/10.1016/S0031-9422\(00\)95189-6](https://doi.org/10.1016/S0031-9422(00)95189-6).
- Passamonti, S., Vrhovsek, U. & Mattivi, F. (2002) The interaction of anthocyanins with bilitranslocase. *Biochemical and Biophysical Research Communications*, 296 (3), p. 631-6, doi:[https://doi.org/10.1016/s0006-291x\(02\)00927-0](https://doi.org/10.1016/s0006-291x(02)00927-0).
- Passamonti, S., et al. (2005) Fast access of some grape pigments to the brain. *Journal of Agricultural and Food Chemistry*, 53 (18), p. 7029-7034, doi:<https://doi.org/10.1021/jf050565k>.
- Patras, A., et al. (2010) Effect of thermal processing on anthocyanin stability in foods; mechanisms and kinetics of degradation. *Trends in Food Science & Technology*, 21 (1), p. 3-11, doi:<https://doi.org/10.1016/j.tifs.2009.07.004>.
- Peckel, R. C. & Small, C. J. (1980) Occurrence, location and development of anthocyanoplasts. *Phytochemistry*, 19 (12), p. 2571-2576, doi:[https://doi.org/10.1016/S0031-9422\(00\)83921-7](https://doi.org/10.1016/S0031-9422(00)83921-7).
- Penny, J. H. J. (1983) Nectar guide color contrast - a possible relationship with pollination strategy. *New Phytologist*, 95 (4), p. 707-721, doi:<https://doi.org/10.1111/j.1469-8137.1983.tb03534.x>.
- Pietta, P. G. (2000) Flavonoids as antioxidants. *Journal of Natural Products*, 63 (7), p. 1035-1042, doi:<https://doi.org/10.1021/np9904509>.
- Pina, F. (1998) Thermodynamics and kinetics of flavylium salts Malvin revisited. *Journal of the Chemical Society, Faraday Transactions*, 94 (15), p. 2109-2116, doi:<https://doi.org/10.1039/A802602E>.
- Pina, F., et al. (2012) Chemistry and applications of flavylium compounds: a handful of colours. *Chemical Society Reviews*, 41 (2), p. 869-908, doi:<https://doi.org/10.1039/c1cs15126f>.

- Post, A. (1990) Photoprotective pigment as an adaptive strategy in the Antarctic moss *Ceratodon purpureus*. *Polar Biology*, 10 (4), p. 241-245, doi:<https://doi.org/10.1007/BF00238420>.
- Preston, N. W. & Timberlake, C. F. (1981) Separation of anthocyanin chalcones by high-performance liquid-chromatography. *Journal of Chromatography A*, 214 (2), p. 222-228, doi:[https://doi.org/10.1016/S0021-9673\(00\)98528-5](https://doi.org/10.1016/S0021-9673(00)98528-5).
- Prior, R. L., et al. (2008) Whole berries versus berry anthocyanins: interactions with dietary fat levels in the C57BL/6J mouse model of obesity. *Journal of Agricultural and Food Chemistry*, 56 (3), p. 647-53, doi:<https://doi.org/10.1021/jf071993o>.
- Qiu, Y. L., et al. (1998) The gain of three mitochondrial introns identifies liverworts as the earliest land plants. *Nature*, 394 (6694), p. 671-674, doi:<https://doi.org/10.1038/29286>.
- Renaud, S. & de Lorgeril, M. (1992) Wine, alcohol, platelets, and the French paradox for coronary heart disease. *Lancet*, 339 (8808), p. 1523-6, doi:[https://doi.org/10.1016/0140-6736\(92\)91277-f](https://doi.org/10.1016/0140-6736(92)91277-f).
- Rodriguez-Saona, L. E., Giusti, M. M. & Wrolstad, R. E. (1998) Anthocyanin pigment composition of red-fleshed potatoes. *Journal of Food Science*, 63 (3), p. 458-465, doi:<https://doi.org/10.1111/j.1365-2621.1998.tb15764.x>.
- Rossi, A., et al. (2003) Protective effects of anthocyanins from blackberry in a rat model of acute lung inflammation. *Free Radical Research*, 37 (8), p. 891-900, doi:<https://doi.org/10.1080/1071576031000112690>.
- Rudolph, H. (1964) Zur frage der membranochromie bei Sphagnen: I. Welche faktoren bestimmen den farbwechesl? *Flora oder Allgemeine Botanische Zeitung*, 155 (2), p. 250-293, doi:[https://doi.org/10.1016/S0367-1615\(17\)33360-8](https://doi.org/10.1016/S0367-1615(17)33360-8).
- Rudolph, H. & Vowinkel, E. (1969) Sphagnorubin, a crystalline membrane pigment from *Sphagnum magellanicum*. *Zeitschrift für Naturforschung B*, B 24 (9), p. 1211-&, doi:<https://doi.org/10.1515/znb-1969-0938>.
- Sadilova, E., Stintzing, F. C. & Carle, R. (2006) Anthocyanins, colour and antioxidant properties of eggplant (*Solanum melongena* L.) and violet pepper (*Capsicum annuum* L.) peel extracts. *Zeitschrift für Naturforschung C*, 61 (7-8), p. 527-35, doi:<https://doi.org/10.1515/znc-2006-7-810>.
- Saito, N., et al. (2003) The first isolation of C-glycosylanthocyanin from the flowers of *Tricyrtis formosana*. *Tetrahedron Letters*, 44 (36), p. 6821-6823, doi:[https://doi.org/10.1016/S0040-4039\(03\)01747-7](https://doi.org/10.1016/S0040-4039(03)01747-7).

- Saito, N., et al. (1995) Acylated cyanidin glycosides in the violet-blue flowers of *Ipomoea purpurea*. *Phytochemistry*, 40 (4), p. 1283-9, doi:[https://doi.org/10.1016/0031-9422\(95\)00369-I](https://doi.org/10.1016/0031-9422(95)00369-I).
- Santos, H., et al. (1993) Elucidation of the multiple equilibria of malvin in aqueous solution by one- and two-dimensional NMR. *Phytochemistry*, 33 (5), p. 1227-1232, doi:[https://doi.org/10.1016/0031-9422\(93\)85054-u](https://doi.org/10.1016/0031-9422(93)85054-u).
- Schwarz, M., Wray, V. & Winterhalter, P. (2004) Isolation and identification of novel pyranoanthocyanins from black carrot (*Daucus carota* L.) juice. *Journal of Agricultural and Food Chemistry*, 52 (16), p. 5095-5101, doi:<https://doi.org/10.1021/jf0495791>.
- Scotter, M. J. (2011) Methods for the determination of European Union-permitted added natural colours in foods: a review. *Food Addit Contam Part A Chem Anal Control Expo Risk Assess*, 28 (5), p. 527-96, doi:<https://doi.org/10.1080/19440049.2011.555844>.
- Seeram, N. P., et al. (2001) Cyclooxygenase inhibitory and antioxidant cyanidin glycosides in cherries and berries. *Phytomedicine*, 8 (5), p. 362-9, doi:<https://doi.org/10.1078/0944-7113-00053>.
- Shanker, N., et al. (2011) Aurones: small molecule visible range fluorescent probes suitable for biomacromolecules. *Journal of Fluorescence*, 21 (6), p. 2173-84, doi:<https://doi.org/10.1007/s10895-011-0919-y>.
- Shih, C. H., et al. (2007) Quantitative analysis of anticancer 3-deoxyanthocyanidins in infected sorghum seedlings. *Journal of Agricultural and Food Chemistry*, 55 (2), p. 254-9, doi:<https://doi.org/10.1021/jf062516t>.
- Shih, P. H., et al. (2011) Protective effects of anthocyanins against amyloid beta-peptide-induced damage in neuro-2A cells. *Journal of Agricultural and Food Chemistry*, 59 (5), p. 1683-9, doi:<https://doi.org/10.1021/jf103822h>.
- Shimokoriyama, M. & Hattori, S. (1953) On a probable enzymatic conversion of hydroxychalcone glycoside into hydroxybenzalcoumaranone glycoside. *Journal of the American Chemical Society*, 75 (9), p. 2277-2277, doi:<https://doi.org/10.1021/ja01105a532>.
- Sigurdson, G. T., et al. (2017) Effects of hydroxycinnamic acids on blue color expression of cyanidin derivatives and their metal chelates. *Food Chemistry*, 234 (Supplement C), p. 131-138, doi:<https://doi.org/10.1016/j.foodchem.2017.04.127>.
- Simmonds, M. S. J. (2003) Flavonoid-insect interactions: recent advances in our knowledge. *Phytochemistry*, 64 (1), p. 21-30, doi:[https://doi.org/10.1016/S0031-9422\(03\)00293-0](https://doi.org/10.1016/S0031-9422(03)00293-0).

- Skaar, I., et al. (2012) New anthocyanidin and anthocyanin pigments from blue plumbago. *Journal of Agricultural and Food Chemistry*, 60 (6), p. 1510-5, doi:<https://doi.org/10.1021/jf2048004>.
- Slimestad, R., Aaberg, A. & Andersen, Ø. M. (1999) Acylated anthocyanins from petunia flowers. *Phytochemistry*, 50 (6), p. 1081-1086, doi:[https://doi.org/10.1016/S0031-9422\(98\)00647-5](https://doi.org/10.1016/S0031-9422(98)00647-5).
- Snell, K. R. S., Convey, P. & Newsham, K. K. (2007) Metabolic recovery of the Antarctic liverwort *Cephaloziella varians* during spring snowmelt. *Polar Biology*, 30 (9), p. 1115-1122, doi:<https://doi.org/10.1007/s00300-007-0269-z>.
- Snell, K. R. S., et al. (2009) Quantifying the metabolic cost to an Antarctic liverwort of responding to an abrupt increase in UVB radiation exposure. *Global Change Biology*, 15 (11), p. 2563-2573, doi:<https://doi.org/10.1111/j.1365-2486.2009.01929.x>.
- Sondheimer, E. (1953) On the relation between spectral changes and pH of the anthocyanin pelargonidin 3-monoglucoside. *Journal of the American Chemical Society*, 75 (6), p. 1507-1508, doi:<https://doi.org/10.1021/ja01102a528>.
- Sousa, M. M., et al. (2008) Flavylum chromophores as species markers for dragon's blood resins from *Dracaena* and *Daemonorops* trees. *Journal of Chromatography A*, 1209 (1-2), p. 153-61, doi:<https://doi.org/10.1016/j.chroma.2008.09.007>.
- Strack, D. & Wray, V. (1994) The anthocyanins. In Harborne, J. B. (ed.) *The Flavonoids*. Boston, USA, Springer US, p. 1-22.
- Sutton, C. L., et al. (2017) Antifungal activity of substituted aurones. *Bioorganic & Medicinal Chemistry Letters*, 27 (4), p. 901-903, doi:<https://doi.org/10.1016/j.bmcl.2017.01.012>.
- Takeda, K., et al. (1994) A blue pigment complex in flowers of *Salvia patens*. *Phytochemistry*, 35 (5), p. 1167-1169, doi:[https://doi.org/10.1016/S0031-9422\(00\)94815-5](https://doi.org/10.1016/S0031-9422(00)94815-5).
- Talavera, S., et al. (2003) Anthocyanins are efficiently absorbed from the stomach in anesthetized rats. *Journal of Nutrition*, 133 (12), p. 4178-4182, doi:<https://doi.org/10.1093/jn/133.12.4178>.
- Tatsuzawa, F., et al. (2004) Diacylated 8-C-glucosylcyanidin 3-glucoside from the flowers of *Tricyrtis formosana*. *Chemical and Pharmaceutical Bulletin*, 52 (5), p. 631-3, doi:<https://doi.org/10.1248/cpb.52.631>.
- Terahara, N., et al. (1990) Acylated anthocyanins of *Clitoria ternatea* Flowers and their acyl moieties. *Phytochemistry*, 29 (3), p. 949-953, doi:[https://doi.org/10.1016/0031-9422\(90\)80053-J](https://doi.org/10.1016/0031-9422(90)80053-J).

- Toki, K., et al. (2008) 7-O-Methylated anthocyanidin glycosides from *Catharanthus roseus*. *Phytochemistry*, 69 (5), p. 1215-9, doi:<https://doi.org/10.1016/j.phytochem.2007.11.005>.
- Torskangerpoll, K. & Andersen, Ø. M. (2005) Colour stability of anthocyanins in aqueous solutions at various pH values. *Food Chemistry*, 89 (3), p. 427-440, doi:<https://doi.org/10.1016/j.foodchem.2004.03.002>.
- Tsuda, T. (2008) Regulation of adipocyte function by anthocyanins; possibility of preventing the metabolic syndrome. *Journal of Agricultural and Food Chemistry*, 56 (3), p. 642-6, doi:<https://doi.org/10.1021/jf073113b>.
- Tsuda, T. (2012) Dietary anthocyanin-rich plants: biochemical basis and recent progress in health benefits studies. *Molecular Nutrition & Food Research*, 56 (1), p. 159-70, doi:<https://doi.org/10.1002/mnfr.201100526>.
- Veitch, N. C. & Grayer, R. J. (2006) Chalcones, dihydrochalcones, and aurones. In Andersen, Ø. M. & Markham, K. R. (eds.) *Flavonoids: chemistry, biochemistry and applications*. Boca Raton, USA, CRC Press/Taylor & Francis, p. 1003-1100.
- Vowinkel, E. (1975) Torfmoosmembranochrome, 2. Die struktur des Sphagnorubins. *Chemische Berichte*, 108 (4), p. 1166-1181, doi:<https://doi.org/10.1002/cber.19751080423>.
- Wallace, T. C. (2011) Anthocyanins in cardiovascular disease. *Advances in Nutrition*, 2 (1), p. 1-7, doi:<https://doi.org/10.3945/an.110.000042>.
- Wang, H., Cao, G. H. & Prior, R. L. (1997) Oxygen radical absorbing capacity of anthocyanins. *Journal of Agricultural and Food Chemistry*, 45 (2), p. 304-309, doi:<https://doi.org/10.1021/jf960421t>.
- Wang, H., et al. (1999) Antioxidant and antiinflammatory activities of anthocyanins and their aglycon, cyanidin, from tart cherries. *Journal of Natural Products*, 62 (2), p. 294-296, doi:<https://doi.org/10.1021/np980501m>.
- Wang, L. S. & Stoner, G. D. (2008) Anthocyanins and their role in cancer prevention. *Cancer Letters*, 269 (2), p. 281-290, doi:<https://doi.org/10.1016/j.canlet.2008.05.020>.
- Wrolstad, R. E. & Culver, C. A. (2012) Alternatives to those artificial FD&C food colorants. *Annual Review of Food Science and Technology*, 3, p. 59-77, doi:<https://doi.org/10.1146/annurev-food-022811-101118>.
- Ye, J., et al. (2010) Effect of purple sweet potato anthocyanins on beta-amyloid-mediated PC-12 cells death by inhibition of oxidative stress. *Neurochemical Research*, 35 (3), p. 357-65, doi:<https://doi.org/10.1007/s11064-009-0063-0>.

-
- Yoshida, K., et al. (2006) Ferric ions involved in the flower color development of the Himalayan blue poppy, *Meconopsis grandis*. *Phytochemistry*, 67 (10), p. 992-8, doi:<https://doi.org/10.1016/j.phytochem.2006.03.013>.
- Yoshida, K., Kondo, T. & Goto, T. (1992) Intramolecular stacking conformation of gentiodelphin, a diacylated anthocyanin from *Gentiana makinoi*. *Tetrahedron*, 48 (21), p. 4313-4326, doi:[https://doi.org/10.1016/S0040-4020\(01\)80442-7](https://doi.org/10.1016/S0040-4020(01)80442-7).
- Zhang, H. B., et al. (2006) New insight into the structures and formation of anthocyanic vacuolar inclusions in flower petals. *BMC Plant Biology*, 6 (1), p. 29, doi:<https://doi.org/10.1186/1471-2229-6-29>.
- Zhao, C. L., et al. (2017) Stability-increasing effects of anthocyanin glycosyl acylation. *Food Chemistry*, 214 (Supplement C), p. 119-128, doi:<https://doi.org/10.1016/j.foodchem.2016.07.073>.
- Zorn, B., et al. (2001) 3-Desoxyanthocyanidins from *Arrabidaea chica*. *Phytochemistry*, 56 (8), p. 831-5, doi:[https://doi.org/10.1016/S0031-9422\(01\)00038-3](https://doi.org/10.1016/S0031-9422(01)00038-3).

Appendix A: Tables of ^1H and ^{13}C NMR data

Appendix A-1: Pigments 1 and 2

^1H and ^{13}C NMR chemical shifts for auronidin 4-heohesperidoside (**1**) and its aglycone auronidin (**2**), isolated from transgenic plants of the liverwort *Marchantia polymorpha*. Recorded in 5 % *d*-TFA in *d*-MeOD (v/v) at 25 °C using 600 MHz and 850 MHz NMR instruments.

pos	1 (^1H)		2 (^1H)	
aglycone				
5	6.826	<i>d</i> 1.6	6.45	<i>d</i> 1.6
7	6.832	<i>d</i> 1.6	6.64	<i>d</i> 1.6
α	8.88		8.74	
3'	7.66		7.55	
6'	7.50		7.46	
4-O-glucosyl				
1''	5.49	<i>d</i> 7.5		
2''	3.86	<i>dd</i> 7.6, 9.1		
3''	3.69	<i>t</i> 9.1		
4''	3.52	<i>dd</i> 9.2, 9.7		
5''	3.60	<i>dd</i> 9.7, 6.2		
6''A	3.94	<i>m</i>		
6''B	3.75	<i>t</i> 8.0		
2''-O-rhamnoside				
1'''	5.42	<i>d</i> 1.8		
2'''	4.03	<i>m</i>		
3'''	3.63	<i>dd</i> 3.3, 9.4		
4'''	3.18	<i>t</i> 9.5		
5'''	3.60	<i>dd</i> 9.5, 6.2		
6'''	0.69	<i>d</i> 6.2		

pos	1 (¹³ C)	2 (¹³ C)
Auronidin		
2	145.94	146.72
3	158.13	159.06
4	157.34	159.51
5	101.61	100.70
6	171.99	172.43
7	94.56	92.43
8	165.67	165.79
9	102.38	101.34
α	129.61	127.65
1'	118.47	117.30
2'	152.56	151.37
3'	105.05	104.06
4'	158.26	156.93
5'	149.96	149.19
6'	112.73	112.67
4-O-glucosyl		
1''	101.46	
2''	81.64	
3''	77.82	
4''	71.25	
5''	78.61	
6''A	62.45	
6''B		
2''-O-rhamnoside		
1'''	103.26	
2'''	72.19	
3'''	72.12	
4'''	73.91	
5'''	70.49	
6'''	17.91	

Appendix A-2: Pigment 5

¹H and ¹³C NMR chemical shifts for Sphagnorubin C (5) isolated from peat moss (*Sphagnum* sp.). Recorded in 5 % *d*-TFA in *d*-MeOD (v/v), 5 % *d*-TFA in *d*-MeOD (v/v), and pure DMSO, at 25 °C using 600 MHz NMR.

pos flav	pos <i>t</i> -chal	MeOD+TFA flav	DMSO+TFA flav	DMSO flav	DMSO <i>t</i> -chal
		¹ H δ (ppm) J (Hz)	¹ H δ (ppm) J (Hz)	¹ H δ (ppm) J (Hz)	¹ H δ (ppm) J (Hz)
3	α	8.41 <i>d</i> 8.9	8.74 <i>d</i> 9.0	8.85 <i>d</i> 9.1	7.97 <i>d</i> 15.4
4	β	9.71 <i>d</i> 8.8	10.04 <i>d</i> 9.1	10.16 <i>s</i> (<i>b</i>)	8.34 <i>d</i> 15.4
5	10	8.47 <i>d</i> 8.8	8.72 <i>d</i> 9.0	8.85 <i>d</i> 9.1	7.87 <i>d</i> 9.2
6	9	8.09 <i>d</i> 8.8	8.20 <i>d</i> 8.9	8.34 <i>d</i> 8.9	7.67 <i>d</i> 9.2
7	8	7.35 <i>s</i>	7.47 <i>s</i>	7.60 <i>s</i>	7.18 <i>s</i>
10	5	9.01 <i>s</i>	9.05 <i>s</i>	9.17 <i>s</i>	8.89 <i>s</i>
12	3	7.86 <i>s</i>	8.13 <i>s</i>	8.26 <i>s</i>	6.90 <i>s</i>
2'	2'	8.00 <i>d</i> 1.2	8.09 <i>d</i> 2.2	8.21 <i>s</i> (<i>b</i>)	7.56 <i>d</i> 2.0
5'	5'	7.21 <i>d</i> 8.5	7.16 <i>d</i> 8.6	7.27 <i>d</i> 8.4	6.93 <i>d</i> 8.2
6'	6'	8.16 <i>dd</i> 1.4, 8.0	8.26 <i>dd</i> 2.2, 8.6	8.40 <i>dd</i> 2.1, 8.6	7.59 <i>dd</i> 2.0, 8.2
MeO-C3'	MeO-C3'	4.20 <i>s</i>	4.03 <i>s</i>	4.16 <i>s</i>	3.87 <i>s</i>
MeO-C11	MeO-C4	4.55 <i>s</i>	4.44 <i>s</i>	4.57 <i>s</i>	4.08 <i>s</i>

s: singlet, *d*: doublet, *dd*: doublet of doublets, *b*: broad, -: not detected

APPENDIX

Position flav	Position t-chal	MeOD+TFA flavylium	DMSO+TFA flavylium	DMSO flavylium	DMSO chalcone
		^{13}C δ (ppm)	^{13}C δ (ppm)	^{13}C δ (ppm)	^{13}C δ (ppm)
2	CO	170.47	168.98	-	187.78
3	α	113.26	113.28	111.82	123.38
4	β	147.74	148.17	147.31	136.88
4a	1	118.56	117.81	117.47	108.77
4b	10a	129.42	129.43	128.01	132.83
5	10	118.15	117.89	117.36	118.60
6	9	132.80	131.49	131.05	128.25
6a	8a	130.92	129.27	129.14	125.74
7	8	112.58	111.95	111.56	111.62
8	7	148.88	147.68	147.52	145.02
9	6	148.93	147.99	147.87	146.10
10	5	113.20	112.43	112.03	112.61
10a	4b	125.11	123.77	123.24	124.12
10b	4a	120.84	119.70	119.34	114.23
11	4	170.27	168.68	168.20	159.91
12	3	97.66	97.68	97.18	98.60
12a	2	159.25	158.35	157.71	156.38
1'	1'	121.17	120.15	-	130.09
2'	2'	112.09	112.18	111.64	111.35
3'	3'	150.18	148.92	148.81	147.69
4'	4'	157.20	155.39	155.49	151.31
5'	5'	118.13	116.83	116.57	115.08
6'	6'	126.46	125.46	125.12	122.84
MeO-C3'	MeO-C3'	56.74	56.49	56.04	55.56
MeO-C11	MeO-C4	58.10	58.15	57.71	55.61

Appendix A-3: Pigments 6 and 7

¹H and ¹³C NMR chemical shifts for erlangidin 5-*O*-(4-(*E*-caffeoyl)-6-(malonyl)-β-glucoside)-3'-*O*-(6-(3-(β-glucosyl)-*E*-caffeoyl)-β-glucoside) (6) and erlangidin 5-*O*-(6-(malonyl)-β-glucoside)-3'-*O*-(6-(3-(β-glucosyl)-*E*-caffeoyl)-β-glucoside) (7) isolated from pink-mauve flowers of *Erlangea tomentosa*. Recorded in 5 % *d*-TFA in *d*-MeOD (v/v) at 25 °C using 600 MHz NMR.

	6		7b		6	7b
	¹ H		¹ H		¹³ C	¹³ C
Erlangidin						
2					162.66	162.4
3					149.19	149.0
4	8.64	<i>s</i>	8.65	<i>d</i> 2.0	129.86	129.8
5					156.00	155.9
6	7.09	<i>d</i> 2.0	7.04	<i>d</i> 2.0	106.65	106.3
7					168.32	168.3
8	7.02	(<i>d</i>)	7.01	<i>dd</i> 2.0, 0.8	97.60	97.4
9					155.68	155.4
10					113.76	113.7
1'					121.24	121.3
2'	8.42	<i>d</i> 2.1	8.43	<i>d</i> 2.2	120.23	120.3
3'					146.89	146.6
4'					157.40	157.1
5'	7.27	<i>d</i> 8.8	7.27	<i>d</i> 8.9	118.90	118.7
6'	8.39	<i>dd</i> 8.8, 2.1	8.39	<i>dd</i> 8.8, 2.2	130.68	130.4
3-OMe	4.25	<i>s</i>	4.25	<i>s</i>	58.35	58.3
5-<i>O</i>-glucoside						
1''	5.35	<i>d</i> 7.8	5.27	<i>d</i> 7.7	102.47	102.5
2''	3.92	<i>dd</i> 9.2, 7.8	3.79	<i>m</i>	74.69	74.5
3''	4.00	<i>t</i> 9.2	3.59	<i>m</i>	75.32	77.5
4''	5.16	<i>dd</i> 9.9, 9.3	3.58	<i>dd</i> 9.8, 9.1	71.94	71.1
5''	4.22	<i>ddd</i> 9.9, 6.6, 3.3	3.94	<i>m</i>	73.90	75.9
6A''	4.44	<i>m</i>	4.70	<i>dd</i> 12.0, 2.0	64.78	65.4
6B''	4.44	<i>m</i>	4.50	<i>dd</i> 12.0, 7.0		
3'-<i>O</i>-glucoside						
1'''	5.16	<i>d</i> 7.6	5.15	<i>d</i> 7.7	102.15	102.0
2'''	3.74	<i>dd</i> 9.1, 7.7	3.72	<i>dd</i> 9.4, 7.7	74.47	74.4
3'''	3.68	<i>t</i> 9.0	3.69	<i>t</i> 8.6	77.56	78.6
4'''	3.49	<i>dd</i> 9.3, 8.9	3.49	<i>m</i>	72.68	72.7
5'''	3.93	<i>m</i>	3.93	<i>ddd</i> 9.6, 6.3, 2.0	76.07	75.9
6A'''	4.94	<i>dd</i> 11.7, 2.3	4.91	<i>dd</i> 11.9, 2.1	64.96	64.9
6B'''	4.32	<i>dd</i> 11.7, 9.6	4.34	<i>dd</i> 12.0, 7.0		
3''-<i>O</i>-glucosyl						

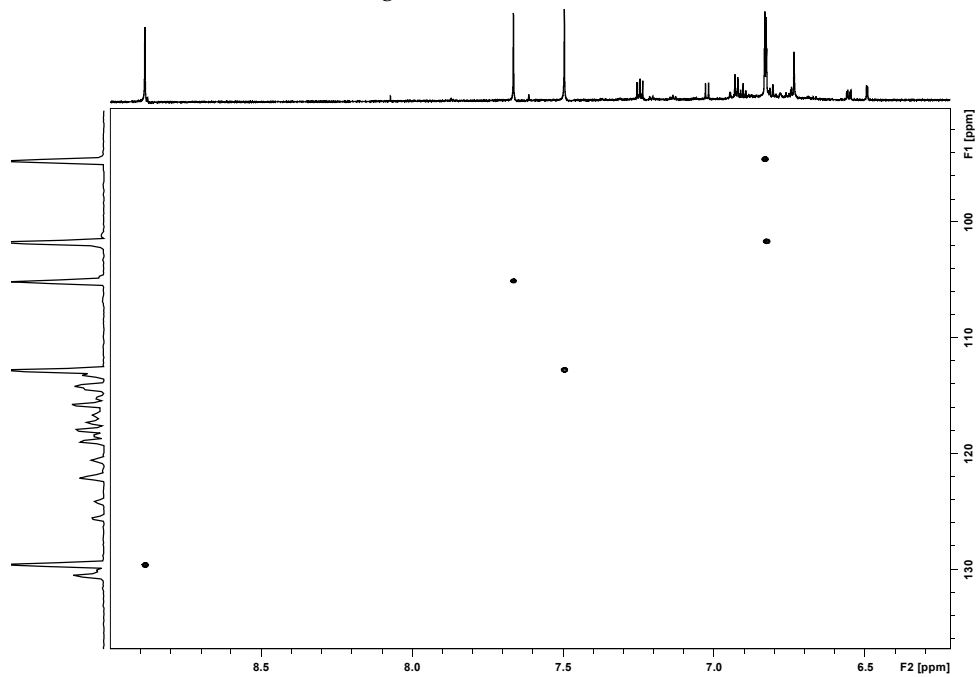
1 ^{'''}	4.69	<i>d</i> 7.6	4.63	<i>d</i> 7.5	103.86	103.8
2 ^{'''}	3.64	<i>dd</i> 9.2, 7.6	3.61	<i>m</i>	74.75	74.9
3 ^{'''}	3.63	<i>t</i> 9.2	3.60	<i>m</i>	77.61	77.4
4 ^{'''}	3.54	<i>dd</i> 9.3, 8.7	3.52	<i>m</i>	71.35	71.3
5 ^{'''}	3.39	<i>m</i>	3.36	<i>m</i>	78.63	78.3
6A ^{'''}	3.98	<i>dd</i> 11.6, 2.1	4.00	<i>dd</i> 11.9; 2.2	62.27	62.4
6B ^{'''}	3.81	<i>dd</i> 11.6, 5.6	3.80	<i>m</i>		
4''-O-caffeoyl						
1 ^I					127.66	
2 ^I	7.18	<i>d</i> 2.1			115.31	
3 ^I					146.85	
4 ^I					149.88	
5 ^I	6.89	<i>d</i> 8.1			116.53	
6 ^I	7.08	<i>dd</i> 8.1, 2.1			123.21	
α ^I	6.45	<i>d</i> 15.9			114.38	
β ^I	7.75	<i>d</i> 15.8			148.13	
COO ^I					168.18	
6'''-O-caffeoyl						
1 ^{II}					126.96	126.8
2 ^{II}	6.96	<i>d</i> 1.8	6.95	<i>d</i> 2.0	116.73	116.6
3 ^{II}					146.89	146.6
4 ^{II}					150.72	150.3
5 ^{II}	6.71	<i>d</i> 8.2	6.70	<i>d</i> 9.3	117.49	117.6
6 ^{II}	6.63	<i>dd</i> 8.2, 1.9	6.63	<i>m</i>	125.11	125.1
α ^{II}	6.10	<i>d</i> 15.9	6.10	<i>d</i> 15.9	115.99	115.9
β ^{II}	7.22	<i>d</i> 15.9	7.21	<i>d</i> 15.9	145.75	145.7
COO ^{II}					168.06	168.2
6''-O-malonyl						
1 ^{III}					168.40	168.9
2 ^{III}	3.58		3.61		41.65	41.4
3 ^{III}					170.25	170.3
1 ^{III} -OMe			3.79	<i>s</i>		52.9

*Weak signal or overlapped by other signals. *s* = singlet, *d* = doublet, *dd* = double doublet, *m* = multiplet. See Figure 23 for structures. The deuteriomethyl ¹³C signal and the residual ¹H signal of the solvent (deuterated methanol) were used as secondary references (δ 49.0 and 3.40 from TMS, respectively).

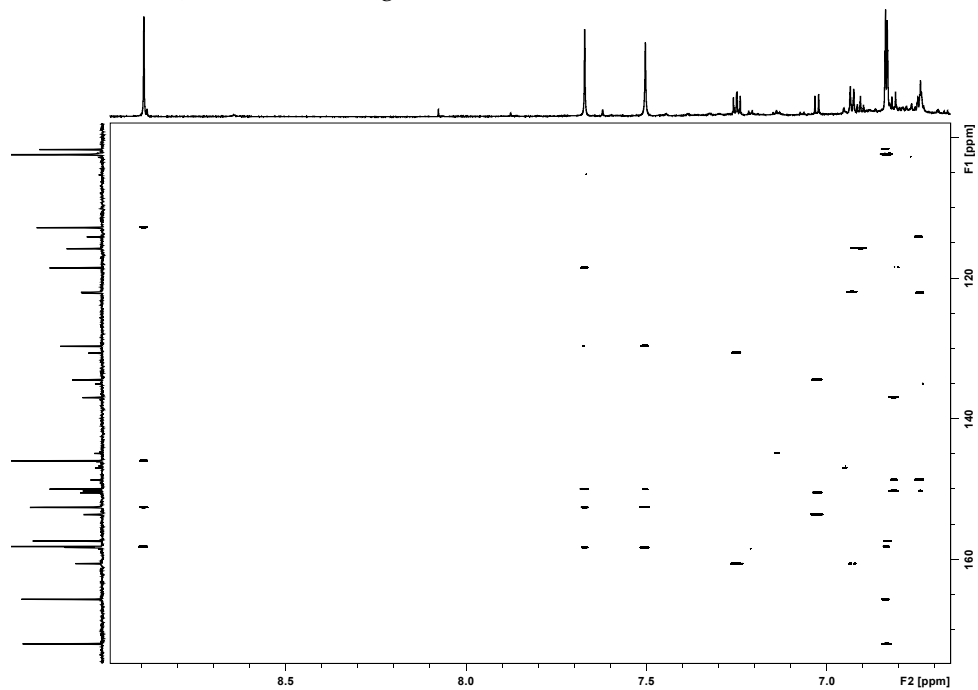
Appendix B: Figures of NMR spectra

Appendix B-1: Pigment 1

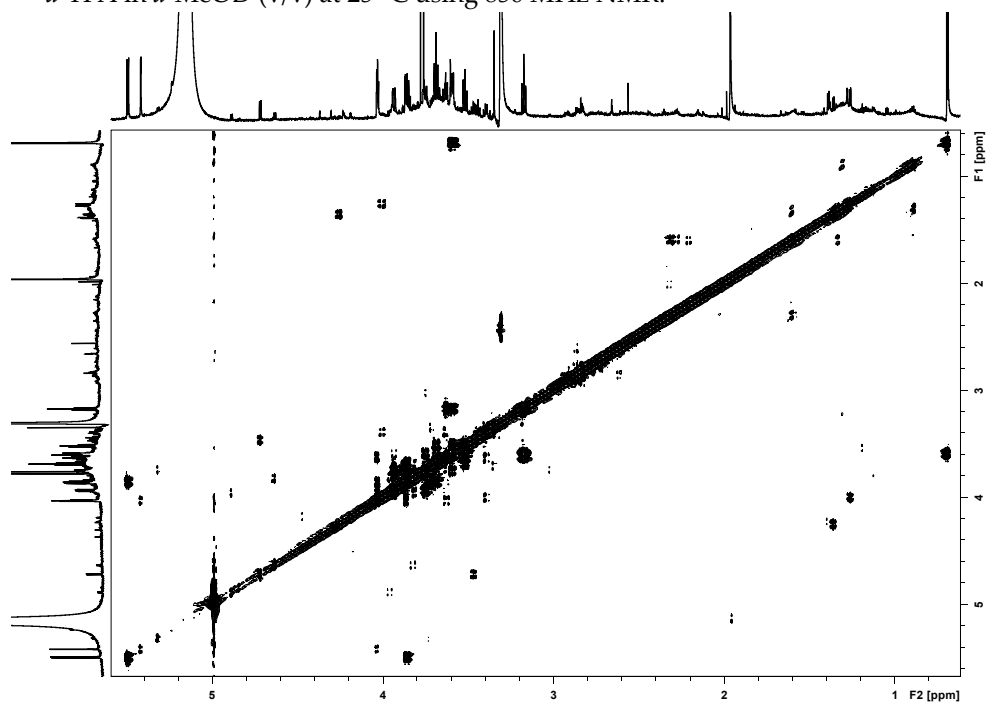
HSQC spectrum of auronidin 4-*O*-neohesperidoside (**1**). Recorded in 5 % *d*-TFA in *d*-MeOD (v/v) at 25 °C using 850 MHz NMR.



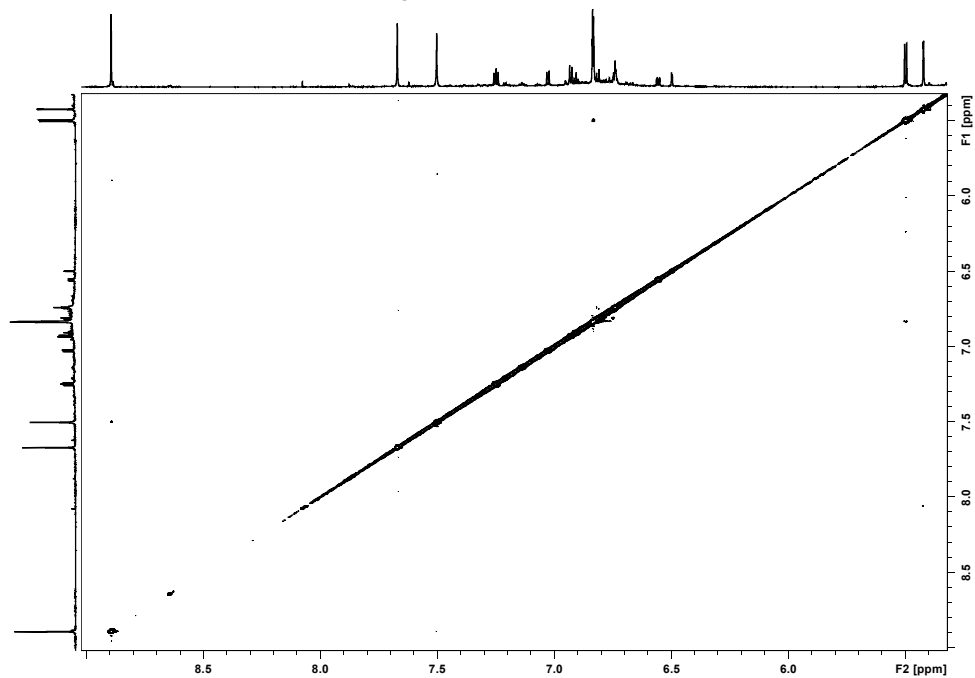
HMBC spectrum of auronidin 4-*O*-neohesperidoside (**1**). Recorded in 5 % *d*-TFA in *d*-MeOD (v/v) at 25 °C using 850 MHz NMR.



DQF-COSY spectrum of auronidin 4-*O*-neohesperidoside (**1**). Recorded in 5 % *d*-TFA in *d*-MeOD (v/v) at 25 °C using 850 MHz NMR.

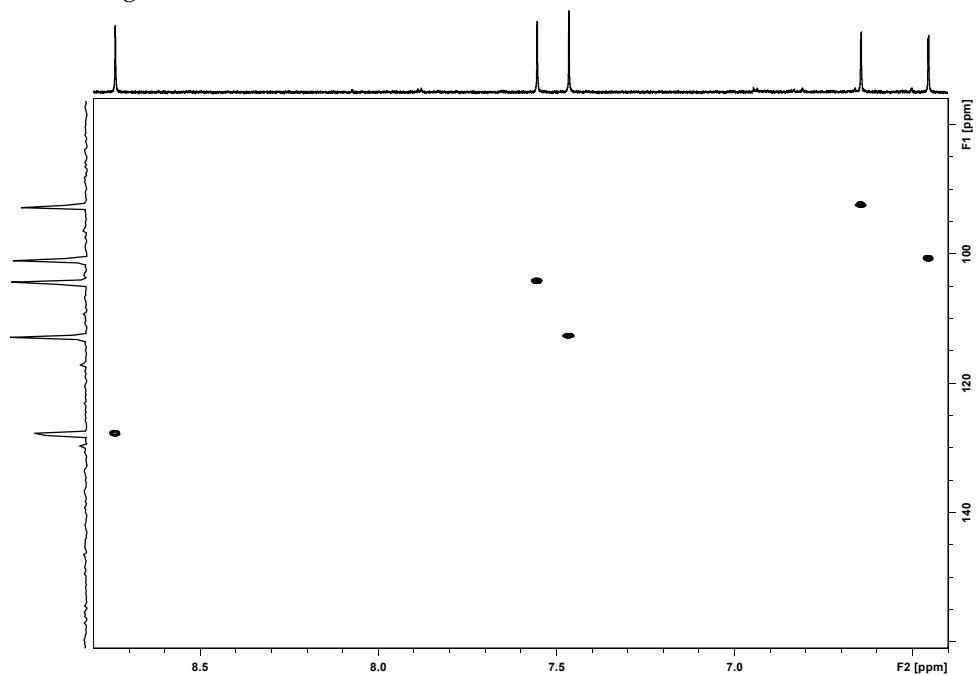


ROESY spectrum of auronidin 4-*O*-neohesperidoside (1). Recorded in 5 % *d*-TFA in *d*-MeOD (v/v) at 25 °C using 850 MHz NMR.

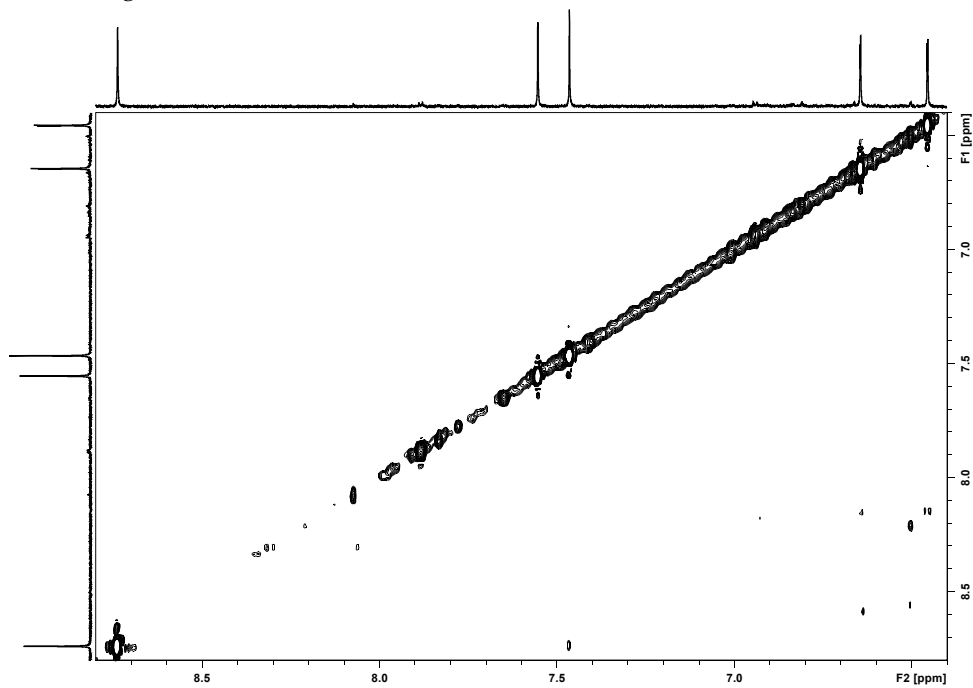


Appendix B-2: Pigment 2

HSQC spectrum of auronidin (2). Recorded in 5 % *d*-TFA in *d*-MeOD (v/v) at 25 °C using 850 MHz NMR.



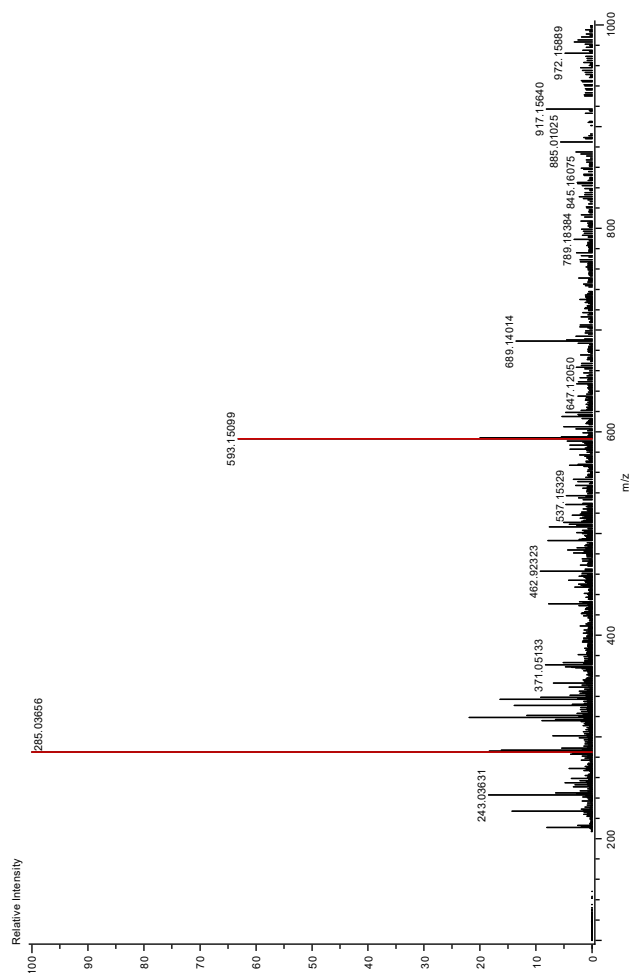
ROESY spectrum of auronidin (2) Recorded in 5 % *d*-TFA in *d*-MeOD (v/v) at 25 °C using 850 MHz NMR.



Appendix C: Figures of MS spectra

Appendix C-1: Pigment 1

High-resolution mass spectrum of auronidin 4-*O*-neohesperidoside (**1**).

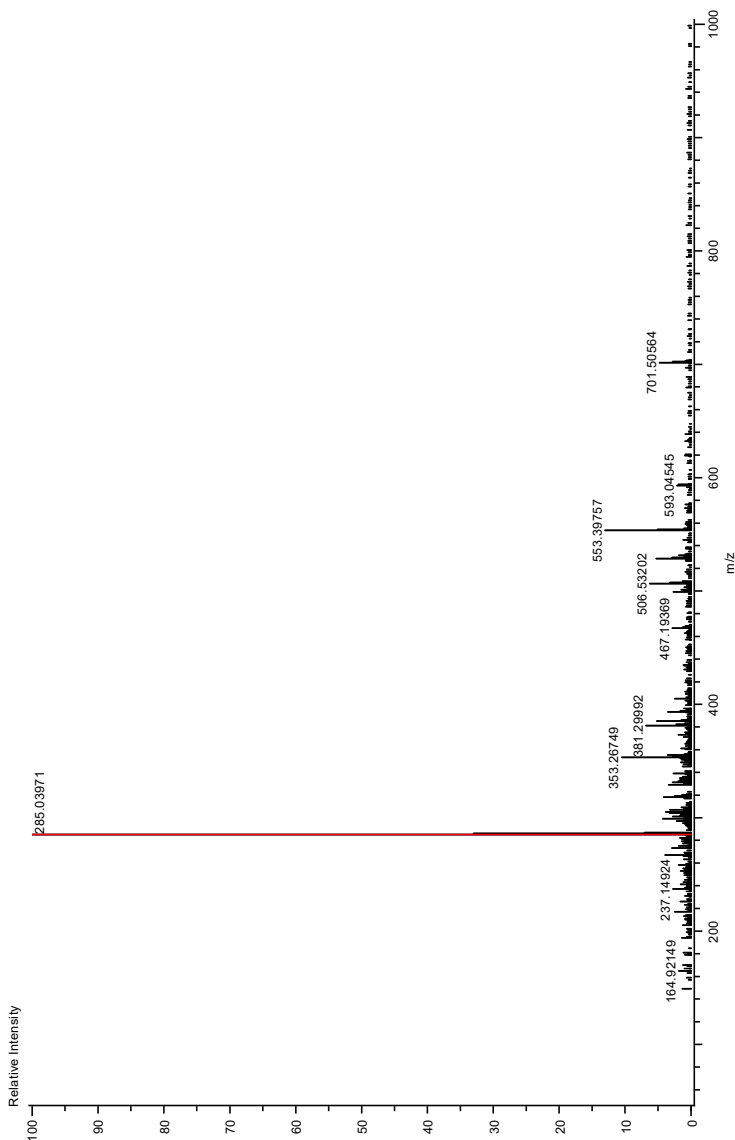


Needle Volt: 2499[V] Orifice1 Volt: 60V Orifice2 Volt: 10[V] Ring Lens Volt: 31[V] Desolvating Chamber Temp: 250[°C] Ion Guide RF Volt: 2500V Ion Guide Bias Volt: 28[V] Pusher Bias Volt: -0.78[V] Data Acquisition Interval: 1[ns] Flight Repetition Interval: 59[μs]
Spec. Record Interval: 0.70[s] Wait Time: 0.023[s] Detector Volt: 2350[V]

Mass	Intensity	Calc. Mass	Mass Difference (ppm)	Possible Formula	¹² C	¹ H	¹⁶ O	Unsaturation Number
285.03656	428954.23	285.03991	-3.35	¹² C ₁₅ ¹ H ₉ ¹⁶ O ₆	15	9	6	11.5
593.15099	270929.59	593.15064	0.34	¹² C ₂₇ ¹ H ₂₉ ¹⁶ O ₁₅	27	29	15	13.5

Appendix C-2: Pigment 2

High-resolution mass spectrum of auronidin (1).



Needle Volt: 2499[V], Orifice1 Volt: 40V, Orifice2 Volt: 10[V], Ring Lens Volt: 20[V] Desolvating Chamber Temp: 220[°C] Orifice1Temp: 120[°C], Ion Guide RF Volt: 1600V Ion Guide Bias Volt: 26[V] Detector Volt: 2350[V], MS Calibration Name: PEG_ESI+_1000 Data Acquisition Interval: 0.5[ns] Flight Repetition Interval: 59 [μs], Ionization Mode: ESI+ Charge number:1 Tolerance:5.00 (mmu)

Mass	Intensity	Calc. Mass	Mass Difference (ppm)	Possible Formula	¹² C	¹ H	¹⁶ O	Unsaturation Number
285.03971	39555.52	285.03991	-0.71	¹² C ₁₅ ¹ H ₉ ¹⁶ O ₆	15	9	6	11.5

Paper I

Auronidins are a previously unreported class of flavonoid pigments that challenges when anthocyanin biosynthesis evolved in plants

Helge Berland, Nick W. Albert, Anne Stavland, Monica Jordheim, Tony K. McGhie, Huaibi Zhang, Simon C. Deroles, Brian R. Jordan, Kevin M. Davis, Øyvind M. Andersen

Proceedings of the National Academy of Sciences (2019)



Auronidins are a previously unreported class of flavonoid pigments that challenges when anthocyanin biosynthesis evolved in plants

Helge Berland^a, Nick W. Albert^b, Anne Stavland^a, Monica Jordheim^a, Tony K. McGhie^b, Yanfei Zhou^b, Huaibi Zhang^b, Simon C. Derolles^b, Kathy E. Schwinn^b, Brian R. Jordan^c, Kevin M. Davies^{b,1}, and Øyvind M. Andersen^{a,1}

^aDepartment of Chemistry, University of Bergen, 5007 Bergen, Norway; ^bNew Zealand Institute for Plant and Food Research Limited, Palmerston North 4410, New Zealand; and ^cFaculty of Agriculture and Life Sciences, Lincoln University, Lincoln 7647, New Zealand

Edited by Richard A. Dixon, University of North Texas, Denton, TX, and approved August 23, 2019 (received for review July 24, 2019)

Anthocyanins are key pigments of plants, providing color to flowers, fruit, and foliage and helping to counter the harmful effects of environmental stresses. It is generally assumed that anthocyanin biosynthesis arose during the evolutionary transition of plants from aquatic to land environments. Liverworts, which may be the closest living relatives to the first land plants, have been reported to produce red cell wall-bound riccionidin pigments in response to stresses such as UV-B light, drought, and nutrient deprivation, and these have been proposed to correspond to the first anthocyanidins present in early land plant ancestors. Taking advantage of the liverwort model species *Marchantia polymorpha*, we show that the red pigments of *Marchantia* are formed by a phenylpropanoid biosynthetic branch distinct from that leading to anthocyanins. They constitute a previously unreported flavonoid class, for which we propose the name “auronidin,” with similar colors as anthocyanin but different chemistry, including strong fluorescence. Auronidins might contribute to the remarkable ability of liverworts to survive in extreme environments on land, and their discovery calls into question the possible pigment status of the first land plants.

anthocyanin | CRISPR | flavonoid | liverwort | *Marchantia*

The flavonoid pathway is thought to be unique to land plants. It is hypothesized to have arisen when plants were first colonizing the land, as an adaptation to cope with the additional abiotic stresses faced from a terrestrial lifestyle (1–4). Both seed plants and basal land plant groups produce a variety of flavonoid types, reflecting adaptations of the biosynthetic pathway during evolution to facilitate colonization of the wide range of environments that plants now occupy (2, 4, 5). However, although more than 8,000 individual flavonoid structures have been characterized (6), the great majority belong to a small number of major flavonoid classes. All land plants studied to date, including the liverworts, considered the probable basal plant group, produce nearly colorless, vacuolar-located flavone or flavonol glycosides, which absorb UV light and are important for ameliorating the damaging effects of UV-B radiation (1, 7–12). Seed plants also produce a variety of vacuolar-located anthocyanidin glycosides (anthocyanins) (13) that provide the majority of water-soluble plant colors, ranging from orange to blue.

Anthocyanins have various functions in plant–environment interactions; they aid pollination and seed dispersal through coloration of flowers and fruit and are also thought to help plants cope with different abiotic stresses (3, 14, 15). The flavonoid pigments of basal land plant groups have not been extensively characterized (16), but liverworts, in response to abiotic stresses, produce red nonglycosylated cell wall-bound riccionidin pigments that are proposed to be early evolved anthocyanidin forms (13, 17–19). The flavonoid biosynthetic pathway to flavones and flavonols, which is part of the larger phenylpropanoid pathway, appears to be conserved across land

plants (17, 20). Anthocyanins share the same initial biosynthetic steps as flavones/flavonols but require additional enzymatic steps that are well defined in seed plants but not in nonseed plants. It is assumed that the branches of the flavonoid biosynthetic pathway that lead to flavones/flavonols and anthocyanins arose during the evolutionary transition of plants from aquatic to land environments (1, 3, 7–9).

Regulation of flavonoid production has been extensively characterized in angiosperms, with R2R3MYB and bHLH family transcription factors found to be the key regulators (21–23). It was recently reported that an R2R3MYB transcription factor, *MpMYB14*, activates flavonoid biosynthesis in the model liverwort *Marchantia polymorpha* (17, 24). Transgenic *Marchantia* plants overexpressing *MYB14* under the *35SCaMV* gene promoter display strong activation of the flavonoid pathway (17, 24), yielding greatly increased amounts of flavone *O*-glycosides and a red pigment (2) assumed to be cell wall-bound riccionidin (18). Using the *Marchantia* model system (25), we show here that the red pigments are formed by a flavonoid biosynthetic branch distinct from that leading to anthocyanins and representing a previously unreported pigment class that raises questions about our current understanding of flavonoid pathway evolution.

Significance

Anthocyanins are flavonoid plant pigments that may be important for coping with environmental stresses, such as high light, drought, and nutrient deprivation. It has been thought that anthocyanin biosynthesis arose when land plants evolved approximately 450 million y ago, and extant basal plants groups, such as liverworts, have been reported to have “primitive” anthocyanins bound to their cell walls. However, here we report that the red pigments of the liverwort *Marchantia* are not anthocyanins, but rather a unique class of phenylpropanoids, for which we propose the name “auronidins.” Auronidins have similar colors as anthocyanins but distinct biosynthesis and color properties, and they may contribute to the remarkable ability of liverwort to survive in extreme environments.

Author contributions: H.B., N.W.A., M.J., S.C.D., B.R.J., K.M.D., and Ø.M.A. designed research; H.B., N.W.A., A.S., T.K.M., and Y.Z. performed research; H.B., N.W.A., A.S., M.J., Y.Z., H.Z., K.E.S., K.M.D., and Ø.M.A. analyzed data; and H.B., N.W.A., K.M.D., and Ø.M.A. wrote the paper.

The authors declare no conflict of interest.

This article is a PNAS Direct Submission.

Published under the PNAS license.

¹To whom correspondence may be addressed. Email: kevin.davies@plantandfood.co.nz or Oyvind.Andersen@uib.no.

This article contains supporting information online at www.pnas.org/lookup/suppl/doi:10.1073/pnas.1912741116/-DCSupplemental.

Results

In addition to the water-insoluble pigment bound to the cell wall, the *35S:MYB14 Marchantia* plants also produce a water-soluble reddish pigment (**1**) in considerable amounts, previously only barely detectable in wild-type (WT) plants (17). We took advantage of these transgenic plants to obtain sufficient quantities of the 2 pigments for isolation and full structural analysis. After preparation of pure compounds, their structures were determined to be 2,3,6,8-tetrahydroxybenzofuro[3,2-*b*]chromen-5-ium-6-*O*-(2-*O*- α -rhamnopyranosyl- β -glucopyranoside) (termed auronidin 4-neohesperidoside) (**1**) and its aglycone (**2**), using various 1D and 2D NMR experiments (Fig. 1 and *SI Appendix, Table S1*). The high-resolution electrospray ionization mass spectrum of **1** showed a molecular ion at m/z 593.15099 corresponding to the empirical formula $C_{27}H_{29}O_{15}^+$ (calc. 593.15064), in agreement with the predicted structure based on NMR. During the elucidation, we recognized that the 2 pigments represented a pigment class distinct from anthocyanidins but probably also derived from the flavonoid pathway. Therefore, we propose the term “auronidin” for this reddish class to reflect its structural resemblance to aurones and anthocyanidins and common color properties with anthocyanidins. Thus, these pigments are auronidin 4-*O*-neohesperidoside (**1**) and its aglycone,

auronidin (**2**). Accordingly, riccionidin A is not an anthocyanidin, although it has been previously characterized as such (17–19, 24).

The auronidin 4-glycoside (**1**) and its aglycone (**2**) have the basic structure of an aurone plus a pyrylium ring (D-ring) similar to the C-ring of the flavylium cationic form of anthocyanidins (Fig. 2A). The conjugation within these rings enables them to facilitate orange through red to magenta colors not far from the color nuances of many anthocyanins (Fig. 2B), in contrast to the more yellow colors (λ_{\max} 370 to 400 nm) reported for most aurones. However, we observed that the color palette expressed by auronidin 4-glycoside when exposed to different pH environments and solvents was based on various proportions of the auronidin and its anionic form in a simple acid-base equilibrium (Fig. 3A and B). This is in contrast to what is observed for anthocyanins, which display a similar but more extended color palette based on various proportions of individual structural forms (chalcones, hemiketals, flavylium, and quinoidal forms) with different colors. The auronidins can be added, alongside anthocyanins, as a flavonoid class that provides coloration to plants suitable for screening in the visible part of the light spectrum but based on distinct chemical expression. In addition, the auronidins **1** and **2** showed strong fluorescence (Fig. 3C and

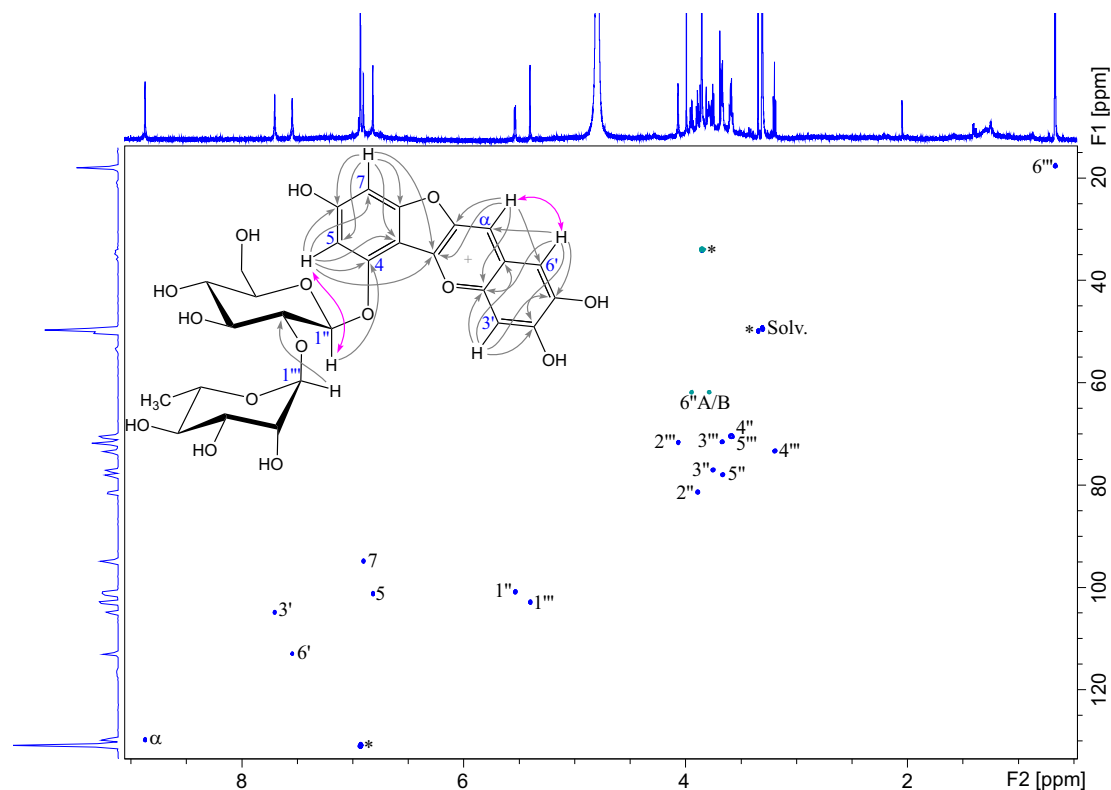


Fig. 1. Selected NMR information from various 1D and 2D NMR spectra used for structural elucidation of auronidin 4-neohesperidoside (**1**). The main annotated spectrum (^1H - ^{13}C heteronuclear single quantum coherence [HSQC]) shows $^1\text{J}_{\text{CH}}$ cross-peaks representing the carbon atoms, which are directly connected to hydrogen atoms. The gray arrows in the included structure show selected long-range ^1H -to- ^{13}C bonding correlations observed as cross-peaks in the heteronuclear multiple bond correlation spectrum, while the 2-sided pink arrows represent ^1H -to- ^1H through-space neighborships observed as cross-peaks in the rotating frame Overhauser spectroscopy spectrum. The ^1H NMR spectrum is shown on top and the ^{13}C projection of the HSQC spectrum on the left. Pigment **1** is dissolved in $\text{CD}_3\text{OD}-\text{CF}_3\text{CO}_2\text{D}$ (95:5, vol/vol), and the NMR spectra are recorded at 25 °C. *SI Appendix, Table S1* provides the chemical shift values for the proton and carbon atoms.

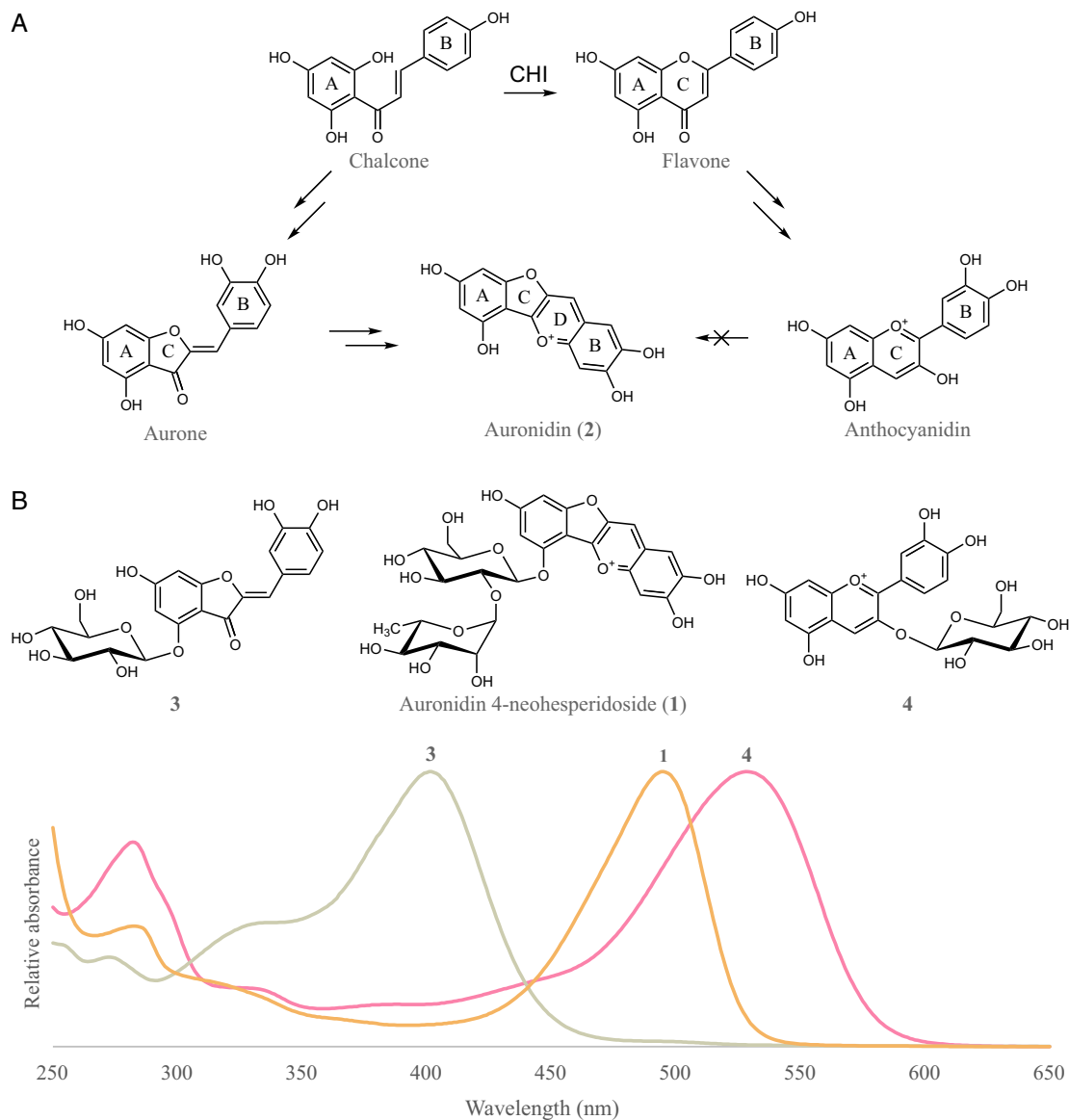


Fig. 2. Proposed biosynthetic relationships among aurones, auronidins, and anthocyanidins and comparison of the UV/visible-light spectra of corresponding glycosides. (A) *Marchantia* plants with a knockout mutation of the single *chi* gene showed no detectable flavones but were unaltered in auronidin production compared with WT plants. Plants with a knockout mutation of the candidate *ppo* aurone biosynthetic gene showed reduced auronidin content but were unaltered in flavone production. (B) Structures and corresponding UV/visible-light spectra recorded in acidified methanol of an aurone, aureusidin 4-glucoside (3) (λ_{\max} = 402 nm); an auronidin, auronidin 4-neohesperidoside (1) (λ_{\max} = 495 nm); and an anthocyanin, cyanidin 3-glucoside (4) (λ_{\max} = 529 nm).

D) at wavelengths that may provide opportunities for new chemistry-based practical applications, for example, as chemosensors in dye-sensitized solar cells (26) or in the base compound of a line of pharmaceutical derivatives (27).

We observed that the hydroxyl substitution pattern of riccionidin A (2) reported as an anthocyanidin (18) did not fit with the standard pattern of anthocyanidins, where the A-ring is derived from the acetate/malonate pathway and the B- and C-rings from

the shikimate/phenylalanine pathway. However, this pattern of hydroxyls would be obtained if ring closure occurred between the B- and C-rings of an aurone with 4,6,3',4'-hydroxylation (4,6,3',4'-tetrahydroxyaurone, termed aureusidin). In this case, the oxygenation pattern of the A-ring is in accordance with condensation of 3 acetate units, and the B-, C- and D-rings fit with the oxygenation pattern of their C₉ skeleton coming from the shikimate/phenylalanine pathway (Fig. 2A). *Marchantia* has

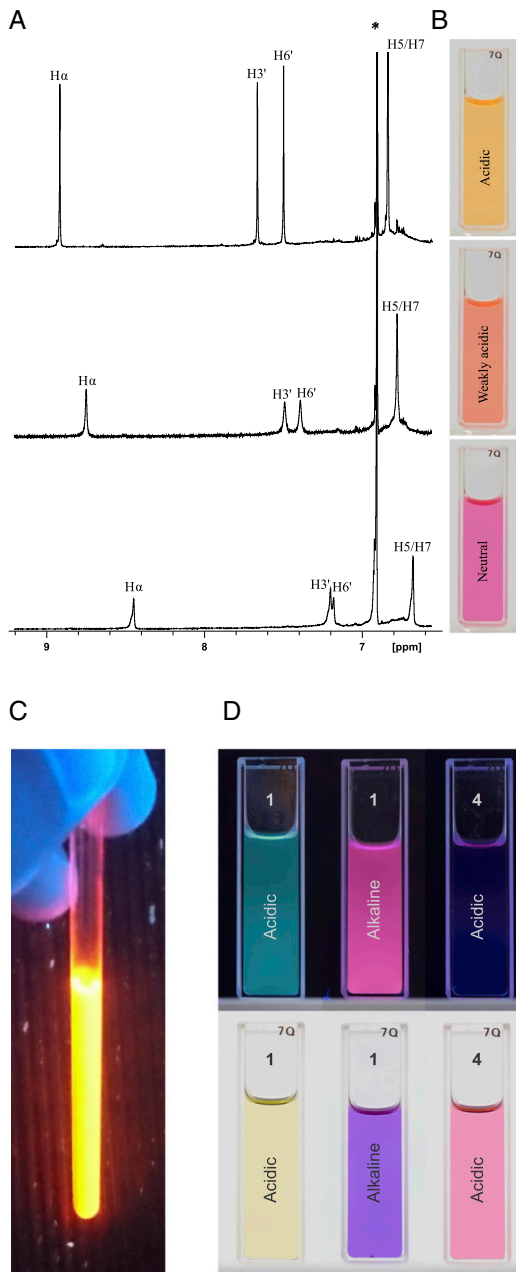


Fig. 3. ^1H NMR spectra, colors, and fluorescence of auronidin 4-neoheperidoside from *Marchantia* in solvents with different acidities, demonstrating lack of some typical anthocyanin properties. (A and B) Auronidin 4-neoheperidoside (1) dissolved in methanol containing various amounts of TFA. The aromatic regions of the corresponding ^1H NMR spectra (A) show that the color changes from orange to pink-purple (B) are in accordance with increased amounts of the anionic form of 1 in an acid-base equilibrium when the acid content is reduced. The lack of additional peaks in the NMR spectra prove the absence of various anthocyanin equilibrium forms expressing different colors. (C) Auronidin 4-

been shown to produce aureusidin 6-O-glucuronide during the reproductive phase (28) and thus possesses the biosynthetic route to the proposed substrate for auronidin formation. Thus, a biosynthetic route to 1 and 2 via aurones was theorized (Fig. 2A and *SI Appendix*, Fig. S1). In this case, the biosynthetic pathway to auronidins and anthocyanins is common through the early steps of the phenylpropanoid pathway (phenylalanine ammonia lyase [PAL], cinnamate 4-hydroxylase, and 4-coumaroyl CoA ligase) and the first steps of the flavonoid specific branch that result in the formation of chalcones (chalcone synthase [CHS] and chalcone isomerase-like [CHIL]). However, the pathways to each compound from chalcones then diverge. The enzyme chalcone isomerase (CHI) that conducts the second committed step of flavonoid biosynthesis is required for flavone and anthocyanin biosynthesis but not for the biosynthesis of aurones (*SI Appendix*, Fig. S1). Aurones are formed from chalcones by variant polyphenol oxidase (PPO) enzymes, with different types of PPOs, termed aureusidin synthase (AUS) and aurone synthase (AS), forming aurones in *Antirrhinum majus* and *Coreopsis grandiflora*, respectively (29–34). The AUS and AS conduct hydroxylation at the B-ring of chalcones, followed by oxidative cyclization into aurones, either before (CgAS) or after (*AmaUS*) glycosylation. The majority of PPOs characterized in angiosperms are localized to the plastid and exert an oxidative action on phenolic substrates that can lead to, for example, the browning that occurs during cell rupture (35). The CgAS has the characteristic N-terminal chloroplast transit peptide and thylakoid transfer domain and so might direct aurone biosynthesis in plastids (33, 34). However, the *AmaUS* lacks the plastid localization signal and is localized to the vacuole (32). As auronidins are a newly identified phenylpropanoid group, there is no information on the possible subsequent biosynthetic steps from aurones to the cell wall-bound or soluble glycosylated auronidin products.

Although a biosynthetic pathway to auronidins via aurones seemed probable, based on the shared structural characteristics with aurones and the characterized function of *MpMYB14* in activating flavonoid biosynthesis, alternative biosynthetic routes could not be excluded. Thus, RNA-seq differential gene expression analysis was conducted to identify candidate genes for auronidin biosynthesis. *Marchantia* produces auronidins when placed under nutrient deprivation stress, and this response is lost in the *myb14* mutant (17). RNA-seq comparisons of the gene expression response of WT and *myb14* plants under nutrient deprivation identified 260 differential genes with a cutoff of an adjusted P value <0.001 and a \log_2 fold increase >1.0 (Fig. 4A and *SI Appendix*, Table S2). Of these, 121 were up-regulated in WT but not *myb14* plants and thus included candidates for auronidin biosynthetic genes. Of the 20 up-regulated transcripts with lowest adjusted P values, 7 encoded known phenylpropanoid biosynthetic enzymes, including those corresponding to PAL (*Mapoly0005s0086*, *Mapoly0005s0088*, and *Mapoly0014s0211*), CHS (*Mapoly0021s0159*), and CHIL (*Mapoly0175s0004*). However, CHI (*Mapoly0167s0012*) was not 1 of these 260 genes, being up-regulated by only 0.5 \log_2 fold with an adjusted P value >0.001 and ranked at 1,627 out of 11,937 gene models on adjusted P value. In addition to the 7 transcript models for characterized phenylpropanoid biosynthetic enzymes, 4 others corresponded to candidates for additional auronidin biosynthetic or localization steps. These included a transcript for a PPO (*Mapoly0021s0041*), which had the lowest adjusted P value of any gene model (2.2×10^{-308}) and

neoesperidoside dissolved in deuterated dimethyl sulfoxide containing 5% TFA in 365-nm UV light. (D) Comparison of auronidin 4-neoheperidoside and the anthocyanin cyanidin 3-glucoside dissolved in methanol containing 0.5% TFA (acidic) or 0.5% 0.2 M NaOH (alkaline). The samples were illuminated by a 365-nm UV lamp (Top) or ambient light (Bottom). The anthocyanin in alkaline is not shown, as it degraded in that solvent.

one of the highest fold differences (8.5 log₂ fold, a baseMean change from 42 to 15,622 reads). To further resolve candidate auronidin biosynthetic genes, comparisons were made to genes up-regulated in 35S:MYB14 transgenics compared with unstressed WT plants, as the 35S:MYB14 *Marchantia* transgenics have greatly increased auronidin content (SI Appendix, Fig. S3). Applying the same adjusted *P* value <0.001 and log₂ fold increase >1.0 cutoff gave 160 transcripts as up-regulated in 35S:MYB14 transgenics (Fig. 4B). Twenty-two transcripts were common across the 2 pairwise comparisons, and 6 of these corresponded to candidate phenylpropanoid biosynthetic enzymes, including the PPO. The pattern of genes up-regulated by MYB14 thus supported a phenylpropanoid biosynthetic route to auronidins but not via chalcones, as *CHI* was not activated. The proposed route via aurones was supported by the strong and coordinated up-regulation of genes for PAL, CHS, CHIL, and a candidate AUS PPO.

To confirm that CHI was not required for auronidin biosynthesis, we analyzed *Marchantia* plants that have CRISPR/Cas9-based mutations in the *CHI* gene (9). Previous studies have identified *CHI* and *CHIL* as single-copy genes in *M. polymorpha* (9, 25). We confirmed this through BLAST analysis of the genome sequence, transcript assemblies of Bowman et al. (25), and our own de novo transcript assemblies based on RNA from the 35S:MYB14 transgenics. In phylogenetic analysis, the MpCHI and MpCHIL sequences fall into the well-characterized separate *CHI* and *CHIL* clades (SI Appendix, Fig. S2), with only 25.4% identity between the deduced amino acid sequences. *CHI* and *CHIL* sequences from *Marchantia paleacea*, termed MpalCHI1 and MpalCHI2, have been characterized for their encoded enzyme activities, with MpalCHI1 able to form flavanones from chalcones with a similar efficiency to *CHI* enzymes from angiosperms but MpalCHI2 lacking any flavanone biosynthetic activity (36). MpCHI and MpCHIL have 90.7% and 92.9% amino acid identity to MpalCHI1 and MpalCHI2, respectively. Wild-type *Marchantia* plants under nutrient deprivation stress produced both flavone *O*-glycosides and the red pigment auronidin (2) (Fig. 5). Plants with knockout mutations of the Mpchi gene produced no detectable flavones, confirming that the single MpCHI gene is required for production of flavanone-derived compounds such as flavones and anthocyanins (SI Appendix, Fig. S1). However, the *chi* mutants were unaltered in auronidin production (Fig. 5). As an additional visualization of the lack of requirement of CHI for auronidin biosynthesis, the *chi* line was crossed with a 35S:MYB14 transgenic line. The (haploid) F₁ lines containing the *chi* mutated allele and 35S:MYB14 transgene were visually indistinguishable from the 35S:MYB14 parental line, showing substantial overproduction of auronidin and deep purple pigmentation (SI Appendix, Fig. S3).

The *chi* mutant analysis confirmed that the auronidin biosynthetic branch differ from that of anthocyanins and does not require flavanone production. The differential gene expression suggested a flavonoid biosynthetic origin. This was tested by analysis of *Marchantia* plants with knockout mutations of the *chil* gene (9). *CHIL* function is unresolved, but mutant studies in *Arabidopsis* and *Ipomoea nil* show that it is generally required for efficient function of the early steps of the flavonoid pathway (37, 38) and may noncatalytically enhance chalcone formation and downstream conversion (39). The Mpchil lines had reduced content of both flavones and auronidin (Fig. 5), supporting a flavonoid origin for auronidins. In accordance with this, plants with a knockout of both the *chi* and *chil* genes, generated by crossing the individual mutant lines, contained almost no detectable flavonoids, with both flavones and auronidins reduced (Fig. 5).

The RNA-seq differential gene analysis identified the PPO gene *Mapoly0021s0041* as a candidate biosynthetic step for auronidins, potentially as an AUS/AS. To investigate this further, we analyzed the *Mapoly0021s0041* predicted amino acid sequence in the context of the *Marchantia* PPO gene family. We found 63 candidate

Marchantia PPO gene models (SI Appendix, Fig. S4), by far the largest PPO gene family identified for any plant species (35), despite the comparatively small number of gene models in the *Marchantia* genome sequence. *Mapoly0021s0041* contained an N-terminal extension, which may be a targeting peptide, and the conserved PPO catalytically active domain of ~40 kDa. However, it lacked the C-terminal domain of ~19 kDa that is thought to shield the active site until cleavage at the site of action. The N-terminal targeting peptide did not have the typical characteristics for plastid localization, with the highest prediction being for secretory. We used CRISPR/Cas9 (40) to generate knockout mutants for *Mapoly0021s0041* (*ppo* plants). The haploid status of the dominant liverwort life stage, the gametophyte, allowed for efficient visual screening of the first transgenic generation for reduced pigmentation when plants were placed under nutrient stress. Thus, 8 independent candidate *ppo* mutants were identified in the initial screen, and the presence of different deletion events in the targeted region of the *Mapoly0021s0041* gene then confirmed for each of these lines

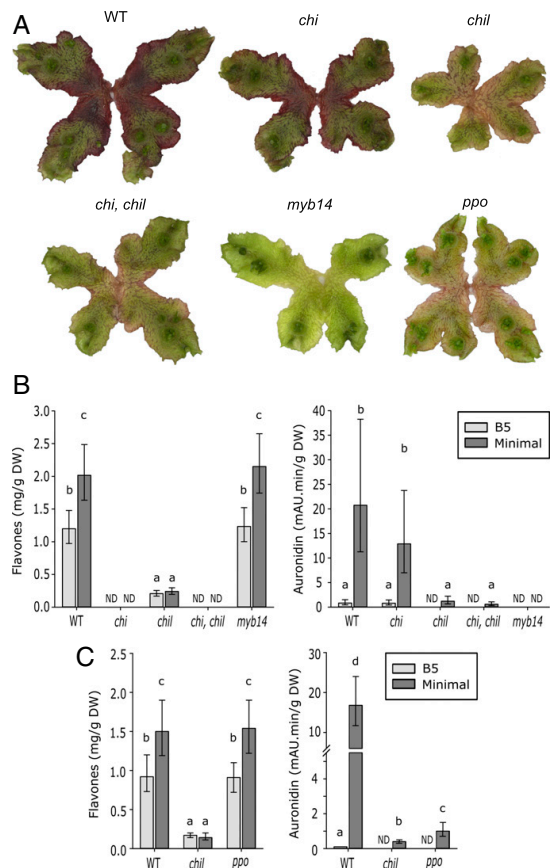


Fig. 5. *Marchantia* genetic mutants showing that auronidins are produced by a different branch of the flavonoid pathway than that producing anthocyanins. WT and mutant *Marchantia* plants were induced to synthesize red auronidin pigments by nutrient deprivation. Lines contain mutations in flavonoid biosynthetic (*chi*, *chil*, and *ppo*) or regulatory (*myb14*) genes. (A) Representative pigmentation phenotypes. (B and C) Flavone and auronidin contents. *n* = 3 biological replicates ± 95% confidence interval. ND, not detected. Means that are significantly different are indicated by different letters (a, b, c, and d).

(SI Appendix, Fig. S5). As the initial screen was visual, rather than an unbiased screening for mutation events, we confirmed the specificity of the *ppo* mutations by sequencing any predicted potential nontarget sites in the genome. No off-target genome sequence changes were found. The *ppo* mutants had reduced auronidin production but WT flavone production (Fig. 5), suggesting a specific role for *Mapoly0021s0041* in auronidin biosynthesis and supporting the proposed aurone biosynthetic route to auronidins.

Discussion

The timing of the evolution of the flavonoid pathway is the subject of current debate (20). Most papers communicate that flavonoids are absent from algae and propose flavonoids arising during the evolution of the first land plants. Although genes for the initial steps of the phenylpropanoid pathway may be present in algae, and there is some evidence of various flavonoid groups (but not the pigmented anthocyanin nor aurone groups) at very low amounts in algae (40), there are no substantiated examples of the flavonoid-specific genes being present in algal genomes. What type of flavonoids the first land plants might have produced is not known. The UV-B-absorbing colorless flavones and flavonols are present in all major extant land plant groups examined, suggesting that they may have been present in the last common ancestor (8–11, 16). When it comes to pigmented flavonoids, anthocyanins are widely distributed in angiosperms and to some extent in gymnosperms. A few deoxyanthocyanidins (rather simple in structure) are reported to occur in nonseed plants, such as ferns and mosses (6, 41).

Anthocyanins serve 2 major functions in plants. In seed plants, they provide a diversity of colors vital for pollination and seed dispersal (14, 15). This color palette is based on several distinct structural elements of the anthocyanins, including various proportions of structurally different equilibrium forms of individual colors. The second function of anthocyanins is in protection against abiotic stress. Although the mechanism by which anthocyanins function is not resolved, they are known to directly absorb or distribute visible light and to have antioxidant activity (2, 3, 7, 8). In the liverwort gametophyte, auronidins obviously serve other functions besides participating in pollination and seed dispersal and (reported as riccionidin) have been found to be stress-induced (17–19). Thus, auronidins may be anthocyanin “replacements” in liverworts with regard to stress tolerance functions—despite the absence of the various structural forms typical of anthocyanins. Auronidins share some color attributes with anthocyanins in the orange to violet part of the light spectrum and are the only other flavonoid group to do so. However, in auronidins, the chromophore system is based on acid-base equilibrium forms and not on the different anthocyanin equilibrium forms. Also, the formation of the auronidin C- and D-rings based on the C9 skeleton is unique among the flavonoid groups. The chemical properties displayed by auronidins in vitro, and the presence of both cell wall-bound and soluble forms in planta, suggest unreported in planta functions that perhaps contribute to the remarkable ability of liverworts to survive in extreme environments.

More than 8,000 flavonoid structures were identified by 2006 (6), and more have been characterized since. We suggest that the development of and within the various flavonoid groups, as well as the regulation of the amounts of individual flavonoids in each plant, are in the evolutionary context of the various plant phyla driven by functional needs. R2R3MYB transcription factors are central regulators of flavonoid production (14, 17, 22, 23). Angiosperm R2R3MYB gene families are substantially larger than those of basal plants such as *Marchantia* (25). In *Marchantia*, a single R2R3MYB gene, *MpMYB14*, is the key regulator of auronidin production in response to stress triggers (17) (Fig. 5). Although these same stress triggers activate the R2R3MYB genes that induce anthocyanin production in angiosperms, additional R2R3MYB genes are required for the production of anthocyanins

or other flavonoid groups in response to a variety of different developmental and environmental stimuli. As a consequence, we suggest that the progress of diversity and complexity of anthocyanin structures with their structurally different equilibrium forms, and associated increased complexity in pathway regulation, are advanced features in seed plants that facilitated communication with the biotic environment via their additional functions in pollination and seed dispersal. Thus, the biosynthesis of anthocyanins in the evolutionary context must be viewed from 2 directions, driven either by its proposed function in stress tolerance or its function in pollination and seed dispersal.

The similarity of the auronidin ring pattern, hydroxyl positions, and glycosylation pattern to that of auronones suggested an aurone precursor for auronidins. The phenotypes of the *chi* and *chil* mutants supported this proposed aurone biosynthetic route; the *chi* mutants lost production of flavanone-derived flavonoids (flavones) but not of auronidins, while the *chil* mutants had reduced production of both flavones and auronidins. The reduced flavone in *chil* plants suggests that CHIL has a similar role in promoting flavonoid production in *Marchantia* as it does in some angiosperms. The flavonoid route to auronidins was also supported by the genes identified as up-regulated by *MpMYB14* coincident with auronidin production. These included the phenylpropanoid pathway enzyme PAL and the flavonoid pathway enzymes CHS and CHIL, as well as a candidate AUS PPO. Thus, the chemistry, *chi/chil* mutant, and RNA-seq analysis data show that auronidins are phenylpropanoid pigments and suggest a biosynthetic origin via auronones. However, a genetic mutation removing the activity of either CHS or a confirmed enzyme in the specific aurone/auronidin biosynthetic branch is required to rule out other possible biosynthetic routes. CHS is a challenging CRISPR/Cas9 target in *Marchantia*. Twenty-four putative CHS genes have been identified in the genome (25), including 9 of the 2,000 most highly expressed genes in the stressed WT RNA-seq data, with no single gene accounting for >25% of the total CHS transcript pool. The auronidin biosynthetic steps following chalcones are unknown; however, the candidate AUS PPO, *Mapoly0021s0041*, was coordinately expressed with auronidin production and the characterized flavonoid biosynthetic genes. In the top 2,000 genes in the stressed WT RNA-seq data, there are only 2 PPO candidates, with *Mapoly0021s0041* accounting for 77% of the total PPO transcript pool, thus making it a suitable CRISPR target. *Mapoly0021s0041* loss-of-function mutants (*ppo* lines) had greatly reduced production of both cell wall-bound auronidin and auronidin glycoside. Thus, *Mapoly0021s0041* probably conducts a biosynthetic step before the cell wall attachment of auronidin (which presumably may involve polymerization), as the auronidin glycoside is thought to be vacuolar-located based on visual localization in cells, including the presence of anthocyanic vacuolar inclusion equivalents (24). It is unlikely that the reduced pigment amounts in the *ppo* plants were due to pathway feedback inhibition from the accumulation of unbound auronidin, as 35S:MYB14 plants accumulate large amounts of auronidin glycoside. The data thus support an aurone biosynthetic route. However, the possibility that *Mapoly0021s0041* (which has an in silico localization prediction as “secretory”) or other *MpPPO* genes are involved in biosynthetic steps in addition to formation of the aurone, such as cell wall binding or polymerization, cannot be ruled out.

Auronones occur sporadically across the embryophyta, and PPOs with differing structures and activities have been adopted for aurone biosynthesis. Tran et al. (35) found that the size of the PPO gene family varied from 0 to 13 across 20 embryophyte genomes analyzed, which included those of the moss *Physcomitrella patens* and the lycophyte *Selaginella moellendorffii*. The same analysis found PPO genes across 5 green algae genomes, suggesting that PPO predates land colonization. In comparison, 63 candidate PPO genes were found in the *Marchantia* genome,

with various predicted protein structures. These included several genes, like the candidate AUS, that are short sequences comparative to angiosperm PPOs. The large gene number and variation in protein structures suggests that the PPO gene family has undergone extensive duplication and neofunctionalization in *Marchantia* and could have roles in biosynthetic processes other than those typically expected for angiosperm PPOs. Whether this is a feature of liverworts in general awaits the completion of genome sequences for additional species.

Liverworts are often considered as the basal plant group with a sister relationship to all extant land plants. The discovery that riccionidin A is an auronidin means that there are now no validated reports of anthocyanins in liverworts. Thus, we suggest that the biosynthesis of anthocyanins arose after the occurrence of the last common ancestor of liverworts and seed plants.

Methods and Materials

Plant Material. Plant material, growth conditions, and stress treatments of *Marchantia polymorpha* L. have been described previously (17). The WT and *mpmyb14-1* lines have been described previously (17). CRISPR/Cas9-mutagenesis of the *MpCHI*, *MpCHL*, and *MpPPO* genes was as described previously (17, 42), using the oligonucleotide guide sequences given in *SI Appendix*. Multiple independent knockout lines were generated, with results shown for representative lines (*mpchi-1*, *mpchil-1*, and *mppo-1*).

1. L. O. Björn, S. Widell, T. Wang, Evolution of UV-B regulation and protection in plants. *Adv. Space Res.* **30**, 1557–1562 (2002).
2. K. Davies, N. Albert, Y. Zhou, K. Schwinn, Functions of flavonoid and betalain pigments in abiotic stress tolerance in plants. *Annu. Plant Rev.* **1**, 1–41 (2018).
3. M. Landi, M. Tattini, K. S. Gould, Multiple functional roles of anthocyanins in plant-environment interactions. *Environ. Exp. Bot.* **119**, 4–17 (2015).
4. J. K. Weng, The evolutionary paths towards complexity: A metabolic perspective. *New Phytol.* **201**, 1141–1149 (2014).
5. J. A. Banks *et al.*, The Selaginella genome identifies genetic changes associated with the evolution of vascular plants. *Science* **332**, 960–963 (2011).
6. Ø. M. Andersen, K. R. Markham, Eds., *The Flavonoids: Chemistry, Biochemistry and Applications* (CRC Press, Boca Raton, FL, 2006), p. 1237.
7. G. Agati, E. Azzarello, S. Pollastri, M. Tattini, Flavonoids as antioxidants in plants: Location and functional significance. *Plant Sci.* **196**, 67–76 (2012).
8. G. Agati *et al.*, Functional roles of flavonoids in photoprotection: New evidence, lessons from the past. *Plant Physiol. Biochem.* **72**, 35–45 (2013).
9. W. A. Clayton *et al.*, UVR8-mediated induction of flavonoid biosynthesis for UVB tolerance is conserved between the liverwort *Marchantia polymorpha* and flowering plants. *Plant J.* **96**, 503–517 (2018).
10. S. Pollastri, M. Tattini, Flavonols: Old compounds for old roles. *Ann. Bot.* **108**, 1225–1233 (2011).
11. L. Wolf, L. Rizzini, R. Stracke, R. Ulm, S. A. Rensing, The molecular and physiological responses of *Physcomitrella patens* to ultraviolet-B radiation. *Plant Physiol.* **153**, 1123–1134 (2010).
12. R. Yin, R. Ulm, How plants cope with UV-B: From perception to response. *Curr. Opin. Plant Biol.* **37**, 42–48 (2017).
13. Ø. M. Andersen, M. Jordeheim, “The anthocyanins” in *The Flavonoids: Chemistry, Biochemistry, and Applications*, Ø. M. Andersen, K. R. Markham, Eds. (CRC Press, Boca Raton, FL, 2006), pp. 471–552.
14. K. M. Davies, N. W. Albert, K. E. Schwinn, From landing lights to mimicry: The molecular regulation of flower colouration and mechanisms for pigmentation patterning. *Funct. Plant Biol.* **39**, 619–638 (2012).
15. K. Valenta, O. Nevo, C. Martel, C. A. Chapman, Plant attractants: Integrating insights from pollination and seed dispersal ecology. *Evol. Ecol.* **31**, 249–267 (2017).
16. Y. Asakawa, A. Ludwiczuk, F. Nagashima, “Chemical constituents of bryophytes: Bio and chemical diversity, biological activity, and chemosystematics” in *Progress in the Chemistry of Organic Natural Products*, A. D. Kinghorn, H. Falk, J. Kobayashi, eds. (Springer, Vienna, 2013), Vol. 95, pp. 1–796.
17. N. W. Albert *et al.*, Genetic analysis of the liverwort *Marchantia polymorpha* reveals that R2R3MYB activation of flavonoid production in response to abiotic stress is an ancient character in land plants. *New Phytol.* **218**, 554–566 (2018).
18. S. Kunz, G. Burkhardt, H. Becker, Riccionidins A and B, anthocyanidins from the cell walls of the liverwort *Ricciocarpos natans*. *Phytochemistry* **35**, 233–235 (1993).
19. K. R. S. Snell *et al.*, Quantifying the metabolic cost to an Antarctic liverwort of responding to an abrupt increase in UVB radiation exposure. *Glob. Change Biol.* **15**, 2563–2573 (2009).
20. J. de Vries, S. de Vries, C. H. Slamovits, L. E. Rose, J. M. Archibald, How embryophytic is the biosynthesis of phenylpropanoids and their derivatives in streptophyte algae? *Plant Cell Physiol.* **58**, 934–945 (2017).
21. V. Cheynier, G. Comte, K. M. Davies, V. Lattanzio, S. Martens, Plant phenolics: Recent advances on their biosynthesis, genetics, and ecophysiology. *Plant Physiol. Biochem.* **72**, 1–20 (2013).
22. W. Xu, C. Dubos, L. Lepiniec, Transcriptional control of flavonoid biosynthesis by MYB-bHLH-WDR complexes. *Trends Plant Sci.* **20**, 176–185 (2015).
23. A. Lloyd *et al.*, Advances in the MYB-bHLH-WD repeat (MBW) pigment regulatory model: Addition of a WRKY factor and co-option of an anthocyanin MYB for betalain regulation. *Plant Cell Physiol.* **58**, 1431–1441 (2017).
24. H. Kubo *et al.*, Biosynthesis of riccionidins and marchantins is regulated by R2R3-MYB transcription factors in *Marchantia polymorpha*. *J. Plant Res.* **131**, 849–864 (2018).
25. J. L. Bowman *et al.*, Insights into land plant evolution garnered from the *Marchantia polymorpha* genome. *Cell* **171**, 287–304.e15 (2017).
26. N. T. R. N. Kumara, A. Lim, C. M. Lim, M. I. Petra, P. Ekanayake, Recent progress and utilization of natural pigments in dye-sensitized solar cells: A review. *Renew. Sustain. Energy Rev.* **78**, 301–317 (2017).
27. S. Demiryak, L. Yurttas, N. Gundogdu-Karaburun, A. C. Karaburun, I. Kayagil, Synthesis and anti-cancer activity evaluation of new aurore derivatives. *J. Enzyme Inhib. Med. Chem.* **30**, 816–825 (2015).
28. K. R. Markham, L. J. Porter, Production of an aurore by bryophytes in the reproductive phase. *Phytochemistry* **17**, 159–160 (1978).
29. B. Boucherle, M. Peuchmaur, A. Boumendjel, R. Haudecoeur, Occurrences, biosynthesis and properties of aurores as high-end evolutionary products. *Phytochemistry* **142**, 92–111 (2017).
30. C. Molitor, S. G. Mauracher, A. Rompel, Aurore synthase is a catechol oxidase with hydroxylase activity and provides insights into the mechanism of plant polyphenol oxidases. *Proc. Natl. Acad. Sci. U.S.A.* **113**, E1806–E1815 (2016).
31. T. Nakayama *et al.*, Aureusidin synthase: A polyphenol oxidase homolog responsible for flower coloration. *Science* **290**, 1163–1166 (2000).
32. E. Ono *et al.*, Localization of a flavonoid biosynthetic polyphenol oxidase in vacuoles. *Plant J.* **45**, 133–143 (2006).
33. C. Kaintz *et al.*, Cloning and functional expression in *E. coli* of a polyphenol oxidase transcript from *Coreopsis grandiflora* involved in aurore formation. *FEBS Lett.* **588**, 3417–3426 (2014).
34. C. Molitor *et al.*, Latent and active aurore synthase from petals of *C. grandiflora*: A polyphenol oxidase with unique characteristics. *Planta* **242**, 519–537 (2015).
35. L. T. Tran, J. S. Taylor, C. P. Constabel, The polyphenol oxidase gene family in land plants: Lineage-specific duplication and expansion. *BMC Genomics* **13**, 395 (2012).
36. A. X. Cheng *et al.*, Identification of chalcone isomerase in the basal land plants reveals an ancient evolution of enzymatic cyclization activity for synthesis of flavonoids. *New Phytol.* **217**, 909–924 (2018).
37. W. Jiang *et al.*, Role of a chalcone isomerase-like protein in flavonoid biosynthesis in *Arabidopsis thaliana*. *J. Exp. Bot.* **66**, 7165–7179 (2015).
38. Y. Morita *et al.*, A chalcone isomerase-like protein enhances flavonoid production and flower pigmentation. *Plant J.* **78**, 294–304 (2014).
39. Z. Ban *et al.*, Noncatalytic chalcone isomerase-fold proteins in *Humulus lupulus* are auxiliary components in prenylated flavonoid biosynthesis. *Proc. Natl. Acad. Sci. U.S.A.* **115**, E5223–E5232 (2018).
40. K. Goiris *et al.*, Detection of flavonoids in microalgae from different evolutionary lineages. *J. Phycol.* **50**, 483–492 (2014).
41. M. F. Cohen, T. Meziane, M. Tsuchiya, H. Yamasaki, Feeding deterrence of *Azolla* in relation to deoxyanthocyanin and fatty acid composition. *Aquat. Bot.* **74**, 181–187 (2002).
42. S. S. Sugano *et al.*, Efficient CRISPR/Cas9-based genome editing and its application to conditional genetic analysis in *Marchantia polymorpha*. *PLoS One* **13**, e0205117 (2018).

Supplementary Information for

Auronidins: A new class of flavonoid pigments that challenges when anthocyanin biosynthesis evolved in plants

Helge Berland, Nick W. Albert, Anne Stavland, Monica Jordheim, Tony K. McGhie, Yanfei Zhou, Huaibi Zhang, Simon C. Deroles, Kathy E. Schwinn, Brian R. Jordan, Kevin M. Davies, Øyvind M. Andersen

Correspondence: Øyvind M. Andersen Email: oyvind.andersen@uib.no or Kevin M. Davies Email: kevin.davies@plantandfood.co.nz

This PDF file includes:

Supplementary Methods
Figs. S1 to S5.
Tables S1 and S2.

Supplementary Methods

Plant Material

The wild-type and *mpmyb14* mutant (*mpmyb14-1*) lines of *Marchantia polymorpha* L., growth conditions used, and stress treatments to induce auronidin production were essentially as described in Albert *et al.* (New Phytologist, 218: 554). Plants used for experiments were G2 generation (at least two rounds of gemmae propagation) or later. Transformation of marchantia and screening for CRISPR/Cas9-generated mutations of the MpCHI, MpCHIL and MpPPO genes were conducted as described in Albert *et al.* and Sugano *et al.* (PloS One, 13: e0205117.).

Oligonucleotide guide sequences used for CRISPR/Cas9 were:

MpCHI sgRNA1 5'-CAGGGAAAGACTCTTGCCAA-3'

MpCHI sgRNA2 5'-GAAAGCTCACTGTCCGAACC-3'

MpCHIL sgRNA1 5'-CAAGGCGACTATGCCGTGGA-3'

MpPPO sgRNA1 5'-CTCAGATGGCGGCTTCGGGG-3'

MpPPO sgRNA2 5'-CTATACCGAGAAGTTGGACA-3'

Multiple independent knockout lines for MpCHI (*Mapoly0167s0012*), MpCHIL (*Mapoly0175s0004*) and MpPPO (*Mapoly0021s0041*) genes were generated. Results are shown for representative mutant lines (*mpchi-1*, *mpchil-1*, *mpppo-1*).

Flavonoid quantification

Quantification of flavone glycoside and auronidin content of *M. polymorpha* lines was conducted as described in Albert *et al.* (New Phytologist, 218: 554), including significance tests (ANOVA + Fisher's Least Significant Difference $\alpha = 0.05$, upon log-transformed data). All analyses used at least three biological replicates, which consisted of at least three plants grown per tissue culture vessel.

Isolation of pigments

Pigments **1** and **2** were extracted from freeze-dried transgenic tissue of *M. polymorpha* with methanol/water/trifluoroacetic acid (80:20:0.5, v/v). The methanol was removed *in vacuo*, and the crude extract was purified using liquid-liquid extraction against ethyl acetate. Pigment **1** was isolated from the water phase on a Toyopearl HW-40F column (50 × 100mm) equilibrated with methanol/water/trifluoroacetic acid (20:80:0.5, v/v), using a step gradient from 20% to 40% methanol, and further purified using preparative HPLC. Pigment **2** was extracted from the ethyl acetate phase using acidified water, and further purified using preparative HPLC. The pigments were elucidated to be 2,3,6,8-tetrahydroxybenzofuro[3,2-*b*]chromen-5-ium-6-*O*-(2-*O*- α -rhamnopyranosyl- β -glucopyranoside), auronidin 4-*O*-neohesperidoside (**1**), and its aglycone, auronidin (**2**) mainly based on various homo- and heteronuclear two-dimensional NMR experiments on a 850 MHz NMR instrument, and high-resolution electrospray ionisation mass spectrometry. Fig. 1 shows a heteronuclear single quantum coherence (HSQC) spectrum showing cross peaks representing all the carbon atoms, which are directly connected to hydrogen atoms. The included structure is annotated with a) selected long-range ^1H to ^{13}C bonding correlations observed as cross peaks in the heteronuclear multiple bond correlation (HMBC) and b) selected ^1H to ^1H through-space neighborhood correlations observed as cross peaks in the rotating frame Overhauser (ROESY) spectrum. These correlations were in particular important for the assignments of the various quaternary carbon atoms of the aglycone, and for determination of the linkage positions of the two sugar units (SI Appendix, Table S1). The anomeric coupling constants, the chemical shifts of the ^{13}C resonances in the sugar region of the HSQC spectrum, and the crosspeaks in the ^1H - ^1H DQF-COSY and ^1H - ^1H TOCSY spectra agreed with a rhamnopyranosyl unit linked in the 2-position on a glucopyranosyl unit connected to the aglycone (SI Appendix, Table S1). The structure of **1** was

confirmed by its HR-ESI-MS spectrum, which showed a molecular ion at m/z 593.15099 corresponding to the empirical formula $C_{27}H_{29}O_{15}^+$ (calc. 593.15064).

Instrumentation

Analytical HPLC

The isolation procedure was monitored by analytical HPLC using an Agilent 1160 HPLC system equipped with an Agilent 1100 diode-array detector and an 250×4.6 mm (5 μ m) Agilent Hypersil 5 ODS C18 column with a flow rate of 1 ml min^{-1} . The solvents A: water/TFA (100:0.5, v/v) and B: acetonitrile/TFA (100:0.5, v/v) were used with the following gradient: Initial conditions of 10% B, followed by a gradient to 14% B (10 min), isocratic elution to 14 min, and subsequent gradients: 18% B (22 min), 23% B (26 min), 28% B (31 min) and 40% B (32 min), and lastly isocratic elution to 37 min. Aliquots of 20 μ l were injected, and filtered through a 0.45 μ m filter prior to injection.

Preparative HPLC

The samples of **1** and **2** were purified by preparative HPLC using a Gilson 321 pump, an Ultimate 3000 variable wavelength detector at 490 nm, and a 250×22 mm (10 μ m) Econosphere C18 column (Grace) at a flow rate of 15 ml min^{-1} . The solvents A: water/TFA (100:0.5, v/v) and B: acetonitrile/TFA (100:0.5, v/v) were used with the following gradient: Initial conditions of 10% B followed by a gradient to 14% B (10 min), isocratic elution to 14 min, and subsequent gradients: 18% B (22 min), 28% B (31 min), 40% B (32 min), 40% B (40 min), and lastly isocratic elution to 45 min. Aliquots were filtered through a 0.45 μ m filter, and 500 μ l were injected.

UV-Visible light spectroscopy

The UV-Visible light absorption spectra were recorded in steps of 1 nm in the range of 250-700 nm using a Biochrom Libra S32 PC spectrophotometer with quartz cells with 1 cm path length.

NMR spectroscopy

Structure elucidation of **1** and **2** were obtained by NMR spectroscopy on a Bruker Ascend™ 850 MHz spectrometer equipped with a TCI CryoProbe at 850.13 MHz and 213.77 MHz for ¹H and ¹³C respectively. 1D ¹H NMR and 2D Heteronuclear single quantum coherence (¹H-¹³C HSQC), Heteronuclear multiple bond correlations (¹H-¹³C HMBC), Double quantum filtered correlation spectroscopy (¹H-¹H DQF-COSY), Total correlation spectroscopy (¹H-¹H TOCSY), and Rotating-frame nuclear Overhauser effect correlation spectroscopy (¹H-¹H ROESY), were performed. Samples were dissolved in *d*₆-MeOD/*d*-TFA (100:5, v/v), and the deuteriomethyl ¹³C and residual ¹H signal of *d*₆-MeOD were used as secondary references at δ 49.15 and δ 3.31, respectively.

Mass spectrometry

The structures of **1** and **2** were confirmed by direct injection of pure samples into a high-resolution mass spectrometer (JEOL AccuTOF JMS-T100LC) with electrospray ionisation and time-of-flight separation (ESI⁺/TOF).

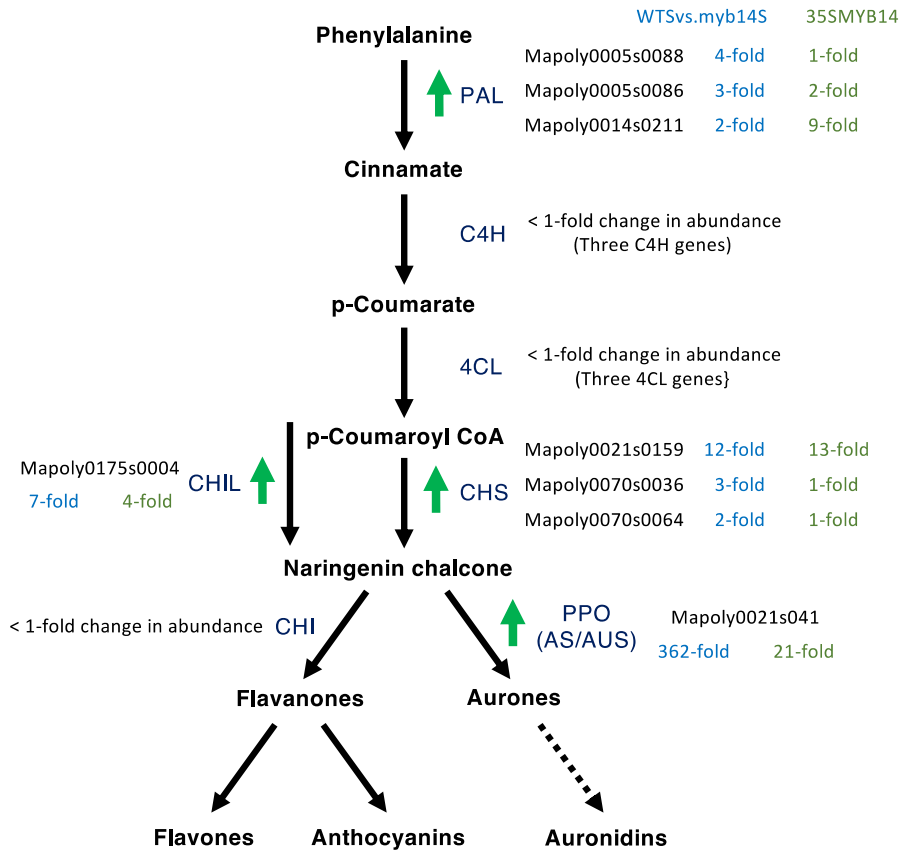


Fig. S1. Changes in transcript abundance for phenylpropanoid biosynthetic enzymes accompanying *MpMYB14* activated auronidin pigment production in *Marchantia polymorpha*. The biosynthetic pathway to flavones, aurones and anthocyanins is shown, with the proposed route to auronidins as a dotted arrow. The fold increase in transcript abundance is shown next to each gene, as determined by RNAseq analysis of wild-type plants under nutrient stress compared to *myb14* mutant plants under stress (WTS vs. *myb14S*, in blue text), and *35S:MYB14* transgenics compared to wild-type plants (*35S:MYB14*, in green text). Enzyme abbreviations are PAL, PHENYLALANINE AMMONIA LYASE; C4H, CINNAMATE 4-HYDROXYLASE; 4CL, COUMAROYL CoA-LIGASE; CHS, CHALCONE SYNTHASE; CHI, CHALCONE ISOMERASE; CHIL, CHALCONE ISOMERASE-LIKE; AS/AUS, AURONE SYNTHASE/AUREUSIDIN SYNTHASE. For PAL and CHS only the genes with significant changes in transcript abundance are shown (from gene families of 10 and 24 members, respectively).

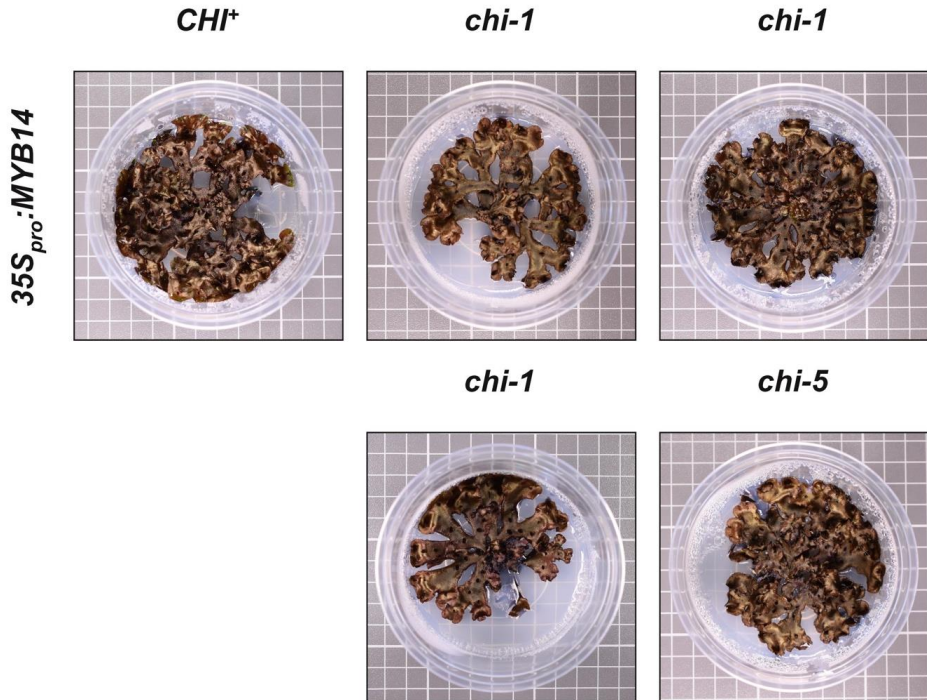
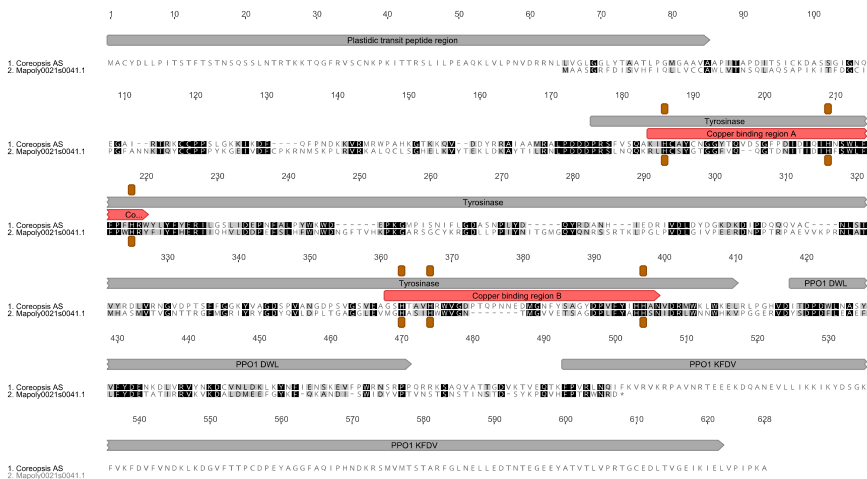


Fig. S3. Chalcone isomerase is not required for auronidin biosynthesis. Transgenic $35S_{pro}:MYB14$ marchantia plants were crossed with the *chi* mutant (*chi-1*). Spores were grown and plants screened for the presence of the MpMYB14 transgene and for the presence of the *chi-1* mutation (102 bp deletion). Plants were further screened for new mutations within *CHI*, because the CRISPR tDNA was also segregating. *chi-5* contains a 1 bp insertion, resulting in a frameshift mutation. Plants containing the $35S_{pro}:MYB14$ construct were always intensely pigmented with auronidin, regardless of whether they were *chi* or *CHI* genotypes.



Mapoly0001s0379.1	Mapoly0071s0078.1	Mapoly0121s0019.1	Mapoly0244s0001.1
Mapoly0021s0034.1	Mapoly0073s0001.1	Mapoly0121s0020.1	Mapoly0244s0002.1
Mapoly0021s0035.1	Mapoly0074s0082.1	Mapoly0134s0001.1	Mapoly0244s0003.1
Mapoly0021s0037.1	Mapoly0080s0086.1	Mapoly0134s0050.1	Mapoly0248s0003.1
Mapoly0021s0041.1	Mapoly0084s0022.1	Mapoly0145s0006.1	Mapoly0266s0001.1
Mapoly0024s0005.1	Mapoly0084s0086.1	Mapoly0145s0008.1	Mapoly0266s0004.1
Mapoly0024s0006.1	Mapoly0091s0043.1	Mapoly0145s0009.1	Mapoly0391s0001.1
Mapoly0032s0136.1	Mapoly0094s0040.1	Mapoly0145s0012.1	Mapoly0595s0001.1
Mapoly0032s0137.1	Mapoly0097s0009.1	Mapoly0149s0028.1	Mapoly0654s0001.1
Mapoly0038s0001.1	Mapoly0106s0029.1	Mapoly0206s0001.1	Mapoly0967s0001.1
Mapoly0038s0002.1	Mapoly0109s0017.1	Mapoly0212s0001.1	Mapoly0994s0001.1
Mapoly0038s0003.1	Mapoly0117s0055.1	Mapoly0212s0002.1	Mapoly2340s0001.1
Mapoly0038s0004.1	Mapoly0117s0058.1	Mapoly0220s0002.1	Mapoly2776s0001.1
Mapoly0038s0112.1	Mapoly0121s0016.1	Mapoly0237s0003.1	Mapoly3313s0001.1
Mapoly0040s0078.1	Mapoly0121s0017.1	Mapoly0237s0004.1	Mapoly3320s0001.1
Mapoly0071s0077.1	Mapoly0121s0018.1	Mapoly0237s0005.1	MapolyY_B0028.1

Fig. S4. The Polyphenol Oxidase gene family of *Marchantia polymorpha*. Blast analysis of the *M. polymorpha* genome sequence and transcriptomes identified 64 PPO gene family members, listed at the bottom of the figure. Two of the gene models (*Mapoly0121s0016.1* and *Mapoly0121s0017.1*) are fragments of the same (non-functional) gene. The upper part of the figure shows the alignment of the deduced amino acid sequence *M. polymorpha* candidate AURONE SYNTHASE (*Mapoly0021s0041.1*) with the characterised AURONE SYNTHASE from *Coreopsis grandiflora*. The transit peptide, copper binding, tyrosinase, DWL, and C-terminal cleaved region of the *C. grandiflora* sequence are marked, along with the copper binding histones.

Table S1. ^1H and ^{13}C NMR spectra data for auronidin 4-neohesperidoside (1) isolated from transgenic material of *Marchantia polymorpha*. Spectral data for 1 were obtained in d_6 -MeOD/ d -TFA (100:5, v/v) at 25°C, at 850.13 MHz and 213.77 MHz for ^1H and ^{13}C respectively. The deuteriomethyl ^{13}C signal and the residual ^1H signal of the solvent were used as secondary references at δ 49.15 and δ 3.31, respectively.

	^{13}C	^1H		^{13}C	^1H		
<i>auronidin</i>			<i>4-glucoside</i>				
2	145.94		1"	101.46	5.49	<i>d</i>	7.5
3	158.13		2"	81.64	3.86	<i>dd</i>	7.6, 9.1
4	157.34		3"	77.82	3.69	<i>t</i>	9.1
5	101.61	6.826	<i>d</i> 1.5	4"	71.25	3.52	<i>dd</i> 9.2, 9.7
6	171.99		5"	78.61	3.60	<i>dd</i>	9.7, 6.2
7	94.56	6.832	<i>d</i> 1.5	6"A	62.45	3.94	<i>m</i> -
8	165.67		6"B		3.75	<i>t</i>	8.0
9	102.38						
α	129.61	8.88	<i>s</i>	<i>2''-rhamnoside</i>			
1'	118.47		1'''	103.26	5.42	<i>d</i>	1.8
2'	152.56		2'''	72.19	4.03	<i>m</i>	-
3'	105.05	7.66	<i>s</i>	3'''	72.12	3.63	<i>dd</i> 3.3, 9.4
4'	158.26		4'''	73.91	3.18	<i>t</i>	9.5
5'	149.96		5'''	70.49	3.60	<i>dd</i>	9.5, 6.2
6'	112.73	7.50	<i>s</i>	6'''	17.91	0.69	<i>d</i> 6.2

s: singlet, *d*: doublet, *t*: triplet, *dd*: double doublet, *m*: multiplet

Table S2. Differential transcript abundance between *Marchantia polymorpha myb14* mutant and wild-type plants undergoing nutrient stress, as analysed by DeSeq2 RNaseq. The BaseMean was calculated for each treatment set using Illumina RNaseq data on RNA from three biological replicates, mapped to the *M. polymorpha* genome predicted gene models. The 260 genes are shown that had an adjusted *p*-value <0.001 and Log2 fold increase >1.0, as well as the PFAM database classification based on the predicted amino acid sequence. (PFAM database: EI-Gebali et al. 2019. Nucleic Acids Research 47: D427–D432.)

Mpoly_primaryTs	bM-myb14S	bM-WT	baseMean	log2 FoldChange	padj	PFAM_Desc
Mapoly0021s0041.1	41.80	15622.17	5269.17	8.54	0	Polyphenol oxidase middle domain; Common central domain of tyrosinase
Mapoly0005s0088.1	2325.03	8663.16	4412.77	1.90	1.30E-239	NA
Mapoly2045s0001.1	3417.76	43.50	1158.69	-6.29	1.93E-238	NA
Mapoly0175s0004.1	759.07	3238.90	1646.80	2.09	4.13E-174	Chalcone-flavanone isomerase-like
Mapoly0021s0159.1	2263.83	23383.03	9311.02	3.37	7.45E-147	Chalcone and stilbene synthases, C-terminal domain; Chalcone and stilbene synthases, N-terminal domain
Mapoly0024s0001.1	51.42	1104.73	457.66	4.43	2.62E-137	NA
Mapoly0020s0078.1	19181.51	6833.62	9085.29	-1.49	1.72E-132	NA
Mapoly0048s0047.1	379.12	1740.62	741.28	2.20	1.79E-127	Transferase family
Mapoly0006s0217.1	9.28	2749.60	946.38	8.22	3.41E-112	Dirigent-like protein
Mapoly0044s0010.1	8237.34	2928.95	4030.08	-1.49	8.44E-88	NA
Mapoly0005s0086.1	773.14	2432.53	1315.19	1.65	3.47E-79	Aromatic amino acid lyase
Mapoly0044s0009.1	4336.02	1908.90	2236.24	-1.18	5.20E-74	NA
Mapoly0092s0006.1	7098.05	3116.68	3719.29	-1.19	1.87E-72	NA
Mapoly0071s0031.1	2507.76	1133.58	1410.33	-1.15	4.77E-60	NA
Mapoly0032s0031.1	1565.20	471.35	754.48	-1.73	7.40E-59	NA
Mapoly0063s0049.1	2602.63	5338.05	2795.55	1.04	3.36E-58	NAD dependent epimerase/dehydratase family
Mapoly0126s0004.1	14114.46	5858.55	7206.31	-1.27	6.70E-57	Phosphate transporter family
Mapoly0009s0202.1	34.58	449.43	448.17	3.71	1.86E-54	Phosphoesterase family
Mapoly0020s0024.1	1676.38	718.08	859.24	-1.22	1.94E-53	Protein kinase domain
Mapoly0006s0216.1	11.47	817.41	287.16	6.15	9.56E-46	Dirigent-like protein
Mapoly0032s0032.1	482.22	2905.00	1646.65	2.59	2.62E-41	Sodium:dicarboxylate symporter family
Mapoly0002s0040.1	6822.37	3246.43	3762.79	-1.07	5.64E-41	Armadillo/beta-catenin-like repeat
Mapoly0147s0044.1	18777.83	6566.59	9364.22	-1.52	2.81E-38	Chitinase class I
Mapoly0031s0159.1	4346.29	1979.68	2255.67	-1.13	5.25E-38	NA
Mapoly0004s0179.1	6904.26	1760.40	3287.17	-1.97	5.18E-37	Protein of unknown function (DUF1399)
Mapoly0014s0211.1	1240.63	2697.76	1620.09	1.12	4.92E-36	Aromatic amino acid lyase
Mapoly0016s0113.1	2270.74	891.91	1187.11	-1.35	2.07E-33	Protein of unknown function (DUF1399)
Mapoly0056s0138.1	21892.13	7096.09	10932.63	-1.63	3.17E-33	Heavy-metal-associated domain FAD-binding domain;Ferric reductase like transmembrane component;Ferric reductase NAD binding domain
Mapoly0043s0144.1	89.14	428.55	236.94	2.27	1.23E-32	C1-like domain;Thioredoxin-like
Mapoly0049s0009.1	43046.51	20959.89	24327.02	-1.04	7.23E-32	Pathogenesis-related protein Bet v I family
Mapoly0064s0111.1	74.89	529.45	253.71	2.82	1.05E-31	PAP2 superfamily
Mapoly0015s0198.1	1602.22	630.78	957.97	-1.34	1.76E-30	Lipase (class 3)
Mapoly0047s0068.1	1074.18	533.27	663.34	-1.01	3.20E-30	Domain associated at C-terminal with AAA;ATPase family associated with various cellular activities (AAA)
Mapoly0165s0017.1	17176.97	5076.86	7755.23	-1.76	1.56E-28	Protein kinase domain
Mapoly0056s0067.1	161.59	446.31	500.89	1.47	3.53E-28	Leucine rich repeat;Leucine rich repeat N-terminal domain;Leucine Rich Repeat;Leucine Rich repeats (2 copies)
Mapoly0118s0002.1	667.13	227.14	346.00	-1.55	1.25E-27	Plant PDR ABC transporter associated; ABC-2 type transporter; ABC-transporter extracellular N-terminal; ABC transporter
Mapoly0125s0012.1	565.22	1156.62	1191.09	1.03	9.86E-27	NA
Mapoly0007s0207.1	439.48	118.56	204.45	-1.89	4.04E-26	NA
Mapoly1150s0001.1	895.02	360.36	526.57	-1.31	4.08E-26	Leucine Rich Repeat
Mapoly0135s0047.1	2699.07	1083.26	1384.72	-1.32	4.37E-26	Protein of unknown function (DUF1399)
Mapoly0109s0013.1	524.73	1263.52	1268.44	1.27	2.03E-25	ABC-2 type transporter;ABC transporter

Mapoly0197s0009.1	689.74	1640.37	807.63	1.25	3.68E-25	Cytochrome P450
Mapoly0111s0014.1	756.80	371.26	512.39	-1.03	6.96E-25	ABC transporter transmembrane region;ABC transporter
Mapoly0039s0023.1	367.84	73.42	156.46	-2.33	3.77E-23	NA
Mapoly0120s0039.1	5375.57	2499.40	2855.53	-1.10	3.19E-22	NA
Mapoly0346s0002.1	2016.22	1004.72	1157.21	-1.00	1.44E-21	NA
Mapoly0073s0006.1	1566.23	311.63	667.52	-2.33	2.66E-21	Ankyrin repeat;Ankyrin repeats (many copies);Ankyrin repeats (3 copies)
Mapoly0010s0119.1	894.32	421.51	884.19	-1.09	3.31E-21	Alpha-L-fucosidase
Mapoly0818s0001.1	8695.99	2959.66	4213.57	-1.55	4.78E-21	Glutathione S-transferase, C-terminal domain;Glutathione S-transferase, N-terminal domain
Mapoly0099s0050.1	3089.99	681.87	1317.98	-2.18	1.07E-20	Ankyrin repeat;Ankyrin repeats (3 copies)
Mapoly0028s0010.1	206.08	514.46	2798.93	1.32	1.12E-20	Pectinesterase
Mapoly0044s0062.1	2050.76	655.58	989.60	-1.65	1.34E-20	Ion transport protein;Cyclic nucleotide-binding domain
Mapoly0160s0025.1	408.17	974.86	1261.18	1.26	2.12E-19	NA
Mapoly0106s0031.1	613.95	173.61	1041.53	-1.82	2.15E-19	PLAT/LH2 domain;Lipoxygenase
Mapoly0061s0098.1	1233.53	3417.20	4836.65	1.47	3.04E-19	Rare lipoprotein A (RlpA)-like double-psi beta-barrel;Pollen allergen
Mapoly0022s0060.1	277.78	30.36	105.54	-3.19	4.74E-19	C2 domain
Mapoly0041s0051.1	13594.28	3794.37	6495.32	-1.84	8.07E-19	NA
Mapoly0074s0030.1	1609.97	628.66	928.68	-1.36	8.08E-19	NA
Mapoly0052s0105.1	2570.91	916.03	1342.66	-1.49	9.38E-19	NA
Mapoly0126s0007.1	568.18	1253.16	1870.60	1.14	9.58E-19	Protein tyrosine kinase;Legume lectin domain
Mapoly0053s0011.1	6805.64	2057.39	3052.08	-1.73	1.58E-18	NA
Mapoly0131s0006.1	2646.63	5436.98	12466.30	1.04	1.65E-18	Xyloglucan endo-transglycosylase (XET) C-terminus;Glycosyl hydrolases family 16
Mapoly2590s0001.1	713.59	2726.40	4746.37	1.93	2.25E-18	NA
Mapoly0033s0082.1	237.39	49.96	109.44	-2.25	1.18E-17	F-box-like
Mapoly0745s0001.1	995.78	2018.93	2828.42	1.02	1.47E-17	Tetratricopeptide repeat;TPR repeat;Thioredoxin
Mapoly0036s0061.1	1202.52	553.65	656.82	-1.12	3.01E-17	Phloem protein 2;F-box domain
Mapoly0064s0010.1	9152.16	3643.71	4702.95	-1.33	3.91E-17	NA
Mapoly0067s0051.1	1521.13	380.98	691.21	-2.00	8.85E-17	Cytochrome P450
Mapoly0070s0012.1	1822.82	22443.99	8322.72	3.62	2.09E-16	Amidohydrolase
Mapoly0030s0137.1	1052.56	319.00	503.01	-1.72	3.43E-16	Pheophorbide a oxygenase;Rieske [2Fe-2S] domain
Mapoly0001s0363.1	482.17	1626.53	1329.10	1.75	3.46E-16	NA
Mapoly0050s0079.1	1155.91	497.58	628.50	-1.22	3.82E-16	NA
Mapoly0203s0002.1	1100.96	492.85	660.81	-1.16	2.25E-15	Lecithin retinol acyltransferase
Mapoly0006s0236.1	2345.15	1155.24	1356.47	-1.02	2.76E-15	DSBA-like thioredoxin domain
Mapoly0365s0001.1	336.64	49.27	134.04	-2.77	3.67E-15	14-3-3 protein
Mapoly0048s0056.1	423.17	1005.36	1291.52	1.25	5.31E-15	GDSL-like Lipase/Acylhydrolase
Mapoly0070s0036.1	6048.51	17573.02	8238.39	1.54	7.50E-15	Chalcone and stilbene synthases, C-terminal domain;Chalcone and stilbene synthases, N-terminal domain
Mapoly0007s0179.1	1631.20	671.78	809.07	-1.28	2.40E-14	Calcium-binding EGF domain;Protein tyrosine kinase;Wall-associated receptor kinase galacturonan-binding
Mapoly0342s0002.1	262.20	6.40	89.88	-5.36	4.16E-14	D-mannose binding lectin
Mapoly0004s0216.1	473.53	139.00	239.34	-1.77	8.88E-14	Protein of unknown function (DUF563)
Mapoly0193s0020.1	35.39	124.00	181.61	1.81	9.78E-14	Cupin
Mapoly0184s0024.1	315.99	151.86	209.26	-1.06	1.11E-13	Protein tyrosine kinase;Leucine rich repeat N-terminal domain;Leucine Rich Repeat;Leucine Rich repeats (2 copies)
Mapoly0030s0112.1	162.55	626.16	741.63	1.95	1.10E-12	Sodium/calcium exchanger protein
Mapoly0006s0280.1	529.81	249.52	314.98	-1.09	2.03E-12	Plant protein of unknown function
Mapoly0166s0024.1	1712.42	454.44	757.62	-1.91	2.51E-12	Lipase (class 3)
Mapoly0155s0011.1	13.41	140.72	54.66	3.38	2.79E-12	Ferritin-like domain
Mapoly0096s0070.1	402.22	877.52	1562.92	1.13	3.03E-12	Peroxidase
Mapoly1060s0001.1	194.38	79.44	113.92	-1.29	4.85E-12	NA
Mapoly0833s0001.1	5.52	71.53	40.38	3.70	4.89E-12	C-5 cytosine-specific DNA methylase
Mapoly0010s0218.1	1002.09	356.41	490.67	-1.49	5.18E-12	Lipase (class 3)
Mapoly0055s0109.1	1935.59	4140.73	9537.73	1.10	5.51E-12	Pectinesterase
Mapoly0007s0096.1	802.68	2246.51	2603.53	1.49	6.60E-12	Pectate lyase

Mapoly0034s0001.1	160.14	19.73	69.83	-3.02	2.10E-11	Cytochrome P450
Mapoly0056s0076.1	2735.04	1286.89	1511.96	-1.09	2.72E-11	NA
Mapoly0188s0001.1	2304.82	475.56	991.35	-2.28	2.79E-11	NB-ARC domain
Mapoly0008s0176.1	1216.45	560.82	1357.20	-1.12	4.11E-11	Chlorophyllase
Mapoly0081s0028.1	885.13	420.83	438.48	-1.07	4.12E-11	NA
Mapoly0073s0049.1	693.88	1402.85	1861.59	1.02	4.43E-11	Alcohol dehydrogenase GroES-like domain;Zinc-binding dehydrogenase
Mapoly0001s0381.1	567.11	244.72	314.13	-1.21	5.29E-11	Cellulase (glycosyl hydrolase family 5)
Mapoly0022s0112.1	382.79	184.18	227.76	-1.06	5.71E-11	NA
Mapoly0016s0100.1	696.80	337.91	358.06	-1.05	1.21E-10	Xyloglucan fucosyltransferase
Mapoly0003s0309.1	150.90	0.00	73.27	-9.81	1.21E-10	Patched family
Mapoly0076s0087.1	158.41	363.08	1462.53	1.20	1.33E-10	NA
Mapoly0001s0382.1	1352.20	609.01	904.06	-1.15	1.65E-10	PQQ-like domain;PQQ enzyme repeat
Mapoly0166s0023.1	164.37	19.26	66.83	-3.09	2.17E-10	Lipase (class 3)
Mapoly0048s0003.1	36486.69	15763.45	18935.27	-1.21	2.38E-10	Peroxidase
Mapoly0983s0001.1	758.29	263.49	380.38	-1.53	3.26E-10	Heavy-metal-associated domain
Mapoly0073s0047.1	2151.25	961.74	1125.71	-1.16	3.64E-10	Enoyl-(Acyl carrier protein) reductase Chalcone and stilbene synthases, C-terminal domain;Chalcone and stilbene synthases, N-terminal domain
Mapoly0070s0064.1	4474.71	9118.92	4859.21	1.03	3.77E-10	AP2 domain
Mapoly0136s0025.1	232.76	92.65	121.52	-1.33	4.03E-10	AP2 domain
Mapoly0003s0267.1	513.50	203.67	249.02	-1.33	5.93E-10	EamA-like transporter family
Mapoly0209s0006.1	2158.74	992.68	1169.30	-1.12	6.79E-10	Calcineurin-like phosphoesterase;Iron/zinc purple acid phosphatase-like protein C
Mapoly0044s0114.1	5191.90	2317.61	2524.68	-1.16	9.36E-10	Aromatic amino acid lyase
Mapoly0141s0002.1	577.42	1222.08	1543.24	1.08	9.84E-10	Pectinesterase
Mapoly0013s0025.1	101.35	246.11	238.91	1.28	1.52E-09	Caspase domain
Mapoly0085s0004.1	1599.25	589.67	979.30	-1.44	2.62E-09	SPFH domain / Band 7 family
Mapoly0056s0025.1	193.53	387.97	486.04	1.00	3.35E-09	Plant invertase/pectin methylesterase inhibitor;Pectinesterase
Mapoly0013s0011.1	2.70	52.47	39.93	4.27	4.18E-09	RNA recognition motif. (a.k.a. RRM, RBD, or RNP domain)
Mapoly0039s0121.1	998.99	498.41	582.75	-1.00	8.31E-09	Leucine rich repeat;Protein kinase domain;Leucine rich repeat N-terminal domain;Leucine rich repeat;Leucine Rich Repeat
Mapoly0125s0001.1	45.39	132.70	224.53	1.55	9.04E-09	Rare lipoprotein A (RlpA)-like double-psi beta-barrel;Pollen allergen
Mapoly0022s0188.1	850.98	417.69	508.89	-1.03	9.22E-09	UDP-glucuronosyl and UDP-glucosyl transferase
Mapoly0103s0042.1	3.05	38.18	23.89	3.65	1.20E-08	NA
Mapoly0307s0001.1	186.23	64.83	434.68	-1.53	1.23E-08	Rare lipoprotein A (RlpA)-like double-psi beta-barrel;Chitin recognition protein
Mapoly0143s0039.1	28.25	109.38	111.33	1.96	1.39E-08	Xylanase inhibitor N-terminal;Xylanase inhibitor C-terminal
Mapoly0042s0095.1	2646.87	1304.88	1678.71	-1.02	1.39E-08	D-mannose binding lectin;Glycosyl hydrolases family 17
Mapoly0100s0004.1	3492.49	755.01	1456.06	-2.21	1.70E-08	Sugar efflux transporter for intercellular exchange
Mapoly0129s0027.1	361.85	170.51	243.94	-1.09	1.76E-08	Leucine Rich repeat
Mapoly0013s0154.1	744.69	347.74	574.68	-1.10	1.76E-08	Multicopper oxidase;Multicopper oxidase;Multicopper oxidase
Mapoly0596s0001.1	335.41	114.81	167.06	-1.55	2.11E-08	Cytochrome P450
Mapoly0116s0045.1	2942.82	1126.76	1898.72	-1.39	2.19E-08	Chitinase class I;Chitin recognition protein
Mapoly0012s0118.1	44.89	113.27	113.66	1.33	2.23E-08	NA
Mapoly0123s0036.1	177.13	33.70	80.26	-2.40	3.95E-08	LysM domain
Mapoly0017s0019.1	1283.50	6.37	430.18	-7.65	4.44E-08	Calmodulin binding protein-like
Mapoly0033s0008.1	361.30	732.48	529.18	1.02	4.46E-08	EF-hand domain;EF hand
Mapoly0185s0032.1	68.26	158.51	193.03	1.22	4.67E-08	Xylanase inhibitor N-terminal;Xylanase inhibitor C-terminal
Mapoly0193s0021.1	18.71	78.42	79.44	2.08	4.88E-08	Cupin
Mapoly0008s0177.1	2712.71	1244.89	2285.92	-1.12	5.37E-08	Chlorophyllase
Mapoly0042s0016.1	3956.78	1060.09	2591.02	-1.90	5.56E-08	Thaumatin family
Mapoly0108s0022.1	316.73	147.68	166.23	-1.10	6.50E-08	F-box domain
Mapoly0049s0126.1	9671.21	4579.44	5125.87	-1.08	7.14E-08	Phosphoenolpyruvate carboxykinase
Mapoly0064s0034.1	113.26	230.43	267.35	1.02	1.11E-07	PLAT/LH2 domain;Lipoxygenase

Mapoly0066s0072.1	9.81	40.54	58.30	2.05	1.55E-07	Xyloglucan endo-transglycosylase (XET) C-terminus;Glycosyl hydrolases family 16
Mapoly3939s0001.1	123.98	504.31	765.06	2.03	1.77E-07	NA
Mapoly0027s0087.1	786.25	1734.21	1837.07	1.14	1.97E-07	Fasciclin domain
Mapoly0070s0055.1	101.66	222.30	281.26	1.13	3.08E-07	Peroxidase
Mapoly0075s0012.1	525.74	255.11	349.21	-1.04	3.99E-07	Leucine Rich Repeat;Leucine Rich repeats (2 copies)
Mapoly0103s0046.1	501.48	172.67	311.08	-1.54	4.25E-07	U1 zinc finger
Mapoly0009s0220.1	379.40	188.69	226.20	-1.01	4.39E-07	von Willebrand factor type A domain
Mapoly0029s0149.1	776.32	1599.36	1109.26	1.04	4.56E-07	Protein of unknown function, DUF538
Mapoly0009s0188.1	598.74	178.40	278.32	-1.75	4.66E-07	Ankyrin repeat;Domain of unknown function;Ankyrin repeats (3 copies)
Mapoly0274s0003.1	166.90	334.62	352.51	1.00	5.10E-07	Protein of unknown function (DUF679)
Mapoly0365s0002.1	155.25	26.01	63.97	-2.58	6.88E-07	14-3-3 protein
Mapoly0008s0235.1	8.01	48.66	67.15	2.61	7.14E-07	NA
Mapoly0124s0014.1	38.96	100.72	130.79	1.37	7.19E-07	Cytokinin dehydrogenase 1, FAD and cytokinin binding;FAD binding domain
Mapoly0043s0030.1	439.77	964.11	1350.78	1.13	7.78E-07	GDLS-like Lipase/Acylhydrolase
Mapoly0008s0126.1	21.31	118.49	75.96	2.47	1.05E-06	NA
Mapoly0036s0139.1	154.66	68.75	123.67	-1.17	1.08E-06	Cysteine-rich secretory protein family
Mapoly0041s0118.1	2755.33	1153.82	1501.36	-1.26	1.13E-06	Chalcone and stilbene synthases, C-terminal domain;Chalcone and stilbene synthases, N-terminal domain
Mapoly0134s0045.1	546.75	249.43	327.71	-1.13	1.19E-06	Embryo-specific protein 3, (ATS3)
Mapoly0030s0038.1	106.62	4.32	38.35	-4.63	1.28E-06	NA
Mapoly0063s0050.1	3823.64	1893.52	2035.29	-1.01	1.42E-06	PLAT/LH2 domain;Lipoxygenase
Mapoly0006s0158.1	14.42	49.37	52.46	1.78	1.62E-06	Rare lipoprotein A (RlpA)-like double-psi beta-barrel;Pollen allergen
Mapoly0201s0003.1	57.26	148.52	100.20	1.37	1.87E-06	Major intrinsic protein
Mapoly0010s0008.1	1823.63	559.24	914.34	-1.71	2.65E-06	NA
Mapoly0026s0014.1	128.29	257.99	301.66	1.01	2.65E-06	Polysaccharide lyase family 4, domain II;Polysaccharide lyase family 4, domain III;Rhamnogalacturonate lyase family
Mapoly0059s0060.1	34.97	80.66	79.21	1.20	2.69E-06	Armadillo/beta-catenin-like repeat
Mapoly0108s0018.1	1.94	48.15	57.86	4.58	2.89E-06	GDLS-like Lipase/Acylhydrolase
Mapoly0002s0059.1	142.88	67.38	80.66	-1.08	2.96E-06	Plant protein of unknown function
Mapoly0003s0127.1	54.54	114.55	94.22	1.07	3.55E-06	Polysaccharide lyase family 4, domain II;Polysaccharide lyase family 4, domain III;Rhamnogalacturonate lyase family
Mapoly0127s0004.1	196.61	399.66	410.04	1.02	3.70E-06	GDLS-like Lipase/Acylhydrolase
Mapoly0013s0012.1	31.58	0.00	45.40	-20.25	4.21E-06	Transketolase, thiamine diphosphate binding domain;Transketolase, pyrimidine binding domain;Transketolase, C-terminal domain
Mapoly0047s0034.1	29.79	74.57	64.52	1.32	4.87E-06	GRAS domain family
Mapoly0015s0037.1	13109.41	33577.98	44271.06	1.36	5.14E-06	NA
Mapoly0116s0046.1	625.36	301.97	785.52	-1.05	6.15E-06	Chitinase class I;Chitin recognition protein
Mapoly0114s0001.1	41.85	128.12	253.28	1.61	6.49E-06	Iron permease FTR1 family
Mapoly0011s0040.1	363.88	158.97	277.72	-1.20	7.14E-06	Glycosyl hydrolase family 46
Mapoly0017s0028.1	1230.55	113.67	482.71	-3.44	7.25E-06	Protein kinase domain
Mapoly0005s0003.1	41.31	127.22	169.52	1.63	9.89E-06	NA
Mapoly0095s0031.1	75.03	243.12	127.33	1.70	1.07E-05	POT family
Mapoly0122s0035.1	1065.32	2142.37	1313.13	1.01	1.10E-05	Calcineurin-like phosphoesterase;Iron/zinc purple acid phosphatase-like protein C
Mapoly0033s0095.1	51.64	137.51	144.70	1.41	1.19E-05	NA
Mapoly0160s0032.1	101.30	206.20	217.69	1.03	1.23E-05	Partial alpha/beta-hydrolase lipase region;alpha/beta hydrolase fold
Mapoly0036s0050.1	43.22	92.26	97.89	1.09	1.50E-05	NA
Mapoly0011s0092.1	3215.02	6481.81	3371.60	1.01	1.52E-05	Phosphoesterase family
Mapoly0580s0001.1	438.80	200.32	352.73	-1.13	1.56E-05	Leucine rich repeat;Leucine Rich Repeat
Mapoly0015s0184.1	14.47	45.87	47.94	1.67	1.65E-05	NA
Mapoly0001s0050.1	786.36	36.68	280.63	-4.42	1.66E-05	F-box domain
Mapoly0040s0053.1	36.25	0.62	13.10	-5.88	1.88E-05	NA
Mapoly0052s0013.1	9.59	41.58	35.45	2.12	1.95E-05	Domain of unknown function DUF21
Mapoly0071s0004.1	127.78	284.89	229.42	1.16	2.50E-05	Development and cell death domain

Mapoly0079s0056.1	17.56	48.22	64.37	1.46	2.57E-05	PLAT/LH2 domain;Lipoxygenase
Mapoly0185s0031.1	57.14	146.34	175.78	1.36	2.87E-05	Xylanase inhibitor N-terminal;Xylanase inhibitor C-terminal
Mapoly0046s0045.1	1627.70	769.42	965.53	-1.08	3.39E-05	Glutathione S-transferase, C-terminal domain;Glutathione S-transferase, N-terminal domain
Mapoly0171s0025.1	104.45	664.32	323.42	2.67	4.42E-05	SNF2 family N-terminal domain;Helicase conserved C-terminal domain;Snf2-ATP coupling, chromatin remodelling complex
Mapoly0015s0192.1	18.99	54.01	37.67	1.51	4.63E-05	Male sterility protein;Male sterility protein
Mapoly0133s0022.1	99.47	37.16	52.44	-1.42	4.92E-05	NA
Mapoly0050s0107.1	133.01	2.66	45.22	-5.63	5.26E-05	Terpene synthase family, metal binding domain
Mapoly0051s0102.1	25.66	112.03	61.36	2.13	5.42E-05	Kinesin motor domain
Mapoly0111s0050.1	49.77	15.02	23.12	-1.73	5.50E-05	Aldo/keto reductase family
Mapoly0006s0107.1	85.61	20.07	40.05	-2.09	5.62E-05	C-5 cytosine-specific DNA methylase
Mapoly0012s0198.1	197.67	83.89	99.94	-1.24	5.78E-05	Retinal pigment epithelial membrane protein
Mapoly0012s0033.1	6.23	27.76	24.34	2.16	6.11E-05	NA
Mapoly0193s0014.1	5.02	43.05	49.73	3.09	6.56E-05	FAD-binding domain;Ferric reductase like transmembrane component;Ferric reductase NAD binding domain
Mapoly0004s0001.1	72.94	159.45	110.28	1.13	7.17E-05	ABC-2 type transporter;ABC transporter
Mapoly0008s0164.1	113.50	251.48	541.19	1.15	7.97E-05	GDSL-like Lipase/Acylhydrolase
Mapoly0112s0025.1	131.18	62.46	113.32	-1.07	8.05E-05	Cupin
Mapoly0090s0006.1	335.10	148.92	190.93	-1.17	8.43E-05	Leucine rich repeat;Leucine rich repeat;Leucine Rich Repeat;NB-ARC domain
Mapoly0193s0024.1	120.61	275.27	702.84	1.19	8.75E-05	Enoyl-(Acyl carrier protein) reductase
Mapoly0166s0025.1	5048.44	2211.61	2439.28	-1.19	8.89E-05	NA
Mapoly0206s0002.1	176.31	399.56	500.92	1.18	8.93E-05	Cyclic nucleotide-binding domain;Sodium/hydrogen exchanger family
Mapoly0037s0062.1	71.94	23.23	39.75	-1.63	9.30E-05	Exostosin family
Mapoly0010s0104.1	450.64	204.27	307.41	-1.14	0.000103683	NA
Mapoly0115s0006.1	17.77	91.08	52.43	2.36	0.000103767	Amino acid permease
Mapoly0008s0124.1	25.55	98.58	55.02	1.95	0.000104332	NA
Mapoly0135s0012.1	72.16	151.99	172.08	1.08	0.000108023	Protein of unknown function (DUF679)
Mapoly0097s0007.1	177.41	64.38	83.76	-1.46	0.000113699	Cysteine-rich secretory protein family
Mapoly0015s0187.1	15.46	51.74	46.50	1.75	0.000118054	NA
Mapoly0137s0006.1	558.74	1333.24	2279.35	1.25	0.000125799	NA
Mapoly0110s0044.1	59.27	125.86	111.69	1.08	0.000145036	F-box domain
Mapoly0342s0001.1	207.21	19.35	101.99	-3.42	0.00015905	D-mannose binding lectin
Mapoly0040s0044.1	1045.26	2565.24	4103.28	1.29	0.000160742	Oxidoreductase family, NAD-binding Rossmann fold;Oxidoreductase family, C-terminal alpha/beta domain
Mapoly0182s0024.1	64.30	128.65	136.24	1.00	0.000184511	Peroxidase
Mapoly0018s0008.1	6112.39	47.35	2054.00	-7.01	0.000189972	Ras family
Mapoly0182s0023.1	112.58	237.32	301.78	1.08	0.00020252	Peroxidase
Mapoly1268s0001.1	1.01	15.68	106.70	3.94	0.000222772	Cupin
Mapoly0026s0013.1	37.62	95.24	88.83	1.34	0.000232014	Polysaccharide lyase family 4, domain II;Polysaccharide lyase family 4, domain III;Rhamnogalacturonate lyase family
Mapoly0077s0034.1	157.97	318.30	293.74	1.01	0.000247977	GDSL-like Lipase/Acylhydrolase
Mapoly0107s0020.1	36.49	99.10	101.47	1.44	0.000257006	Major intrinsic protein
Mapoly0010s0035.1	152.33	69.00	110.35	-1.14	0.000292679	SAM dependent carboxyl methyltransferase
Mapoly0009s0002.1	495.61	163.77	262.29	-1.60	0.000294596	D-mannose binding lectin;Glycosyl hydrolases family 17
Mapoly0004s0210.1	256.63	109.24	187.41	-1.23	0.000326225	NA
Mapoly0282s0002.1	23.98	60.84	65.31	1.34	0.000328627	Partial alpha/beta-hydrolase lipase region;Alpha/beta hydrolase family
Mapoly0086s0060.1	42.28	86.27	70.27	1.03	0.00036252	Protein kinase domain;PAN-like domain;D-mannose binding lectin
Mapoly0202s0006.1	20.00	1.23	8.46	-4.02	0.000373742	Xyloglucan fucosyltransferase
Mapoly0018s0021.1	1334.64	8.74	448.06	-7.25	0.000374211	RING/Ubox like zinc-binding domain
Mapoly0203s0007.1	67.22	182.18	117.17	1.44	0.000388791	Xyloglucan endo-transglycosylase (XET) C-terminus;Glycosyl hydrolases family 16
Mapoly0185s0030.1	11.35	31.38	42.97	1.47	0.000410775	Xylanase inhibitor N-terminal;Xylanase inhibitor C-terminal

Mapoly0030s0160.1	126.16	271.82	148.50	1.11	0.000460881	NA
Mapoly0307s0003.1	723.85	338.59	470.60	-1.10	0.000478348	Rare lipoprotein A (RlpA)-like double-psi beta-barrel;Chitin recognition protein
Mapoly0019s0118.1	382.43	141.32	184.85	-1.44	0.000479599	NA
Mapoly0088s0038.1	149.61	56.44	96.08	-1.41	0.000495639	Leucine rich repeat
Mapoly0054s0093.1	480.68	968.17	1145.74	1.01	0.000496794	NA
Mapoly0071s0079.1	84.44	177.31	119.60	1.07	0.00052569	EF-hand domain pair
Mapoly0017s0009.1	1680.31	10.21	563.74	-7.36	0.000534847	CCT motif;tify domain;GATA zinc finger
Mapoly0049s0062.1	2289.87	659.47	1122.15	-1.80	0.000550496	Trichodiene synthase (TRI5)
Mapoly0027s0190.1	208.74	439.73	399.70	1.08	0.000561124	NA
Mapoly0739s0001.1	141.16	66.83	96.93	-1.08	0.000613684	Ankyrin repeat;Domain of unknown function;Ankyrin repeats (3 copies)
Mapoly0061s0017.1	40.31	93.04	184.30	1.21	0.000625714	Protein kinase domain;S-locus glycoprotein family;D-mannose binding lectin
Mapoly0106s0033.1	286.52	2791.46	1274.87	3.28	0.000673832	NA
Mapoly0017s0003.1	6925.19	42.22	2323.12	-7.36	0.000673832	RNA recognition motif. (a.k.a. RRM, RBD, or RNP domain)
Mapoly0016s0185.1	23.92	63.71	47.62	1.42	0.000679391	GDSL-like Lipase/Acylhydrolase
Mapoly0012s0095.1	0.00	8.28	6.94	5.45	0.000695611	SEC-C motif;OTU-like cysteine protease
Mapoly0003s0211.1	154.71	77.06	104.50	-1.00	0.000759113	SAM dependent carboxyl methyltransferase
Mapoly0020s0081.1	16.35	0.92	6.82	-4.15	0.000759113	Xyloglucan fucosyltransferase
Mapoly0061s0054.1	30.55	96.29	93.37	1.66	0.00078223	Cyclin, N-terminal domain
Mapoly0017s0004.1	803.03	6.91	269.98	-6.86	0.000787337	RNA recognition motif. (a.k.a. RRM, RBD, or RNP domain)
Mapoly0182s0012.1	29.83	68.50	45.96	1.20	0.00080592	NA
Mapoly0060s0038.1	51.15	14.59	24.17	-1.81	0.000831003	NA
Mapoly0066s0038.1	310.41	131.51	175.94	-1.24	0.00084005	Polysaccharide deacetylase;Chitin recognition protein
Mapoly0068s0087.1	0.65	24.71	132.35	5.19	0.000874892	Chlorophyll A-B binding protein

Paper II

Characterization of a natural, stable, reversible and colourful anthocyanidin network from *Sphagnum* moss based mainly on the yellow *trans*-chalcone and red flavylum cation forms

Helge Berland, Øyvind M. Andersen

Molecules, Special issue 'Natural colorants' (2021)

Article

Characterization of a Natural, Stable, Reversible and Colourful Anthocyanidin Network from *Sphagnum* Moss Based Mainly on the Yellow *Trans*-Chalcone and Red Flavylium Cation Forms

Helge Berland * and Øyvind M. Andersen *

Department of Chemistry, University of Bergen, P.O. 7803, N-5020 Bergen, Norway

* Correspondence: helge.berland@uib.no (H.B.); oyvind.andersen@uib.no (Ø.M.A.)

Abstract: Anthocyanins with various functions in nature are one of the most important sources of colours in plants. They are based on anthocyanidins or 3-deoxyanthocyanidins having in common a C15-skeleton and are unique in terms of how each anthocyanidin is involved in a network of equilibria between different forms exhibiting their own properties including colour. Sphagnorubin C (1) isolated from the cell wall of peat moss (*Sphagnum* sp.) was in fairly acidic and neutral dimethyl sulfoxide characterized by nuclear magnetic resonance (NMR) and ultraviolet–visible (UV–vis) absorption techniques. At equilibrium, the network of 1 behaved as a two–component colour system involving the reddish flavylium cationic and the yellow *trans*–chalcone forms. The additional D- and E-rings connected to the common C15-skeleton extend the π -conjugation within the molecule and provide both bathochromic shifts in the absorption spectra of the various forms as well as a low isomerization barrier between the *cis*- and *trans*-chalcone forms. The hemiketal and *cis*-chalcone forms were thus not observed experimentally by NMR due to their short lives. The stable, reversible network of 1 with good colour contrast between its two components has previously not been reported for other natural anthocyanins and might thus have potential in future photochromic systems. This is the first full structural characterization of any naturally occurring anthocyanin chalcone form.

Keywords: 3-deoxyanthocyanidin; A–E rings; *trans*-chalcone; structure elucidation; equilibrium network; colours; NMR

Citation: Berland, H.; Andersen, Ø. M.; Characterization of a Natural, Stable, Reversible and Colourful Anthocyanidin Network from *Sphagnum* Moss Based Mainly on the Yellow *Trans*-Chalcone and Red Flavylium Cation Forms. *Molecules* **2021**, *26*, 709. <https://doi.org/10.3390/molecules26030709>

Academic Editors: Eulogio J. Llorent-Martínez and Ruperto Bermejo-Román
Received: 31 December 2020
Accepted: 25 January 2021
Published: 29 January 2021

Publisher's Note: MDPI stays neutral with regard to jurisdictional claims in published maps and institutional affiliations.



Copyright: © 2021 by the authors. Licensee MDPI, Basel, Switzerland. This article is an open access article distributed under the terms and conditions of the Creative Commons Attribution (CC BY) license (<http://creativecommons.org/licenses/by/4.0/>).

1. Introduction

Anthocyanins are ubiquitous in plants, and the total number of anthocyanin structures identified after isolation from plant extracts is about 800. These pigments are mainly divided into two groups, anthocyanins and 3-deoxyanthocyanins, with the latter group lacking an oxygen-function on the anthocyanidin 3-position on the C-ring [1]. The vast majority of the common anthocyanins are based on just 6 different aglycones (anthocyanidins) varying with the substitutions on the B-ring, and range in colour from salmon red to dark purple and blue [2]. In addition, a third heterogenous group (pyranoanthocyanins) [3,4] formed from anthocyanins during storage and processing in plant-derived foods, has gained much attention mostly because of their influence on colour evolution in wine during maturation [5]. A couple of pyranoanthocyanins have also been reported to occur in minor amounts in intact plant materials, for instance strawberries [6]. The various pyranoanthocyanins have in common an extra pyranic ring formed by cyclic addition onto both carbon 4 and the hydroxyl group at carbon 5 of the anthocyanidin skeleton. In solution, each anthocyanin exists in a network of reactions between the flavylium cation, hemiketals, chalcones and quinoidal bases [7–9]. The vast majority of structure elucidation

tions of anthocyanins have been undertaken in acidic environments on the flavylium cation form, which is considered to be the most stable form. In recent years it has been shown that synthetic flavylium compounds analogous to anthocyanidins also possess the same general network of chemical reactions [10].

In this context, pigment **1**, Sphagnorubin C isolated from sphagnum moss, is an interesting molecule belonging to the 3-deoxyanthocyanidin group. However, due to the two extraordinary aromatic rings connected to the A-ring, this pigment possesses properties not previously highlighted for any natural anthocyanidin/anthocyanin before. The purpose of this work was to present the first full structural characterization of a naturally occurring anthocyanidin/anthocyanin chalcone form. Other aims were to focus on how the extra aromatic rings of **1** extend the type of network of equilibrium forms displayed by natural anthocyanins, and to reveal the colours of the different forms of **1** in this network and their potential use.

2. Results

2.1. Structural Elucidation

The structures of the different forms of **1** present in deuterated dimethyl sulfoxide (*d*-DMSO), with and without deuterated trifluoroacetic acid (*d*-TFA), were elucidated using a combination of 1D (¹H) and 2D (heteronuclear single quantum coherence (HSQC), heteronuclear multiple bond coherence (HMBC), double-quantum filtered correlation spectroscopy (DQF-COSY)) NMR experiments and high-resolution electrospray ionisation mass spectrometry (HR-ESI-MS).

2.1.1. Elucidation of the Flavylium Cationic Form of **1**

The ¹H spectrum of **1** dissolved in 5% *d*-TFA in *d*-DMSO (*v/v*) showed an aromatic region corresponding to 10 proton signals (see supplementary Figure S1). Three of these protons belonged to an AMX coupling pattern at δ 8.09 ppm (d, 2.2 Hz; H2'), δ 7.16 ppm (d, 8.6 Hz; H5') and δ 8.26 ppm (dd, 2.2, 8.6 Hz; H6'), which together with one methoxy group at δ 4.03 ppm coupled to C3' shown through cross-peaks in the HMBC spectrum (Supplementary Figure S2), were similar to the corresponding signals of the B-ring of the anthocyanidin peonidin [11]. The rest of the proton and carbon atoms of the B-ring were assigned (Table 1) based on the HMBC and HSQC spectra (Supplementary Figure S3). The aromatic region also contained a signal with a rather downfield chemical shift (10.04 ppm) typical for anthocyanidin H4 protons. This signal having a coupling constant of 9.1 Hz, was shown by the DQF-COSY spectrum (Supplementary Figure S4) to be coupled to a proton at δ 8.74 ppm (H3). Both H4 and H3 as well as H2' had cross-peaks with C2 (δ 168.98 ppm) in the HMBC spectrum, supporting the assignment of a 3-deoxyanthocyanidin C-ring. The rest of the carbon atoms of this ring was assigned by the HMBC spectrum. In this spectrum the proton at δ 8.13 ppm (H12) has in common with H4 a cross-peak with C12a (δ 158.35 ppm), and in common with H3 a cross-peak with C4a (δ 117.81 ppm). The H12 proton also helped to assign the second methoxy group to C11, by its cross-peaks with this carbon (δ 168.68 ppm) (Figure 1). The remaining carbon atoms of the A-ring, C10b and C4b, were assigned by cross-peaks with H12 (δ 8.13/119.70 ppm) and H4 (δ 10.04/129.43 ppm), respectively.

The elucidation of the unusual D- and E-rings started with assignment of H5 (δ 8.72 ppm, d 9.0 Hz) having in common with H12 (δ 8.13 ppm, s) a cross-peak to C10b (δ 8.72/119.70 ppm) in the HMBC spectrum (Figure 1). H5 showed in the DQF-COSY spectrum cross-peak at δ 8.72/8.20 ppm, used for assignment of H6. This latter proton had in common with H4 cross-peak to C4b (δ 8.20/129.43 ppm), and in common with H7 (δ 7.47 ppm, s) cross-peak to C10a (δ 8.20/123.77 ppm) in the HMBC spectrum. The last carbon of the D-ring, C6a, was assigned by the cross-peak at δ 8.72/129.27 ppm (H5/C6a). This carbon also showed a cross-peak to H10 of the E-ring (δ 9.05/129.27 ppm). H10 had another ³J_{HC} cross-peak to C8 (δ 9.05/147.57 ppm). The assignments of the remaining C-atom of E-

ring, C9, was revealed by the $^3J_{\text{HC}}$ cross-peak between H7 and C9 (δ 7.47/147.99 ppm). With all the proton signals assigned, the HSQC spectrum confirmed the chemical shifts of the corresponding tertiary carbon atoms (Figure 1). The positive mode HR-ESI-MS spectrum of **1** in acidified DMSO showed a molecular ion at m/z 415.11833 corresponding to the empirical formula $\text{C}_{25}\text{H}_{19}\text{O}_6^+$ (calc. m/z 415.11816), which is in agreement with **1** in its flavylum cationic form. See supplementary figure S7 for the MS spectrum.

Table 1. Sphagnorubin C (**1**) ^1H and ^{13}C -NMR data of the flavylum cation form in 5% *d*-TFA in *d*-DMSO (*v/v*) and the *trans*-chalcone form (after 24 h of equilibration) in pure *d*-DMSO.

Position flav	Position <i>t</i> -chal	^1H δ (ppm) <i>J</i> (Hz) flav	^1H δ (ppm) <i>J</i> (Hz) <i>t</i> -chal	^{13}C δ (ppm) flav	^{13}C δ (ppm) <i>t</i> -chal
2	CO			168.98	187.78
3	α	8.74 <i>d</i> 9.0	7.97 <i>d</i> 15.4	113.28	123.38
4	β	10.04 <i>d</i> 9.1	8.34 <i>d</i> 15.4	148.17	136.88
4a	1			117.81	108.77
4b	10a			129.43	132.83
5	10	8.72 <i>d</i> 9.0	7.87 <i>d</i> 9.2	117.89	118.60
6	9	8.20 <i>d</i> 8.9	7.67 <i>d</i> 9.2	131.49	128.25
6a	8a			129.27	125.74
7	8	7.47 <i>s</i>	7.18 <i>s</i>	111.95	111.62
8	7			147.68	145.02
9	6			147.99	146.10
10	5	9.05 <i>s</i>	8.89 <i>s</i>	112.43	112.61
10a	4b			123.77	124.12
10b	4a			119.70	114.23
11	4			168.68	159.91
12	3	8.13 <i>s</i>	6.90 <i>s</i>	97.68	98.60
12a	2			158.35	156.38
1'	1'			120.15	130.09
2'	2'	8.09 <i>d</i> 2.2	7.56 <i>d</i> 2.0	112.18	111.35
3'	3'			148.92	147.69
4'	4'			155.39	151.31
5'	5'	7.16 <i>d</i> 8.6	6.93 <i>d</i> 8.2	116.83	115.08
6'	6'	8.26 <i>dd</i> 2.2, 8.6	7.59 <i>dd</i> 2.0, 8.2	125.46	122.84
MeO-C3'	MeO-C3'	4.03 <i>s</i>	3.87 <i>s</i>	56.49	55.56
MeO-C11	MeO-C4	4.44 <i>s</i>	4.08 <i>s</i>	58.15	55.61

s: singlet, *d*: doublet, *dd*: doublet of doublets

2.1.2. Elucidation of the *Trans*-Chalcone Form of **1**

The ^1H spectrum of **1** dissolved in pure *d*-DMSO and equilibrated at room temperature for 24 h showed, in addition to signals of the flavylum cationic form, a set of peaks corresponding to another form of **1**. Resonances of three of these protons (H2', H5' and H6') had a similar AMX coupling pattern as elucidated for the B-ring of the flavylum form (Table 1). The carbon resonances of this ring were determined by the cross-peaks in the HSQC and HMBC spectra of this sample (Figure 1). Interestingly, both H2' and H6' had cross-peaks in the HMBC spectrum to the same carbon at δ 187.78 ppm corresponding to a carbonyl function. This carbonyl group also showed cross-peaks to two protons (H α and H β) (Figure 1), which coupled with each other with a large coupling constant (15.4 Hz) typical for a *trans*-alkene. The H α proton also had a cross-peak to C1 (δ 7.97/108.77 ppm), while H β also showed cross-peaks to C1 (δ 8.34/108.77 ppm) and C2 (δ 8.34/156.38 ppm), which were in accordance with an 'open C-ring' of a chalcone form. The ^1H - ^1H coupling patterns of the five remaining protons of this second form of **1** in the proton and

DQF-COSY spectra were similar to the corresponding patterns of the analogous protons of the A-, D- and E-rings of the flavylium cationic form of **1**. See supplementary figure S5 for the DQF-COSY spectrum. As described above for the flavylium cationic form, the tertiary carbon atoms of the A-, D- and E-rings of the second form were assigned from cross-peaks in the HSQC spectrum (see supplementary Figure S6) after cross-referencing to cross-peaks in the HMBC spectrum (Figure 1). After assignments of the remaining quaternary carbon atoms of these rings (Table 1) by the cross-peaks in the HMBC spectrum, the second form of **1** was elucidated to be the *trans*-chalcone form of **1**. The negative mode HR-ESI-MS spectrum of a sample of this *trans*-chalcone form showed a molecular ion at m/z 431.11338 corresponding to the empirical formula $C_{25}H_{19}O_7$ (calc. m/z 431.11308), in agreement with a deprotonated *trans*-chalcone form of **1**. See supplementary figure S8 for the MS spectrum.

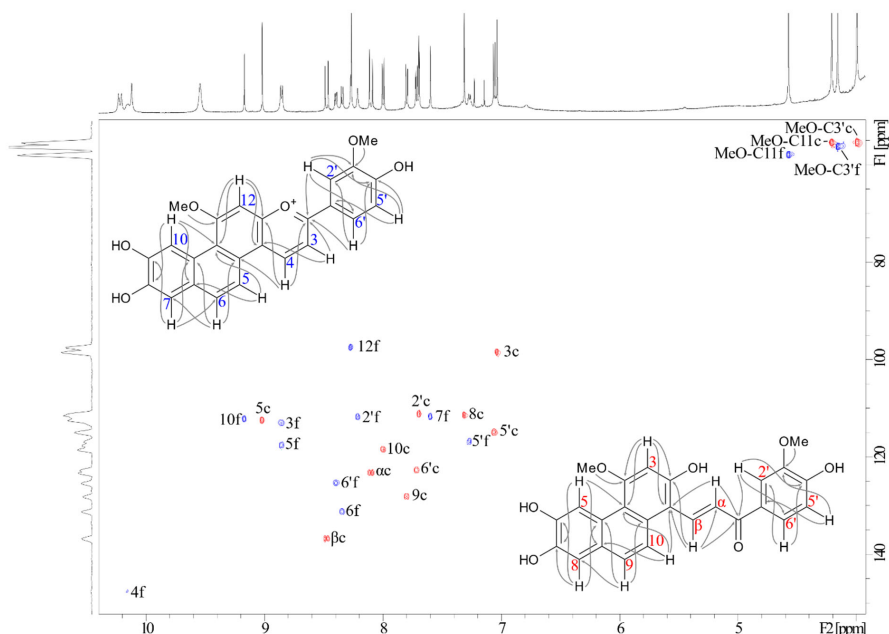
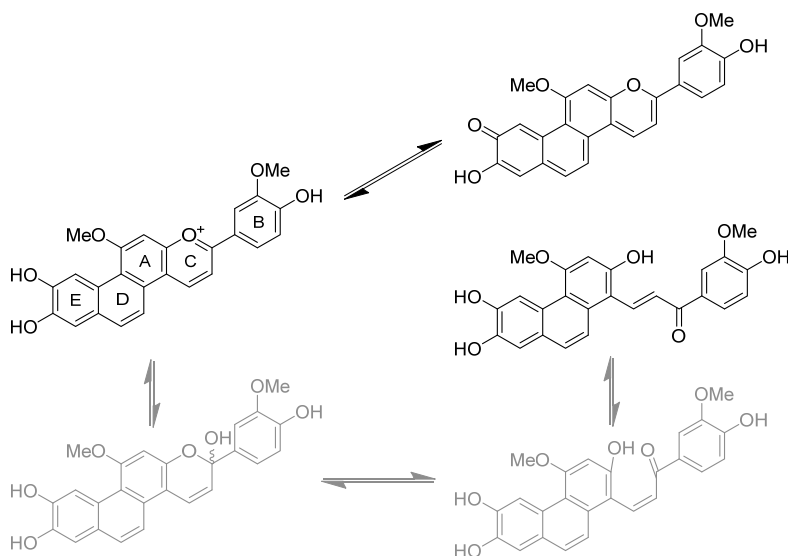


Figure 1. Heteronuclear single quantum coherence (HSQC) nuclear magnetic resonance (NMR) spectrum of Sphagnorubin C (**1**) in pure deuterated dimethyl sulfoxide (*d*-DMSO) after equilibration for 24 h, showing the ^1H - ^{13}C cross-peaks of both the flavylium cation (blue) and the *trans*-chalcone (red) forms. The ^1H -NMR spectrum and the ^{13}C -NMR projection of **1** are aligned on the top and left axes, respectively. The flavylium cation (blue numbers) and *trans*-chalcone (red numbers) structures are supplied with arrows showing long-range ^1H - ^{13}C heteronuclear multiple bond coherence (HMBC) cross-peaks. The flavylium cation HMBC cross-peaks are collected from a sample of **1** dissolved in 5% deuterated trifluoroacetic acid (*d*-TFA) in *d*-DMSO.

2.2. The Network of Anthocyanin Forms

The red sample of **1** dissolved in 5% *d*-TFA in *d*-DMSO (*v/v*) (sample A), showed in the NMR spectra only the presence of signals corresponding to the flavylium cation form, also during storage for 88 days at -20 °C. When **1** was dissolved in pure *d*-DMSO (sample B), the first ^1H spectrum recorded after 30 min also revealed the presence of just the flavylium cationic form. However, by regular recordings of ^1H spectra throughout 24 h at room temperature another set of peaks belonging to the characterised *trans*-chalcone form, were recognized. During this period the flavylium cation and *trans*-chalcone forms were

stabilised at a 1:1 equilibrium ratio, and the colour of the sample had turned orange. No hemiketal or *cis*-chalcone forms nor any degradation products were detected in the NMR spectra. After storage for 76 days at $-20\text{ }^{\circ}\text{C}$, sample B was acidified with 5% *d*-TFA. Following 1 h of storage of this ‘new’ sample B at room temperature, the NMR spectra still revealed an approximate 1:1 equilibrium ratio of the *trans*-chalcone and flavylium forms without distinctive signs of other compounds. However, after 6 days in a frozen solvent at $-20\text{ }^{\circ}\text{C}$ the flavylium cation and only minor amounts of the *trans*-chalcone form occurred in the sample, and this latter form was completely gone after 4 more days. This network consisting of the pure reddish flavylium cation and the orange coloured flavylium cation/*trans*-chalcone mixture (1:1) as endpoints (Scheme 1), thus seemed to be both fully stable and reversible under the changing pH conditions described above, without any signs of plausible hemiketal or *cis*-chalcone forms nor any degradation products.



Scheme 1. The hemiketal and *cis*-chalcone forms were short-lived and not experimentally detected (represented in the figure with faded structures). The quinoidal base in the figure represents various structures differing in the position of the carbonyl function.

The colours of the network of various anthocyanidin forms of **1** were also studied using visible absorption spectroscopy having faster sampling time and less demand for sample amounts per experiment compared to the NMR experiments. To reduce possible effects of residual water and acid coming from the isolation process, the bulk sample from where samples A and B originated was treated according to Section 4.2 to give samples C–F. Sample C (**1** dissolved in 0.5% TFA in DMSO) had the characteristic red colour of the flavylium cationic form with a λ_{max} around 540 nm in its visible absorption spectrum. When **1** was dissolved in pure DMSO (sample D), a relatively slow transformation from red, though orange, to yellow was observed. The yellow solution had its λ_{max} around 420 nm (Figure 2a), in accordance with the transformation from the red flavylium cationic form into the yellow *trans*-chalcone form observed in the NMR experiments described above. However, contrary to sample B, sample D showed an almost complete conversion from the flavylium cation form to the *trans*-chalcone form (reasoned by the low absorbance of the flavylium cation form at 540 nm, Figure 2a) reaching equilibrium after circa 14 h. After another 24 h, sample D was acidified with 5% TFA (*v/v*) (sample E). Similarly, as

observed in the NMR experiments described above, a slow transformation of the *trans*-chalcone form back to the flavylum cationic form was recognized by colour change from yellow to red, reaching equilibrium after circa 16 h (Figure 2b). After another 24 h period, the flavylum cation absorbance of sample E was at 97% of its initial absorbance at 540 nm in sample D. The 3% reduction in absorbance at 540 nm in sample E was in accordance with the volume of the added acid to sample D. The flavylum cationic form thus seemed to be fully regenerated from the *trans*-chalcone form, without any sign of degradation.

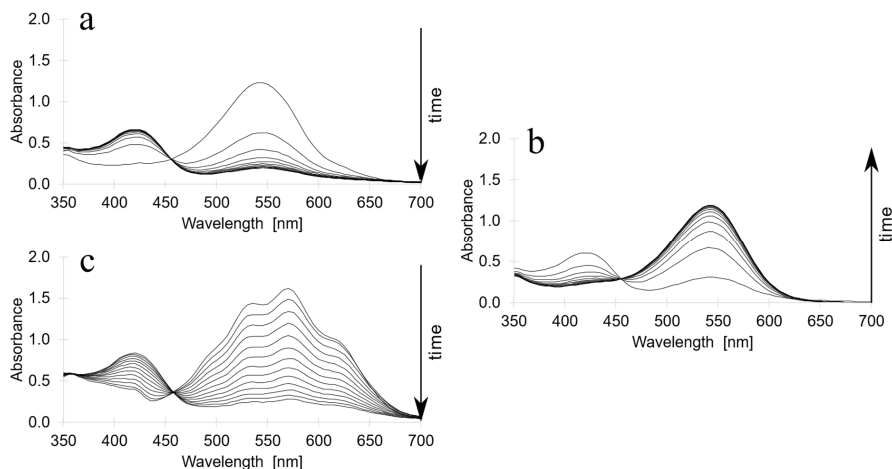


Figure 2. Visible absorption spectra of samples of Sphagnorubin C (1) recorded at 2-h intervals for 24 h, with different pre-treatments of the samples (see section 4.2). (a) Sample D dissolved in pure DMSO: The spectra show the decrease of the flavylum cation form (λ_{\max} at 540 nm) and the increase of the *trans*-chalcone form (λ_{\max} at 420 nm) with time. Equilibration is obtained after circa 14 h. (b) Sample E (Sample D after 24 h acidified with 5% TFA): The spectra show the increase of the flavylum cation form and the decrease of the *trans*-chalcone form with time. (c) Sample F₃ (see section 4.2) dissolved in pure *d*-DMSO: The spectra show the decrease of the quinoidal forms and the increase of the *trans*-chalcone form with time. F₃ has initially a dark blue/purple colour typical for quinoidal forms. 5% TFA was also added to sample F₃ after 24 h, which gave virtually identical results to those described for sample E. Note the isosbestic point at 455 nm in all the three spectra series. The spectra were recorded at room temperature.

A typical anthocyanidin network also includes quinoidal structures, which are formed in simple acid-base reactions starting with the flavylum cation under near neutral to basic pH conditions [7]. The importance of the impact of minor amounts of residual water/acid in the pigment 1 sample (here sample F) on such acid-base reactions is visualized in Figure 3. The red line represents the first recorded visible absorption spectrum of sample F₁ purified at the same stage as sample D (see Section 4.2). Here sample F₁ has its λ_{\max} at 540 nm, in accordance with the flavylum cationic form. The purple and blue lines in represent the first recorded visible absorption spectrum of samples F₂ and F₃, respectively. Samples F₂ and F₃ were prepared by adding respectively one and two purification steps in addition to those used for preparation of F₁. Each of these purification steps included adding pure methanol to the pigment sample followed by evaporation to dryness under a stream of nitrogen before pure DMSO (*d*-DMSO for F₃) finally was added as solvent. In these additional steps minor amounts of residual water/acid was removed from the sample, and the pigment obtained its neutral form. Sample F₃ gave initially a dark blue/purple colour when dissolved in pure deuterated DMSO. The initial visible absorption spectrum of this sample (blue line in Figure 3) having its λ_{\max} at 570 nm and additional shoulders above 600 nm, was in accordance with quinoidal forms of 1. The initial visible

absorption spectrum of sample F₂ (purple line in Figure 3) showed an intermediate spectrum between the spectra of F₁ and F₃, respectively, in accordance with a mixture of flavylum cation and quinoidal forms of **1**. Visible absorption spectra of sample F₃ were also recorded every 2 h for 24 h (Figure 2c), which also showed the slow transformation from the quinoidal forms to the *trans*-chalcone. These observations were in accordance with the formation of the flavylum cationic form from the quinoidal forms before the reactions towards the thermodynamically more stable *trans*-chalcone started (Scheme 1), as described above for sample D.

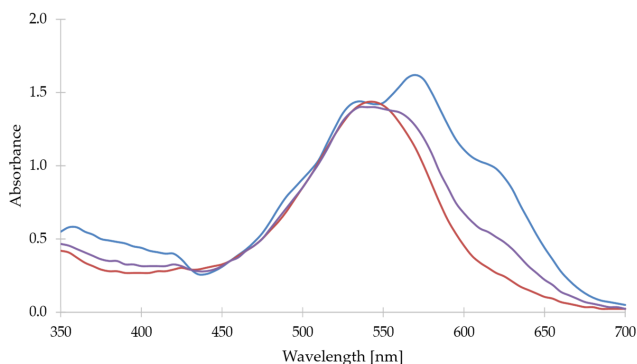


Figure 3. Visible absorption spectra of samples F₁ (red), F₂ (purple) and F₃ (blue) of Sphagnorubin C (**1**). The samples, which have different pre-treatment (see Section 4.2), were dissolved in pure DMSO/*d*-DMSO. The spectra show that different amounts of the flavylum cationic form were transformed into quinoidal forms depending on the pre-treatment of each of the samples. The spectra are normalised to the isosbestic point at 455 nm.

3. Discussion

The structure of Sphagnorubin C (**1**) in its flavylum cation form has previously been elucidated using derivatisation techniques in combination with ultraviolet–visible (UV–Vis), infrared (IR) and ¹H spectroscopy and mass spectrometry [12,13]. In a comparison of the assignments of ¹H shift values verified for **1** in its flavylum cation form in the same solvent (DMSO), complete assignments of H2' and H6' and a switch between H12 and H7 were the only differences, which in the present study were determined by 2D NMR techniques.

Pigment **1** has previously not been supplied with ¹³C-NMR data. However, highly relevant for the present paper, the 3'-OH analogue (Sphagnorubin B) of **1** has previously been made into a pentaacetate-chalcone derivative in the slightly alkaline solvent when reacted with ethanoic anhydride and pyridine [13]. This derivative was supplied with ¹³C-NMR data, although many of the signals were not completely assigned.

Anthocyanidins and anthocyanins (anthocyanidin with glycosidic moieties) are outstanding compounds by virtue of the way they are involved in a series of equilibrium reactions giving rise to several forms (secondary structures). However, proper ¹H and ¹³C-NMR structural assignments of other forms than the flavylum cationic form, have with just a couple of exceptions not been addressed for anthocyanins and anthocyanidins. As far as we know the first proper spectroscopic data (UV–visible absorption spectrum) for any natural anthocyanin in its chalcone form was published by Brouillard, et al. [14]. In 1993, Santos, et al. [15] studied various equilibrium forms of malvidin 3,5-*O*-diglucoside (malvin), which coexisted in slightly acidic aqueous conditions. Two-dimensional nuclear Overhauser effect spectroscopy (NOESY) exchange correlation NMR spectra provided

valuable information about the structural transformations, including evidence for the relationship between the various equilibrium forms of malvin. For the first time the chalcone forms of a natural anthocyanin were characterized by assignments of the chemical shifts of the four protons of the anthocyanidin. Later the chemical proton shifts of the chalcone forms of malvidin 3-*O*-glucoside [16] and cyanidin 3-*O*-glucoside [17] have been assigned. Several forms of the pyranoanthocyanin vitisin A., including the chalcone form, have previously been reported to be distinguished by NMR [3]. However, the authors reported that complete unambiguous assignment of the ^{13}C -NMR signals of the chalcone form was not possible. More recently it has clearly been demonstrated that pyranoanthocyanins like vitisins are not able to form hemiketals [18,19], and as a consequence unable to form chalcone forms. Thus, the assignments of all ^1H and ^{13}C -NMR signals of the *trans*-chalcone structure of **1** is as far as we know, the first full structural characterization of a naturally occurring anthocyanin chalcone form.

The difference in structure between anthocyanidins and 3-deoxyanthocyanidins is the lack of oxygen function in the 3-position in the C-ring of the latter group. The impact of a reduced chromophore gives the common 3-deoxyanthocyanins (apigeninidin, luteolinidin and tricetinidin) yellow colours under acidic conditions compared to more scarlet to blue colours of analogous flavylum cationic forms of the common anthocyanins. Another even more striking effect of this hypsochromic shift in the absorption spectra under less acidic/neutral conditions is displayed by the colourless chalcone forms of the common 3-deoxyanthocyanins contrasting the yellow chalcone forms of the analogous anthocyanins. However, the colours of 3-deoxyanthocyanidins are positively reckoned to be much more stable than the colours of the analogous anthocyanins under slightly acidic conditions [20]. The network consisting of the flavylum cationic and *trans*-chalcone forms of pigment **1** in the present paper, proved the best of both of these attributes. The additional D- and E-rings extended the π -conjugation within the molecule and provided bathochromic shifts in the absorption spectra of the various forms of **1** compared to 3-deoxyanthocyanidins comprising only the normal A–C rings. Thus, the red flavylum cationic form of **1** had its absorption maximum (λ_{max}) at 540 nm, while the *trans*-chalcone form revealed a yellow colour and had its λ_{max} at 420 nm in pure DMSO.

How was it verified that pigment **1** had higher colour stability than the common anthocyanins (in this paper represented by peonidin 3-*O*-glucoside, **2**) under slightly acidic to neutral conditions? The flavylum cation and the two hemiketal enantiomers of **2** were in the ^1H NMR spectra in Figure 4 (right) represented by their anomeric protons (see Supplementary Table S1 for aromatic and anomeric ^1H -NMR data). In pure *d*-DMSO the flavylum cationic form of **2** was transferred within hours into two hemiketal forms (64% within 1.4 h or 93% after 4.9 h) (Figure 4, right, a–d), according to Scheme 2. Few traces of the probable yellow chalcone forms were observed (Figure 4, right). This is in accordance with previous papers reporting the chalcone forms to constitute typically less than 10% of the various equilibrium forms of anthocyanins (not 3-deoxyanthocyanidins) in slightly acidic or neutral aqueous solutions [8]. The important factor in this context was that the hemiketal forms of **2** (or other anthocyanins) were colourless, making the colour of the solution fade proportionally with the increase of the hemiketal forms. However, opposite to this pattern the red flavylum cation and the yellow *trans*-chalcone forms occurred in various proportions when **1** was examined under similar conditions as described for **2** (Figure 4, left, a–d). The *trans*-chalcone and flavylum cationic forms in the ^1H -NMR spectra are in Figure 4 (left) represented by their H3 and H6' protons, respectively. Since no colourless forms of **1** were observed in the NMR spectra, a gradual change from reddish flavylum cation colour towards yellow *trans*-chalcone colours were observed in the NMR spectra of this sample taken during storage (Figure 4, left, a–d). To characterize the reversibility of the two-components system described above between the flavylum cation and *trans*-chalcone forms of **1**, acid (5% *d*-TFA, *v/v*) was added to the equilibrated neutral sample (Figure 4, left, e–f). After 5–6 days of equilibration, the sample had turned back to its red flavylum cationic form, leaving only traces of the *trans*-chalcone form (Figure 4, left, g).

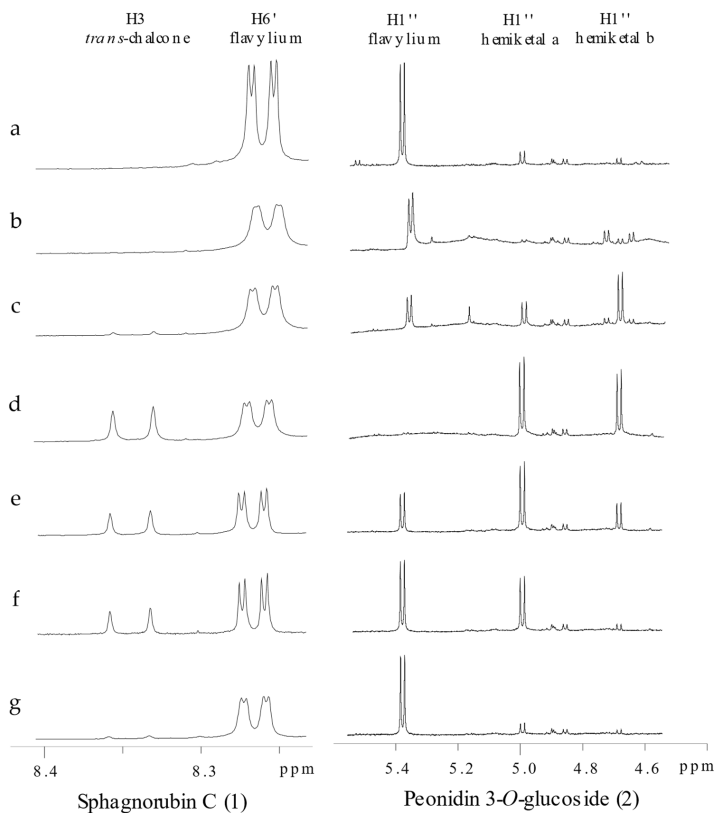
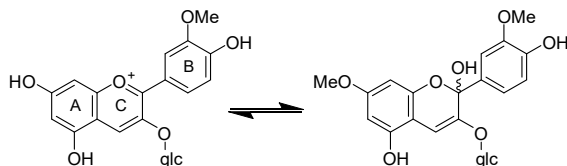


Figure 4. $^1\text{H-NMR}$ spectra of Sphagnorubin C (**1**, left) and peonidin 3-*O*-glucoside (**2**, right) showing selected signals of different equilibrium forms belonging to each of the pigments. The spectra are recorded when **1** and **2** are separately (a) dissolved in 5% *d*-TFA in *d*-DMSO, (b) dissolved in pure *d*-DMSO, (c) after samples **b** have been equilibrated for 1 h, (d) after samples **c** have been equilibrated for 3–7 days, (e) after samples **d** have been acidified with 5% *d*-TFA, (f) after samples **e** have been equilibrated for 1 h, (g) after samples **f** have been equilibrated for 5–6 days. The flavylium cation and *trans*-chalcone forms of **1** are represented by their $\text{H6}'$ and H3 protons, respectively, while both the flavylium cation and the two hemiketal enantiomers of **2** are represented by their anomeric $\text{H1}''$ protons. The spectra were recorded at 21 °C.



Scheme 2. Peonidin 3-*O*-glucoside (**2**) dissolved in pure *d*-DMSO. After 24 h storage the two hemiketal enantiomers were present at a 56:44 ratio, and only traces of other potential equilibrium forms were revealed.

It is well known that all anthocyanins, including 3-deoxyanthocyanidins, are represented by a network of chemical forms, which are reversibly interconverted by external stimuli such as pH variation, light, etc. [8]. Based on the results described above, the network depicted for **1** is presented in Scheme I. It can be viewed as a single acid-base equilibrium involving the flavylum cation and the overall conjugated base. The conjugated base represents both the quinoidal bases, hemiketal forms and the *cis*- and *trans*-chalcones. The hemiketal and *cis*-chalcone forms are short-lived, transient forms, which were not observed in the NMR spectra. In this network there is a low isomerization barrier between the *cis*- and *trans*-chalcone forms. Thus, at low pH values the reddish flavylum cationic form (λ_{\max} at 540 nm) is the only form occurring in considerable amounts, while at more moderately acidic and at neutral pH values the yellow *trans*-chalcone form (λ_{\max} at 420 nm) is increasing with pH to be the most dominant form. The group of Pina [10] has previously reported a similar network with similar colours for the synthetic compound 2-(4-hydroxystyryl)-1-naphthopyrylium. Here they reported that a photochromic system with good switching colours from yellow to red (or from orange to red depending on pH) based on this network could be designed. Another interesting paper from this group has also reported a similar natural photochromic system based on dracoflavylum [21]. However, this compound does not have the conjugation of the D- and E-rings of compound **1**, which gives less colour (λ_{\max} at 374 nm) and less occurrence of the *trans*-chalcone form compared to **1**. The occurrence of the *trans*-chalcone form was in this paper improved by stabilization of the *trans*-chalcone form in the presence of β -cyclodextrin. The common anthocyanins (but the 3-deoxyanthocyanins) have similar colours as **1** for their flavylum cationic and *trans*-chalcone forms. However, opposite to the network of **1**, these natural anthocyanins have a high isomerization barrier between their *cis*- and *trans*-chalcone forms and turn into colourless hemiketal forms under moderately acidic to neutral conditions. However, photochemistry of the colourless hemiketal forms of common anthocyanins have been shown to have a potential role in plant protection from UV-B radiation [22]. The stable, reversible two-component colour system involving the reddish flavylum cation and the yellow *trans*-chalcone forms of **1** might thus be of advantage compared to previously reported multistate systems of natural anthocyanins.

4. Materials and Methods

4.1. Isolation of *Sphagnorubin C* (**1**)

Sphagnorubins are natural pigments tightly bound to the cell walls of peat moss (*Sphagnum* sp.) [23], which makes them quite difficult to isolate. Additionally, in contrast to most anthocyanins, they are not soluble in water, and poorly soluble in pure methanol.

Brightly red coloured peat moss (8 kg wet wt.) was collected in the western part of Norway (60.2744 N, 5.4974 E), air dried and homogenised using a blender. The dried plant material was extracted 4 times for 24 h in 8 L 0.5% TFA in methanol (*v/v*). The combined extracts were concentrated to a low volume under reduced pressure. A low volume of 0.5% TFA in water (*v/v*) was added and the remaining methanol was removed under reduced pressure. The extract was partitioned against ethyl acetate, where three layers formed: water on the bottom, a thick layer of precipitate containing most of the Sphagnorubins in the middle and ethyl acetate on the top. The water and middle layer were removed and partitioned six more times against ethyl acetate. The purified extract was evaporated to dryness, recovered using a minimal volume of 0.5% TFA in methanol (*v/v*) and applied to a column of Amberlite XAD-7 resin (Supelco, Bellefonte, United States). Most of the pigments were eluted as a precipitate using 0.5% TFA in water (*v/v*), the eluate was evaporated to dryness under reduced pressure. Sphagnorubin C (**1**) was isolated from the extract using semi-preparative high-performance liquid chromatography (HPLC), which produced pure pigment suitable for 1D and 2D NMR spectroscopy and visible absorption spectroscopy.

4.2. Samples for Analysis

Each injection on the semi-preparative HPLC system yielded about 0.15 mg of pure **1**. One batch was used to produce sample A, which was dissolved in 5% *d*-TFA in *d*-DMSO for analysis on NMR. Another batch was used to produce sample B, which was dissolved in pure *d*-DMSO for analysis on NMR. A third batch was dissolved in 10 mL 0.5% TFA in methanol and aliquoted into samples appropriate for visible absorption spectroscopy. Each aliquot was evaporated to dryness under a stream of nitrogen. These aliquots were used to produce samples C, D, and F₁–F₄. Sample C was dissolved in 0.5% TFA in DMSO and sample D was dissolved in pure DMSO. Sample F₁ was identical to sample D, while samples F₂–F₄ was prepared by adding respectively one, two and three purification steps in addition to those used for preparation of F₁. Each of these purification steps included adding pure methanol to pigment sample followed by evaporation to dryness under a stream of nitrogen. Samples F₃ and F₄ gave identical results.

4.3. Semi-Preparative High-Performance Liquid Chromatography (HPLC)

Semi-preparative HPLC were performed using a Gilson 321 pump (Gilson, Inc., Middleton, WI, United States) equipped with an UltiMate 3000 variable wavelength detector (Thermo Fisher Scientific, Waltham, MA, United States) set at 540 nm, a 25 × 2.2 cm (10 μm particle size) Econosphere C18 column (Grace, Columbia, MD, United States). The mobile phases were A, 1% TFA in water (*v/v*), and B, 1% TFA in methanol (*v/v*), used at a flow of 15 mL/min. A solvent elution profile consisted of initial conditions of 30% B and the following isocratic and gradient elution: 0–14 min gradient to 40% B, 14–20 min gradient to 50% B, 20–30 min isocratic, 30–32 min gradient to 80% B, 32–38 min isocratic, and a finally 38–41 min gradient to 30% B. Prior to injections, samples were filtered through a 0.45 μm filter.

4.4. Analytical HPLC

Analytical HPLC was used to assess the purity of the extract during each step of the isolation procedure. The instrument used was an HP Agilent 1200 analytical HPLC system (HP/Agilent, Santa Clara, United States) equipped with a diode array detector at 520 nm and 280 nm, and a 250 × 25 mm (4.5 μm particle size) Ascentis RP-Amide column (Supelco, Bellefonte, United States). The mobile phases were A, 1% TFA in water (*v/v*), and B, 1% TFA in acetonitrile (*v/v*), used at a flow of 1 mL/min. A solvent elution profile consisted of initial conditions of 30% B and the following isocratic and gradient elution: 0–7 min gradient to 40% B, 7–10 min gradient to 50% B, 10–15 min isocratic, 15–17 min gradient to 80% B, 17–22 min isocratic, and 22–25 min gradient to 30%. Injections were 20 μL aliquots injected by an auto-sampler. Prior to injections, samples were filtered through a 0.45 μm filter.

4.5. Nuclear Magnetic Resonance (NMR) Spectroscopy

The NMR experiments were obtained using a Bruker Ultrashield Plus AV-600 MHz (Bruker, Billerica, MA, United States) at 600.13 and 150.92 MHz for ¹H and ¹³C spectra respectively, recorded at 21 °C. Deuterated dimethyl sulfoxide (*d*-DMSO) and deuterated trifluoroacetic acid (*d*-TFA) were used as solvents. ¹H and ¹³C signals of the spectra were calibrated using the *d*-DMSO residual signal at 2.50 ppm and 39.51 ppm, respectively.

4.6. Mass Spectrometry

Purified samples of both the flavylum cation and the *trans*-chalcone of **1** were analysed by high-resolution electron spray ionisation mass spectrometry (HR-ESI-MS). The spectra were recorded using a JEOL AccuTOF instrument (JEOL USA, Inc., Peabody, MA, United States). See supplementary Figures S7 and S8 for details about the individual MS spectra.

4.7. Visible Absorption Spectroscopy

A HunterLab UltraScan PRO spectrophotometer (Hunter Associates Laboratory, Inc., Reston, VA, United States) was used to record visible absorption spectra. Pure solvents were used as background and extracted from each spectrum. The instrument was calibrated every 24 h. During 24 h of interval sampling, the cuvettes were covered with parafilm. The data from the instrument were imported to Microsoft Excel for data analysis.

Supplementary Materials: Supplementary Table S1: Peonidin 3-*O*-glucoside (**2**) ¹H-NMR data. Supplementary Figure S1: ¹H-NMR spectrum of the flavylum cation form of Sphagnorubin C (**1**) dissolved in 5 % *d*-TFA in *d*-DMSO. Supplementary Figure S2: Heteronuclear Multiple Bond Correlation (HMBC) NMR spectrum of the flavylum cation form of Sphagnorubin C (**1**) dissolved in 5 % *d*-TFA in *d*-DMSO. Supplementary Figure S3: Heteronuclear Single Quantum Coherence (HSQC) NMR spectrum of the flavylum cation form of Sphagnorubin C (**1**) dissolved in 5 % *d*-TFA in *d*-DMSO. Supplementary Figure S4: Double-quantum filtered correlation spectroscopy (DQF-COSY) NMR spectrum of the flavylum cation form of Sphagnorubin C (**1**) dissolved in 5 % *d*-TFA in *d*-DMSO. Supplementary Figure S5: DQF-COSY NMR spectrum of the flavylum cation and *trans*-chalcone forms of Sphagnorubin C (**1**) dissolved in pure *d*-DMSO and equilibrated for 24 h before recording. Supplementary Figure S6: HMBC NMR spectrum of the flavylum cation and *trans*-chalcone forms of Sphagnorubin C (**1**) dissolved in pure *d*-DMSO and equilibrated for 24 h before recording. Supplementary Figure S7: Mass spectrometry spectrum of the flavylum cation form of Sphagnorubin C (**1**), and instrument settings used for the recording. Supplementary Figure S8: Mass spectrometry spectrum of the *trans*-chalcone form of Sphagnorubin C (**1**), and instrument settings used for the recording.

Author Contributions: Conceptualization, H.B. and Ø.M.A.; methodology, H.B.; writing—original draft preparation, H.B. and Ø.M.A.; writing—review and editing, H.B. and Ø.M.A.; supervision, Ø.M.A. All authors have read and agreed to the published version of the manuscript.

Funding: This research received funding for open access publication from the university library of University of Bergen, Bergen, Norway.

Institutional Review Board Statement: Not applicable.

Informed Consent Statement: Not applicable.

Data Availability Statement: The data presented in this study are available on request from the corresponding author.

Acknowledgments: We would like to thank Bjarte Holmelid for his support in recording HR-ESI-MS spectra of the samples of **1**, Kristiane Eikeland for providing initial thoughts on the isolation of **1**, and Ingrid Kyrkjebø for isolating the sample of **2**.

Conflicts of Interest: The authors declare no conflict of interest.

References

1. Stich, K.; Forkmann, G. Biosynthesis of 3-deoxyanthocyanins with flower extracts from *Sinningia cardinalis*. *Phytochemistry* **1988**, *27*, 785–789.
2. Andersen, Ø.M.; Jordheim, M. Chemistry of flavonoid-based colors in plants. In *Comprehensive Natural Products II: Chemistry and Biology*; Andersen, Ø.M., Markham, K.R., Eds.; Elsevier Science: Amsterdam, The Netherlands, 2010; Volume 3, pp. 547–614.
3. Bakker, J.; Bridle, P.; Honda, T.; Kuwano, H.; Saito, N.; Terahara, N.; Timberlake, C.F. Identification of an anthocyanin occurring in some red wines. *Phytochemistry* **1997**, *44*, 1375–1382.
4. Bakker, J.; Timberlake, C.F. Isolation, identification, and characterization of new color-stable anthocyanins occurring in some red wines. *J. Agric Food Chem.* **1997**, *45*, 35–43.
5. de Freitas, V.; Mateus, N. Formation of pyrananthocyanins in red wines: a new and diverse class of anthocyanin derivatives. *Anal. Bioanal. Chem.* **2011**, *401*, 1463–1473.
6. Andersen, Ø.M.; Fossen, T.; Torskangerpoll, K.; Fossen, A.; Hauge, U. Anthocyanin from strawberry (*Fragaria ananassa*) with the novel aglycone, 5-carboxypyranopelargonidin. *Phytochemistry* **2004**, *65*, 405–410.
7. Brouillard, R.; Delaporte, B. Chemistry of anthocyanin pigments .2. Kinetic and thermodynamic study of proton-transfer, hydration, and tautomeric reactions of malvidin 3-glucoside. *J. Am. Chem Soc.* **1977**, *99*, 8461–8468.
8. Pina, F.; Melo, M.J.; Laia, C.A.; Parola, A.J.; Lima, J.C. Chemistry and applications of flavylum compounds: a handful of colours. *Chem. Soc. Rev.* **2012**, *41*, 869–908.

9. Jurd, L. Anthocyanins and related compounds. I. Structural transformations of flavylum salts in acidic solutions. *J. Org. Chem.* **1963**, *28*, 987–991.
10. Gavara, R.; Leydet, Y.; Petrov, V.; Pina, F. Photochemistry of 2-(4-hydroxystyryl)-1-naphthopyrylium. *Photochem. Photobiol. Sci.* **2012**, *11*, 1691–1699.
11. Saito, N.; Tatsuzawa, F.; Kasahara, K.; Yokoi, M.; Iida, S.; Shigihara, A. Acylated peonidin glycosides in the slate flowers of *Pharbitis nil*. *Phytochemistry* **1996**, *41*, 1607–1611.
12. Vowinkel, E. Torfmoosmembranochrome, 2. Die Struktur des Sphagnorubins. *Chem. Ber.* **1975**, *108*, 1166–1181.
13. Mentlein, R.; Vowinkel, E. Die roten Wandfarbstoffe des Torfmooses *Sphagnum rubellum*. *Liebigs Ann. Chem.* **1984**, *1984*, 1024–1035.
14. Brouillard, R.; Delaporte, B.; EL Hage Chahine, J.M.; Dubois, J.E. Chemistry of anthocyanin pigments. 4- Absorption spectrum of the chalcone form of malvidin 3- Glucoside. *J. Chim. Phys.* **1979**, *76*, 273–276.
15. Santos, H.; Turner, D.L.; Lima, J.C.; Figueiredo, P.; Pina, F.S.; Maçanita, A.L. Elucidation of the multiple equilibria of malvin in aqueous solution by one- and two-dimensional NMR. *Phytochemistry* **1993**, *33*, 1227–1232.
16. Houbiers, C.; Lima, J.C.; Maçanita, A.L.; Santos, H. Color stabilization of malvidin 3-glucoside: Self-aggregation of the flavylum cation and copigmentation with the Z-chalcone form. *J. Phys. Chem. B* **1998**, *102*, 3578–3585.
17. Fernandes, A.; Ivanova, G.; Brás, N.F.; Mateus, N.; Ramos, M.J.; Rangel, M.; de Freitas, V. Structural characterization of inclusion complexes between cyanidin-3-O-glucoside and β -cyclodextrin. *Carbohydr. Polym.* **2014**, *102*, 269–277.
18. Oliveira, J.; Mateus, N.; de Freitas, V. Network of carboxypyranomalvidin-3-O-glucoside (vitisin A) equilibrium forms in aqueous solution. *Tetrahedron Lett.* **2013**, *54*, 5106–5110.
19. Oliveira, J.; Mateus, N.; Silva, A.M.S.; de Freitas, V. Equilibrium forms of vitisin B pigments in an aqueous system studied by NMR and visible spectroscopy. *J. Phys. Chem. B* **2009**, *113*, 11352–11358.
20. Mazza, G.; Brouillard, R. Recent developments in the stabilization of anthocyanins in food-products. *Food Chem.* **1987**, *25*, 207–225.
21. Lopes-Costa, T.; Basílio, N.; Pedrosa, J.M.; Pina, F. Photochromism of the natural dye 7, 4'-dihydroxy-5-methoxyflavylium (dracoflavylum) in the presence of (2-hydroxypropyl)- β -cyclodextrin. *Photochem. Photobiol. Sci.* **2014**, *13*, 1420–1426.
22. Costa, D.; Galvão, A.M.; Di Paolo, R.E.; Freitas, A.A.; Lima, J.C.; Quina, F.H.; Maçanita, A.L. Photochemistry of the hemiketal form of anthocyanins and its potential role in plant protection from UV-B radiation. *Tetrahedron* **2015**, *71*, 3157–3162.
23. Rudolph, H.; Vowinkel, E. Notizen: Sphagnorubin, ein kristallines Membranochrom aus *Sphagnum magellanicum*. *Zeitschrift für Naturforschung B* **1969**, *24*, 1211–1212.

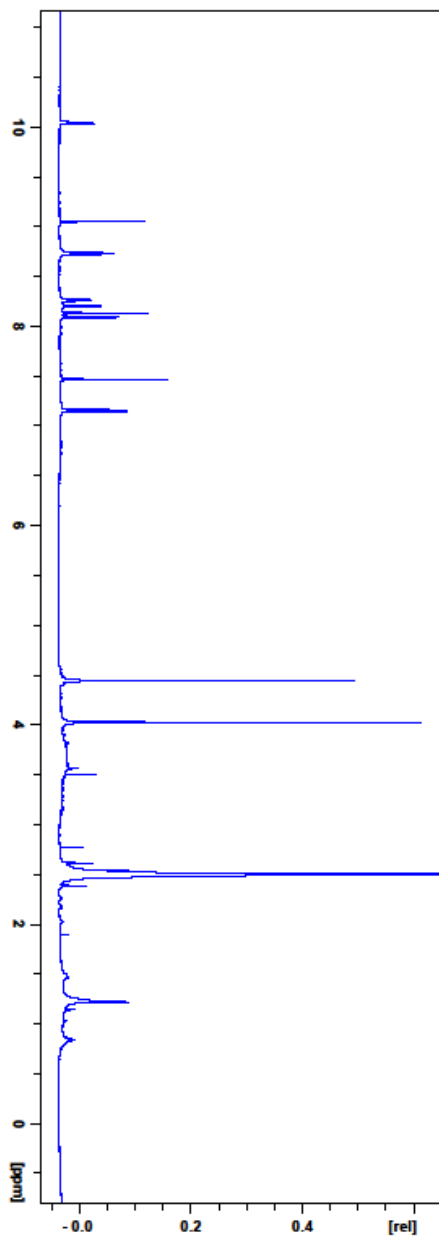


Figure S1 1H NMR SPHC flavylum.pdf

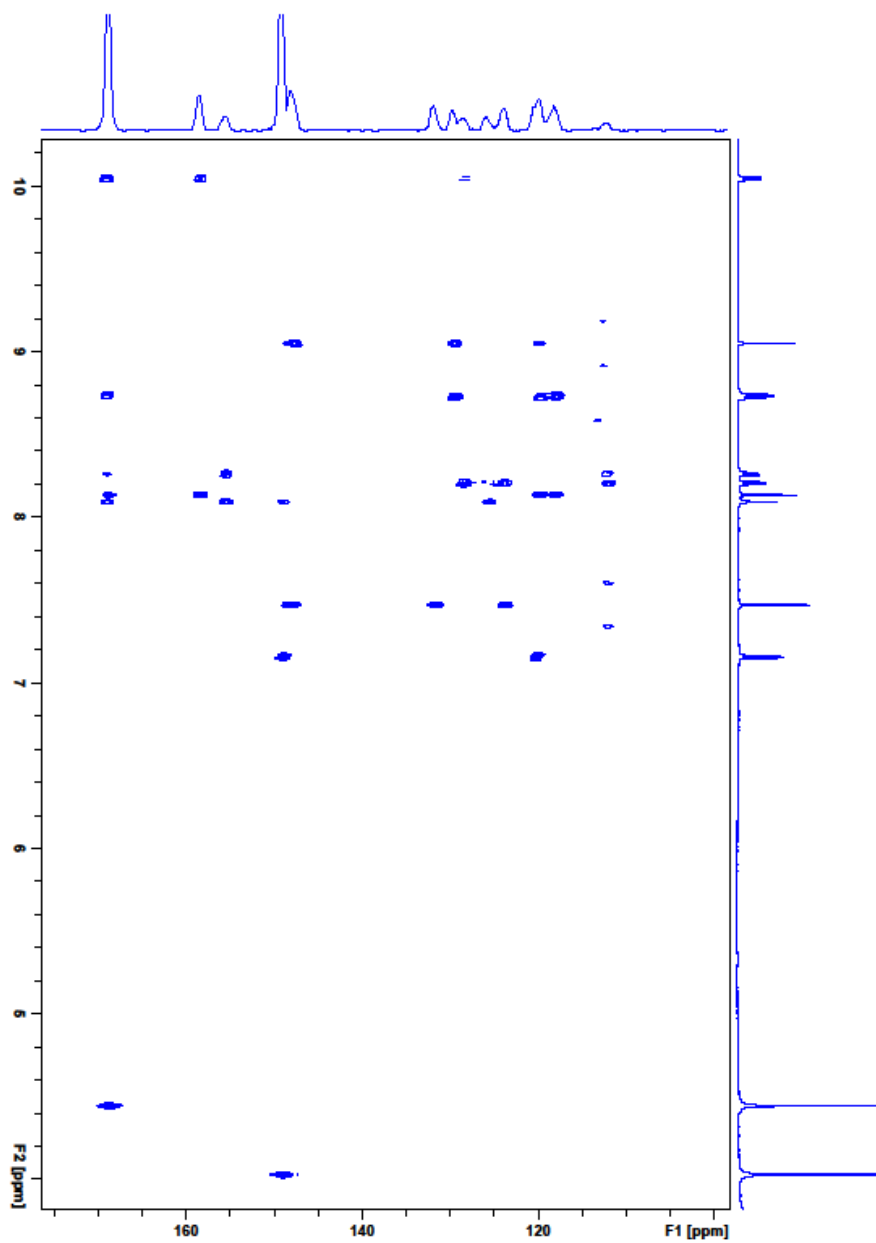


Figure S2 HMBC in acidic DMSO.pdf

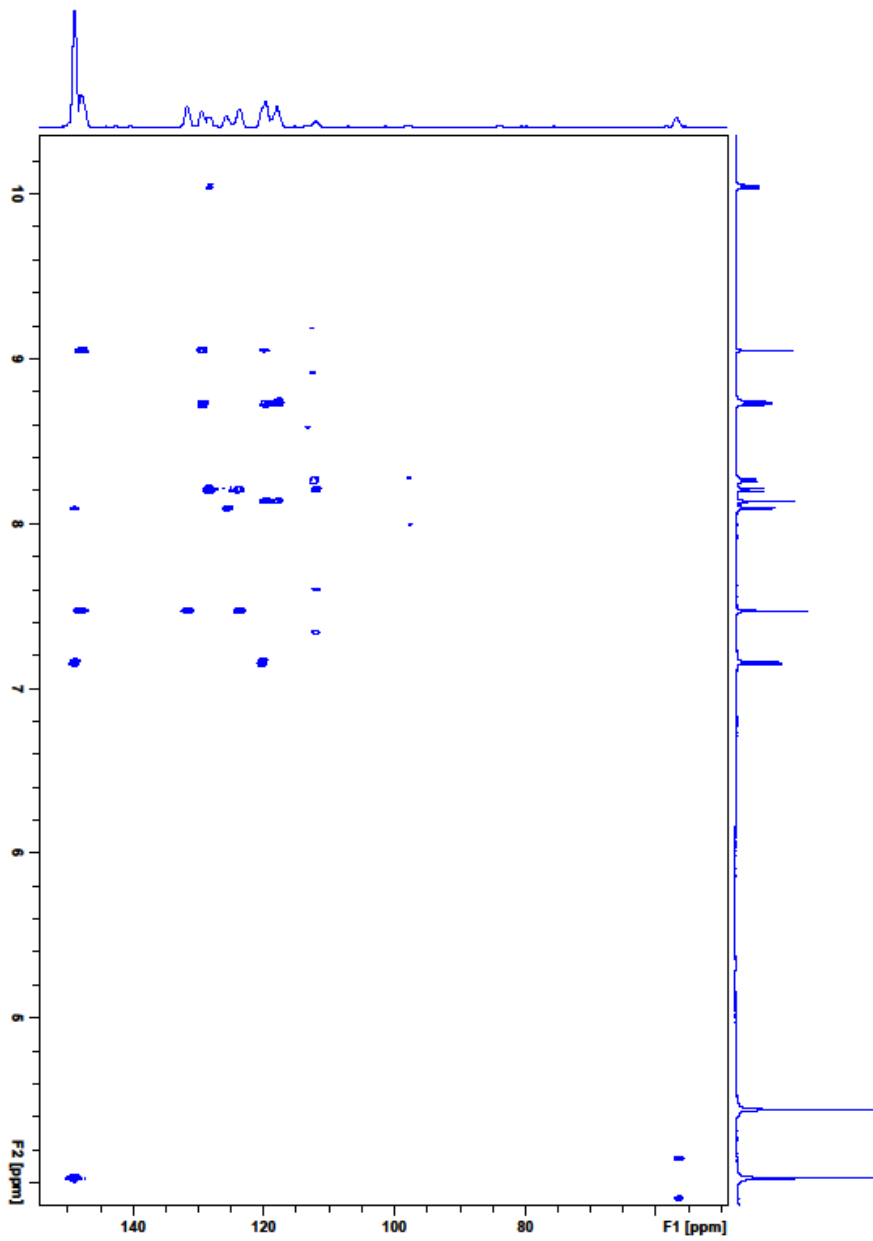


Figure S3 HSQC in acidic DMSO.pdf

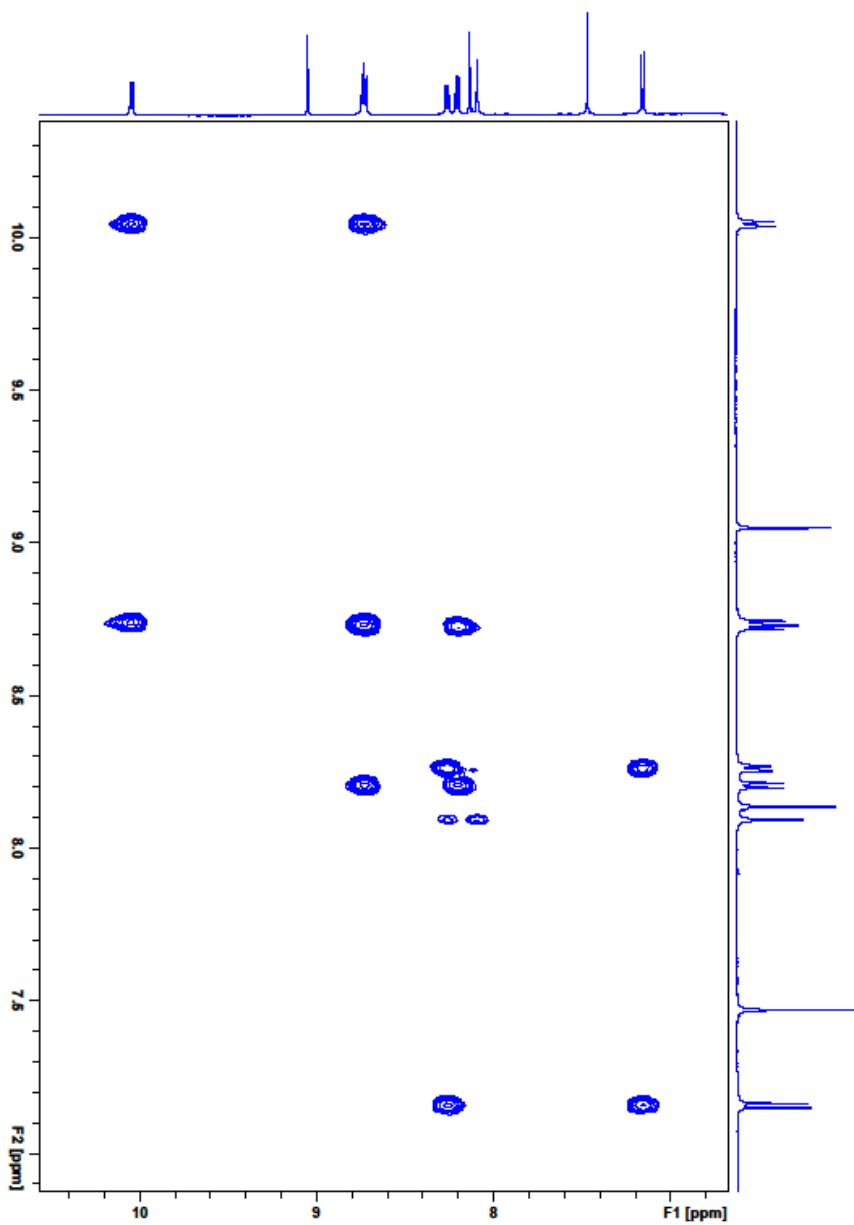


Figure S4 DQF-COSY in acidic DMSO.pdf

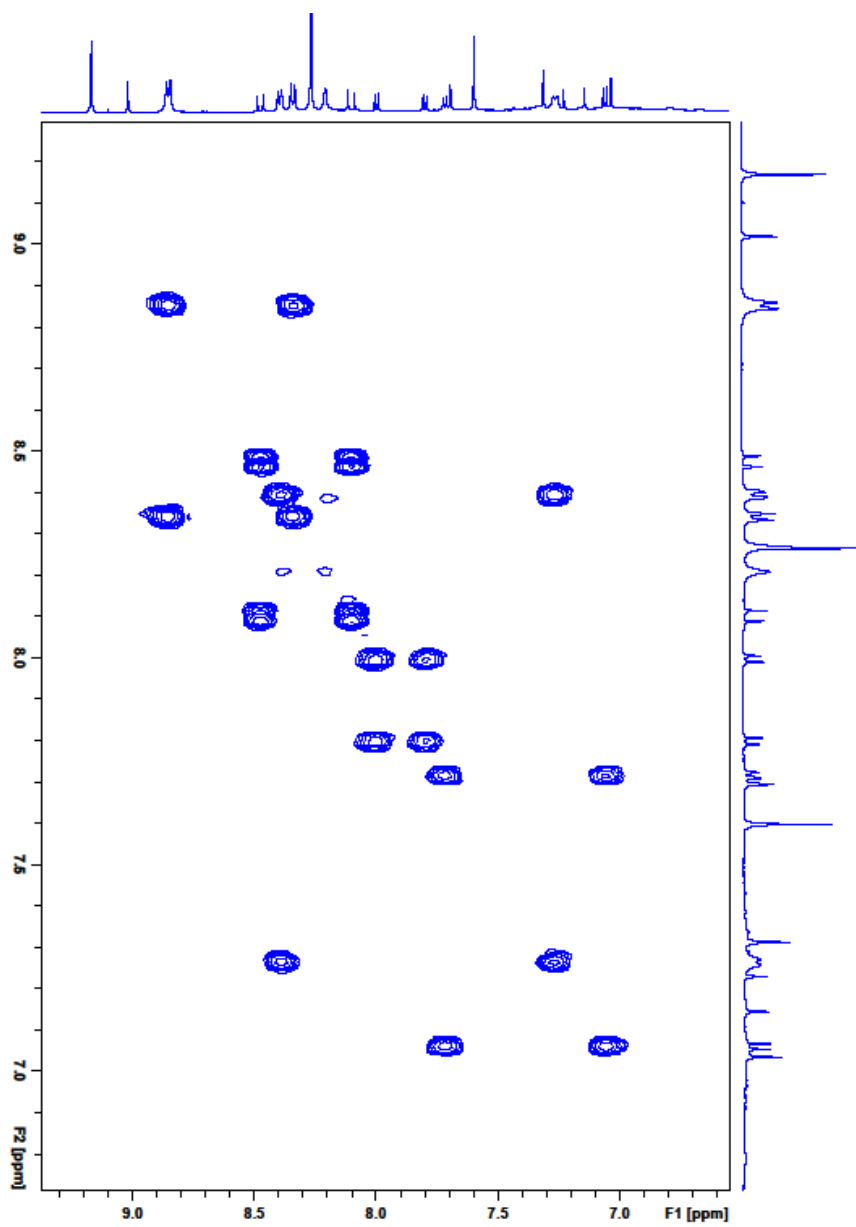


Figure S5 DQF-COSY d-DMSO.pdf

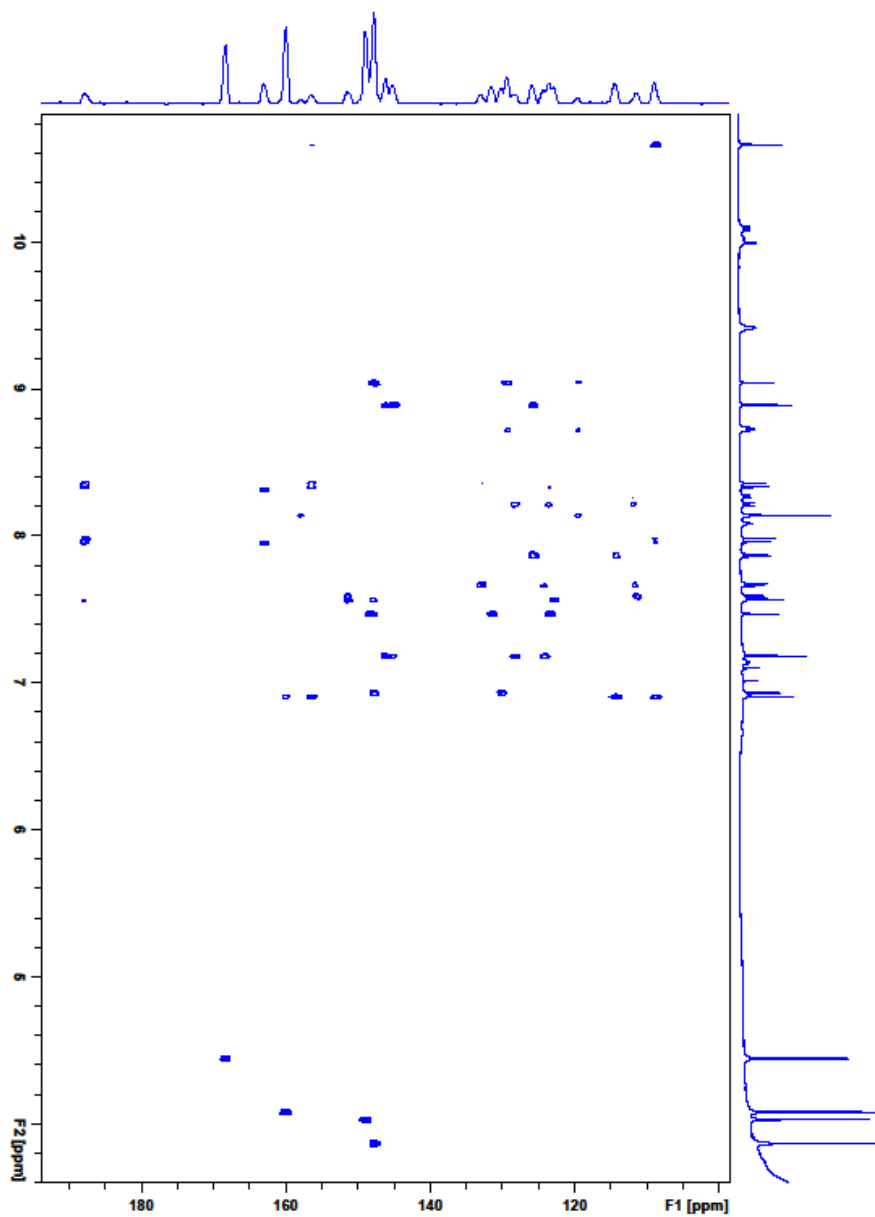
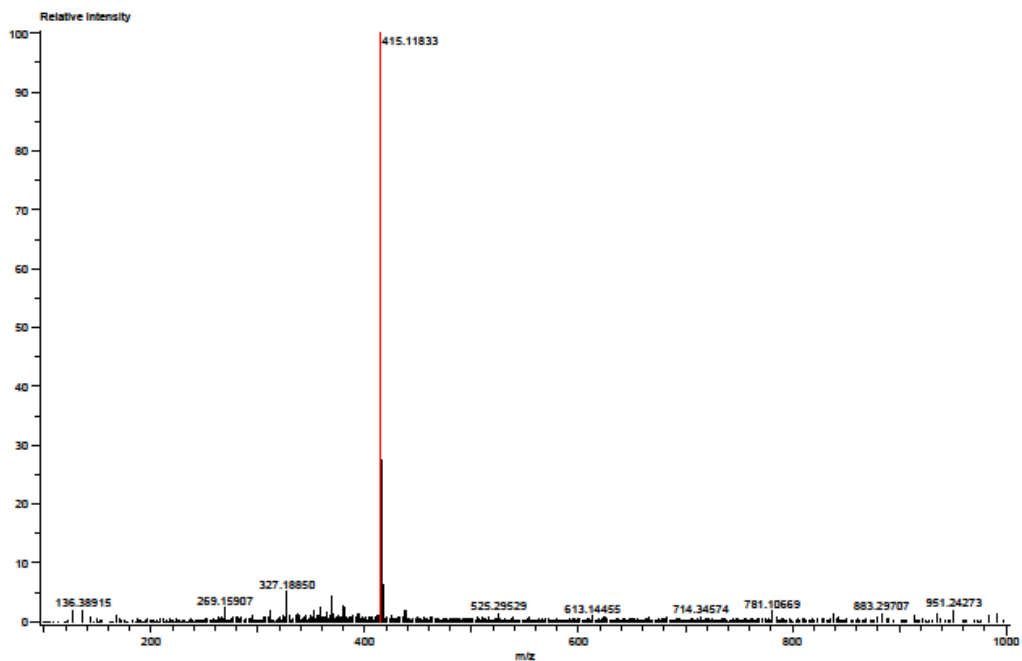


Figure S6 HMBC d-DMSO.pdf

Experiment
 Needle Volt: 2499[V]
 Ring Lens Volt: 13[V]
 Ion Guide Bias Volt: 30[V]
 Acquired m/z Range: 100.00..1000.00
 Spec. Record Interval: 0.60[s]

Orifice1 Volt: 30V
 Desolvating Chamber Temp: 250[°C]
 Pusher Bias Volt: -0.80[V]
 Data Acquisition Interval: 1[ms]
 Wait Time: 0.023[s]

Ionization Mode: ESI+
 Orifice2 Volt: 10[V]
 Ion Guide RF Volt: 2000V
 Detector Volt: 2350[V]
 Flight Repetition Interval: 59[μs]
 Detector Volt: 2350[V]



Ionization Mode: ESI+
 History: Determine m/z [Peak Detect [Centroid, 50, Area], Correct Base [5.0%], Correct Base [5.0%], Smooth [3], Average ...

Created: 8/9/2016 13:28:22
 Created by: Accutorf

Charge number: 1
 Element: ¹²C: 0 .. 100, ¹H: 0 .. 200, ¹⁶O: 0 .. 10

Tolerance: 5.00 (mmu)

Unsaturation Number: -1.5 .. 40.0 (Fraction: Both)

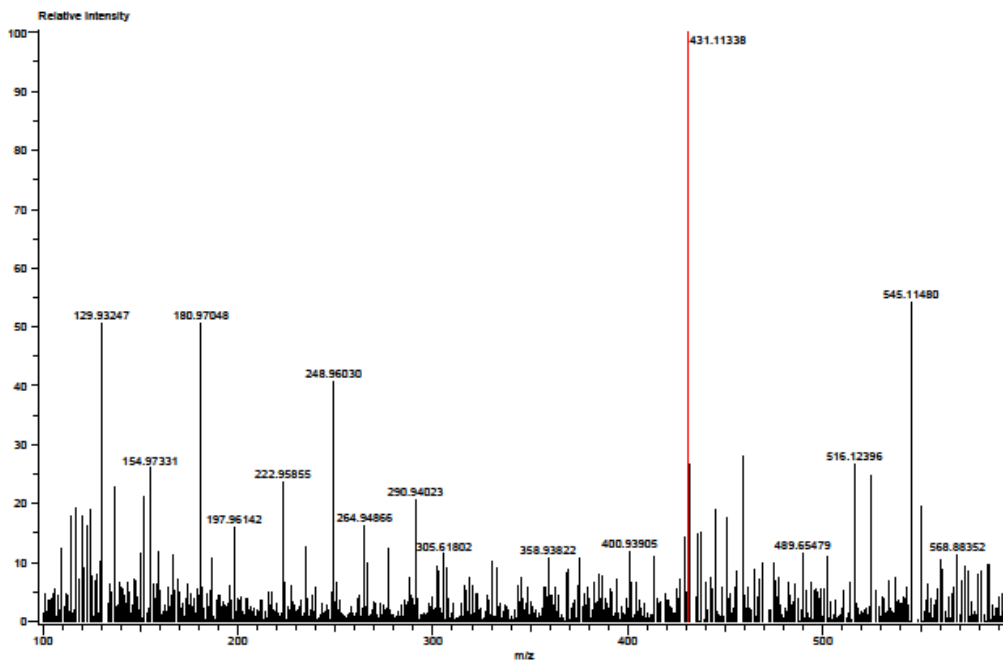
Mass	Intensity	Calc. Mass	Mass Difference (mmu)	Possible Formula	¹² C	¹ H	¹⁶ O	Unsaturation Number
415.11833	578919.85	415.11816	0.17	¹² C ₂₅ ¹ H ₁₉ ¹⁶ O ₅	25	19	5	16.5

Figure S7 ESI+ HR-MS flavylum cation form.pdf

Experiment
 Needle Volt: -2200[V]
 Ring Lens Volt: -10[V]
 Ion Guide Bias Volt: -30[V]
 Acquired m/z Range: 100.00..1000.00
 Spec. Record Interval: 0.60[s]

Orifice1 Volt: -23V
 Desolvating Chamber Temp: 250[°C]
 Pusher Bias Volt: 0.80[V]
 Data Acquisition Interval: 1[ms]
 Wait Time: 0.023[s]

Ionization Mode: ESI-
 Orifice2 Volt: -6[V]
 Ion Guide RF Volt: 1600V
 Detector Volt: 2350[V]
 Flight Repetition Interval: 59[us]
 Detector Volt: 2350[V]



History:Determine m/z[Peak Detect[Centroid,50,Area];Correct Base[5.0%];Average[MS[1] 0.494..0.519]-1.0*Avera... Created by:Accutof

Charge number:1

Element:¹²C:0 .. 100, ¹H:0 .. 200, ¹⁶O:0 .. 10

Tolerance:10.00(mmu)

Unsaturation Number:-1.5 .. 40.0 (Fraction:Both)

Mass	Intensity	Calc. Mass	Mass Difference (mmu)	Possible Formula	¹² C	¹ H	¹⁶ O	Unsaturation Number
431.11338	26125.29	431.11308	0.31	¹² C ₂₈ ¹ H ₁₈ ¹⁶ O ₇	28	18	7	16.5
		431.10720	6.18	¹² C ₂₈ ¹ H ₁₈ ¹⁶ O ₂	32	18	2	25.5

Figure S8 ESI- HR-MS trans-chalcone form.pdf

Table S1: Peonidin 3-glucoside (**2**) ^1H NMR data of the flavylum cation form in 5 % *d*-TFA in *d*-DMSO (v/v) and the two hemiketal forms a and b in pure *d*-DMSO recorded after 24 hours of equilibration.

Position	^1H δ (ppm) J (Hz)	^1H δ (ppm) J (Hz)	^1H δ (ppm) J (Hz)
flav	flavylum	hemiketal a	hemiketal b
4	8.94 <i>s</i>	6.35 <i>s</i>	6.16 <i>s</i>
6	6.72 <i>d</i> 2.0	5.90 <i>m</i>	5.90 <i>m</i>
8	7.04 <i>d</i> 2.0	5.65 <i>m</i>	5.65 <i>m</i>
2'	8.18 <i>d</i> 2.2	7.15 <i>d</i> 1.9	7.01 <i>d</i> 2.0
5'	7.09 <i>d</i> 8.6	6.70 <i>d</i> 8.0	6.69 <i>d</i> 8.0
6'	8.28 <i>dd</i> 8.6, 2.2	6.75 <i>dd</i> 8.0, 1.9	6.85 <i>dd</i> 8.2, 2.0
4'-OMe	3.92 <i>s</i>	3.74 <i>s</i>	3.72 <i>s</i>
1''	5.38 <i>d</i> 7.8	4.68 <i>d</i> 8.1	4.99 <i>d</i> 8.1

s: singlet, *d*: doublet, *dd*: doublet of doublets, *m*: multiplet

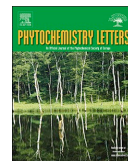
Paper III

Anthocyanins from mauve flowers of *Erlangea tomentosa* (*Bothriocline longipes*) based on erlangidin – The first reported natural anthocyanidin with C-ring methoxylation

Christopher Adaku, Irene Skaar, Helge Berland, Robert Byamukama, Monica Jordheim, Øyvind M. Andersen

Phytochemistry letters (2019)





Anthocyanins from mauve flowers of *Erlangea tomentosa* (*Bothriocline longipes*) based on erlangidin – The first reported natural anthocyanidin with C-ring methoxylation

Christopher Adaku^a, Irene Skaar^b, Helge Berland^b, Robert Byamukama^a, Monica Jordheim^b, Øyvind M. Andersen^{b,*}

^a Chemistry Department, Makerere University, P.O. Box 7062, Kampala, Uganda

^b Department of Chemistry, University of Bergen, Allég. 41, 5007, Bergen, Norway

ARTICLE INFO

Keywords:

Erlangea tomentosa
Bothriocline longipes
Compositae
Anthocyanins
Erlangidin
Analytical characteristics

ABSTRACT

Above 700 different anthocyanins have been isolated from plants. These flavonoid pigments are grouped after the number and position of hydroxy- and methoxy-groups on their anthocyanidin A- and B-rings, which influence their properties. In this study two new anthocyanins, erlangidin 5-O-(4''-(E-caffeoyl)-6''-(malonyl)-β-glucopyranoside)-3'-O-(6''-(3''-(β-glucopyranosyl)-E-caffeoyl)-β-glucopyranoside) and erlangidin 5-O-(6''-(malonyl)-β-glucopyranoside)-3'-O-(6''-(3''-(β-glucopyranosyl)-E-caffeoyl)-β-glucopyranoside) were isolated from purple flowers of *Erlangea tomentosa* (*Bothriocline longipes*) Oliv. & Hiern (Asteraceae) in amounts of ~1.6 and 0.6 mg/g fr. wt., respectively. They were found to contain the first reported natural anthocyanidin with a methoxy-group on the heterocyclic C-ring, which we have given the name erlangidin. During extraction, isolation and storage in acidified methanolic solvents the two anthocyanins were both partly converted to their demalonylated and methylmalonyl esterified forms. Spectroscopic and chromatographic characteristics for erlangidin in comparison with the common anthocyanidins, which it might be mistaken for, are included.

1. Introduction

The last two decades have witnessed renewed research activities on anthocyanins, mainly related to their potential health-promoting properties, their use as natural food colorants, and their appearance in cultivars and plant mutants with new colors and color patterns (Andersen and Jordheim, 2010; Davies, 2009; Zhao et al., 2017). Besides affecting the colors, various anthocyanin structures, including type of aglycone (anthocyanidin), have in many papers been reported to have different impact on the biological activity of these flavonoids. The position and number of hydroxy- and methoxy-groups on the various anthocyanidins have been considered as pivotal features for their stability and reactivity (Cabrita et al., 2000; Kamonpatana et al., 2012). The type of anthocyanidin have been shown to influence the bioavailability and degradation routes of anthocyanins, and their ability to form various phase II metabolites in metabolism (Andersen and Jordheim, 2013; Jakesevic et al., 2013; Sinela et al., 2017).

Around 92% of the reported anthocyanins (above 700 in 2018; Andersen, unpublished data) are based on the six anthocyanidins, cyanidin, delphinidin, pelargonidin, malvidin, peonidin and petunidin,

referred to as the common anthocyanidins. These anthocyanidins have different number of hydroxyl- and methoxy-groups on their B-rings. Nearly all anthocyanins isolated from plants have an O-glycosyl moiety located at their anthocyanidin 3-positions. The exceptions are the 3-deoxyanthocyanins (which are lacking any substitution at their 3-positions) found in several sources, including mainly bryophytes, ferns, sorghum and some Gesneriaceae (Andersen and Jordheim, 2010), and two anthocyanins found in the blue flowers of African water lily (*Nymphaea caerulea*) (Fossen and Andersen, 1999) and two anthocyanins isolated from red onion (*Allium cepa*) (Fossen et al., 2003) having a free hydroxyl group in their anthocyanidin 3-positions.

In our continuing survey of the East-African flora looking for new nutraceutical or pigmentation sources, an investigation of *Erlangea tomentosa* (Oliv. & Hiern) S.Moore (*Bothriocline longipes* (Oliv. & Hiern) N.E.Br.) (family Compositae) a native tropical African plant widely distributed in South, Central and East Africa (Bailey, 1939), revealed that the relative complex anthocyanins isolated from its mauve flowers were based on an extraordinary anthocyanidin. In Uganda, *E. tomentosa* has been used to treat various health conditions including colic pains, stomachache, syphilis, fever, miscarriage, mental confusion,

* Corresponding author.

E-mail address: oyvind.andersen@kj.uib.no (Ø.M. Andersen).

conjunctivitis, and convulsion in children (Asimwe et al., 2014). With exception of the content of the seed oil (Phillips et al., 1969), the phytochemical composition of *E. tomentosa* is largely unknown.

The aim of this paper is to report anthocyanins from nature with methoxylation of the anthocyanidin C-ring for the first time, and to provide chromatographic and spectroscopic characteristics of this unusual anthocyanidin.

2. Results and discussion

2.1. Structural elucidation

HPLC analysis (detection at 520 ± 20 nm) of fresh flower extract of *E. tomentosa* revealed the presence of mainly two anthocyanins (**1** and **2**) in quantitative amounts found to be 1.55 and 0.60 mg/g fr. wt., respectively. The extract was purified by partition against ethyl acetate followed by Amberlite XAD-7 column chromatography before individual anthocyanins were isolated using combinations of Sephadex LH-20 column chromatography and reversed phase preparative HPLC.

The 1D ^1H NMR spectrum of **1** showed in the area downfield for the sugar region signals corresponding to sixteen protons. Three of these at δ 8.42 ($d, J = 2.1$ Hz, H-2'), δ 8.39 ($dd, J = 2.1, 8.8$ Hz, H-6') and δ 7.27 ($d, J = 8.8$ Hz, H-5') were caused by the AMX-system of the anthocyanidin B-ring, while δ 8.64 (s, H-4), δ 7.09 ($d, J = 2.0$ Hz, H-6) and δ 7.02 (d (broad), H-8) belonged to the A- and C-rings, respectively (Table 1). The chemical shifts of the corresponding carbons of the aglycone of **1** were assigned from the HSQC NMR experiment, whereas the remaining quaternary carbon atoms of the aglycone were assigned from the HMBC spectrum (Table 1) indicating an anthocyanidin with a similar substitution pattern as cyanidin. However, a strong cross-peak at δ 4.25/149.19 (C-3) was observed in the HMBC spectrum of **1** (Fig. 2). This proton signal at δ 4.25 was integrated to three protons in the ^1H NMR spectrum, in accordance with a methoxy group extraordinary located at the 3-position of the anthocyanidin. This location of a methoxy group on an anthocyanidin was also supported by the cross-peak in the NOESY spectrum at δ 8.64/4.25 between H-4 and the methoxy group (Fig. 2). A fragment ion $[\text{F}]^+$ at m/z 301.0853 in the HR-ESI-MS spectrum of **1** was in accordance with a 3-methoxy-5,7,3',4'-tetrahydroxyflavylium cation (3-methoxycyanidin) (calcd 301.0707 Da, $\text{C}_{16}\text{H}_{13}\text{O}_6^+$). No anthocyanidin with a methoxy group on its C-ring has previously been isolated from nature, and we suggest to name this anthocyanidin erlangidin.

Five of the protons in the downfield ^1H NMR region were due to coupled aromatic proton resonances at δ 6.96 ($d, J = 1.8$ Hz, H-2^{II}), δ 6.71 ($d, J = 8.2$ Hz, H-5^{II}) and δ 6.63 ($dd, J = 8.2, 1.9$ Hz, H-6^{II}), and the coupled olefinic resonances at δ 7.22 ($d, J = 15.9$ Hz, β^{II}) and δ 6.10 ($d, J = 15.9$ Hz, α^{II}) (Table 1). These signals together with resonances for the three quaternary carbons at δ 150.72 (C-4^{II}), δ 146.89 (C-3^{II}) δ 126.96 (C-1^{II}) and the ester carbonyl carbon at δ 168.06 showed the presence of one *p*-caffeoyl moiety. Similarly, the remaining five protons in the downfield region were found to belong to the second *p*-caffeoyl moiety (Table 1). The *E*-configuration of the double bond of both of the caffeoyl moieties were established by the coupling constant (15.9 Hz) of the olefinic protons.

The sugar region of the ^1H and TOCSY spectra of **1** indicated the presence of three sugar units. Starting from the anomeric proton at δ 5.35 ($d, J = 7.8$ Hz, H-1^{III}), the observed cross-peak at δ 5.35/3.92 in the DQF-COSY spectrum supported by the cross-peak in the HSQC spectrum at δ 5.35/102.47, permitted the assignment of H-2^{III}. Similarly, the chain of coupled protons H-2^{III}, H-3^{III}, H-4^{III}, H-5^{III}, H-6A^{III}/H-6B^{III} and their coupling constants were assigned in accordance with a β -glucopyranosyl (Table 1). A cross-peak at δ 5.35/156.00 in the HMBC spectrum between H-1^{III} and C-5 of the aglycone and the cross-peak at δ 5.35/7.09 in the NOESY spectrum between H-1^{III} and H-6 (Fig. 2) showed that this sugar was connected to the aglycone 5-position. By using the doublet at δ 5.16 ($J = 7.6$ Hz) as the starting point in the DQF-COSY spectrum it

Table 1

^1H and ^{13}C NMR spectral data for the anthocyanins erlangidin 5-O-(4^{III}-(*E*-caffeoyl)-6^{III}-(malonyl)- β -glucoside)-3'-O-(6^{III}-(β -glucosyl)-*E*-caffeoyl)- β -glucoside (**1**) and erlangidin 5-O-(6^{III}-(methylmalonyl)- β -glucoside)-3'-O-(6^{III}-(β -glucosyl)-*E*-caffeoyl)- β -glucoside (**2b**) isolated from mauve flowers of *Erlangea tomentosa* (*Bothriocline longipes*) recorded in $\text{CF}_3\text{COOD-CD}_3\text{OD}$ (5:95, v/v) at 25 °C.

	1 (^1H)		2b (^1H)		1 (^{13}C)		2b (^{13}C)	
Erlangidin								
2					162.66	162.4		
3					149.19	149.0		
4	8.64	s	8.65	<i>d</i> 2.0	129.86	129.8		
5					156.00	155.9		
6	7.09	<i>d</i> 2.	7.04	<i>d</i> 2.0	106.65	106.3		
7					168.32	168.3		
8	7.02	(<i>d</i>)	7.01	<i>dd</i> 2.0, 0.8	97.60	97.4		
9					155.68	155.4		
10					113.76	113.7		
1'					121.24	121.3		
2'	8.42	<i>d</i> 2.1	8.43	<i>d</i> 2.2	120.23	120.3		
3'					146.89	146.6		
4'					157.40	157.1		
5'	7.27	<i>d</i> 8.8	7.27	<i>d</i> 8.9	118.90	118.7		
6'	8.39	<i>dd</i> 8.8, 2.1	8.39	<i>dd</i> 8.8, 2.2	130.68	130.4		
3-O-Me	4.25	s	4.25	s	58.35	58.3		
5-O-glucoside								
1 ^{III}	5.35	<i>d</i> 7.8	5.27	<i>d</i> 7.7	102.47	102.5		
2 ^{III}	3.92	<i>dd</i> 9.2, 7.8	3.79	<i>m</i>	74.69	74.5		
3 ^{III}	4.00	<i>t</i> 9.2	3.59	<i>m</i>	75.32	77.5		
4 ^{III}	5.16	<i>dd</i> 9.9, 9.3	3.58	<i>dd</i> 9.8, 9.1	71.94	71.1		
5 ^{III}	4.22	<i>dd</i> 9.9,	3.94	<i>m</i>	73.90	75.9		
		6.6, 3.3						
6A ^{III}	4.44	<i>m</i>	4.70	<i>dd</i> 12.0, 2.0	64.78	65.4		
6B ^{III}	4.44	<i>m</i>	4.50	<i>dd</i> 12.0, 7.0				
3'-O-glucoside								
1 ^{III'}	5.16	<i>d</i> 7.6	5.15	<i>d</i> 7.7	102.15	102.0		
2 ^{III'}	3.74	<i>dd</i> 9.1, 7.7	3.72	<i>dd</i> 9.4, 7.7	74.47	74.4		
3 ^{III'}	3.68	<i>t</i> 9.0	3.69	<i>t</i> 8.6	77.56	78.6		
4 ^{III'}	3.49	<i>dd</i> 9.3, 8.9	3.49	<i>m</i>	72.68	72.7		
5 ^{III'}	3.93	<i>m</i>	3.93	<i>ddd</i> 9.6,	76.07	75.9		
				6.3, 2.0				
6A ^{III'}	4.94	<i>dd</i> 11.7, 2.3	4.91	<i>dd</i> 11.9, 2.1	64.96	64.9		
6B ^{III'}	4.32	<i>dd</i> 11.7, 9.6	4.34	<i>dd</i> 12.0, 7.0				
3 ^{II} -O-glucosyl								
1 ^{III''}	4.69	<i>d</i> 7.6	4.63	<i>d</i> 7.5	103.86	103.8		
2 ^{III''}	3.64	<i>dd</i> 9.2, 7.6	3.61	<i>m</i>	74.75	74.9		
3 ^{III''}	3.63	<i>t</i> 9.2	3.60	<i>m</i>	77.61	77.4		
4 ^{III''}	3.54	<i>dd</i> 9.3, 8.7	3.52	<i>m</i>	71.35	71.3		
5 ^{III''}	3.39	<i>m</i>	3.36	<i>m</i>	78.63	78.3		
6A ^{III''}	3.98	<i>dd</i> 11.6, 2.1	4.00	<i>dd</i> 11.9, 2.2	62.27	62.4		
6B ^{III''}	3.81	<i>dd</i> 11.6, 5.6	3.80	<i>m</i>				
4 ^{II} -O-caffeoyl								
1 ^I					127.66			
2 ^I	7.18	<i>d</i> 2.1			115.31			
3 ^I					146.85			
4 ^I					149.88			
5 ^I	6.89	<i>d</i> 8.1			116.53			
6 ^I	7.08	<i>dd</i> 8.1, 2.1			123.21			
α^{I}	6.45	<i>d</i> 15.9			114.38			
β^{I}	7.75	<i>d</i> 15.8			148.13			
COO ^I					168.18			
6 ^{III} -O-caffeoyl								
1 ^{III'}					126.96	126.8		
2 ^{III'}	6.96	<i>d</i> 1.8	6.95	<i>d</i> 2.0	116.73	116.6		
3 ^{III'}					146.89	146.6		
4 ^{III'}					150.72	150.3		
5 ^{III'}	6.71	<i>d</i> 8.2	6.70	<i>d</i> 9.3	117.49	117.6		
6 ^{III'}	6.63	<i>dd</i> 8.2, 1.9	6.63	<i>m</i>	125.11	125.1		
$\alpha^{\text{III'}}$	6.10	<i>d</i> 15.9	6.10	<i>d</i> 15.9	115.99	115.9		
$\beta^{\text{III'}}$	7.22	<i>d</i> 15.9	7.21	<i>d</i> 15.9	145.75	145.7		
COO ^{III'}					168.06	168.2		
6 ^{III} -O-malonyl								
1 ^{III''}					168.40	168.9		
2 ^{III''}	3.58		3.61		41.65	41.4		
3 ^{III''}					170.25	170.3		
1 ^{III''} -OMe			3.79	s		52.9		

s = singlet, d = doublet, dd = double doublet, m = multiplet. See Fig. 1 for structures.

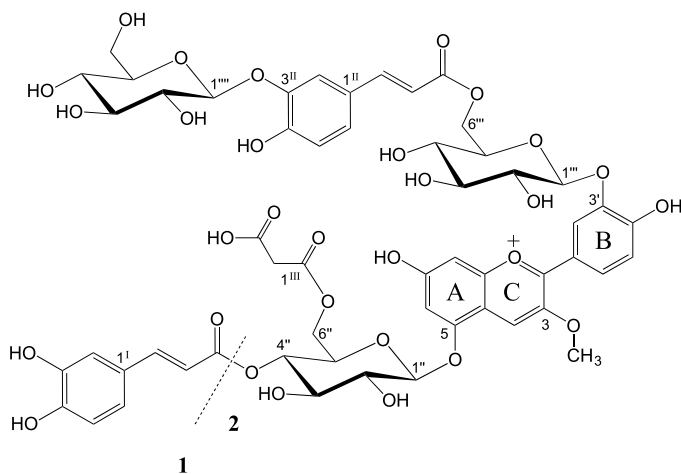


Fig. 1. Structures of erlangidin 5-*O*-(4''-(*E*-caffeoyl)-6''-(malonyl)- β -glucopyranoside)-3'-*O*-(6'''-(3''-(β -glucopyranosyl)-*E*-caffeoyl)- β -glucopyranoside) (1) and erlangidin 5-*O*-(6''-(malonyl)- β -glucopyranoside)-3'-*O*-(6'''-(3''-(β -glucopyranosyl)-*E*-caffeoyl)- β -glucopyranoside) (2) isolated from mauve flowers of *Erlangea tomentosa* (*Bothriocline longipes*). Compounds **1a** and **2a** are the demalonylated derivatives of **1** and **2**, while **1b** and **2b** are the 6''-(methylmalonyl)-derivatives of **1** and **2**, respectively.

was likewise possible to assign all the chemical shifts for the second monosaccharide moiety, β -glucopyranosyl (Table 1). In cases where sugar protons had overlapping chemical shifts, the assignment was assisted by the TOCSY experiment. A cross-peak at δ 5.16/146.89 (H-1''/C-3') in the HMBC spectrum and the cross-peak at δ 5.16/8.42 in the NOESY spectrum between H-1''' and H-2' (Fig. 2) showed that this sugar unit was connected to the 3'-position of the aglycone. The third and last anomeric doublet at δ 4.69 ($J = 7.6$ Hz) was also identified to be part of a β -glucopyranosyl moiety (Table 1). The chair conformation of the three β -glucopyranosyls were confirmed by cross-peaks in the NOESY spectrum between H-1, H-3 and H-5 of all three moieties (Fig. 2).

A cross-peak at δ 4.69/146.89 (H-1''/C-3'') in the HMBC spectrum and the cross-peak at δ 4.69/6.96 in the NOESY spectrum between H-1'' and H-2'' (Fig. 2) showed that this sugar unit was connected to the 3''-position of the second caffeoyl moiety. This aromatic acyl group was itself found to be linked at the glucosyl 6'''-position by the crosspeaks between H-6A''' and the C'''-carbonyl (δ 4.94/168.06) and between H-6B''' and the C'''-carbonyl (δ 4.32/168.06) in the HMBC spectrum, while the other caffeoyl moiety was confirmed to be linked at the glucosyl 4''-position by the crosspeak between H-4'' and the C''-carbonyl (δ 5.16/168.18) in the HMBC spectrum (Fig. 2). Furthermore, an aliphatic acyl moiety was found to be connected in the glucosyl 6''-position by the crosspeak at δ 4.44/168.40 between H-6A''/6B'' and the C''-carbonyl (Fig. 2). This group was identified as malonyl by the crosspeaks at δ 3.58/168.40 (H-2'''/C-1'''-carbonyl) and δ 3.58/170.25 (H-2'''/C-3'''-carbonyl) in the HMBC spectrum and at δ 3.58/41.65 (H-2'''/C-2''') in the HSQC spectrum. The HR-ESI-MS spectrum of **1** showed a molecular ion at m/z 1197.2903 corresponding to the empirical formula $C_{55}H_{57}O_{30}^+$ (calc. 1197.2929 Da) in agreement with the novel compound erlangidin 5-*O*-(4''-(*E*-caffeoyl)-6''-(malonyl)- β -glucopyranoside)-3'-*O*-(6'''-(3''-(β -glucopyranosyl)-*E*-caffeoyl)- β -glucopyranoside) (Fig. 1).

During extraction, isolation and storage in acidified methanolic solvents, **1** and **2** were partly converted to **1a/1b** and **2a/2b**, respectively (Fig. 3), and the NMR assignments in the structure elucidation of **2** were mainly based on NMR spectra recorded for **2b** (Table 1). The compounds (**1**, **1a**, **1b**, **2**, **2a** and **2b**) showed UV-vis spectra with $\lambda_{\text{vis-max}}$ values around 530 nm (Table 2) for all compounds. However, while **1**, **1a** and **1b** showed strong local λ -values around 325 nm, indicating anthocyanins acylated with two aromatic acyl groups, the lower intensity of the local absorption maxima around 322 nm for **2**, **2a** and **2b** indicated that these compounds were acylated with only one aromatic acyl group (Table 2). Based on analogous NMR assignments as reported

for **1**, the identity of **2** was confirmed to be **1** lacking one caffeoyl moiety. The HR-ESI-MS spectrum of **2** showed a molecular ion at m/z 1035.2709 corresponding to the empirical formula $C_{46}H_{51}O_{27}^+$ (calc. 1035.2612 Da) in agreement with the novel compound erlangidin 5-*O*-(6''-(malonyl)- β -glucopyranoside)-3'-*O*-(6'''-(3''-(β -glucopyranosyl)-*E*-caffeoyl)- β -glucopyranoside) (Fig. 1).

The difference of 85.9890 Da in the high-resolution ESI-MS spectra of **1** and **1a** (Table 2) was in accordance with the lack of an aliphatic acyl moiety (malonyl) in **1a**. Compound **1a** was thus made by demalonylation of the malonyl unit of **1**, and the HR-ESI-MS spectrum of **1a** showed a molecular ion at m/z 1111.3013 (Table 2) in agreement with erlangidin 5-*O*-(4''-(*E*-caffeoyl)- β -glucopyranoside)-3'-*O*-(6'''-(3''-(β -glucopyranosyl)-*E*-caffeoyl)- β -glucopyranoside). The difference of 14.0164 Da between of **1** and **1b** (Table 2) was confirmed by an extra methoxy signal at δ 3.77 in the ^1H spectrum, a crosspeak at δ 3.77/53.3 (CH₃O) in the HSQC spectrum, and a crosspeak at δ 3.77/170.16 (CH₃O/C-3'''-carbonyl) in the HMBC spectrum of **1b**. Compound **1b** was thus made by methyl esterification of the free carboxyl group of the malonyl unit of **1**, and the HR-ESI-MS spectrum of **1b** showed a molecular ion at m/z 1211.3067 (Table 2) in agreement with erlangidin 5-*O*-(4''-(*E*-caffeoyl)-6''-(methylmalonyl)- β -glucopyranoside)-3'-*O*-(6'''-(3''-(β -glucopyranosyl)-*E*-caffeoyl)- β -glucopyranoside). In a similar way **2a** and **2b** were identified as erlangidin 5-*O*- β -glucopyranoside-3'-*O*-(6'''-(3''-(β -glucopyranosyl)-*E*-caffeoyl)- β -glucopyranoside) and erlangidin 5-*O*-(6''-(methylmalonyl)- β -glucopyranoside)-3'-*O*-(6'''-(3''-(β -glucopyranosyl)-*E*-caffeoyl)- β -glucopyranoside), respectively.

Numerous studies have confirmed that aromatic acyl groups situated on the glycosyl moieties increase the *in vitro* and *in vivo* stability of anthocyanins (Dangles et al., 1993; Yoshida et al., 2009; Andersen and Jordheim, 2010; Trouillas et al., 2016; Zhao et al., 2017). Anthocyanins without aromatic acylation are assumed to be more quickly transformed into non-cyanic forms by hydration at the 2-position of the anthocyanidin nucleus. The aromatic acyl moieties seem to protect against nucleophilic attack by water at this position. The shift to more bluish colors of in particular acylated anthocyanins based on delphinidin (Yoshida et al., 2009; Andersen and Jordheim, 2010), have in some cases been indicated to be achieved by intramolecular copigmentation involving stacking between the anthocyanidin and one or two of the aromatic acyl groups, which stabilize the cyanic forms of the anthocyanidin. It has also been shown for 3-deoxyanthocyanidins how *O*-glycosidation can perturb the acid-base properties of the chromophore and with a large impact on the distribution of colored and colorless forms in aqueous solution (Basilio et al., 2016; Sigurdson et al.,

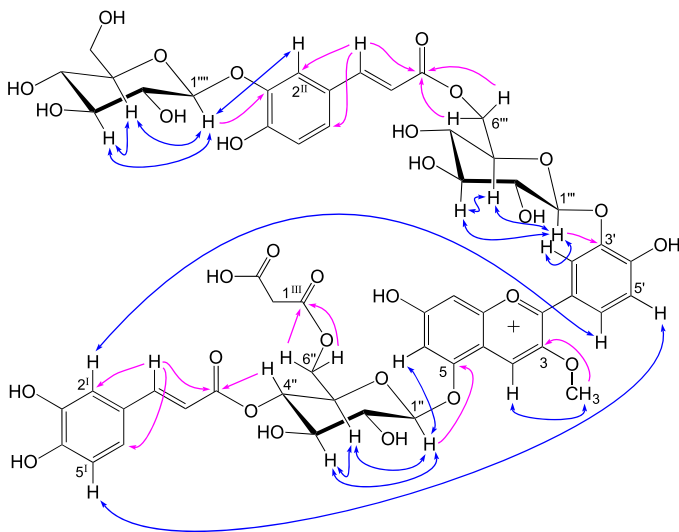


Fig. 2. Highlighted NMR correlations observed as cross-peaks in ^1H - ^1H NOESY (two-sided blue arrows from ^1H to ^1H) and ^1H - ^{13}C HMBC (one-way pink arrows from ^1H to ^{13}C) spectra of erlangidin 5-O-(4''-(*E*-caffeoyl)-6''-(malonyl)- β -glucopyranoside)-3'-O-(6''-(3''- β -glucopyranosyl)-*E*-caffeoyl)- β -glucopyranoside) (**1**) isolated from mauve flowers of *Erlangea tomentosa* (*Bothriocline longipes*).

2018). Pigment **1** isolated from *E. tomentosa* flowers contains two caffeoyl moieties, situated at the glucosyl moieties at the 5- and 3'-position, respectively, on the anthocyanidin (erlangidin). Based on the cross-peaks between H-5' and H-5'' (δ 7.27/6.89) and between H-6' and H-2' (δ 8.39/7.18) in the NOESY NMR spectrum of **1** (Fig. 2), it is obvious that there is proximity between erlangidin and the caffeoyl moiety connected to the 5-glucosyl. This proximity might be achieved by intramolecular folding of the 5-glucosyl unit placing the aromatic ring of the coumaroyl moiety on top or bottom of the B-ring of erlangidin. However, the flowers of *E. tomentosa* might be described as mauve – not bluish, and the visible part of the absorption spectra of **1** and **2** are nearly identical (Table 2), even though pigment **2** is lacking the caffeoyl moiety connected to the 5-glucosyl of pigment **1**. Thus, the aromatic acylated anthocyanins **1** and **2**, which are based on erlangidin, do not achieve the bluing effect typical for aromatic acylated anthocyanins based on delphinidin.

2.2. Diagnostic features of erlangidin

For diagnostic purposes in the identification of anthocyanins based on anthocyanidins with a 3-methoxyl group on their C-ring, we want to highlight three points after comparison with own results on a variety of anthocyanins: a) Erlangidin (made by acid hydrolysis of **1** and **2**) was compared with common anthocyanidins with respect to retention times (TLC and HPLC) and spectral data (UV-vis) (Table 3). The most characteristic feature was the relatively high R_f value of erlangidin in an acidified aqueous TLC system – even when compared with peonidin having the same number of hydroxyl and methoxyl substituents as erlangidin.

b) The chemical carbon shifts of the B-ring methoxyl groups of anthocyanins are observed at 56.7–57.3 ppm in acidified deuterated methanolic solvents, while the carbons of the A-ring methoxyl groups are observed at 57.7–57.9 ppm. The chemical carbon shift of the C-ring 3-methoxyl carbon (58.3 ppm in the erlangidin-derivatives **1** and **2b**)

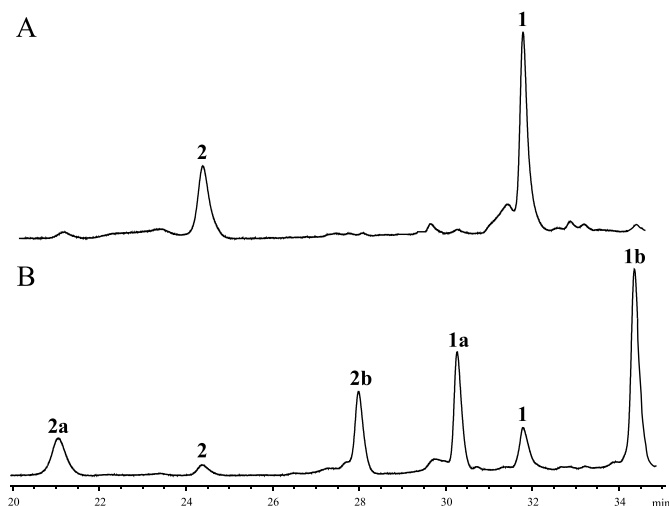


Fig. 3. HPLC profiles of raw extracts (methanol containing 0.5% TFA) of *Erlangea tomentosa* (*Bothriocline longipes*) detected at 520 ± 20 nm. A: After 24 h extraction at 4 °C. B: After 1-month storage at 4 °C showing how the two anthocyanins (**1** and **2**) are converted partly to their respective demalonylated (**1a** and **2a**) and methylmalonylated (**1b** and **2b**) derivatives. See Fig. 1 for structures.

Table 2

Online HPLC, and high-resolution electrospray ionization mass spectral data recorded for anthocyanins **1** and **2** isolated from *Erlangea tomentosa* (*Bothriocline longipes*) and their respective demalonylated (**1a** and **2a**) and methylmalonylated (**1b** and **2b**) derivatives. See Fig. 1 for structures.

	t_r (min)	Vis-max (nm)	Local UV-max (nm)	$A_{440}/A_{vis-max}$ (%)	$A_{UV-max}/A_{vis-max}$ (%) (m/z)	$[M]^+$ (obsd) (m/z)	$[M]^+$ (calcd) (m/z)	molecular formula
1	31.78	530	282 (sh), 294, 326	18	95	1197.2903	1197.2929	$C_{55}H_{57}O_{30}^+$
1a	30.25	530	280 (sh), 296, 324	19	106	1111.3013	1111.2925	$C_{53}H_{55}O_{27}^+$
1b	34.30	530	282 (sh), 296, 326	18	87	1211.3067	1211.3086	$C_{56}H_{59}O_{30}^+$
2	24.32	530	278, 294 (sh), 322	19	65	1035.2709	1035.2612	$C_{46}H_{51}O_{27}^+$
2a	21.11	528	278, 294 (sh), 320	20	63	949.2653	949.2608	$C_{43}H_{49}O_{24}^+$
2b	27.95	530	278, 294 (sh), 322	19	61	1049.2837	1049.2769	$C_{47}H_{53}O_{27}^+$

Table 3

Retention times (TLC and HPLC) and spectral data (UV-vis) recorded for erlangidin compared to five common anthocyanidins.

Aglycone	R_f TLC (FHW)	t_r HPLC (min)	UV-Vis _{max} (nm)	$A_{440}/A_{vis-max}$ (%)
Delphinidin	0.13	18.2	532	25
Cyanidin	0.23	23.7	525	25
Petunidin	0.20	24.9	534	20
Erlangidin	0.42	28.5	525	27
Peonidin	0.34	33.2	526	26
Malvidin	0.30	33.8	533	24

may thus be indicated by their downfield chemical shift effect.

c) The chemical proton shifts of the B-ring methoxyl groups are observed at 4.06–4.13 ppm in acidified deuterated methanolic solvents, while the protons of the A-ring methoxyl groups are observed at 4.17–4.21 ppm. 3-Methoxy protons located at the C-ring (4.25 ppm in the erlangidin-derivatives **1** and **2b** may thus be identified by their small downfield chemical shift effect compared to similar values for A- and B-ring methoxyl protons.

2.3. Concluding remarks

In this paper a novel natural anthocyanidin (erlangidin) with methoxylation of the heterocyclic C-ring is identified for the first time. Two anthocyanins having erlangidin as aglycone, erlangidin 5-O-(4'-*E*-caffeoyl)-6''-(malonyl)- β -glucopyranoside)-3'-O-(6''-(3''- β -glucopyranosyl)-*E*-caffeoyl)- β -glucopyranoside) (**1**) and erlangidin 5-O-(6''-(malonyl)- β -glucopyranoside)-3'-O-(6''-(3''- β -glucopyranosyl)-*E*-caffeoyl)- β -glucopyranoside) (**2**) are isolated from mauve flowers of *E. tomentosa* either intact, as 6''-(methylmalonyl)-derivatives (**1b** and **2b**), or as demalonylated derivatives (**1a** and **2a**). Most of the more than 700 reported anthocyanins (> 90%) found in plants are based on only common 6 anthocyanidins. In addition, three 6-hydroxyanthocyanidins, nine 3-deoxyanthocyanidins, ten anthocyanidins with mono- or dimethoxylation on their A-rings and some anthocyanidins with extended C15-skeleton (pyranoanthocyanidins, sphagnorubins) have previously been reported. The finding of erlangidin-glycosides with methoxylated C-rings will thus expand the diversity of known anthocyanidin structures and have chemotaxonomic significance.

Nearly all previously reported anthocyanins occur as anthocyanidin 3-glycoside derivatives. Further examinations of erlangidin 3-methoxy derivatives may contribute in the understanding of anthocyanidin equilibrium forms and thus anthocyanin chemistry (color, stability etc.) and the potential nutraceutical value of anthocyanins.

3. Experimental

3.1. General experimental procedures

The analytical HPLC system used for the anthocyanins (**1** and **2**) and

anthocyanidins was the Agilent 1100 series equipped with a HP 1050 diode array detector and a 200 × 4.6 mm i.d., 5 μ m ODS Hypersil column (Supelco, Bellefonte, PA). Two solvents, A) H₂O (+ 0.5% TFA, v/v) and B) acetonitrile (+ 0.5% TFA, v/v), were used for elution. The elution profile started with 90% A and 10% B followed by linear gradient elution for the next 10 min to 14% B, isocratic elution (10–14 min), and the subsequent linear gradient conditions: 14–22 min (to 18% B), 22–26 min (to 23% B), 26–31 min (to 28% B), and 31–32 min (to 40% B), with isocratic elution at 32–40 min (40% B), and linear gradient elution at 40–43 min (back to 10% B). The gradient used for separation of anthocyanidins started with 90% A and 10% B followed by linear gradient conditions: 0–10 min (to 18% B), 10–20 min (to 22% B), 20–35 min (to 25% B), 35–36 min (to 40% B), with isocratic elution at 36–41 min (40% B) and linear gradient elution at 41–43 min (back to 10% B). The flow rate was 1.0 ml/min, and aliquots of 15 μ l were injected with an Agilent 1100 series microautosampler. Prior to injection, all samples were filtered through a 0.45 μ m Millipore membrane filter. The UV-vis absorption spectra were recorded online during HPLC analysis over the wavelength range of 240–600 nm in steps of 2 nm.

High-Resolution LC-Electrospray mass spectrometry (ESI⁺/TOF), spectra were recorded using a JEOL AccuTOF JMS-T100LC instrument in combination with an Agilent Technologies 1200 Series HPLC system. A Zorbax SB-C18 (50 × 2.1 mm, length × i.d., 1.8 μ m) column was used for separation. Two solvents, A) H₂O (+ 0.5% TFA, v/v) and B) acetonitrile (+ 0.5% TFA, v/v), were used for elution. The following solvent compositions were used: 0–1.25 min (10–22% B, linear gradient), 1.25–5 min (to 30% B, linear gradient), 5–7 min (30% B, isocratic), 7–8 min (to 40% B, linear gradient), 8–14 min (40% B, isocratic) and 14–15 min (back to 10% B, linear gradient). The flow rate was 0.4 ml/min.

TLC was carried out on microcrystalline cellulose (F5556, Merck) with the solvent FHW (HCO₂H/concentrated HCl/H₂O; 51.4:7.2:41.4, v/v).

One-dimensional ¹H, compensated attached proton test (CAPT), 2D heteronuclear single quantum coherence (¹H-¹³C HSQC), heteronuclear multiple bond correlation (¹H-¹³C HMBC), 2D correlation spectroscopy (¹H-¹H COSY), and 2D total correlation spectroscopy (¹H-¹H TOCSY) were obtained on a Bruker Biospin Ultrashield Plus AV-600 MHz instrument equipped with a TCI ¹H-¹³C/¹⁵N CryoProbehead at 298 K. Sample temperatures were stabilized at 298 K. The deuteriomethyl ¹³C signal and the residual ¹H signal of the solvent (CF₃COOD-CD₃OD; 5:95, v/v) were used as secondary references (δ 49.0 and 3.40 from TMS, respectively).

3.2. Plant material

Fresh flowers of *E. tomentosa* were collected from the margins of Zika forest in Entebbe, Uganda in May 2014. The plant was identified by the staff at the Herbarium of Botany Department of Makerere University, where a voucher specimen, Adaku No. 4, was deposited.

3.3. Extraction and isolation

The fresh mauve corollas of the flowers (300 g) were extracted with 0.8 l methanol containing trifluoroacetic acid (0.5%, v/v) (MeOH-TFA) for 12 h. The filtered extract was concentrated under reduced pressure at 28 °C, purified by partition against ethyl acetate (three times) and applied to an Amberlite XAD-7 column. The anthocyanins adsorbed to the column were washed with water to remove polar non-phenolic impurities, and eluted from the column with MeOH-TFA. The concentrated anthocyanin eluate was applied to a Sephadex LH-20 column and separated by gradient elution using H₂O–MeOH–TFA (from 79.5:20:0.5 to 69.5:30:0.5, v/v/v) solvent. The separated anthocyanins were purified by a preparative HPLC system equipped with a Gilson 321 pump, an Ultimate 3000 Variable Wavelength Detector, a 25 × 2.2 cm (10 μm) Econosphere C18 column (Grace, USA), and the solvents, A) H₂O (0.5% TFA, v/v) and B) acetonitrile (0.5% TFA, v/v). The elution profile consisted of initial conditions with 90% A and 10% B followed by linear gradient elution for the next 10 min to 14% B, isocratic elution (10–14 min), and the subsequent linear gradient conditions; 14–18 min (to 16% B), 18–22 min (to 18% B), 22–26 min (to 23% B), 26–31 min (to 28% B) and 31–32 min (to 40% B), isocratic elution 32–40 min (40% B), and linear gradient elution 43–46 min (back to 10% B). The flow rate was 15 ml/min, and aliquots of 250 μl were injected.

3.4. Preparation of anthocyanidins

Pigments from blueberries (*Vaccinium myrtillus*) (Prior et al. (1998)), *Fuchsia* spp. flowers (Jordheim et al. (2011)) and *E. tomentosa* flowers were subjected to acid hydrolysis by dissolving them in 1 ml water and 1 ml 6 M HCl at 90 °C and incubated for 120 min in sealed ampules. The reactions were monitored by TLC (every 30 min) and HPLC (every 60 min).

3.5. Quantitative determinations

Four samples (4–9 g) of *E. tomentosa* flowers were extracted with methanol containing 0.5% TFA (11–21 mL) at 3 °C for 24 h. The supernatants were concentrated under reduced pressure, dissolved in methanol containing 0.5% TFA (2.5–4.5 mL), filtered through a 0.45 μm Millipore membrane filter, before the quantitative amounts of anthocyanins 1 and 2 in the four samples (three HPLC replicates of each) were determined from a HPLC standard curve based on cyanidin 3-glucoside isolated from black rice (Lee, 2010). The purity of cyanidin 3-glucoside was > 99% based on integration of the signals in the aromatic region of its ¹H NMR spectrum. Each of the three concentration points of the standard curve was based on averaged data calculated from three HPLC replicates. The averaged quantitative results are presented as milligrams per cyanidin 3-glucoside equivalents per gram of fresh flower weight.

Acknowledgements

We are grateful to Dr. Bjarte Holmelid (Dept. of Chemistry,

University of Bergen) for recording of high-resolution mass spectra. This study was initiated by the EU project called MUTHI (Multidisciplinary University Traditional Health Initiative, FP7-AFRICA 2010, Grant Agreement 266,005). The team at Makerere University gratefully acknowledges Carnegie Cooperation of New York for a fellowship.

References

- Andersen, Ø.M., Jordheim, M., 2010. Chemistry of flavonoid-based colors in plants. In: Mander, L.N., Liu, H.W. (Eds.), *Comprehensive Natural Products II: Chemistry and Biology*, vol.3. Elsevier, Oxford, pp. 547–614.
- Andersen, Ø.M., Jordheim, M., 2013. Basic anthocyanin chemistry and dietary sources. In: Wallace, T.C., Giusti, M.M. (Eds.), *Anthocyanins in Health and Disease*. CRC Press, Boca Raton, pp. 13–90.
- Asimwe, S., Namutebi, A., Borg-Karlsson, A., Kamatenesi, M.M., Oryem-Origa, H., 2014. Documentation and consensus of indigenous knowledge on medicinal plants used by the local communities of western Uganda. *J. Nat. Prod. Plant Resour.* 4, 34–42.
- Bailey, L.H., 1939. *The Standard Cyclopedia of Horticulture*, vol. 1. The Macmillan Company, New York, pp. 1136.
- Basilio, N., Al Bittar, S., Mora, N., Dangles, O., Pina, F., 2016. Analogs of natural 3-deoxyanthocyanins: O-glucosides of the 4',7'-dihydroxyflavylium ion and the deep influence of glycosylation on color. *Int. J. Mol. Sci.* 17 1751/1–1751/14.
- Cabrira, L., Fossen, T., Andersen, Ø.M., 2000. Colour and stability of the six common anthocyanidin 3-glucosides in aqueous solutions. *Food Chem.* 68, 101–107.
- Dangles, O., Saito, N., Brouillard, R., 1993. Anthocyanin intramolecular copigment effect. *Phytochemistry* 34, 119–124.
- Davies, K.D., 2009. Modifying anthocyanin production in flowers. In: Gould, K., Davies, K., Winefield, C. (Eds.), *Anthocyanins Biosynthesis, Functions, and Applications*. Springer Science, New York, pp. 49–80.
- Fossen, T., Andersen, Ø.M., 1999. Delphinidin 3'-galloylgalactosides from blue flowers of *Nymphaea caerulea*. *Phytochemistry* 50, 1185–1188.
- Fossen, T., Slimestad, R., Andersen, Ø.M., 2003. Anthocyanins with 4'-glucosidation from red onion, *Allium cepa*. *Phytochemistry* 64, 1367–1374.
- Jakešević, M., Xu, J., Aaby, K., Jeppsson, B., Ahrne, S., Molin, G., 2013. Effects of bilberry (*Vaccinium myrtillus*) in combination with lactic acid bacteria on intestinal oxidative stress induced by ischemia-reperfusion in mouse. *J. Agric. Food Chem.* 61, 3468–3478.
- Jordheim, M., Skaar, I., Lunder, H., Andersen, Ø.M., 2011. Anthocyanins from *Fuchsia* flowers. *Nat. Prod. Commun.* 6, 35–40.
- Kamonpatana, K., Giusti, M.M., Chitthumronchokchai, C., MorenoCruz, M., Riedl, K.M., Kumar, P., Failla, M.L., 2012. Susceptibility of anthocyanins to ex vivo degradation in human saliva. *Food Chem.* 135, 738–747.
- Lee, J.H., 2010. Identification and quantification of anthocyanins from the grains of black rice (*Oryza sativa* L.) varieties. *Food Sci. Biotechnol.* 19, 391–397.
- Phillips, B.E., Smith, C.R., Hagemann, J.R., Hagemann, J.W., 1969. Glyceride structure of *Erlangea tomentosa* seed oil, a new source of vernolic acid. *Lipids* 4, 473–477.
- Prior, R.L., Cao, G., Martin, A., Sofic, E., McEwen, J., O'Brien, C., Lischner, N., Ehrenfeldt, M., Kalt, W., Krewer, G., Mainland, C.M., 1998. Antioxidant capacity as influenced by total phenolic and anthocyanin content, maturity, and variety of *Vaccinium* species. *J. Agric. Food Chem.* 46, 2686–2693.
- Sigurdson, G.T., Robbins, R.J., Collins, T.M., Giusti, M.M., 2018. Impact of location, type, and number of glycosidic substitutions on the color expression of o-dihydroxylated anthocyanidins. *Food Chem.* 268, 416–423.
- Sinela, A., Rawat, N., Mertz, C., Achir, N., Fulcrand, H., Dornier, M., 2017. Anthocyanins degradation during storage of *Hibiscus sabdariffa* extract and evolution of its degradation products. *Food Chem.* 214, 234–241.
- Trouillas, P., Sancho-Garcia, J.C., De Freitas, V., Gierschner, J., Otyepka, M., Dangles, O., 2016. Stabilizing and modulating color by copigmentation: insights from theory and experiment. *Chem. Rev.* 116, 4937–4982.
- Yoshida, K., Mori, M., Kondo, T., 2009. Blue flower color development by anthocyanins: from chemical structure to cell physiology. *Nat. Prod. Rep.* 26, 884–915.
- Zhao, C.-L., Yu, Y.-Q., Chen, Z.-J., Wen, G.-S., Wei, F.-G., Zheng, Q., Wang, C.-D., Xiao, X.-L., 2017. Stability-increasing effects of anthocyanin glycosyl acylation. *Food Chem.* 214, 119–128.

Supporting Information

Anthocyanins from mauve flowers of *Erlangea tomentosa* based on erlangidin – the first reported natural anthocyanidin with C-ring methoxylation

Christopher Adaku^a, Irene Skaar^b, Helge Berland^b, Robert Byamukama^a, Monica Jordheim^b, Øyvind M. Andersen^{b,*}

^a Chemistry Department, Makerere University, P.O. Box 7062, Kampala, Uganda

^b Department of Chemistry, University of Bergen, Allégt. 41, 5007, Bergen, Norway

*Corresponding author. Phone: +47 555 83460.
e-mail address: oyvind.andersen@uib.no (Øyvind M. Andersen)

Content:

Figure S1: ¹H NMR spectrum of **1**.

Figure S2: ¹H-¹³C HSQC NMR spectra of **1**.

Figure S3: ¹H-¹H TOCSY NMR spectra of **1** – sugar region.

Figure S4: ¹H-¹H COSY NMR spectra of **1** – sugar region.

Figure S5: ¹H-¹³C HMBC NMR spectra of **1**.

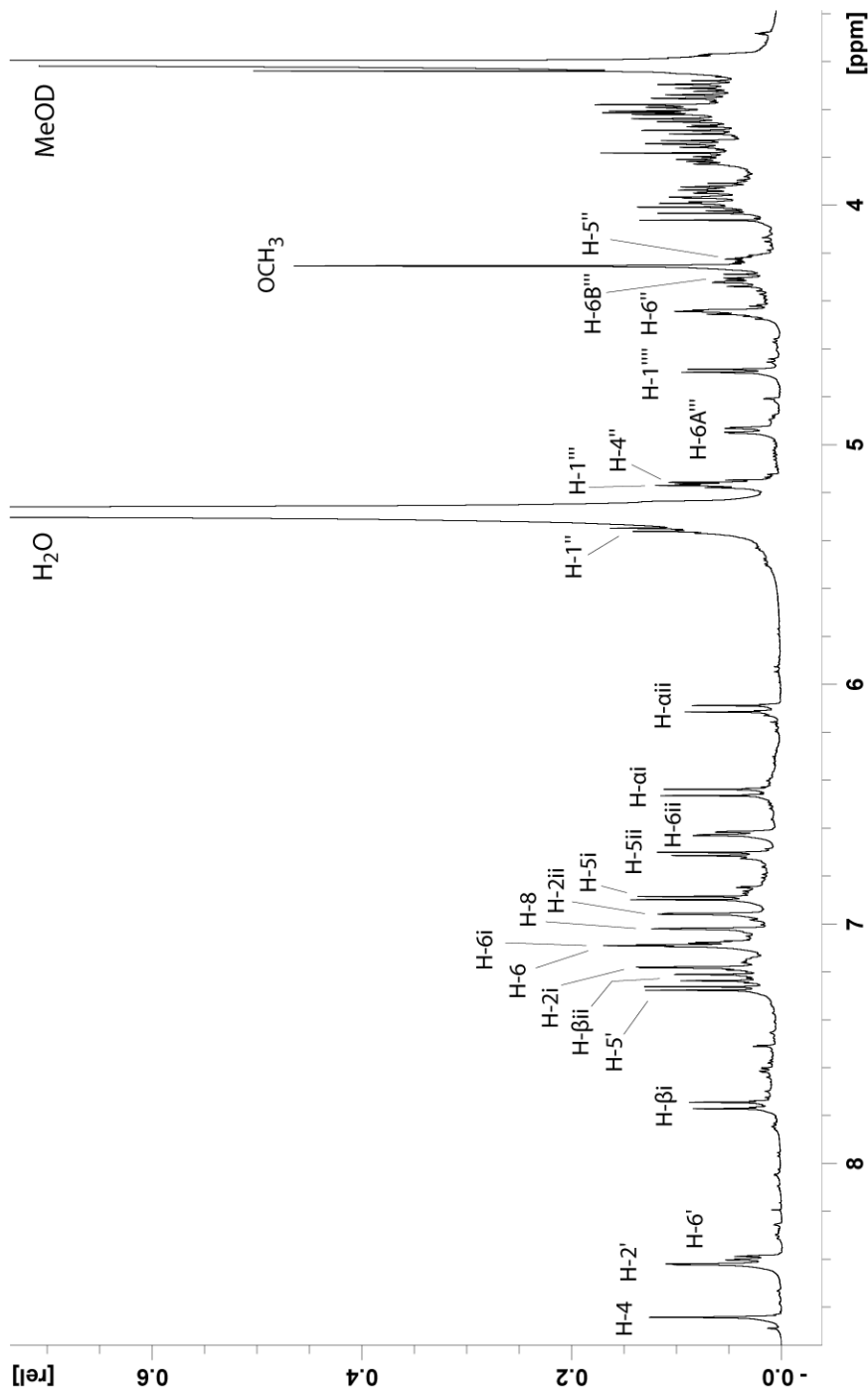


Figure S1. ¹H NMR spectrum (600.17 MHz) of erlangidin 5-*O*-(4''-(*E*-caffeoyl)-6''-(malonyl)-β-glucopyranoside)-3'-*O*-(6'''-(3''-(β-glucopyranosyl)-*E*-caffeoyl)-β-glucopyranoside) (1) in CD₃OD-CF₃CO₂D (95:5, v/v) recorded at 25°C.

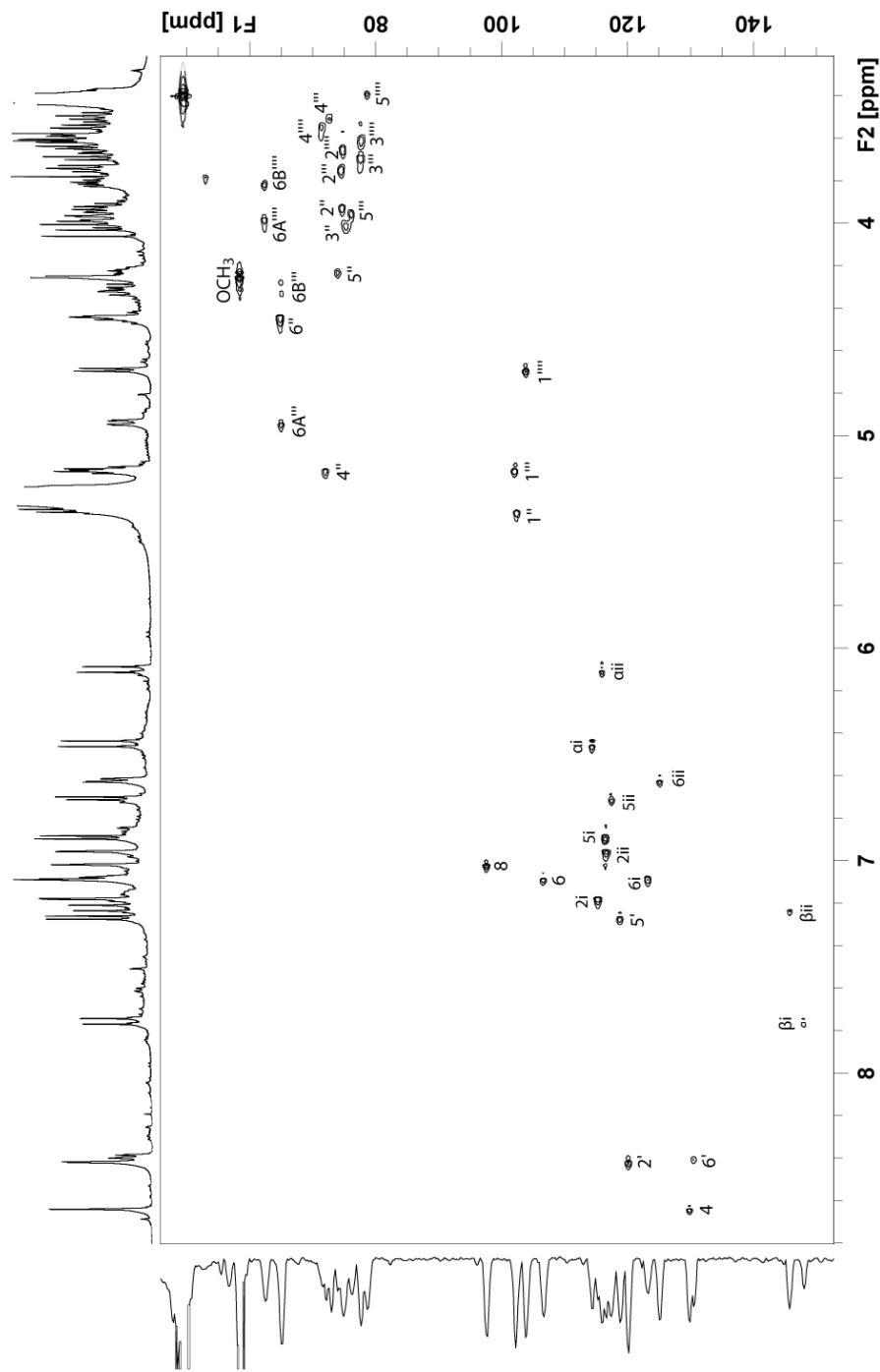


Figure S2. ^1H - ^{13}C HSQC NMR spectra of erlangidin 5-O-(4''-(*E*-caffeoyl)-6''-(malonyl)- β -glucopyranoside)-3'-O-(6'''-(3''-(β -glucopyranosyl)-*E*-caffeoyl)- β -glucopyranoside) (1) in $\text{CD}_3\text{OD}-\text{CF}_3\text{CO}_2\text{D}$ (95:5, v/v) recorded at 25°C, with annotations.

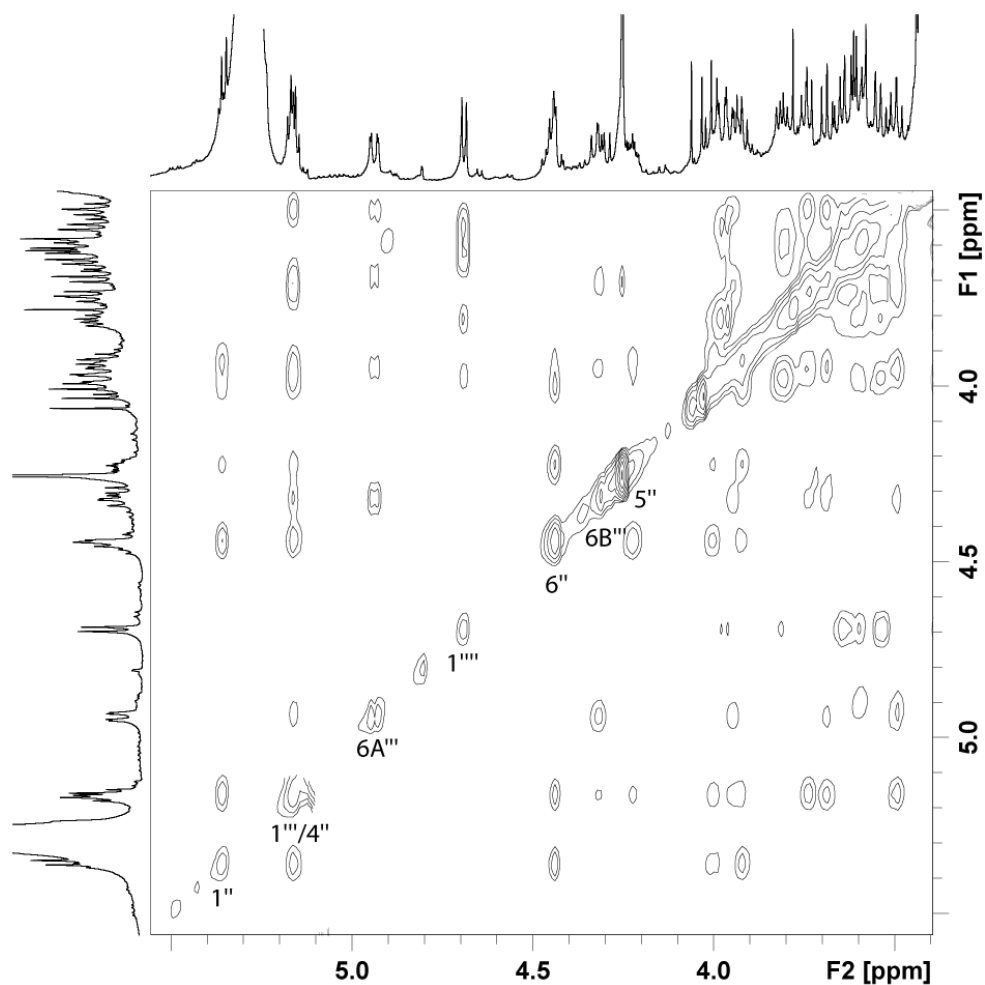


Figure S3. Sugar region of the ^1H - ^1H TOCSY NMR spectra of erlangidin 5-*O*-(4''-(*E*-caffeoyl)-6''-(malonyl)- β -glucopyranoside)-3'-*O*-(6'''-3''L-(β -glucopyranosyl)-*E*-caffeoyl)- β -glucopyranoside) (**1**) in $\text{CD}_3\text{OD}-\text{CF}_3\text{CO}_2\text{D}$ (95:5, v/v) recorded at 25°C. Selected diagonal crosspeaks are assigned.

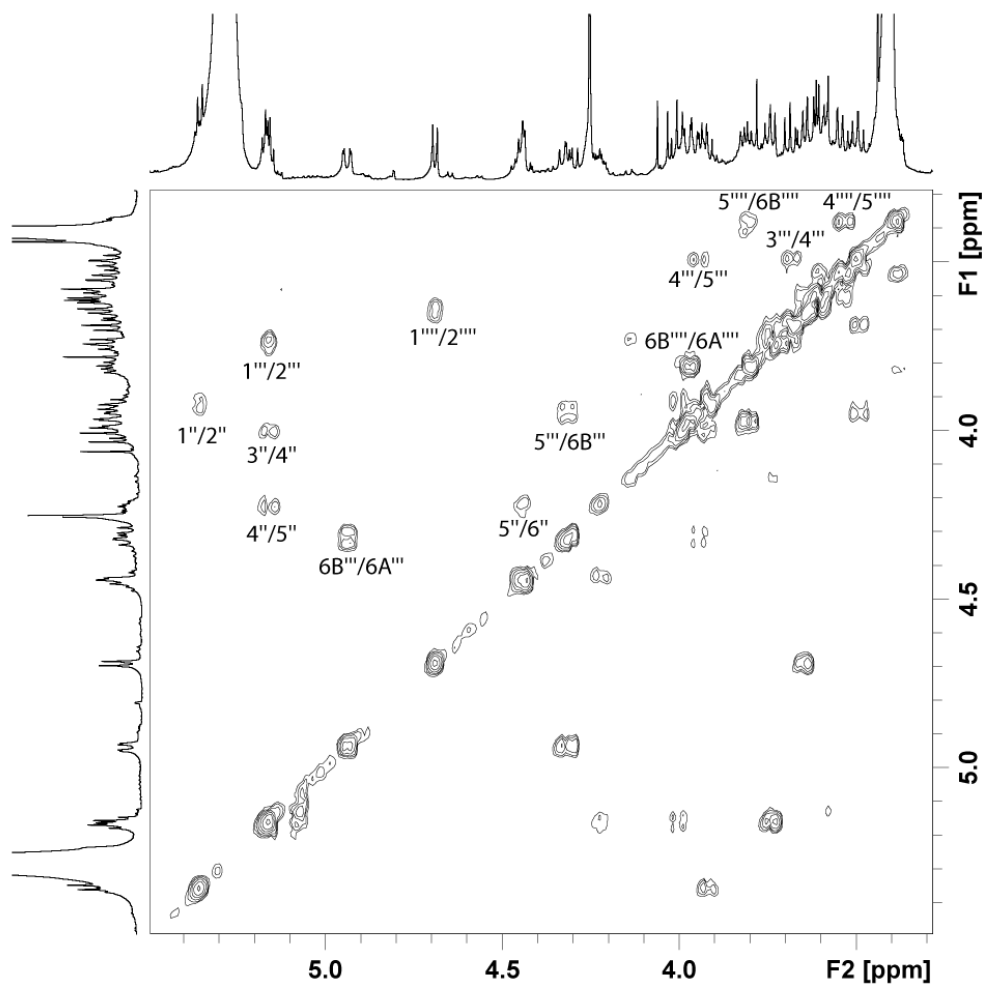


Figure S4. Sugar region of the ^1H - ^1H COSY NMR spectra of erlangidin 5-*O*-(4''-(*E*-caffeoyl)-6''-(malonyl)- β -glucopyranoside)-3'-*O*-(6'''-(3^{II}- β -glucopyranosyl)-*E*-caffeoyl)- β -glucopyranoside (**1**) in CD_3OD - $\text{CF}_3\text{CO}_2\text{D}$ (95:5, v/v) recorded at 25°C. Selected crosspeaks are assigned.

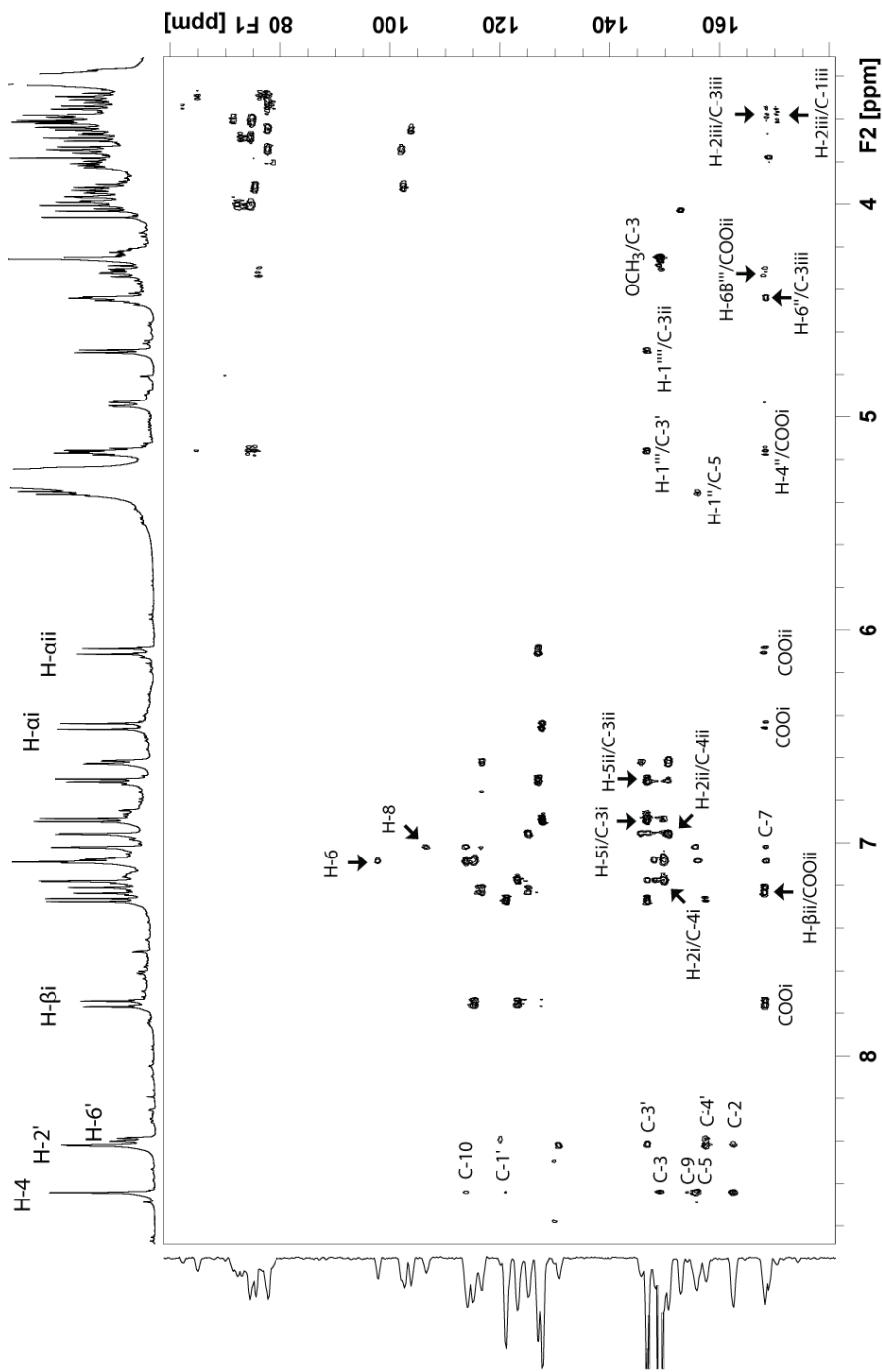


Figure S5. ^1H - ^{13}C HMBC NMR spectra of erlangidin 5-*O*-(4''-(*E*-caffeoyl)-6''-(malonyl)- β -glucopyranoside)-3'-*O*-(6'''-(3''-(β -glucopyranosyl)-*E*-caffeoyl)- β -glucopyranoside) (**1**) in $\text{CD}_3\text{OD}-\text{CF}_3\text{CO}_2\text{D}$ (95:5, v/v) recorded at 25°C. Quarternary carbon atoms have been assigned.

Paper IV

Nutraceutical characterization of anthocyanin-rich fruits produced by 'Sun Black' tomato line

Federica Blando, Helge Berland, Gabriele Maiorano, Miriana Durante, Andrea Mazzucato, Maurizio E. Picarella, Isabella Nicoletti, Carmela Gerardi, Giovanni Mita, Øyvind M. Andersen

Frontiers in Nutrition (2019)



Nutraceutical Characterization of Anthocyanin-Rich Fruits Produced by “Sun Black” Tomato Line

Federica Blando^{1*}, Helge Berland², Gabriele Maiorano¹, Miriana Durante¹, Andrea Mazzucato³, Maurizio E. Picarella³, Isabella Nicoletti⁴, Carmela Gerardi¹, Giovanni Mita¹ and Øyvind M. Andersen²

¹ Institute of Sciences of Food Production, (ISPA), CNR, Lecce, Italy, ² Department of Chemistry, University of Bergen, Bergen, Norway, ³ Department of Agriculture and Forest Sciences, University of Tuscia, Viterbo, Italy, ⁴ Institute for Biological Systems (ISB), CNR, Rome, Italy

OPEN ACCESS

Edited by:

Antonio Ferrante,
University of Milan, Italy

Reviewed by:

Chafik Haidar,
Institut National de la Recherche
Agronomique de Tunisie, Tunisia
Eugenio Butelli,
John Innes Centre (JIC),
United Kingdom

*Correspondence:

Federica Blando
federica.blando@ispa.cnr.it

Specialty section:

This article was submitted to
Nutrition and Food Science
Technology,
a section of the journal
Frontiers in Nutrition

Received: 30 April 2019

Accepted: 09 August 2019

Published: 28 August 2019

Citation:

Blando F, Berland H, Maiorano G,
Durante M, Mazzucato A,
Picarella ME, Nicoletti I, Gerardi C,
Mita G and Andersen ØM (2019)
Nutraceutical Characterization of
Anthocyanin-Rich Fruits Produced by
“Sun Black” Tomato Line.
Front. Nutr. 6:133.
doi: 10.3389/fnut.2019.00133

Tomato (*Solanum lycopersicum* L.) is one of the most cultivated vegetable in the world and it represents a large source of bioactive compounds, including carotenoids and polyphenols (phenolic acids and flavonoids). However, the concentration of flavonoids in tomato is considered sub-optimal, particularly because anthocyanins are not generally present. Therefore, this crop has been the object of an intense metabolic engineering in order to obtain anthocyanin-enriched tomatoes by using either breeding or transgenic strategies. Some wild tomato species, such as *S. chilense* and *S. cheesmaniae*, biosynthesize anthocyanins in the fruit sub-epidermal tissue, and some alleles from those genotypes have been introgressed into a new developed purple tomato line, called “Sun Black” (SB). It is a tomato line with a purple skin color, both in green and in red fruit stages, due to the biosynthesis of anthocyanins in the peel, and a normal red color pulp, with a taste just like a traditional tomato. SB is the result of a breeding programme and it is not a genetically modified (GM) product. We report the chemical characterization and structure elucidation of the attractive anthocyanins found in the peel of SB tomato, as well as other bioactive compounds (carotenoids, polyphenols, vitamin C) of the whole fruit. Using one- and two-dimensional NMR experiments, the two main anthocyanins were identified to be petunidin 3-O-[6''-O-(4'''-O-E-p-coumaroyl- α -rhamnopyranosyl)- β -glucopyranoside]-5-O- β -glucopyranoside (petanin) and malvidin 3-O-[6''-O-(4'''-O-E-p-coumaroyl- α -rhamnopyranosyl)- β -glucopyranoside]-5-O- β -glucopyranoside (negretein). The total anthocyanins in the whole ripe fruit was 1.2 mg/g dry weight (DW); 7.1 mg/100g fresh weight (FW). Chlorogenic acid (the most abundant phenolic acid) was 0.6 mg/g DW; 3.7 mg/100g FW. The main flavonol, rutin was 0.8 mg/g DW; 5 mg/100g FW. The total carotenoid content was 211.3 μ g/g DW; 1,268 μ g/100g FW. The total phenolic content was 8.6 mg/g DW; 52.2 mg/100g FW. The vitamin C content was 37.3 mg/100g FW. The antioxidant activities as measured by the TEAC and ORAC assays were 31.6 and 140.3 μ mol TE/g DW, respectively (193 and 855.8 μ mol TE/100g FW, respectively). The results show the unique features of this new tomato genotype with nutraceutical properties.

Keywords: tomato, tomato breeding, bioactive compounds, anthocyanins, functional food

INTRODUCTION

The tomato (*Solanum lycopersicum* L.) is one of the most cultivated vegetables in the world, whose production was around 182 million tons (FAOSTAT)¹ in 2017. The average annual consumption of tomato fruit is 18 kg per capita in Europe and 8 kg in the US, with regular dietary intake in fresh, cooked and processed form, depending on the local habit (1). The tomato fruit has a high nutritional value, thanks to the presence of numerous antioxidant compounds such as carotenoids, phenolic compounds, vitamin C and E. These compounds are supposed to be responsible for the beneficial effects on health, such as reduced risk of inflammatory processes, cancer and cardiovascular diseases (2–5). Since tomatoes are an important component of the Mediterranean diet, probably their consumption contributes to the decreased risk of some chronic diseases in the Mediterranean area (6). However, among phenolic compounds, one sub-class of these secondary metabolites is scarce in tomato, i.e., flavonoids, whose concentration is considered sub-optimal, particularly because anthocyanins are not generally present in the fruit. Therefore, tomato is an ideal candidate for anthocyanin enrichment due to its widespread consumption over the world, year-round.

A great variation in size, shape and color exists in the modern tomato varieties. Some cultivated varieties show dark skin color ("black" or "purple") as a result of mutations in carotenoid biosynthesis or chlorophyll breakdown (7). The red color of the tomato fruit results from the accumulation of lycopene, the most present carotenoid in the fruit. Conventional tomato genotypes accumulate anthocyanins on vegetative tissues, but not on fruit (8). On the contrary, the fruit of different wild *Solanum* species, closely related to cultivated tomato, accumulates anthocyanins in the peel (7, 9).

Anthocyanins belonging to the flavonoid family are a group of natural pigments represented by over 700 different molecular structures responsible for the red-blue color of many fruits and vegetables (10), having strong antioxidant properties (11). Anthocyanins are of particular interest to the agri-food industry, because of their potential health benefits, as well as their unique feature to confer vibrant colors to a variety of products (12–14). Recent studies using purified anthocyanins or anthocyanin-rich extracts on *in vitro* experimental systems have shown anti-inflammatory and anti-atherosclerotic effects (15–17). *In vivo* animal experiments and human clinical trials have given reason of the efficacy and biological activities of anthocyanins in the prevention of cardio-vascular disease (CVD) and cancer [(18–20) and references therein].

Giving these premises, it is not surprising that in the last 20 years there has been an increasing interest in developing highly consumed food, such as tomato, rich in flavonoids and particularly anthocyanins. To this purpose, transgenic approaches have been applied to modify the biosynthesis of phenylpropanoids, in order to alter the flavonoid composition of the tomato fruit. The ectopic expression in tomato of specific transcription factor (TF) genes from maize (*Lc* and *C1*), lead

to 60% increase of flavonol (kaempferol) content at the whole fruit level (8). Conversely, the overexpression of TFs *Del* and *Ros1* from snapdragon (*Antirrhinum majus* L.), under the fruit-specific *E8* promoter resulted in high anthocyanin accumulation throughout the fruit of Micro-Tom, a model cultivar for tomato research (21). The same approach, using TFs *Del* and *Ros1* from *A. majus*, as used by in Butelli et al. (21) was applied to an Indian commercial cultivar (22). Recently, Scarano et al. (23) reported the engineering of a new tomato line, named "Bronze," expressing the TFs *Del* and *Ros1* from *A. majus* (inducing anthocyanin biosynthesis), *MYB12* from *A. thaliana* (regulating flavonol biosynthesis), and the biosynthetic gene *StSy* (from *V. vinifera*) controlling the production of resveratrol.

A strategy more likely to receive consumer acceptance is the conventional breeding using interspecific crosses with wild *Solanum* species, which transfers to cultivated varieties the ability to produce anthocyanins in the fruit. Some wild tomato species, such as *S. chilense*, *S. cheesmaniae*, *S. lycopersicoides*, and *S. habrochaites*, biosynthesize anthocyanins in the sub-epidermal tissue of the fruit, and some alleles from those genotypes have been introgressed into cultivated genetic backgrounds. At Tuscia University (Viterbo, Italy), a 20-years breeding activity has produced new tomato lines by intervarietal crossing or backcrossing mutant genes (for fruit color) to commercial cultivars used as recurrent parents (24). In particular, the combination of different alleles, responsible for the anthocyanin biosynthesis (*Aft* and *atv*), led to select a line (*AftAft/atvatv*) with a "purple" skin color, due to the biosynthesis of anthocyanins in the peel, having still a red colored flesh and a taste just like a traditional tomato (25). This selection was named "Sun Black" due to the requirement of light for anthocyanin accumulation, as phytochromes are known to be involved in light-mediated regulation of anthocyanins biosynthesis (26). The molecular nature of the introgressions underlying the "Sun Black" phenotype has been recently clarified. A dominant gene located on Chr10 and encoding an *R2R3-MYB* TF activating anthocyanin biosynthesis is thought to underlie the *Aft* variant (27), although it is still uncertain which of the three paralogs located in the involved genomic region is the actual responsible for the phenotype (28). More recently, the identity of the *atv* variant has been also identified as a mutation of an *R3-MYB* located on Chr7 and acting as a repressor of anthocyanin biosynthesis (29, 30).

We report here the chemical characterization and structure elucidation of the anthocyanins found in the peel of "Sun Black" tomato, as well as nutraceutical features of the whole fruit.

MATERIALS AND METHODS

Plant Material (Genetic Characteristics of SB Tomato)

Purple tomatoes were bred by crossing a line carrying the *Anthocyanin fruit* introgression (*Aft*, LA1996) and the *atroviolaceum* mutant line (*atv*, LA0797) as described (25).

A stable *AftAft/atvatv* purple line (line V710448, called "Sun Black," SB) was selected in parallel with a stable

¹FAOSTAT. Available online at: <http://www.fao.org/faostat/en/#home>

line with red fruits (*aftaft/AtvAtv*) (line V710445, hereafter referred to as WT, standing for "wild type") used as a wild type reference. The two lines were selected for having the same vegetative and fruit characteristic, except for the fruit color phenotype. The term "Sun Black" has been protected as a trademark and the cultivars selected from the Tuscia University breeding programme are now commercialized (cv "Solenero" and others). The genetic combination giving rise to anthocyanin accumulation on the tomato peel is the same exploited in other commercial genotypes, such as cv "Indigo Rose" (<https://extension.oregonstate.edu/news/purple-tomato-debuts-indigo-rose>). Differently from "Indigo Rose" which is an indeterminate genotype, the SB line is a semi-indeterminate genotype.

Plants of the two lines were grown in an unheated tunnel in Viterbo, Italy (42°25'07" N, 12°06'34" E) arranged in twin rows and grown with the same agronomic techniques and inputs, corresponding to the standard agronomic practices for fresh market tomatoes. All genotypes were grown on tutors; axillary shoots were systematically removed, and the canopy reduced to expose the fruits to natural light. Plants were left to open pollination to set fruits.

Reagents and Standards

Reagents were purchased from various suppliers as follows: Authentic standards of kuromanin (cyanidin 3-O-glucoside chloride), chlorogenic acid (3-caffeoylquinic acid), gentisic acid, rutin (quercetin 3-O-rutinoside) (Extrasynthèse, Genay, France); the standard for carotenoids (lutein, carotene, α -carotene, β -carotene and lycopene) were purchased from CaroteNature (Lupsingen, Switzerland); gallic acid, Folin-Ciocalteu's phenol reagent, Trolox [(S)-(-)-6-hydroxy-2,5,7,8-tetramethylchroman-2-carboxylic acid], ABTS [2,2'-azino-bis(3-ethylbenzothiazoline-6-sulfonic acid)], fluorescein disodium, AAPH [2,2'-azobis(2-methyl-proprionamide)], ascorbic acid, *meta*-phosphoric acid, DTT (dithiothreitol), BHT (butylated hydroxytoluene) as well as acetonitrile, ethanol, methanol, acetone, methyl tert-butyl ether, formic acid and acetic acid (all HPLC grade) (Sigma-Aldrich, St. Louis, MO, USA). In all experiments Milli-Q (Merck Millipore, Darmstadt, Germany) water was used.

Sample Extraction

Fruits were collected from the two lines (WT and SB) at three developmental stages: mature green (MG, fruit fully developed with surface of the tomato completely green), breaker (BR, about 50% of the fruit with color changed to red) and red ripe (RR, fruit completely ripe with red color). Developmental stages in purple fruits were inferred by inspecting the blossom end that is usually lacking anthocyanin accumulation.

Tomato fruits (at least three fruits for each developmental stage) were collected from three plants of both lines, immediately cooled at 4°C, washed, cut into pieces and reduced to a fine powder with a Waring blender, in presence of liquid N₂. The powder was then freeze-dried using a Freezone[®] 2.5 model 76530 lyophiliser (Labconco Corp., Kansas City, MO, USA) for 48 h and stored in polyethylene tubes at -20°C (-80°C for

carotenoids), until analysis. For ascorbic acid determination, aliquots of fresh fruit were stored at -80°C until analysis.

Anthocyanin extraction (for structure elucidation) was done from the peel of at least 1 kg (fresh weight, FW) of SB tomato at MG and RR stages. Freeze-dried peel (25 g) was extracted with Methanol:Water:Trifluoroacetic acid (70:29.5:0.5 v/v/v), with a ratio 1/20 (W/V), o.n., in static at room temperature. After centrifugation at 3,500 g for 10 min., the extraction was repeated for 1 h in the same condition, the supernatants were combined and solvent evaporated at 32°C to 1/3 of the initial volume, then freeze-dried.

Polyphenols (including anthocyanins, for quantitative purposes) were extracted in triplicate from 100 mg freeze dried material (whole fruit), macerated overnight at 4°C in 10 mL of extraction solvent [Methanol:Ethanol:Water:Formic acid (35:35:28:2 v/v/v/v)]. After centrifugation at 3,500 g for 10 min., the extraction was repeated on a rotary shaker at room temperature, the supernatants were combined and organic solvent evaporated at 32°C, then brought to a known volume with acidified water (0.1% formic acid). Extracts were filtered through a 0.45 μ m nylon membrane (PTFE) (Millipore, Bedford, MA), stored at -20°C and analyzed in triplicates within 1 month.

Carotenoids were extracted from triplicate aliquots of freeze-dried tomato powder (50 mg, whole fruit) by the method of Sadler et al. (31) modified by Perkins-Veazie et al. (32). Carotenoids were extracted with 20 mL mixture of hexane/ethanol/acetone (2/1/1 v/v/v) containing 0.05% of BHT. Samples were shaken on an orbital shaker at 180 rpm for 15 min. Then, 3 mL of distilled water was added and the suspension was centrifuged at 4,500 g for 10 min. The organic phase was dried under nitrogen, resuspended in 1 mL of ethyl acetate and analyzed by HPLC.

Ascorbic acid extraction was done from 1 g fresh tomato fruit (from freshly-grounded fruits in Waring blender with liquid N₂) in 10 mL 5% *meta*-phosphoric acid, centrifuging at 10,000 g for 20 min at 4°C.

Analysis of Anthocyanins, Other Polyphenols, Carotenoids, and Vitamin C

The concentrated filtered freeze-dried anthocyanin extract was purified using partition against ethyl acetate and Amberlite XAD-7 column chromatography. Isolation of individual compounds was performed using Sephadex LH-20 column chromatography and preparative HPLC. Structural elucidations of the main anthocyanins were mainly based on the following NMR experiments: One-dimensional ¹H, 2D heteronuclear single quantum coherence (¹H-¹³C HSQC), heteronuclear multiple bond correlation (¹H-¹³C HMBC), double quantum filtered correlation (¹H-¹H DQF-COSY), and total correlation (¹H-¹H TOCSY) spectroscopy [experimental procedure according to Skaar et al. (33)]. See **Table 1** for assignments of individual ¹H and ¹³C chemical shifts for anthocyanin **1** and **2**, and **Figures S1, S2** for the HSQC and HMBC spectra of anthocyanin **1**.

Sample extracts were analyzed for phenolic compounds by an HPLC apparatus with photodiode array (PDA) detection

TABLE 1 | ^1H and ^{13}C NMR spectral data for the anthocyanins petunidin 3-O-[6''-O-(4'''-O-E-p-coumaroyl- α -rhamnopyranosyl)- β -glucopyranoside]-5-O- β -glucopyranoside (petanin, **1**) and malvidin 3-O-[6''-O-(4'''-O-E-p-coumaroyl- α -rhamnopyranosyl)- β -glucopyranoside]-5-O- β -glucopyranoside (negreitein, **2**) isolated from the peel of "Sun Black" tomato recorded in $\text{CF}_3\text{COOD-CD}_3\text{OD}$ (5:95, v/v) at 25°C.

	1 (^1H)	2 (^1H)	1 (^{13}C)	2 (^{13}C)
ANTHOCYANIDIN				
2			164.34	164.66
3			146.03	146.32
4	9.06	9.02	133.92	135.41
5			156.56	156.86
6	7.11	7.04	105.63	105.90
7			169.40	169.95
8	7.16	7.14	97.24	97.76
9			156.94	157.45
10			112.82	113.31
1'			119.71	119.75
2'	8.11	8.04	109.48	111.16
3'			149.65	149.84
4'			146.35	147.35
5'			147.56	149.84
6'	7.94	8.04	113.95	111.16
OMe	4.10	4.01	57.04	57.44
3-O-GLUCOSIDE				
1''	5.59	5.50	102.26	106.14
2''	3.82	3.70	74.47	75.00
3''	3.67	3.59	78.29	78.58
4''	3.56	3.47	71.51	71.76
5''	3.91	3.81	77.81	78.05
6A''	4.11	4.01	67.30	67.59
6B''	3.82	3.73	67.30	67.59
6''-O-RHAMNOSYL				
1'''	4.80	4.71	101.63	102.13
2'''	3.88	3.80	72.34	72.50
3'''	3.92	3.82	70.34	70.61
4'''	5.01	4.91	75.27	75.52
5'''	3.83	3.71	67.17	67.71
6'''	1.09	0.98	17.73	18.21
5-O-GLUCOSIDE				
1''''	5.28	5.20	102.36	102.90
2''''	3.78	3.69	74.64	75.02
3''''	3.66	3.59	77.97	78.51
4''''	3.63	3.54	70.90	71.31
5''''	3.73	3.69	76.81	78.29
6A''''	4.03	3.94	62.05	62.37
6B''''	3.87	3.79	62.05	62.37
4'''-E-p-COUMAROYL				
1			127.06	127.29
2	7.53	7.43	130.64	131.27
3	6.90	6.81	116.39	117.03
4			161.17	161.39
5	6.90	6.81	116.39	117.03
6	7.53	7.43	130.66	131.27
α	6.35	6.27	114.38	115.07
β	7.67	7.57	146.58	147.40
COO			168.80	169.06

See Figure 2B for structures.

(Agilent 1100 series, Agilent Technologies, Santa Clara, CA, USA). Instrument control, data acquisition and processing were provided by the ChemStation software (Agilent Technologies). Separations were performed at 30°C on a Luna RP-C18 column (250 × 4.6 mm, 5 μm internal diameter) (Phenomenex, Torrance, CA, USA) equipped with a guard cartridge column. The samples were eluted following the multi-segment linear gradient employed in Gerardi et al. (14), using 5% (v/v) formic acid both in water (mobile phase A) and in acetonitrile (mobile phase B). UV-visible spectra were recorded in the 200–800 nm range and chromatograms were acquired at 280 and 520 nm. Individual polyphenolic compounds were identified by comparing their peak retention times and UV-visible spectra with those of commercial standards, and by co-chromatography of samples spiked with the standards.

The identified phenolic compounds were quantified by the external standard method using calibration graphs obtained with solutions of available authentic standards at six different concentration within the linearity range of concentration.

Anthocyanins were quantified by using a calibration graph (six concentration levels from 0.001 to 0.5 $\mu\text{g/L}$, analyzed in triplicate) constructed with petanin standard purified in house.

Carotenoids analyses were carried out using an Agilent 1100 Series HPLC system as described by Durante et al. (34).

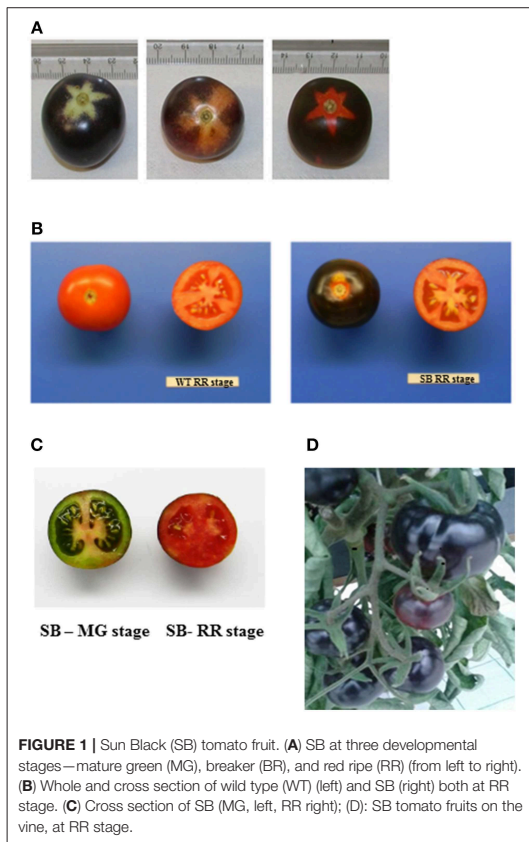
Determination of vitamin C (Ascorbic acid, AA, plus Dehydroascorbic acid, DHA) was done according to Sánchez-Moreno et al. (35), with some modifications. Samples were kept in the dark and on ice all the time. The total AA + DHA was obtained after reduction of DHA to AA by DTT. Sample extract (0.2 mL) and DTT solution (50 mg/mL) (0.2 mL) were mixed and diluted to 1 mL with 5% meta-phosphoric acid and let to react at room temperature in darkness for 2 h, then injected onto the HPLC system, following the same conditions as in Gerardi et al. (14). DHA content was obtained by subtracting the initial AA content to the final total AA content after reduction.

Antioxidant Capacity Analysis

The Folin-Ciocalteu (F-C) reducing capacity assay, the TEAC and the ORAC assays were evaluated in WT and SB hydrophilic extracts, as described in Gerardi et al. (14). A rapid microplate methodology, using a microplate reader (Infinite M200, Tecan Trading AG, Switzerland) and 96-well plates (Costar, 96-well black round bottom plate, Corning) were used. All experiments were performed in triplicate, and two independent assays were performed for each sample.

Statistical Analysis

Assays were carried out in triplicate and the results were expressed as mean values \pm standard deviation (SD). Differences between samples were analyzed by one-way analysis of variance (ANOVA) with Tukey's HSD *post hoc* test. A *p*-value lower than 0.05 was considered statistically significant. Statistical analysis was performed using SigmaPlot version 13.0 software (SyStat Software Inc., Chicago, IL).



RESULTS

Occurrence and Profile of Polyphenolic Compounds: Comparison of "Sun Black" and Wild Type Tomatoes Anthocyanins

The presence of anthocyanin pigment in SB tomato fruit was visually detected already at the immature (MG) stage, making difficult the inspection of developmental stages, unless to focus on the calix imprint or shaded area where anthocyanin biosynthesis was not activated by the light (**Figure 1**).

The only but very significant difference between WT and SB tomato fruits was the color of the peel (**Figure 1A**), instead the flesh was regularly red, both at immature (MG) and mature (RR) stage (**Figures 1B,C**).

The HPLC profile of SB fruit extracts, regardless of the ripening stage, showed two major peaks (corresponding to pigments **1** and **2**), in addition to small amounts of other anthocyanins (**Figure 2A**).

The downfield part of the ^1H NMR spectrum of anthocyanin **1** showed a 1H singlet at δ 9.06 (H-4), a 2H AX system at δ 8.11 (H-2') and δ 7.94 (H-6'), and a 2H AX system

at δ 7.16 (H-8) and δ 7.11 (H-6) (**Table 1**). A singlet at δ 4.10 integrating for 3H, corresponding to a methoxy group, identified the aglycone as petunidin. The acyl moiety was identified as *p*-coumaric acid by the 4H AA'XX' spin system at δ 7.53 (H-2,6) and δ 6.90 (H-3,5) and the AX system at δ 7.67 (H- β) and δ 6.35 (H- α). A coupling constant of 15.8 Hz between H- α and H- β showed the *E*-configuration. The chemical shifts of the carbons of the aglycone and acyl moiety assigned by the HMBC and HSQC NMR experiments were also in agreement with the presence of petunidin and one *p*-coumaroyl acid moiety (**Table 1**). In the ^1H NMR spectrum three anomeric proton signals were detected. The proton and carbon resonances belonging to the respective sugar moieties were assigned by DQF-COSY, TOCSY, and HSQC experiments to be in accordance with two glucopyranosyl and one rhamnopyranosyl units (**Table 1**).

The connection sites of the sugars of **1** on the aglycone were derived from the HMBC experiment. Cross-peaks between the anomeric proton at δ 5.59 and the carbon at δ 146.03 (C-3), and the anomeric proton at δ 5.28 and the carbon at δ 156.56 (C-5), revealed that the aglycone 3- and 5-positions were both connected to a glucopyranosyl with β -linkages showing coupling constants of 7.8 Hz. A cross-peak between the anomeric proton at δ 4.80 and the carbon at δ 67.30 revealed that the rhamnopyranosyl was connected to the 6'-position on the 3-glucopyranoside. The downfield shift (5.25 ppm) of the 6'-carbon resonance compared to the analogous signal of the 5-glucopyranosyl (**Table 1**) also confirmed this connection site. A downfield shift of H-4''' (δ 5.01) together with a cross-peak in the HMBC spectrum between this resonance and the carbon signal at δ 168.80, revealed that the *p*-coumaroyl moiety was connected to the rhamnosyl 4'''-position. Thus, **1** was identified as petunidin 3-*O*-[6''-*O*-(4'''-*O*-*E*-*p*-coumaroyl- α -rhamnopyranosyl)- β -glucopyranoside]-5-*O*- β -glucopyranoside called petanin [**Figure 2B**; (36)].

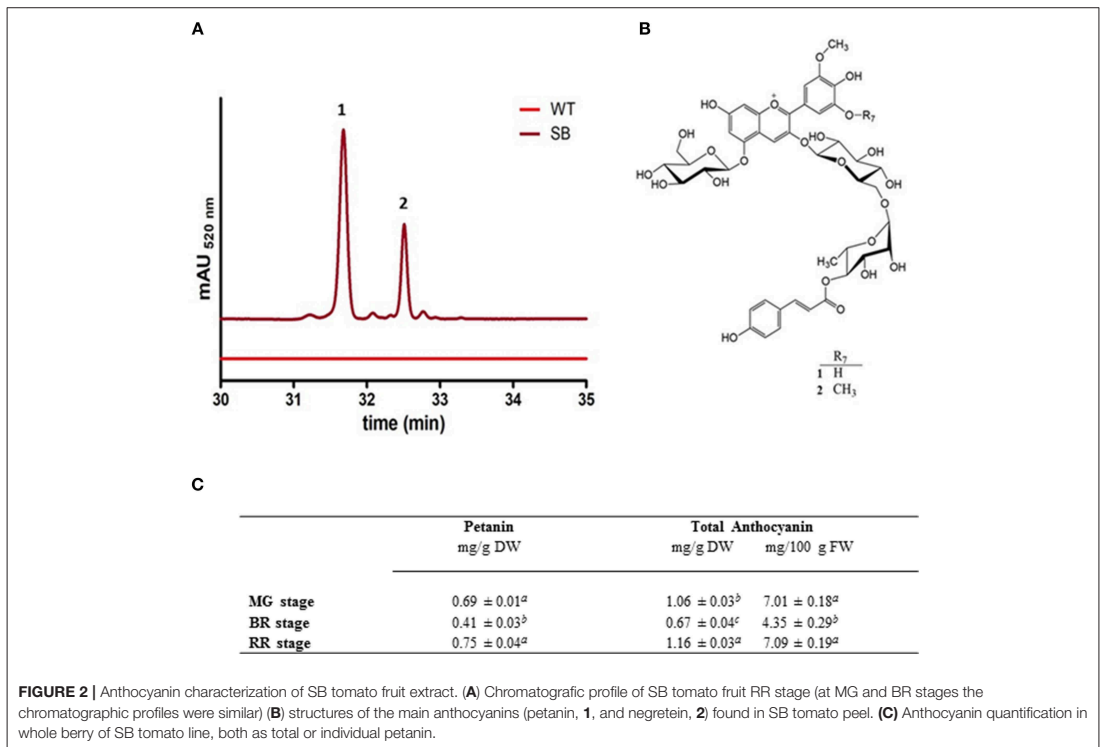
The NMR spectra of anthocyanin **2** showed many similarities with the corresponding spectra of **1** (**Table 1**). After assignments of the proton and carbon resonances, pigment **2** revealed an anthocyanidin B-ring with one hydroxyl group replaced with a methoxy group compared to that of **1**, in accordance with malvidin. Thus, **2** was identified as malvidin 3-*O*-[6''-*O*-(4'''-*O*-*E*-*p*-coumaroyl- α -rhamnopyranosyl)- β -glucopyranoside]-5-*O*- β -glucopyranoside called negretein [**Figure 2B**; (37)].

Petanin and negretein represented 56.6 and 21.4% of the total anthocyanins in SB peel, respectively.

No anthocyanin compound was detected in WT tomato fruit (flesh or peel) nor in the flesh of SB fruit (data not shown). The quantification of anthocyanin in SB (whole fruit) was done using standard curves based on petanin, the standard purified in house. This has made the quantification more reliable than in other reports, where aglycone standard curves were used. **Figure 2C** reports the anthocyanin quantification in whole berry of SB line, both as total or individual petanin.

Phenolic Acids and Flavonols

For the analysis of polyphenols we used a reproducible extraction protocol using aqueous acidified methanol/ethanol



as extraction solvent. This solvent was able to extract polar and semi-polar compounds, and to stabilize anthocyanins on their flavylium forms due to the acid content. Each sample was extracted in triplicate and two technical replicates were adopted to assure reliable results as recovery and repeatability.

We decided to conduct the study with the whole fruit in order to simulate the conditions while eating the fresh fruit.

With the chromatographic method already established in our laboratory (14) we were able to identify several peaks corresponding to phenolic compounds commonly found in traditional tomatoes (38) (Figure 3A).

The chromatographic profile of SB tomato extract at 280 and 320 nm appeared much more complex than other purple tomato genotype (ex. V118 from Ontario) (39) for the more polar compounds eluting earlier (hydroxycinnamic acids). SB extract showed a group of predominant peaks, eluting before chlorogenic acid, which could be assigned, on the basis of similarity to V118 purple tomato, to the unknown peak 1, tentatively identified as caffeic acid hexoside by the authors (39).

The quantification of polyphenolic compounds is reported in Figure 3B and Table S1. In addition to anthocyanins, not present in WT, also phenolic acids and flavonols were found at higher level in SB tomato.

As a quantity, chlorogenic acid was the most abundant phenolic compound quantified in SB tomato extract (from 0.5 to 1.3 mg/g DW, depending on the developmental stage).

Among flavonols, only two peaks were present with maximum absorbance at $\lambda = 350$ nm. Rutin (RT = 29 min) was identified and quantified (Table S1). The peak with RT = 25.9 min showed an absorption spectrum similar to rutin, and from literature data on tomato, particularly in tomato bearing *high pigment (hp)* gene, it has been tentatively assigned to rutin pentoside (24, 38). Total flavonols were quantified as Rutin Equivalent (RE) based on the area of rutin plus rutin pentoside (Table S1).

A more detailed characterization of unknown phenolic compounds present in SB extract will be addressed in a future study; here we report a general characterization of nutraceutical components of the new bred purple tomato SB, in respect to the wild type fruit.

Carotenoids Profile and Their Occurrence

The identification and quantification of carotenoids by HPLC is shown in Table 2.

On a dry weight basis, at the MG stage both in WT and SB the main carotenoid was lutein, followed by β - and α -carotene, respectively, in both genotypes, while lycopene was not detected. When compared, the various carotenoids occurred at the MG

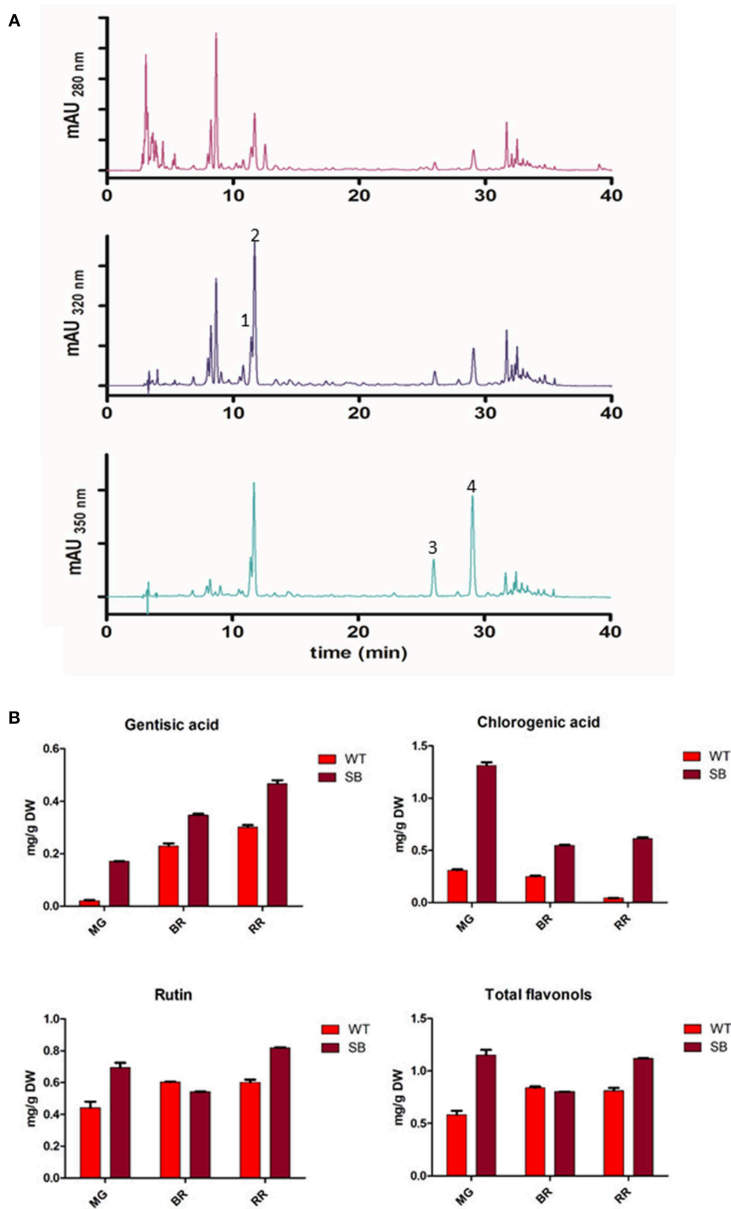


FIGURE 3 | Phenolic acids and flavonols in SB tomato extract. **(A)** Chromatographic profile of SB tomato fruit extract at $\lambda = 280\text{-}320\text{-}350\text{ nm}$. **(B)** Quantification of some phenolic acids and flavonols. Peak 1, genticic acid; peak 2, chlorogenic acid; peak 3, rutin pentoside; peak 4, rutin.

stage in similar amounts in both genotypes. At the BR stage, differences could be found between WT and SB: The content of lutein and α -carotene was higher in SB than in WT. At the RR

stage, the total carotenoids content was statistically similar in the SB and WT lines. However, the β -carotene content was significant higher in the SB sample, while the lycopene content was lower.

TABLE 2 | Carotenoid contents ($\mu\text{g/g}$ dry weight, DW, and $\mu\text{g/g}$ fresh weight, FW) in wild type (WT) and Sun Black (SB) tomato at different stages of ripening, mature green (MG), breaker (BR), and red ripe (RR).

Sample	Lutein		β -carotene		α -carotene		Lycopene		Total carotenoids	
	$\mu\text{g/g}$ DW	$\mu\text{g}/100\text{g}$ FW	$\mu\text{g/g}$ DW	$\mu\text{g}/100\text{g}$ FW	$\mu\text{g/g}$ DW	$\mu\text{g}/100\text{g}$ FW	$\mu\text{g/g}$ DW	$\mu\text{g}/100\text{g}$ FW	$\mu\text{g/g}$ DW	$\mu\text{g}/100\text{g}$ FW
WT-MG	39.75 \pm 3.29 ^{a,b}	278.25 \pm 23.03 ^a	21.33 \pm 2.61 ^b	149.31 \pm 18.27 ^b	3.49 \pm 0.53 ^b	24.43 \pm 3.71 ^b	ND	ND	64.58 \pm 6.44 ^c	452.06 \pm 45.08 ^d
WT-BR	29.70 \pm 0.58 ^c	187.11 \pm 4.06 ^b	37.20 \pm 0.86 ^b	234.36 \pm 5.41 ^b	4.07 \pm 0.61 ^b	25.64 \pm 3.84 ^b	24.67 \pm 0.84 ^c	155.42 \pm 5.29 ^c	95.65 \pm 2.9 ^{b,c}	602.59 \pm 18.27 ^{b,d}
WT-RR	35.58 \pm 1.20 ^{b,d}	273.96 \pm 9.24 ^a	46.33 \pm 0.82 ^b	356.74 \pm 6.31 ^b	4.11 \pm 0.12 ^b	31.64 \pm 0.92 ^b	75.42 \pm 2.58 ^a	580.73 \pm 19.86 ^a	161.46 \pm 4.73 ^a	1243.24 \pm 36.42 ^{a,c}
SB-MG	41.92 \pm 2.55 ^a	276.67 \pm 16.83 ^a	24.20 \pm 3.88 ^b	159.72 \pm 25.60 ^b	4.58 \pm 0.16 ^b	30.22 \pm 0.99 ^b	ND	ND	70.71 \pm 6.69 ^{b,c}	466.68 \pm 44.15 ^{b,d}
SB-BR	44.31 \pm 1.79 ^a	288.01 \pm 11.63 ^a	49.23 \pm 5.34 ^b	319.99 \pm 34.71 ^b	9.82 \pm 1.49 ^a	63.83 \pm 9.69 ^a	22.26 \pm 3.58 ^c	144.69 \pm 23.27 ^c	125.64 \pm 12.22 ^b	816.66 \pm 79.43 ^{b,c}
SB-RR	31.75 \pm 2.28 ^{c,d}	190.5 \pm 13.68 ^b	112.79 \pm 43.11 ^a	676.74 \pm 256.66 ^a	4.71 \pm 0.25 ^b	28.26 \pm 1.5 ^b	62.07 \pm 6.0 ^b	372.42 \pm 36.0 ^b	211.33 \pm 51.65 ^a	1267.98 \pm 309.9 ^a

The same letters in the same column indicate that mean values ($n = 3$) are not significantly different ($p < 0.05$).

Phenolic Content and Antioxidant Capacity

The antioxidant capacity of SB was evaluated by considering only the hydrophilic extract, which is the main contributor to the total antioxidant capacity in fruits and vegetables, particularly in the purple tomato (39).

The total phenols content was measured by the Folin-Ciocalteu (F-C) assay, as reported in Gerardi et al. (14), and it increased during ripening, in both tomato genotypes.

In case of SB tomato at MG stage, the phenolic content (5.8 mg GAE/g DW) was higher than WT by 152%, and at RR stage (8.6 mg GAE/g DW) by 134%. On a fresh weight base, at MG stage, SB had more phenols than WT by 137%, at RR stage SB had 85% more phenols than WT (Table 3).

The TEAC value for SB at RR stage (31.6 $\mu\text{mol TE/g DW}$) was 200% more than WT (10.3 $\mu\text{mol TE/g DW}$); instead the ORAC value for SB, at the same stage of ripening (140.3 $\mu\text{mol TE/g DW}$) was 86% higher than WT (75.5 $\mu\text{mol TE/g DW}$) (Table 3).

The antioxidant capacity of SB assessed by TEAC and ORAC at MG stage (22.9 and 104.1 $\mu\text{mol/TE g DW}$, respectively) was much lower than at RR stage, probably because of the great increase in polyphenols accumulation during ripening (from 5.8 to 8.6 mg GAE/g DW, in MG and RR, respectively).

The HPLC ascorbate determination was done on WT and SB extracts only at RR stage, revealing a much higher total ascorbic acid (AA + DHA) content in SB than WT (37.3 \pm 1.4 vs. 27.1 \pm 1.1 mg/100 g FW, respectively). The ascorbic acid (AA, reduced form) was 82% of total AA (30.8 \pm 1.1 mg/100 g FW) in SB, while in WT was much lower (around 50%, 13.2 \pm 0.79 mg/100 g FW) (data not shown).

DISCUSSION

Despite the remarkable success in increasing flavonoid content in tomato fruits by transgenic approaches (8, 21, 23), in the last 15 years there has been a growing interest in breeding a high flavonoid GM-free tomato (40). This interest is motivated by customers' reluctance to consume transgenic food and by restriction in EU Countries to cultivate genetically modified plants (Directive EU 2015/412).

The exploitation of the biodiversity available in the wild germplasm can allow a remarkable success for specifically exploring metabolic pathways to produce healthier food. This approach has been followed by the Soressi's group in order to combine different alleles from tomato-related wild species into cultivated tomato, promoting anthocyanin production (25, 41).

The characterization of phytochemicals in naturally bred purple tomatoes has already been reported in different genotypes, from the US accession LA1996 (9) and the Canadian purple tomato line V118 (39) to the Brazilian (42) and the Japanese ones (43). Here we report the characterization of the anthocyanin content and other nutraceuticals of "Sun Black" (SB), an Italian tomato line with purple skin color, both in green and in red fruit stages. The latter is caused by the biosynthesis of anthocyanins in the peel, whereas the flesh is red color, similar to the wild type.

TABLE 3 | Total phenols and antioxidant capacity (by TEAC and ORAC assays) of wild type (WT) and "Sun Black" (SB) tomato at different stages of ripening, mature green (MG), breaker (BR), and red ripe (RR).

Sample	Total phenolics [§]		TEAC [°]		ORAC [°]	
	mg GAE/g DW	mg GAE/100g FW	μmol TE/g DW	μmol TE/100g FW	μmol TE/g DW	μmol TE/100g FW
WT- MG	2.28 ± 0.26 ^d	15.96 ± 1.82 ^d	6.93 ± 1.21 ^d	48.51 ± 8.47 ^d	60.04 ± 3.24 ^c	420.28 ± 23.32 ^c
WT- BR	4.34 ± 0.34 ^c	27.34 ± 2.14 ^c	12.11 ± 0.92 ^c	76.29 ± 5.79 ^c	64.48 ± 5.80 ^c	406.27 ± 36.54 ^c
WT- RR	3.66 ± 0.37 ^c	28.18 ± 2.84 ^c	10.35 ± 0.82 ^c	79.69 ± 6.31 ^c	75.49 ± 5.93 ^c	581.32 ± 45.66 ^b
SB- MG	5.76 ± 0.35 ^b	38.01 ± 2.31 ^b	22.95 ± 2.53 ^b	151.47 ± 16.69 ^b	104.13 ± 3.05 ^b	687.25 ± 20.13 ^b
SB- BR	6.03 ± 0.41 ^b	39.19 ± 2.66 ^b	19.9 ± 2.08 ^b	129.35 ± 13.52 ^b	129.44 ± 9.28 ^a	841.36 ± 60.32 ^a
SB- RR	8.56 ± 0.08 ^a	52.21 ± 0.48 ^a	31.64 ± 3.91 ^a	193 ± 23.85 ^a	140.30 ± 9.18 ^a	855.83 ± 55.98 ^a

[§]Total Phenols as GAE = Gallic Acid Equivalent; [°]Antioxidant Capacity as TE = Trolox Equivalent. The same letters in the same column indicate that mean values (n = 3) are not significantly different (p < 0.05).

In SB tomato, the anthocyanidin (aglycone) composition has previously been reported as detected mass (*m/z*) of delphinidin, petunidin and malvidin (44). In the present study, the structure of the major anthocyanins has been elucidated for the first time.

The anthocyanin composition of SB peel is similar to the one previously reported in other purple breeding lines (9, 39). Probably all these genotypes share a common genetic base. In the V118 line (39), petunidin-derivatives accounted for approximately 91.9% of the total anthocyanins, more than in SB (which was 56.6%). In the triple mutant genotype *Aft/atv/hp2*, mostly petunidin and lower amount of delphinidin, in acylated form, were found (42).

The GM purple tomato from C. Martin's Lab. contains (both in the peel and in the flesh) acylated derivatives of delphinidin and petunidin, and at lower extent, malvidin (45). Moreover, in a recent study on a transgenic *Del/Ros1* tomato, two malvidin-based anthocyanins were reported (46).

The similarity of the anthocyanin structures (delphinidin-based) in cross-bred and transgenic tomatoes (overexpressing the *SIANT* gene) demonstrated that the biosynthetic machinery for anthocyanin biosynthesis is under control of the same *MYB* transcription factors (47), although two candidates remain to underlie the *Aft* variant (*SIANT* and *SIAN2*) (28). In addition, the first anthocyanidin product (delphinidin) is promptly methylated by the action of methyltransferases (48) in the two systems.

The anthocyanin content of SB tomato fruit (1.2 mg/g DW or 7.1 mg/100 FW) is comparable to some anthocyanin-rich vegetables (eggplant or red lettuce) or fruits (light-colored strawberries or cherries).

The not linear anthocyanin accumulation in SB tomato at different ripening stages (Figure 2C) could be explained by the different developmental behavior of the fruit: while at immature stage the biosynthesis of anthocyanin is already promptly activated (by the light), at the breaker stage the fruit undergoes cells division and expansion, with fruit enlargement and metabolite biosynthesis slowdown. At ripe stage the full development of the fruit and the anthocyanin biosynthesis (as well all the other typical metabolites of the ripe fruit) is completed.

The anthocyanin content in the peel of SB tomato is controlled by environmental factors, light in particular. It is known that

the anthocyanin biosynthesis is subjected to the environmental activation on regulatory genes (*MYB* transcription factors), by light or cold (26, 49). In the environmental condition described here (unheated tunnel, Central Italy), the anthocyanin content of SB fruits was 1.16 mg/g DW. When SB tomatoes were hydroponically grown in South Italy (where light irradiation is generally higher), preliminary data suggest that at the RR stage both anthocyanin content and ORAC antioxidant capacity were 20% higher than the values reported here (data not reported). In purple tomato V118, the authors reported a total anthocyanin content of nearly 0.25 mg/g DW (39). SB tomato contains four times more anthocyanin as determined more precisely using a real standard (petanin) purified in house.

In transgenic anthocyanin-rich tomatoes a much higher anthocyanin content was reported, as expected, because of the presence of anthocyanins in the flesh (21, 46).

For colorless phenolic compounds, the HPLC chromatographic profile of the SB tomato extract was not different (for major peaks) from the WT. However, the peaks area was greater, revealing a higher content of hydrophilic polyphenolic compounds. Indeed the phenolic content assessed by Folin-Ciocalteu was higher by 100% and more in SB extract than in WT.

Genetic and chlorogenic acids were present in SB tomato extracts at higher level in respect to WT, for each stages of ripening. Rutin was more abundant in SB, except for breaker stage. Total flavonols were not different in SB and WT at RR stage. It is interesting to note that, while during ripening the content of genetic and chlorogenic acids followed a linear trend (increasing for genetic, decreasing for chlorogenic), for rutin, total flavonols, and total anthocyanins the trend was not linear. As already discussed above in the anthocyanin section, during ripening and particularly at the breaker stage, the fruit undergoes many physiological and metabolic changes, not consistent with the other stages. While analyzing three stages of ripening, we focused our interest to the ripe stage, which is important for consumers.

Genetic acid content was present in SB tomato at higher level than reported in the V118 purple tomato genotype, while chlorogenic acid was at the same level (39).

The total carotenoids content in SB (RR stage) was similar to the average amount reported for tomatoes (50), particularly for greenhouse-grown tomatoes (1), and even similar to the reported values in other purple genotypes, as the breeding line V118 from Ontario, although the carotenoid profile was different (39). Borghesi et al. (44) reported a higher content of carotenoids in SB tomatoes, and a very different pattern in lycopene, β -carotene and lutein than reported in our study on the same tomato line. In that study, tomatoes were hydroponically grown, that probably influenced the carotenoid biosynthesis. Moreover, difference in carotenoid analysis methodology can greatly influence the final metabolite quantification.

As far as the cross-talk between lipophilic carotenoids and hydrophilic flavonoids was concerned, interestingly, when transgenic lines with altered carotenoid contents were analyzed, no significant differences were found in phenolic or flavonoid content (51). Breeding or transgenic lines for increased phenylpropanoids did not show an increase of flavonoids at expenses of carotenoids (7, 21). In a transgenic tomato cultivar, total carotenoid and lycopene levels did not vary, in spite of a higher anthocyanin content of 13 mg/100 g FW (22). It has been supposed that both classes of compounds have different role and subcellular localization (plastids for carotenoids vs. vacuoles for anthocyanins), and do not compete for precursors (42).

In tomatoes bearing *high pigment (hp)* gene, with phenotypic effects similar to those due to the *Aft* locus, a slight increased level of carotenoids and polyphenols in respect to the control line was reported (24).

Recently, the potential health benefits of anthocyanins have been related to not yet identified chemical properties beyond the antioxidant capacity of the molecules (12). However, the antioxidant properties of a food extract, assessed *in vitro*, is an inceptive parameter to be tested when studying the nutraceutical properties of a food. Our results on antioxidant capacity of SB hydrophilic extract show a significantly higher value in respect to WT.

The phenolic content (by F-C assay) of SB tomato, at all stage of ripening, was significantly higher than that one found in WT, and in other selected tomato lines (24). At RR stage of ripening phenolic content of SB tomato was higher than the reported value for the Canadian purple tomato V118 (39).

Two different chemical assays (TEAC and ORAC) have been adopted for evaluating the antioxidant capacity of SB extract, as it has been recommended in order to take into account the different mechanisms of action (52). In both assays, the antioxidant capacity (hydrophilic) of SB tomato, at the three stages of ripening, was significantly higher than WT at the same stage, due to the presence of anthocyanin compounds in the peel, and to an increased content of other polyphenolic compounds.

The TEAC of WT tomato was in agreement with the reported value for commercial tomato cultivar (1, 53). The TEAC value for SB tomato was 200% more than WT, thanks to the increased polyphenolic content. The ABTS assay has been previously applied to SB tomato samples, on skin area with different level of pigmentation, revealing increased antioxidant capacity with increasing anthocyanin content, although not comparable to our results which are on whole fruit (54).

The TEAC antioxidant capacity of our SB tomato was lower, as expected, than the value reported for transgenic tomatoes, because of the anthocyanin presence at whole berry fruit (21).

The antioxidant capacity (as ORAC assay) in SB tomato, at all stage of ripening, was statistically higher than that one found in WT. At RR stage of ripening, ORAC was lower in SB than in the Canadian purple tomato V118, in spite of a higher phenolic content in SB (39).

Tomato fruit is considered a good source of vitamin C. The vitamin C content was quite high both in WT and SB, with reference to commercial cultivar or purple tomato (1, 42). SB extracts at RR stage had a higher vitamin C content than WT. The ascorbic acid (AA, reduced form) was much higher in SB than WT. One possible explanation is the protective function of the increased polyphenol content in SB, which protects AA from oxidation. Anyway, the contribution of the ascorbic acid to the antioxidant capacity of plant extract is usually low. As it has been reported, the main contributor to the antioxidant capacity of hydrophilic extracts is not ascorbate but rather polyphenols (55).

It has been reported that purple tomatoes both obtained by transgenesis or conventional breeding showed improved shelf life compared to wild-type, with a delayed ripening and a reduced pathogen susceptibility, due to anthocyanin accumulation and increased level of natural antioxidant (54, 56). Postharvest losses by pathogenic infection can reduce the yield of vegetable crops, therefore the harvest of tomato when green and firm, and successive ethylene exposition, is a usual technique to induce color and ripeness, without developing flavor and aroma. This is likely the main reason why the marketed tomatoes are often characterized by extremely low flavor regardless of the cultivar. Preliminary panel tests on SB at commercial stage of ripeness showed a good performance for flavor, aroma and texture (data not reported). Moreover, ripening SB tomatoes showed that the ethylene climacteric peak was delayed, resulting in a higher firmness at commercial stage of ripening (57). Since SB has been bred to promote fresh consumption of a tomato rich in bioactive compounds, all this information taken together make SB tomato valuable both for nutraceutical and market qualities.

CONCLUSION

From the Kuopio study which demonstrated that the consumption of large amount of anthocyanin-rich food significantly lowered the risk of CVD (58) to the recent advancement in anthocyanin health benefits (12), it can be concluded that consuming anthocyanin-rich fruits and vegetables is a recommended style of eating.

Transgenesis has been always seen in a suspicious way, due to the consumer's concerns over the consumption of GM foods. Moreover, EU rules discourage the application of transgenic cultivations. Therefore, the naturally bred SB tomato can be a valuable alternative to transgenic purple tomato, despite its lower

concentration of anthocyanins and antioxidant phytochemicals. On the other hand, the anthocyanin (and phenolic) content of SB is comparable to some anthocyanin-rich vegetables (eggplant or red lettuce) or fruits (light-colored strawberries or cherries), with the advantage that tomatoes are highly consumed in many countries, and are available all year-round. In conclusion, consumption of SB tomatoes can contribute to ameliorate human health, thanks to the increased content of nutraceutical compounds.

DATA AVAILABILITY

All datasets generated for this study are included in the manuscript and/or the **Supplementary Files**.

AUTHOR CONTRIBUTIONS

FB, HB, GMa, MD, IN, and CG performed the experiments. AM and MP produced the plant material. FB, IN, GMi, HB, and ØA designed the experiments. FB, HB, GMa, MD, IN, GMi, and ØA analyzed and interpreted the data. FB wrote the manuscript with the input from all the authors.

REFERENCES

- Raiola A, Rigano MM, Calafiore R, Frusciantè L, Barone A. Enhancing the health-promoting effects of tomato fruit for biofortified food. *Mediators Inflamm.* (2014) 2014:139873. doi: 10.1155/2014/139873
- Campbell JK, Canene-Adams K, Lindshield BL, Boileau TW, Clinton SK, Erdman JW Jr. Tomato phytochemicals and prostate cancer risk. *J Nutr.* (2004) 134 (12 Suppl.):3486S–92S. doi: 10.1093/jn/134.12.3486S
- Serio F, Bonasia AAO, Santamaria P. Antioxidant properties and health benefits of tomato. In: Govil JN, SingVK, Arunachalam C, editors. *Recent Progress in Medicinal Plants Vol. 13—Search for Natural Drugs*. Houston, TX: Studium Press LLC (2006). p. 163–83.
- Rao AV, Rao LG. Carotenoids and human health. *Pharmacol Res.* (2007) 55:207–16. doi: 10.1016/j.phrs.2007.01.012
- Alshatwi AA, Al Obeaid MA, Al Sedairy SA, Al-Assaf AH, Zhang JJ, Lei KY. Tomato powder is more protective than lycopene supplement against lipid peroxidation in rats. *Nutr Res.* (2010) 30:66–73. doi: 10.1016/j.nutres.2009.12.002
- Weisburger JH. Evaluation of the evidence on the role of tomato products in disease prevention. *Proc Soc Exp Biol Med.* (1998) 218:140–3. doi: 10.3181/00379727-218-44281
- Mes PJ, Boches P, Myers JR, Durst R. Characterization of tomatoes expressing anthocyanins in the fruit. *J Am Soc Hort Sci.* (2008) 133:262–9. doi: 10.21273/JASHS.133.2.262
- Bovy AG, de Vos R, Kemper M, Schiljen EGWM, Almenar Pertejo M, Muir S, et al. High flavonol tomatoes resulting from the heterologous expression of the maize transcription factor genes *LC* and *Cl*. *Plant Cell.* (2002) 14:2509–26. doi: 10.1105/tpc.004218
- Jones CM, Mes, PJ, Myers JR. Characterization and inheritance of the *Anthocyanin fruit* (Aft) tomato. *J Hered.* (2003) 94:449–56. doi: 10.1093/jhered/egq093
- Andersen ØM, Jordheim M. Basic anthocyanin chemistry and dietary sources. In: Wallace TC, Giusti MM, editors. *Anthocyanins in Health and Disease*. Boca Raton, FL: CRC Press; Taylor & Francis Group (2014). p. 13–90. doi: 10.1201/b15554-3
- Wu X. Antioxidant activities of anthocyanins. In: Wallace TC, Giusti MM, editors. *Anthocyanins in Health and Disease*. Boca Raton, FL: CRC Press; Taylor & Francis Group (2014). p. 141–64. doi: 10.1201/b15554-6
- Tsuda T. Dietary anthocyanin-rich plants: biochemical basis and recent progress in health benefits studies. *Mol Nutr Food Res.* (2012) 56:159–70. doi: 10.1002/mnfr.201100526
- Gerardi C, Frassinetti S, Caltavuturo L, Leone A, Lecci R, Calabriso N, et al. Anti-proliferative, anti-inflammatory and anti-mutagenic activities of a *Prunus mahaleb* L. anthocyanin-rich fruit extract. *J Funct Food.* (2016) 27:537–48. doi: 10.1016/j.jff.2016.09.024
- Gerardi C, Albano C, Calabriso N, Carluccio M, Durante M, Mita G, et al. Techno-functional properties of tomato puree fortified with anthocyanin pigments. *Food Chem.* (2018) 240:1184–92. doi: 10.1016/j.foodchem.2017.08.057
- Amin HP, Czank C, Raheem S, Zhang QZ, Botting NP, Cassidy A, et al. Anthocyanin and their physiologically relevant metabolites alter the expression of IL-6 and VCAM-1 in CD40L and oxidized LDL challenged vascular endothelial cells. *Mol Nutr Food Res.* (2015) 59:1095–106. doi: 10.1002/mnfr.201400803
- Olejnik A, Kowalska K, Kidon M, Czapski J, Rychlik J, Olkiewicz M, et al. Purple carrot anthocyanins suppress lipopolysaccharide-induced inflammation in the co-culture of intestinal Caco-2 and macrophage RAW264.7 cells. *Food Funct.* (2016) 7:557–64. doi: 10.1039/C5FO00890E
- Blando F, Calabriso N, Berland H, Maiorano G, Gerardi C, Carluccio MA, et al. Radical scavenging and biological activities of representative anthocyanin groupings from pigment-rich fruits and vegetables. *Int J Mol Sci.* (2018) 19:169. doi: 10.3390/ijms19010169
- Nunez MF, Magnuson BA. Anthocyanins in health and diseases prevention. In: Wallace TC, Giusti MM, editors. *Anthocyanins in Health and Disease*. Boca Raton, FL: CRC Press; Taylor & Francis Group (2014). p. 1–12. doi: 10.1201/b15554-2
- Wallace TC, Slavin M, Frankenfeld CL. Systematic review of anthocyanins and markers of cardiovascular disease. *Nutrients.* (2016) 8:32. doi: 10.3390/nu8010032
- Lin B-W, Gong C-C, Song H-F, Cui Y-Y. Effects of anthocyanins on the prevention and treatment of cancer. *Br J Pharmacol.* (2017) 174:1226–43. doi: 10.1111/bph.13627

FUNDING

This research was financed by the Italian Ministry for University and Research (MIUR), Research Projects: High-Convenience Fruits and Vegetables: New Technologies for Quality and New Products, PON01_01435. We also thank the Apulia Regional Project Rete di Laboratori per l'Innovazione degli Alimenti Funzionali (LAIFF) (PO Puglia FESR 2007–2013 Asse I, Linea 1.2—PO Puglia FSE 2007–2013 Asse IV) which allowed the spectrofluorimeter Infinite M-200 (Tecan Group Ltd., Männedorf, Switzerland) purchasing.

ACKNOWLEDGMENTS

We are grateful to L. D'Amico, Dr. C. Albano, and Dr. C. Chiriatti for their technical assistance in HPLC and ORAC experiments.

SUPPLEMENTARY MATERIAL

The Supplementary Material for this article can be found online at: <https://www.frontiersin.org/articles/10.3389/fnut.2019.00133/full#supplementary-material>

21. Butelli E, Titta L, Giorgio M, Mock H-P, Matros A, Peterek S, et al. Enrichment of tomato fruit with health-promoting anthocyanins by expression of select transcription factors. *Nature Biotechnol.* (2008) 26:1301–8. doi: 10.1038/nbt.1506
22. Maligeppagal M, Chandra GS, Navale PM, Deepa H, Rajeev PR, Asokan R, et al. Anthocyanin enrichment of tomato (*Solanum lycopersicum* L.) fruit by metabolic engineering. *Curr Sci.* (2013) 105:72–80. Available online at: <https://www.jstor.org/stable/24092679>
23. Scarano A, Butelli E, De Santis S, Cavalcanti E, Hill L, De Angelis M, et al. Combined dietary anthocyanins, flavonols, and stilbenoids alleviate inflammatory bowel disease symptoms in mice. *Front Nutr.* (2018) 4:75. doi: 10.3389/fnut.2017.00075
24. Minoggio M, Bramati L, Simonetti P, Gardana C, Iemoli L, Santangelo E, et al. Polyphenol pattern and antioxidant activity of different tomato lines and cultivars. *Ann Nutr Metab.* (2003) 47:64–9. doi: 10.1159/000069277
25. Mazzucato A, Willems D, Bernini R, Picarella ME, Santangelo E, Ruiu F, et al. Novel phenotype related to the breeding of purple-fruited tomatoes and effect of peel extracts on human cancer cell proliferation. *Plant Physiol Biochem.* (2013) 72:125–33. doi: 10.1016/j.plaphy.2013.05.012
26. Kerckhoffs LHJ, Kendrick RE. Photocontrol of anthocyanins biosynthesis in tomato. *J Plant Res.* (1993) 110:141–9. doi: 10.1007/BF02506853
27. Schreiber G, Reuveni M, Evenor D, Oren-Shamir M, Ovadia R, Sapir-Mir R, et al. Anthocyanin1 from *Solanum chitense* is more efficient in accumulating anthocyanin metabolites than its *Solanum lycopersicum* counterpart in association with the anthocyanin fruit phenotype of tomato. *Theor Appl Genet.* (2012) 124:295–307. doi: 10.1007/s00122-011-1705-6
28. Kiferle C, Fantini E, Bassolino L, Povero G, Spelt C, Buti S, et al. Tomato R2R3-MYB proteins SlANT1 and SlAN2: same protein activity, different roles. *PLoS ONE.* (2015) 10:e0136365. doi: 10.1371/journal.pone.0136365
29. Cao X, Qiu Z, Wang X, Van Giang T, Liu X, Wang J, et al. A putative R3 MYB repressor is the candidate gene underlying *atroviolealum*, a locus for anthocyanin pigmentation in tomato fruit. *J Exp Bot.* (2017) 68:5745–58. doi: 10.1093/jxb/erx382
30. Colanero S, Perata P, Gonzali S. The *atrovioleacea* gene encodes an R3-MYB protein repressing anthocyanin synthesis in tomato plants. *Front Plant Sci.* (2018) 9:830. doi: 10.3389/fpls.2018.00830
31. Sadler G, Davis J, Dezman D. Rapid extraction of lycopene and β -carotene from reconstituted tomato paste and pink grapefruit homogenates. *J Food Sci.* (1990) 55:1460–1. doi: 10.1111/j.1365-2621.1990.tb03958.x
32. Perkins-Veazie P, Collins JK, Pair SD, Roberts W. Lycopene content differs among red-fleshed watermelon cultivars. *J Sci Food Agric.* (2001) 81:983–7. doi: 10.1002/jfsa.880
33. Skaar I, Jordheim M, Byamukama R, Mbabazi A, Wubshet AG, Kiremire B, et al. New anthocyanidin and anthocyanin pigments in blue plumbago. *J Agric Food Chem.* (2012) 60:1510–5. doi: 10.1021/jf2048004
34. Durante M, Lenucci MS, Marrese PP, Rizzi V, De Caroli M, Piro G, et al. α -Cyclodextrin encapsulation of supercritical CO₂ extracted oleoresins from different plant matrices: a stability study. *Food Chem.* (2016). 199:684–93. doi: 10.1016/j.foodchem.2015.12.073
35. Sánchez-Moreno C, Plaza L, de Ancos B, Cano MP. Nutritional characterization of commercial traditional pasteurized tomato juices: carotenoids, vitamin C and radical-scavenging capacity. *Food Chem.* (2006) 98:749–56. doi: 10.1016/j.foodchem.2005.07.015
36. Andersen ØM, Opheim S, Aksnes DW, Frøystein NÅ. Structure of petanin, an acylated anthocyanin isolated from *Solanum tuberosum*, using homo- and hetero-nuclear two-dimensional nuclear magnetic resonance techniques. *Phytochem Anal.* (1991) 2:230–6. doi: 10.1002/pca.2800020510
37. Slimestad R, Aaberg A, Andersen ØM. Acylated anthocyanins from petunia flowers. *Phytochemistry.* (1999) 50:1081–6. doi: 10.1016/S0031-9422(98)00647-5
38. Gómez-Romero M, Segura-Carretero A, Fernández Gutiérrez A. Metabolite profiling and quantification of phenolic compounds in methanol extracts of tomato fruits. *Phytochemistry.* (2010) 71:1848–64. doi: 10.1016/j.phytochem.2010.08.002
39. Li H, Deng Z, Liu R, Young JC, Zhu H, Loewen S, et al. Characterization of phytochemicals and antioxidant activities of a purple tomato (*Solanum lycopersicum* L.). *J Agric Food Chem.* (2011) 59:11803–11. doi: 10.1021/jf202364v
40. Willits MG, Kramer CM, Prata RTN, De Luca V, Potter BG, Steffens JC, et al. Utilization of the genetic resources of wild species to create a nontransgenic high flavonoid tomato. *J Agric Food Chem.* (2005) 53:1231–6. doi: 10.1021/jf049355i
41. Gonzali S, Mazzucato A, Perata P. Purple as a tomato towards high anthocyanin tomatoes. *Trends Plant Sci.* (2009) 14:237–41. doi: 10.1016/j.tplants.2009.02.001
42. Sestari I, Zsögön A, Garcia Rehder G, de Lira Teixeira L, Ayamoto Hassimoto NM, Purgatto E, et al. Near-isogenic lines enhancing ascorbic acid, anthocyanin and carotenoid content in tomato (*Solanum lycopersicum* L. cv Micro-Tom) as a tool to produce nutrient-rich fruits. *Sc Hort.* (2014) 175:111–20. doi: 10.1016/j.scienta.2014.06.010
43. Ooe E, Ogawa K, Horiuchi T, Tada H, Murase H, Tsuruma K, et al. Analysis and characterization of anthocyanins and carotenoids in Japanese blue tomato. *Biosci Biotechnol Biochem.* (2016) 80:341–9. doi: 10.1080/09168451.2015.1091715
44. Borghesi E, González-Miret ML, Escudero-Gilete ML, Malorgio F, Heredia FJ, Meléndez-Martínez AJ. Effects of salinity stress on carotenoid, Anthocyanins and color of diverse tomato genotypes. *J Agric Food Chem.* (2011) 59:11676–82. doi: 10.1021/jf2021623
45. Tohge T, Zhang Y, Peterek S, Matros A, Rallapalli G, Tandron YA, et al. Ectopic expression of snapdragon transcription factors facilitates the identification of genes encoding enzymes of anthocyanin decoration in tomato. *Plant J.* (2015) 83:686–704. doi: 10.1111/tpj.12920
46. Su X, Xu J, Rhodes D, Shen Y, Song W, Katz B, et al. Identification and quantification of anthocyanins in transgenic purple tomato. *Food Chem.* (2016) 202:184–8. doi: 10.1016/j.foodchem.2016.01.128
47. Mathews H, Clendennen SK, Caldwell CG, Liu XL, Connors K, Matheis N, et al. Activation tagging in tomato identifies a transcriptional regulator of anthocyanin biosynthesis, modification, and transport. *Plant Cell.* (2003) 15:1689–703. doi: 10.1105/tpc.012963
48. Liu Y, Tikunov Y, Schouten R, Marcelis LFM, Visser RGF, Bovy A. Anthocyanin biosynthesis and degradation mechanisms in Solanaceae vegetables: a review. *Front Chem.* (2018) 6:52. doi: 10.3389/fchem.2018.00052
49. Azuma A, Yakushiji H, Koshita Y, Kobayashi S. Flavonoid biosynthesis-related genes in grape skin are differentially regulated by temperature and light conditions. *Planta.* (2012) 236:1067–80. doi: 10.1007/s00425-012-1650-x
50. Guil-Guerrero JL, Rebolloso-Fuentes MM. Nutrient composition and antioxidant activity of eight tomato (*Lycopersicon esculentum*) varieties. *J Food Comp Anal.* (2009) 22:123–9. doi: 10.1016/j.jfca.2008.10.012
51. Long M, Millar DJ, Kimura Y, Donovan G, Rees J, Fraser PD, et al. Metabolite profiling of carotenoid and phenolic pathways in mutant and transgenic lines of tomato: identification of a high antioxidant fruit line. *Phytochemistry.* (2006) 67:1750–7. doi: 10.1016/j.phytochem.2006.02.022
52. Prior RL, Wu X, Schaich K. Standardized methods for the determination of antioxidant capacity and phenolics in foods and dietary supplements. *J Agric Food Chem.* (2005) 53:4290–302. doi: 10.1021/jf0502698
53. Giuntini D, Graziani G, Lercari B, Fogliano V, Soldatini GF, Ranieri A. Changes in carotenoid and ascorbic acid contents in fruits of different tomato genotypes related to the depletion of UV-B radiation. *J Agric Food Chem.* (2005) 53:3174–81. doi: 10.1021/jf0401726
54. Bassolino L, Zhang Y, Schoonbeek H-J, Kiferle C, Perata P, Martin C. Accumulation of anthocyanins in tomato skin extends shelf life. *New Phytol.* (2013) 200:650–5. doi: 10.1111/nph.12524
55. Gil IM, Tomás-Barberán FA, Hess-Pierce B, Kader AA. Antioxidant capacity, phenolic compounds, carotenoids, and vitamin C contents of nectarine, peach

- and plum cultivars from California. *J Agric Food Chem.* (2002) 50:4976–82. doi: 10.1021/jf020136b
56. Zhang Y, Butelli E, De Stefano R, Schoonbeek H-J, Magusin A, Pagliarini C, et al. Anthocyanins double the shelf life of tomatoes by delaying overripening and reducing susceptibility to gray mold. *Current Biol.* (2013) 23:1094–100. doi: 10.1016/j.cub.2013.04.072
57. Borghesi E, Ferrante A, Gordillo B, Rodríguez-Pulido FJ, Cocetta G, Trivellini A, et al. Comparative physiology during ripening in tomato rich-anthocyanins fruits. *Plant Growth Regul.* (2016) 80:207–14. doi: 10.1007/s10725-016-0158-y
58. Rissanen TH, Voutilainen S, Virtanen JK, Venho B, Vanharant M, Mursu J, et al. Low intake of fruits, berries and vegetables is associated with excess mortality in men: the Kuopio Ischemic Heart Disease Risk Factor (KIHD) Study. *J Nutr.* (2003) 133:199–204. doi: 10.1093/jn/133.1.199

Conflict of Interest Statement: AM and MP are participating as inventors in owning the trademark "Sun Black" and the rights on the registered variety "Solenero." The ownership is the University of Tuscia, Viterbo, Italy.

The remaining authors declare that the research was conducted in the absence of any commercial or financial relationships that could be construed as a potential conflict of interest.

Copyright © 2019 Blando, Berland, Maiorano, Durante, Mazzucato, Picarella, Nicoletti, Gerardi, Mita and Andersen. This is an open-access article distributed under the terms of the Creative Commons Attribution License (CC BY). The use, distribution or reproduction in other forums is permitted, provided the original author(s) and the copyright owner(s) are credited and that the original publication in this journal is cited, in accordance with accepted academic practice. No use, distribution or reproduction is permitted which does not comply with these terms.

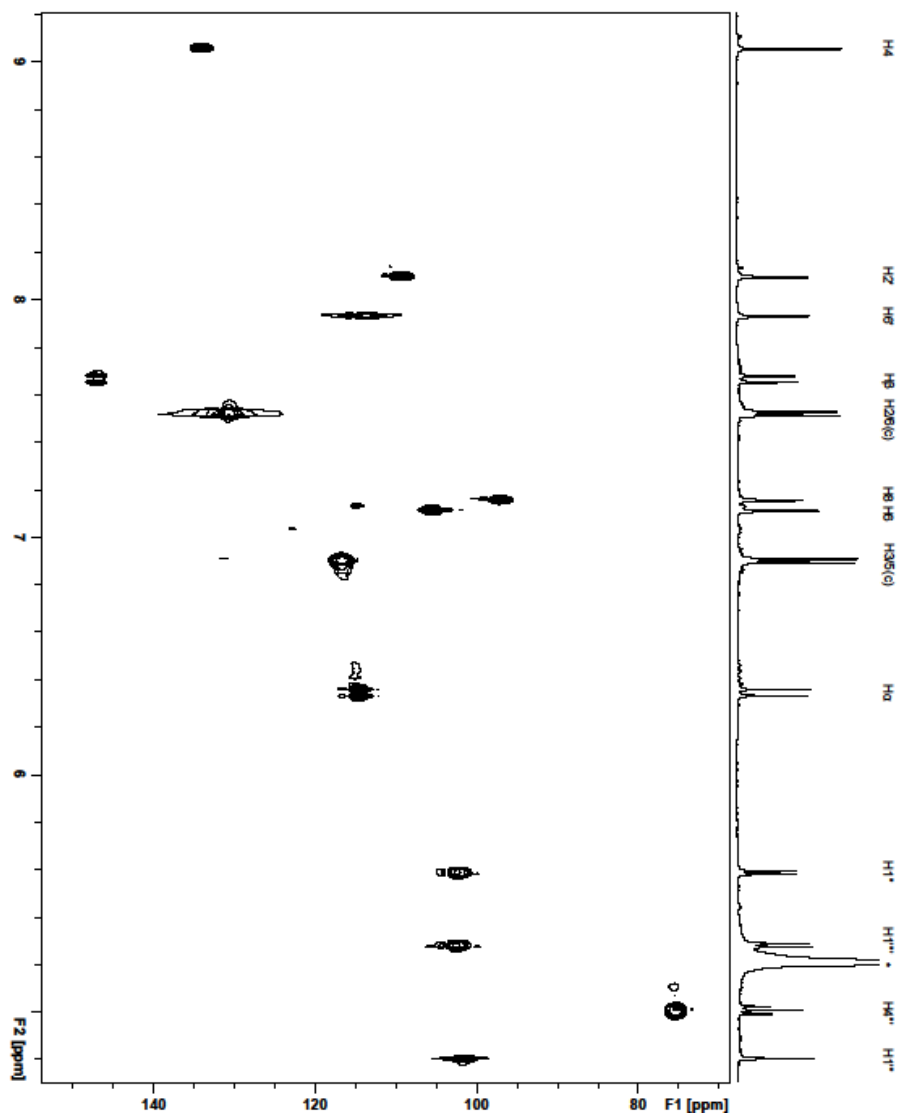


Figure S1: The aromatic and sugar anomeric part of the heteronuclear single quantum coherence (^1H - ^{13}C HSQC) NMR spectra of anthocyanin **1**, petunidin 3-*O*-[6''-*O*-(4'''-*O*-*E*-*p*-coumaroyl- α -rhamnopyranosyl)- β -glucopyranoside]-5-*O*- β -glucopyranoside (petanin) isolated from the peel of 'Sun Black' tomato, recorded in $\text{CF}_3\text{COOD-CD}_3\text{OD}$ (5:95, v/v) at 25 °C. (c) = *p*-coumaroyl moiety; * = water residual peak.

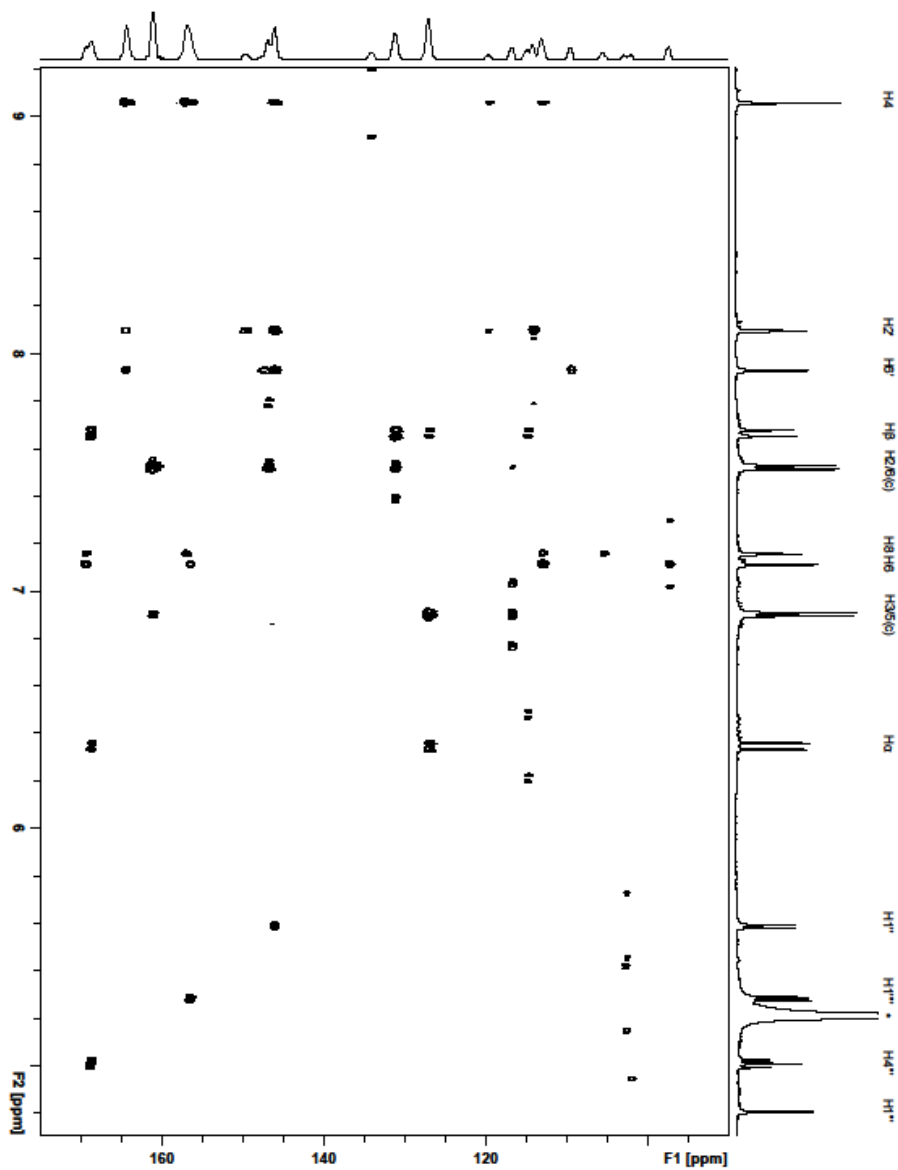


Figure S2: The aromatic and sugar anomeric part of the heteronuclear multiple bond quantum coherence (^1H - ^{13}C HMBC) NMR spectra of anthocyanin **1**, petunidin 3-*O*-[6''-*O*-(4'''-*O*-*E*-*p*-coumaroyl- α -rhamnopyranosyl)- β -glucopyranoside]-5-*O*- β -glucopyranoside recorded in $\text{CF}_3\text{COOD-CD}_3\text{OD}$ (5:95, v/v) at 25 °C. (c) = *p*-coumaroyl moiety; * = water residual peak.

TABLE S1 | Content of gentisic acid, chlorogenic acid, rutin and total flavonols in wild type (WT) and Sun Black (SB) tomato at different stages of ripening, mature green (MG), breaker (BR) and red ripe (RR).

Sample	Gentisic acid		Chlorogenic acid		Rutin		Total flavonols	
	mg/g DW	mg/100 g FW	mg/g DW	mg/100 g FW	mg/g DW	mg/100 g FW	mg/g DW	mg/100 g FW
WT - MG	0.021 ± 0.003 ^f	0.149 ± 0.020 ^e	0.309 ± 0.013 ^d	2.221 ± 0.094 ^c	0.442 ± 0.054 ^f	3.180 ± 0.392 ^b	0.583 ± 0.052 ^b	4.200 ± 0.371 ^c
	0.229 ± 0.014 ^d	1.445 ± 0.088 ^c	0.249 ± 0.012 ^c	1.571 ± 0.075 ^d	0.603 ± 0.003 ^{bd}	3.800 ± 0.019 ^b	0.839 ± 0.019 ^b	5.284 ± 0.121 ^b
WT - RR	0.301 ± 0.012 ^c	2.314 ± 0.092 ^b	0.043 ± 0.002 ^f	0.328 ± 0.015 ^e	0.602 ± 0.023 ^b	4.632 ± 0.176 ^a	0.811 ± 0.038 ^a	6.247 ± 0.296 ^a
	0.099 ± 0.005 ^e	0.652 ± 0.032 ^d	1.314 ± 0.041 ^a	8.674 ± 0.272 ^a	0.694 ± 0.069 ^b	4.581 ± 0.458 ^a	1.152 ± 0.069 ^a	7.603 ± 0.458 ^a
SB - BR	0.346 ± 0.008 ^b	2.251 ± 0.051 ^b	0.546 ± 0.009 ^c	3.551 ± 0.059 ^b	0.542 ± 0.001 ^{ade}	3.523 ± 0.004 ^b	0.803 ± 0.001 ^b	5.218 ± 0.004 ^a
	0.467 ± 0.018 ^a	2.846 ± 0.112 ^a	0.613 ± 0.018 ^b	3.740 ± 0.111 ^b	0.818 ± 0.005 ^a	4.990 ± 0.030 ^a	1.119 ± 0.005 ^a	6.825 ± 0.030 ^a

The same letters in the same column indicate that mean values (n=3) are not significantly different ($p < 0.05$).

Paper V

Radical scavenging and anti-inflammatory activities of representative anthocyanin groupings from pigment-rich fruits and vegetables


Federica Blando, Nadia Calabriso, Helge Berland, Gabriele Maiorano, Carmela Gerardi, Maria A. Carluccio, Øyvind M. Andersen

International Journal of Molecular Sciences (2018)



Article

Radical Scavenging and Anti-Inflammatory Activities of Representative Anthocyanin Groupings from Pigment-Rich Fruits and Vegetables

Federica Blando ^{1,*} , Nadia Calabriso ², Helge Berland ³, Gabriele Maiorano ¹, Carmela Gerardi ¹, Maria Annunziata Carluccio ² and Øyvind M. Andersen ³

¹ Institute of Sciences of Food Production (ISPA), National Research Council (CNR), Via Prov.le Lecce-Monteroni, 73100 Lecce, Italy; gabriele.maiorano@gmail.com (G.M.); carmela.gerardi@ispa.cnr.it (C.G.)

² Institute of Clinical Physiology (IFC), National Research Council (CNR), Via Prov.le Lecce-Monteroni, 73100 Lecce, Italy; nadia.calabriso@ifc.cnr.it (N.C.); maria@ifc.cnr.it (M.A.C.)

³ Department of Chemistry, University of Bergen, Allegt 41, 5007 Bergen, Norway; Helge.Berland@kj.uib.no (H.B.); oyvind.andersen@kj.uib.no (Ø.M.A.)

* Correspondence: federica.blando@ispa.cnr.it; Tel.: +39-0832-422617

Received: 2 December 2017; Accepted: 3 January 2018; Published: 6 January 2018

Abstract: Anthocyanins, the naturally occurring pigments responsible for most red to blue colours of flowers, fruits and vegetables, have also attracted interest because of their potential health effects. With the aim of contributing to major insights into their structure–activity relationship (SAR), we have evaluated the radical scavenging and biological activities of selected purified anthocyanin samples (PASs) from various anthocyanin-rich plant materials: two fruits (mahaleb cherry and blackcurrant) and two vegetables (black carrot and “Sun Black” tomato), differing in anthocyanin content (ranging from 4.9 to 38.5 mg/g DW) and molecular structure of the predominant anthocyanins. PASs from the abovementioned plant materials have been evaluated for their antioxidant capacity using Trolox Equivalent Antioxidant Capacity (TEAC) and Oxygen Radical Absorbance Capacity (ORAC) assays. In human endothelial cells, we analysed the anti-inflammatory activity of different PASs by measuring their effects on the expression of endothelial adhesion molecules VCAM-1 and ICAM-1. We demonstrated that all the different PASs showed biological activity. They exhibited antioxidant capacity of different magnitude, higher for samples containing non-acylated anthocyanins (typical for fruits) compared to samples containing more complex anthocyanins acylated with cinnamic acid derivatives (typical for vegetables), even though this order was slightly reversed when ORAC assay values were expressed on a molar basis. Concordantly, PASs containing non-acylated anthocyanins reduced the expression of endothelial inflammatory antigens more than samples with aromatic acylated anthocyanins, suggesting the potential beneficial effect of structurally diverse anthocyanins in cardiovascular protection.

Keywords: non-acylated anthocyanins; anthocyanins with aromatic acylation; structure–activity relationship (SAR); mahaleb cherry; blackcurrant; black carrot; “Sun Black” tomato; VCAM-1; ICAM-1; endothelial adhesion molecules.

1. Introduction

Anthocyanins are naturally occurring pigments responsible for the red to dark blue colour (in some cases perceived as black by the human eye) of most flowers, fruits and vegetables, and constitute a sub-class of flavonoids within the broad class of polyphenols. They are characterised by having, under acidic conditions, a common 2-phenylbenzopyrylium (flavylium) cationic aglycone

with various oxygen functions (anthocyanidin), which may occur on other equilibrium forms when the pH in their surroundings changes. Twenty anthocyanidins having a C15 skeleton without skeleton extension are known to occur in plants; however, in nearly all fruits and vegetables only six of them are present: pelargonidin, cyanidin, delphinidin, peonidin, petunidin and malvidin. Anthocyanins are present in almost all plants as anthocyanidin glycosides. The sugar moieties (most often mono-, di- or tri-glycosides) can be further acylated with aliphatic and aromatic acids. More than 700 natural anthocyanins have been identified [1,2], revealing the plasticity of their biosynthetic pathway.

Over the last few decades, a huge amount of research has been focused on the possible health effects of anthocyanins relative to the consumption of fruit and vegetables containing these bioactive phytochemicals [3–6]. Many of these health activities have been attributed to the intense antiradical and antioxidant activity of anthocyanin. The relationship between anthocyanins' chemical structure and their corresponding chemical and biological activity (structure–activity relationship, SAR) is a challenging area of research that has been tackled in several studies [7–13]. In these papers, the chemical features of anthocyanins (type of aglycone, type of glycosylation, non-acylated anthocyanins, acylated anthocyanins with aliphatic acids or with hydroxycinnamic acids) have been put in the context of biological activity. Here are some examples: The radical scavenging activity of anthocyanins has been strongly related to their chemical structure, including the substituents on the flavylium cation [14]. The type, position and number of hydroxyl/methoxyl groups, as electron-donating structures, have been considered pivotal features in relation to the antioxidant activity of anthocyanidins; the presence of 3',4'-ortho-dihydroxyl groups in the flavylium B-ring [7,14] and a 3-hydroxyl in the C-ring [12] seem to represent important structural elements for anthocyanins in suppressing oxidative stress. Acylation of a sugar moiety will on the one hand increase the in vitro and in vivo chemical stability of the anthocyanin; however, on the other hand, a change in the ring orientation of the molecule causes hydrogen atom transfer from hydroxyl groups to unpaired electrons to be difficult, making acylated anthocyanins less potent antioxidants than non-acylated ones [13].

Data from epidemiological studies have shown an inverse relationship between anthocyanin intake and cardiovascular risk prevention [15] and mortality [16]. Several clinical and experimental studies with anthocyanins or anthocyanin-rich foods have demonstrated an improvement in vascular function [17,18] and a decrease in atherosclerotic plaque development [19–21]. The initial steps of atherosclerotic process consist of the recruitment and adhesion of circulating monocytes to endothelial cells and subsequent trans-endothelial migration into the intima of the vascular wall [22]. The adhesion of monocytes to the endothelium involves the concerted expression on the surface of the activated endothelium of adhesion molecules, such as vascular cell adhesion molecule-1 (VCAM-1) and intercellular adhesion molecule-1 (ICAM-1) [23], two pivotal vascular inflammatory antigens; therefore, their inhibition by natural compounds could counteract the atherosclerotic process and related *sequelae* of cardiovascular injuries. Recent studies have also documented the ability of anthocyanins to abrogate the adhesion of human monocytes to inflamed endothelial cells [24–26]; however, the relationship between different anthocyanin groupings and biological activities remains elusive.

With the aim of contributing major insights into the challenging structure–activity relationship (SAR) of anthocyanin compounds in a nutraceutical context, we have evaluated the radical scavenging and biological activities of selected purified anthocyanin samples (PASs) from various plant materials. When comparing the anthocyanin sources of our diet, it is obvious that the anthocyanins of vegetables in general are considerably more complex than those of fruits: In vegetables, the proportion of simple anthocyanins without acyl groups and just one or two monosaccharide units is 16%. The corresponding number in the fruits is 74%. Around 70% of anthocyanins in vegetables have one or more aromatic acyl groups, while only 11% of the anthocyanins in the fruits contain an aromatic acyl group [6]. Since there exists a distinct difference between the anthocyanin content in vegetables and fruits of our diet, at least with respect to the aromatic acylation and number of monosaccharide units, we have chosen to compare the activity of PASs from two anthocyanin-rich fruits (mahaleb cherry and blackcurrant) and

vegetables (black carrot and “Sun Black” tomato). These samples contain anthocyanins representative of a typical anthocyanin-rich fruit and vegetable diet.

The antioxidative capacities of different PASs, and the anti-inflammatory activity by measuring the expression of endothelial adhesion molecule (VCAM-1 and ICAM-1), in human endothelial cells under inflamed conditions, are reported in relation to the different chemical structures.

2. Results and Discussion

2.1. Anthocyanin Composition of Selected Fruits and Vegetables

Anthocyanins and other polyphenolic compounds were extracted from (a) mahaleb cherry (*Prunus mahaleb* L.), a marginal fruit crop producing cherry-like dark-purple drupes, rich in non-acylated cyanidin 3-glycosides; (b) blackcurrant (*Ribes nigrum* L.), a well-known berry with high amounts of non-acylated cyanidin and delphinidin 3-glycosides; (c) black carrot (*Daucus carota* L. ssp. *sativus* var. *atrorubens* Alef.), an anthocyanin-rich carrot producing mostly cyanidin 3-glycosides acylated with various cinnamic acid derivatives; and (d) “Sun Black” tomato, a new genotype of tomato synthesising anthocyanins in the peel, based mainly on petunidin and malvidin 3,5-diglycosides acylated with *p*-coumaric acid (Table 1). The relative quantities of the individual anthocyanins in the various PASs are shown in Table 1, while the total anthocyanin contents of the purified samples are shown in Table 2. Accordingly, four groupings of anthocyanins were tested, including two non-acylated anthocyanidin 3-glycosides groupings from fruits (cyanidin-based or delphinidin-based) and two anthocyanidin 3-glycosides groupings acylated with aromatic acyl groups from vegetables. The structural differences of the two acylated anthocyanin groupings reside in the presence or absence of methoxy groups on the anthocyanidin B-ring, in the glycoside type and position (3-glycoside versus 3,5-diglycoside) and the nature of the cinnamic acid involved (Figure 1).

Table 1. Relative anthocyanin proportions in purified extracts of mahaleb cherry, blackcurrant, black carrot and “Sun Black” tomato.

Source	%
Mahaleb Cherry	
Cyanidin 3-(6-(rhamnosyl)glucoside) (4)	34.3
Cyanidin 3-glucoside (2)	33.4
Cyanidin 3-(6-(rhamnosyl)-2-(xylosyl)glucoside) (3)	21.3
Cyanidin 3-(2-(xylosyl)glucoside) (1)	10.9
Blackcurrant	
Delphinidin 3-(6-(rhamnosyl)glucoside) (6)	56.1
Cyanidin 3-(6-(rhamnosyl)glucoside) (4)	32.4
Delphinidin 3-glucoside (5)	5.9
Cyanidin 3-glucoside (2)	3.3
Black Carrot	
Cyanidin 3-(6-(6-(feruloyl)glucosyl)-2-(xylosyl)galactoside) (10)	77.1
Cyanidin 3-(6-(6-(sinapoyl)glucosyl)-2-(xylosyl)galactoside) (9)	9.9
Cyanidin 3-(2-(xylosyl)galactoside) (8)	4.9
Cyanidin 3-(6-(glucosyl)-2-(xylosyl)galactoside) (7)	4.8
Cyanidin 3-(6-(6-(<i>p</i> -coumaroyl)glucosyl)-2-(xylosyl)galactoside) (11)	3.1
“Sun Black” Tomato	
Petunidin 3-(6-(4-(<i>E-p</i> -coumaroyl)rhamnosyl)glucoside)-5-glucoside (petanin) (12)	56.6
Malvidin 3-(6-(4-(<i>E-p</i> -coumaroyl)rhamnosyl)glucoside)-5-glucoside (13)	21.4
Unknown	22.0

Table 2. Anthocyanin content (TA) in purified anthocyanin samples (PASs) of mahaleb cherry, blackcurrant, black carrot and “Sun Black” tomato (as dry weight, DW) and their antioxidant activity measured in TEAC and ORAC assays.

Source	TA	TEAC	TEAC	ORAC	ORAC
	mg AntE/g DW	$\mu\text{mol TE/mg PAS}$	$\mu\text{mol TE}/\mu\text{mol PAS}$	$\mu\text{mol TE/mg PAS}$	$\mu\text{mol TE}/\mu\text{mol PAS}$
Mahaleb cherry	38.5 ± 1.50^a	6.01 ± 0.46^a	3.44 ± 0.31^a	$15.32 \pm 1.73^{a,b}$	8.77 ± 0.63^b
Blackcurrant	32.2 ± 2.33^b	6.44 ± 0.51^a	3.89 ± 0.32^a	17.88 ± 1.87^a	11.02 ± 0.62^a
Black carrot	12.1 ± 0.48^c	2.53 ± 0.59^b	2.24 ± 0.28^b	12.66 ± 1.86^b	11.20 ± 0.87^a
“Sun Black” tomato	4.9 ± 0.26^d	1.30 ± 0.13^c	1.26 ± 0.22^c	11.44 ± 1.56^b	10.68 ± 0.38^a
Significance	***	***	***	**	**

AntE means anthocyanin equivalent; *** and ** significant at $p \leq 0.001$ and 0.01 , respectively. For each parameter, the same letters in the same column indicate that mean values are not significantly different ($p = 0.05$).

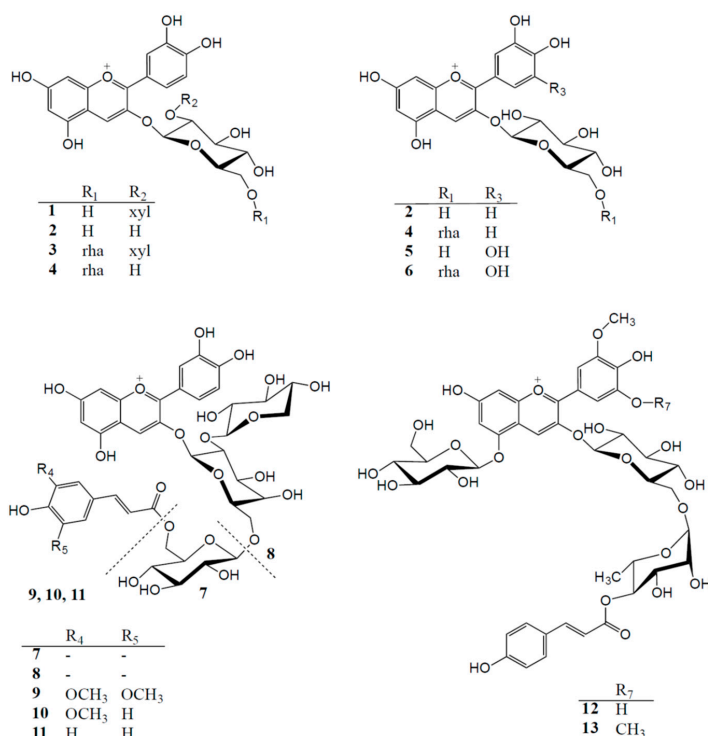


Figure 1. Anthocyanins in purified extracts of mahaleb cherry (1–4), blackcurrant (2, 4–6), black carrot (7–11) and “Sun Black” tomato (12, 13).

2.2. Antioxidative Capacity of Different Anthocyanin Groupings from Selected Fruits and Vegetables

In this study, the radical scavenging activity of purified anthocyanin samples (PASs) from two fruits (mahaleb cherry and blackcurrant) and two vegetables (black carrot and “Sun Black” tomato) have been compared *in vitro* using two of the most commonly used methods (TEAC and ORAC), which account for different mechanisms of action, as recommended by Niki [27].

Mahaleb cherry PAS, which is rich in cyanidin 3-glucoside, cyanidin 3-rutinoside and other cyanidin 3-glycosides, showed a TEAC value of $6.01 \pm 0.46 \mu\text{mol TE/mg PAS}$ and a ORAC value

of $15.32 \pm 1.73 \mu\text{mol TE/mg PAS}$; on molar basis, the values were 3.44 ± 0.31 and $8.77 \pm 0.63 \mu\text{mol TE}/\mu\text{mol PAS}$, respectively (Table 2).

Cyanidin 3-glucoside is the most widely distributed anthocyanin in edible fruits [28]. This anthocyanin has attracted extensive research on its physicochemical behavior, biosynthesis and role in food and health effects [29], and has also been considered the most potent anthocyanin against peroxy radicals [30]. After administration of ^{13}C -labelled cyanidin 3-glucoside in humans, the relative bioavailability was found to be around 12% on the basis of the total elimination of the absorbed ^{13}C dose via the urine and breath [31]. This latter work suggested that anthocyanins are more bioavailable than previously perceived, and their metabolites seem to be present in the circulation for 48 h after ingestion. The same group prepared various cyanidin 3-glucoside metabolites, and reported these metabolites to be active at physiological concentration to suppress inflammation in human vascular endothelial cells [32]. However, it has recently been reported that dietary supplementation with mono- or di-glycosylated cyanidins (from blackberry or black raspberry) had no effect on body weight, food intake, body composition and metabolic risk factors (fasting blood glucose and insulin sensitivity) in high-fat diet-fed mice [33].

Blackcurrant PAS contained more delphinidin 3-glycosides (delphinidin 3-glucoside and delphinidin 3-rutinoside) (62%) than cyanidin-glycosides (cyanidin 3-glucoside and cyanidin 3-rutinoside) (35.7%). This sample was compared to mahaleb PAS, which only contains cyanidin 3-glycosides (Table 1); a similar antioxidant capacity was expressed as the TEAC value ($6.44 \pm 0.51 \mu\text{mol TE/mg PAS}$, or $3.89 \pm 0.32 \mu\text{mol TE}/\mu\text{mol PAS}$) and an increased ORAC value ($17.88 \pm 1.87 \mu\text{mol TE/mg PAS}$, or $11.02 \pm 0.62 \mu\text{mol TE}/\mu\text{mol PAS}$), particularly when expressed on a molar basis (Table 2). These results indicate the slightly higher antioxidant activity of delphinidin 3-glycosides in comparison with analogous cyanidin 3-glycosides when tested with an ORAC assay. TEAC and ORAC assays are based on different reaction mechanisms: electron transfer for TEAC and hydrogen atom transfer for ORAC. Moreover, results from ORAC reflect more than just a radical scavenging activity, being the only assay that combines both inhibition time and degree of inhibition, ending in a complete reaction [30]. Together these features are responsible for the different values of antioxidant capacity assessed with different assays.

Delphinidin, having three hydroxyl-groups on the B-ring, has been shown to have the highest antioxidant activity among the six most common anthocyanidins [8,12]. Previous studies have revealed that delphinidin-type anthocyanins have shown higher biological activity compared to cyanidin-type anthocyanins. When feeding mice with a 1% blackcurrant diet, weight gain was suppressed and glucose metabolism improved, and the effects were suggested to be exerted by involvement of metabolites generated by enteric bacteria [34]. Moreover, since delphinidin 3-rutinoside (from blackcurrant) was demonstrated not to undergo substantial breakage into degradation products inside the gastrointestinal tract, the biological activities (improvement of insulin sensitivity) following its administration have been associated to this anthocyanin structure by itself [35]. Therefore, the difference in the biological activities of different anthocyanins has been suggested to be related to their structure and their individual metabolism in the gut [33].

The purified anthocyanin samples from black carrot and "Sun Black" tomato peel, containing mainly anthocyanins acylated with cinnamic acid derivatives, showed lower antioxidant activity (except for ORAC, expressed on a molar basis) than the non-acylated anthocyanin groupings from the fruits (Table 2). The black carrot PAS had a TEAC value of $2.53 \pm 0.59 \mu\text{mol TE/mg PAS}$ ($2.24 \pm 0.28 \mu\text{mol TE}/\mu\text{mol PAS}$) and an ORAC value of $12.66 \pm 1.86 \mu\text{mol TE/mg PAS}$ ($11.2 \pm 0.87 \mu\text{mol TE}/\mu\text{mol PAS}$), while "Sun Black" tomato peel PAS had a TEAC value of $1.30 \pm 0.13 \mu\text{mol TE/mg PAS}$ ($1.26 \pm 0.22 \mu\text{mol TE}/\mu\text{mol PAS}$), and an ORAC value of $11.44 \pm 1.56 \mu\text{mol TE/mg PAS}$ ($10.68 \pm 0.38 \mu\text{mol TE}/\mu\text{mol PAS}$). The black carrot sample contains anthocyanins based on the same aglycone (cyanidin) as the mahaleb cherry sample. Although the sugar moieties of the anthocyanins in the two samples are different (Table 1), they are all linked to the cyanidin 3-position. Thus, the main difference between the anthocyanin content of the two samples is the absence of

aromatic acylation of all the anthocyanins from mahaleb cherries. Accordingly, the 58% reduction of TEAC activity and 17.4% reduction of ORAC activity of the black carrot PAS relative to the mahaleb cherry PAS indicate the considerable impact of anthocyanin acylation with cinnamic acid derivatives on the antioxidant activity of this type of anthocyanin. The statistically significant difference between the two anthocyanin sources is maintained when the results are expressed on a molar basis. These results are also in accordance with other reports in the field [9,33]. However, when the antioxidant activities of the two major anthocyanins from eggplant, delphinidin 3-rutinoside-5-glucoside and delphinidin 3-(6-(4-(*E-p*-coumaroyl)rhmannosyl)glucoside)-5-glucoside (Nasunin) were measured by DPPH assay and linoleic acid radical scavenging activity assays, the non-acylated anthocyanins showed lower activity than the acylated anthocyanin [36]. In some studies, acylated anthocyanins from black carrot have shown less bioavailability compared to non-acylated anthocyanins, probably due to their larger size and different polarity, which prevent their partition into the lipid bilayer or the interaction with bilitranslocase for transport across the gut epithelium [37,38].

The antioxidative capacity of “Sun Black” tomato PAS ranks this source as the lowest (except for ORAC, expressed on a molar basis, due to the high molecular weight of petanin) among the different tested anthocyanin groupings, particularly along the ABTS assay. “Sun Black” tomato is a trademark protected tomato line obtained at Tuscia University (Viterbo, Italy), characterised by deep purple pigmentation in the epicarp due to an increased level of anthocyanins on the peel. Such a line is a product of breeding, and the anthocyanin pigments accumulate in the fruit epidermis and underlying cell layers, particularly on the side most exposed to the sun; instead, the flesh keeps the same red tone as usual [39]. Even though the antioxidative capacity of petanin, the principal anthocyanin found in PAS from the “Sun Black” tomato, resulted in a somewhat lower antioxidative capacity than the other sources, it must be considered that the anthocyanins in this source give increased value to the total antioxidant capacity of this new tomato genotype in comparison with the bioactive compounds normally found in traditional tomatoes.

Acylated anthocyanins (from black carrot, red cabbage, red radish, red and blue potatoes, red corn, etc.) are more suitable than their non-acylated analogues to be applied in food products with pH ranging from acid to neutral and slightly alkaline, due to their higher resistance to colour fading with increased pH [40]. To this list of vegetables providing acylated anthocyanins we can add the “Sun Black” tomato. For several food products these “vegetable anthocyanins” represent attractive alternatives to the addition of synthetic colorants, even if it must be underlined the somewhat less potent antioxidative and biological activities of anthocyanins acylated with cinnamic acid derivatives in comparison with their non-acylated ones (Table 2).

2.3. Vascular Anti-Inflammatory Properties of Selected Anthocyanin Groupings in Endothelial Cells

The vascular protective effects of different anthocyanin groupings from pigment-rich fruits (mahaleb cherry and blackcurrant) and vegetables (black carrot and “Sun Black” tomato) were analysed using a model of vascular inflammation, represented by cultured human microvascular endothelial cells-1 (HMEC-1) challenged with the pro-inflammatory cytokine, tumour necrosis factor- α (TNF- α). In this model, the anti-inflammatory properties of different PASs were evaluated by measuring the TNF- α -stimulated expression of endothelial adhesion molecules, VCAM-1 and ICAM-1. In endothelial cells, treatment with TNF- α induced cell surface expression of VCAM-1 and ICAM-1 (Figure 2). We found that the pre-exposure of endothelial cells with all the various PASs displayed anti-inflammatory properties by inhibiting the TNF- α -induced VCAM-1 and ICAM-1 expression, although their activities were scaled differently (Figure 2). PASs from mahaleb cherry and blackcurrant, containing non-acylated anthocyanins (Table 1), were shown to be the most effective. They significantly reduced the TNF- α stimulated expression of VCAM-1 in a concentration-dependent manner (Figure 2A), with 10 $\mu\text{g}/\text{mL}$ as the lowest significant concentration for both PASs. Similarly to VCAM-1, the exposure of endothelial cells to mahaleb cherry and blackcurrant PASs inhibited the TNF- α -induced expression of ICAM-1, although to a lesser degree, with 25 $\mu\text{g}/\text{mL}$ as the lowest

effective concentration (Figure 2B). Thus, PASs from mahaleb and blackcurrant exhibited similar vascular anti-inflammatory effects, despite their somewhat different anthocyanin composition. Indeed, mahaleb cherry PAS mainly contained cyanidin 3-rutinoside (about 34%) and cyanidin 3-glucoside (about 33%), while blackcurrant PAS contained delphinidin 3-rutinoside (about 56%) and cyanidin 3-rutinoside (about 32%) as major anthocyanins (Table 1). Previous studies have shown vascular anti-inflammatory properties for either cyanidin 3-glycoside or delphinidin 3-glycosides, reporting their ability to decrease the expression of VCAM-1 and ICAM-1 in endothelial cells challenged with several oxidant and inflammatory triggers [32,41,42]. In accordance with the reduced expression of endothelial adhesion molecules, anthocyanins were also able to reduce the adhesion of monocytes to TNF- α -activated endothelial cells at physiologically relevant concentrations, with delphinidin 3-glucoside as the most efficient [43]. The anti-inflammatory effects of anthocyanins have also been shown by their gut metabolites [43], highlighting the beneficial properties of both native and metabolised forms.

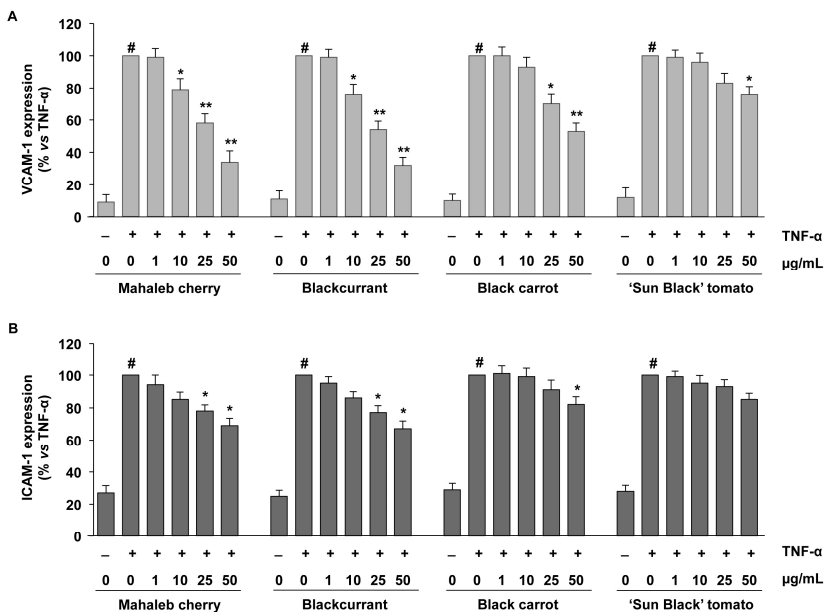


Figure 2. Inhibitory effects of PASs from the mahaleb cherry, blackcurrant, black carrot and “Sun Black” tomato on the expression of endothelial adhesion molecules. Endothelial cells were pre-treated with PASs at different concentrations (1, 10, 25 and 50 $\mu\text{g}/\text{mL}$) or vehicle (control) for 24 h and then stimulated with TNF- α (10 ng/mL) for 16 h. Cell surface expression of VCAM-1 (A) and ICAM-1 (B) was analysed by cell-surface enzyme immunoassay (EIA). Each experiment was performed in triplicate. Data are expressed as the percentage of TNF- α induced expression (mean \pm S.D.). # $p < 0.01$ vs. control; * $p < 0.05$, ** $p < 0.01$ vs. TNF- α alone.

Moreover, the present findings confirm our previous study about the ability of mahaleb cherry extract to decrease the stimulated expression of endothelial adhesion molecules [44], and highlight that the mahaleb fraction responsible for anti-inflammatory activity is represented by its anthocyanin-enriched content.

In addition, we analysed the anti-inflammatory properties of samples containing mainly anthocyanins acylated with cinnamic acid derivatives, from both black carrot and “Sun Black” tomato peel. PAS from black carrot efficiently reduced the TNF- α -induced VCAM-1 expression

in a concentration-dependent manner, with 25 $\mu\text{g}/\text{mL}$ as the lowest effective concentration (Figure 2A). PAS from “Sun Black” tomato inhibited TNF- α -induced VCAM-1 expression significantly only at 50 $\mu\text{g}/\text{mL}$ (Figure 2A). In TNF- α stimulated HMEC-1, black carrot PAS was also able to inhibit ICAM-1 expression, but only at the highest concentration (50 $\mu\text{g}/\text{mL}$); “Sun Black” tomato PAS showed a tendency to reduce ICAM-1; however, the inhibitory effect was not statistically significant (Figure 2B).

Overall, all tested PASs were able to decrease (although to a different degree) the stimulated endothelial adhesion molecules' expression, without affecting the expression of the constitutive endothelial surface antigen E1/1 or the endothelial cell vitality, as determined by cell count and Trypan blue exclusion.

Our findings showed that anthocyanins acylated with cinnamic acid derivatives exhibited a certain degree of anti-inflammatory activity, with lesser efficacy than non-acylated ones. Indeed, when comparing the activity of PASs from mahaleb cherry and black carrot, containing anthocyanins based on the same aglycone (cyanidin) the non-acylated anthocyanins from mahaleb cherry were the most effective in the reduction of the endothelial expression of inflammatory antigens: Mahaleb cherry PAS was effective at concentrations of 10 $\mu\text{g}/\text{mL}$ for VCAM-1 and 25 $\mu\text{g}/\text{mL}$ for ICAM-1, respectively, while black carrot PAS was effective at 25 $\mu\text{g}/\text{mL}$ for VCAM-1 and 50 $\mu\text{g}/\text{mL}$ for ICAM-1, respectively.

The differences in biological properties observed for the non-acylated and acylated anthocyanins were related to the antioxidant activity of their respective PASs, with the non-acylated anthocyanins in the mahaleb cherry and blackcurrant samples having the most effective activity, followed by the anthocyanins acylated with cinnamic acid derivatives in the black carrot and lastly “Sun Black” tomato samples. Notably, in this study we analysed the biological activities of different PASs by referring to the dry weight of each extract (μg of PAS in mL of medium, Figure 2). Comparing different PASs at the same concentration expressed as $\mu\text{g}/\text{mL}$ (Table 3), the anthocyanins with acylation had less molar concentration than the non-acylated anthocyanins because of higher molecular weight, which might partially explain their lower efficacy. In any case, our results regarding the endothelial anti-inflammatory effect of anthocyanins with aromatic acylation from vegetables were supported by the *in vivo* study showing that purple sweet potato anthocyanins suppressed the development of atherosclerotic lesions and enhancements of oxidative stress and soluble VCAM-1 in an animal model of atherosclerosis [19].

Table 3. Molar concentration ($\mu\text{mol}/\text{L}$) of purified anthocyanin samples (PAS) used in cell culture experiments.

PAS	$\mu\text{mol}/\text{L}$			
Mahaleb cherry	1.7	17.5	43.6	87.3
Blackcurrant	1.6	16.2	40.5	81.1
Black carrot	1.1	11.3	28.2	56.5
“Sun Black” tomato	1.1	10.7	26.8	53.5
$\mu\text{g}/\text{mL}$	1	10	25	50

Overall, our findings show that anthocyanins may play a positive role in the context of cardiovascular health due to their anti-inflammatory and anti-atherosclerotic effects. However, comparative analyses suggested that the anthocyanin structure affected the protective action, with non-acylated anthocyanins having a greater inhibitory effect on TNF- α -induced expression of VCAM-1 and ICAM-1 in endothelial cells than anthocyanins acylated with cinnamic acid derivatives. These findings could be useful for food valorization and the development of anthocyanin-rich functional foods.

3. Materials and Methods

3.1. Standards and Chemical Reagents

Reagents were purchased from various suppliers as follows: authentic standards of kuromanin chloride (cyanidin 3-*O*-glucoside chloride), keracyanin chloride (cyanidin 3-*O*-rutinoside chloride), myrtillin chloride (delphinidin 3-*O*-glucoside chloride), delphinidin 3-*O*-rutinoside chloride, *p*-coumaric acid, chlorogenic acid (3-caffeoylquinic acid), rutin (quercetin 3-*O*-rutinoside), and isoquercitrin (quercetin 3-*O*-glucoside) (Extrasynthèse, Genay, France); Trolox ((*S*)-(–)-6-hydroxy-2,5,7,8-tetramethylchroman-2-carboxylic acid), FL (fluorescein disodium), ABTS (2,2'-azino-bis (3-ethylbenzothiazoline-6-sulfonic acid)), AAPH (2,2'-azobis (2-methyl-propionamide dihydrochloride)), as well as acetonitrile (HPLC grade), ethanol, methanol, formic acid (Sigma-Aldrich, St. Louis, MO, USA). In all experiments Milli-Q (Merck Millipore, Darmstadt, Germany) water was used.

Petanidin 3-(6-(4-(*E-p*-coumaroyl)rhamnosyl)glucoside)-5-glucoside (Petanin) (**12**) and malvidin 3-(6-(4-(*E-p*-coumaroyl)rhamnosyl)glucoside)-5-glucoside (Negretein) (**13**) were isolated from blue potatoes (*Solanum tuberosum* cv. Congo and *S. tuberosum* cv. Vitelotte noire, respectively): Diced and frozen potatoes were extracted three times with acidified methanol (0.5% TFA), and the combined filtered extract was purified using partition against ethyl acetate followed by Amberlite XAD-7 column chromatography. Petanin and Negretein were isolated from their respective purified extracts using Sephadex LH-20 column chromatography and preparative HPLC. Their structures were elucidated by 1D and 2D NMR and high-resolution mass spectrometry (MS).

3.2. Plant Material, Preparation of Purified Anthocyanin Samples (PASs) and Anthocyanin Identification

All fruits and vegetables were harvested at their ripened stage. Extractions from respectively mahaleb cherry (*Prunus mahaleb* L.), blackcurrant (*Ribes nigrum* L.), black carrot (*Daucus carota* L. ssp. *sativus* var. *atrorubens* Alef.) and "Sun Black" tomato (*Solanum lycopersicum* L.) peel were done from 500 mg dry weight (DW) plant material, macerated with 50 mL extraction solvent (35% methanol + 35% ethanol + 28% water + 2% formic acid), at 4 °C, overnight. After centrifugation of the slurry (10 min at 2000 g), the supernatant was collected. A further 50 mL of extraction solvent was added to the pellet, and the extraction was repeated on a rotary shaker for one hour. Pooled supernatants were evaporated *in vacuo* at 32 °C using a R-205 Büchi rotavapor (Büchi Labortechnik AG, Flawil, Switzerland) and re-suspended in acidified water (0.5% formic acid). This crude extract (CE) was purified by solid-phase extraction, using C-18 cartridge solid phase extraction (SPE) (STRATA C-18E, Phenomenex, Torrance, CA, USA). Firstly, washing with acidified water (0.5% formic acid) removed water-soluble compounds, and secondly, a mixture of water:ethyl acetate:methanol (35:45:20) removed non-anthocyanin polyphenols, and finally methanol:water:formic acid (40:59.5:0.5) eluted the purified anthocyanins. The respective purified anthocyanin samples (PASs) were concentrated *in vacuo* at 34 °C, and characterised by HPLC (Figure 3). The respective CEs were also filtered through a 0.45 µm CA syringe filter (Filtres Fioroni, Ingré, France), portioned and stored at –20 °C before HPLC analysis (Figure 3).

The individual anthocyanins in the respective PASs (Table 1 and Figure 1) were identified by a combination of co-chromatography (diode-array detection (DAD) during HPLC) with authentic standards and comparison with the literature: mahaleb cherry [45], blackcurrant [46] and black carrot [47]. The two main anthocyanins in "Sun Black" tomato PAS were identified to be petanin (**12**) [48] and negretein (**13**) [49] by using DAD-HPLC and high-resolution LC-MS in comparison with authentic standards.

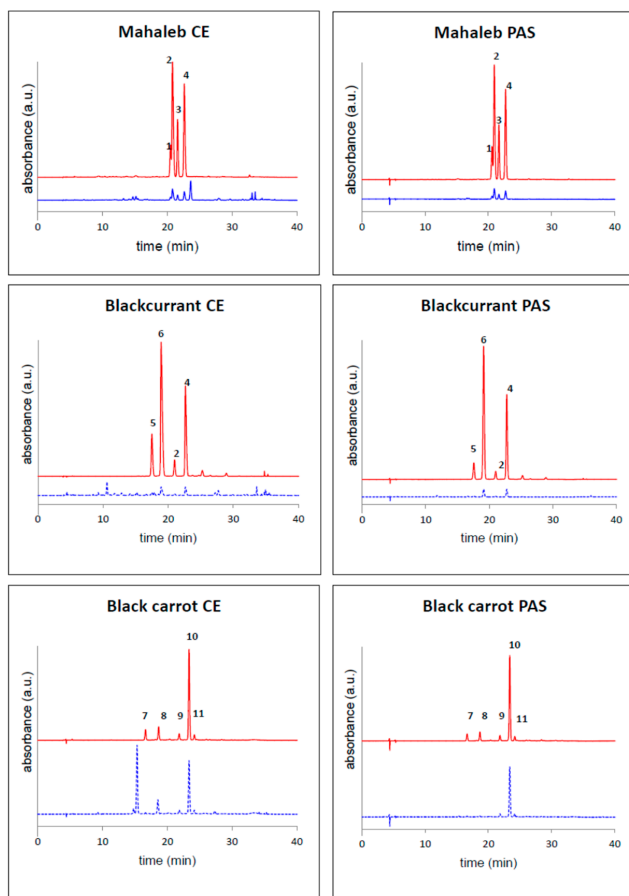


Figure 3. HPLC chromatograms of crude extracts (CE) and purified anthocyanin samples (PASs) of mahaleb cherry, blackcurrant and black carrot, detected at $\lambda = 520$ nm (red line) and 280 nm (blue line). See Table 1 for identities.

3.3. Quantification of Anthocyanin Content

The relative quantities of the individual anthocyanins in the PASs were established by integration of HPLC peaks detected at $\lambda = 520 \pm 20$ nm. The total anthocyanin content of the CEs as well as PASs were quantified by HPLC, using a standard curve based on the main anthocyanin in the sample (if commercially available) or, in the case of black carrot and “Sun Black” tomato PASs, based on the cyanidin 3-glucoside standard. The amounts of each anthocyanin calculated as an external standard equivalent were then multiplied by a molecular weight correction factor [50].

3.4. Antioxidant Activity Assays

The anthocyanin content of the PASs was normalised to 60 $\mu\text{g}/\text{mL}$ and tested at suitable dilutions. The antioxidant capacity of the PASs was measured using the ABTS (TEAC) and the ORAC assays as described by Gerardi et al. (2015) [51], and expressed as a function of the Trolox reference standard (μmol Trolox equivalents (TE)/g of DW). A rapid microplate methodology, using a microplate reader (Infinite M-200, Tecan Group Ltd., Männedorf, Switzerland) and 96-well plates (Costar, 96-well clear

round bottom plate, Corning) was applied. All experiments were performed in triplicate, and at least two independent assays were performed for each sample. The activity was also calculated on a molar basis using a weighted average of the molar weights of the pigments in each PAS and the identified relative quantities (assuming the un-identified portion is similar to the average).

3.5. Cell Culture and Treatments

The human microvascular endothelial cell line (HMEC-1), obtained from Dr. Thomas J. Lawley, was cultured as previously described [52]. Before treatment, confluent cells were shifted to media containing 4% foetal bovine serum, and incubated in the absence (vehicle) or presence of PASs at different concentrations (final concentrations of 1, 10, 25 and 50 µg/mL cell culture medium) for 24 h, and then stimulated with TNF-α (10 ng/mL) for additional 16 h. The effects of vehicle control or different PASs on cell viability were evaluated through a variety of techniques, including cell count and Trypan blue exclusion. In preliminary experiments aimed at evaluating phytochemical toxicity, treatment of HMEC-1 with up to 50 µg/mL PAS for 24 h did not produce any sign of toxicity.

3.6. Detection of Endothelial Cell Molecules

Endothelial surface expression of VCAM-1 and ICAM-1 was assayed by employing a cell surface enzyme immunoassay (EIA), using primary mouse anti-human monoclonal antibodies against VCAM-1 (Millipore) and ICAM-1 (HU5/3), or the monoclonal antibody against the non-cytokine-inducible and constitutive endothelial cell antigen E1/1, as previously described [53].

3.7. Statistical Analysis

Values were expressed as mean ± SD for the indicated number of experiments. Differences between two groups were settled by unpaired Student's *t* test. One-way analysis of variance (ANOVA) followed by the Fisher's least significant difference (LSD) post hoc test was used to determine significant differences among groups.

4. Conclusions

In the present study we demonstrated that purified anthocyanin samples from four plant sources (mahaleb cherry, blackcurrant, black carrot and "Sun Black" tomato) containing structurally different anthocyanins, were biologically active. They all exhibited antioxidant capacity, which was highest for samples containing non-acylated anthocyanins versus samples containing anthocyanins with aromatic acylation, even though this order was reversed when ORAC assay values were expressed on a molar basis. These purified anthocyanin samples were also able to reduce the expression of endothelial inflammatory antigens, suggesting their potential beneficial effect in cardiovascular protection. When compared, the vascular anti-inflammatory capacity of non-acylated anthocyanins was higher than the similar capacity of anthocyanins acylated with cinnamic acid derivatives in accordance with their corresponding antioxidant activity. Future studies might better clarify the underlying mechanisms of structurally different anthocyanins related to vascular health.

Acknowledgments: This work was supported by the Italian Ministry of University and Research (MIUR) Research Projects: "High-Convenience Fruits and vegetables: New Technologies for Quality and New Products", PON 01_01435. We also thank the Regional Project "Rete di Laboratori per l'Innovazione degli Alimenti Funzionali (LAIFF)" (PO Puglia FESR 2007–2013 Asse I, Linea 1.2—PO Puglia FSE 2007–2013 Asse IV) which allowed the spectrofluorimeter "Infinite M-200" (Tecan Group Ltd., Männedorf, Switzerland) purchasing. We thank Andrea Mazzucato, Tuscia University, Viterbo, Italy, for providing "Sun Black" tomatoes, and "Aureli" farm, Ortucchio (AQ), Italy for providing black carrots.

Author Contributions: Federica Blando and Maria Annunziata Carluccio conceived and designed the experiments; Federica Blando, Gabriele Maiorano, Nadia Calabriso and Helge Berland performed the experiments; Federica Blando, Gabriele Maiorano, Carmela Gerardi, Maria Annunziata Carluccio, Helge Berland and Øyvind M. Andersen analysed the data; Federica Blando, Maria Annunziata Carluccio, Nadia Calabriso, Helge Berland and Øyvind M. Andersen wrote the paper.

Conflicts of Interest: The authors declare no conflict of interest.

Abbreviations

PAS	Purified Anthocyanin Sample
TEAC	Trolox Equivalent Antioxidant Capacity
ORAC	Oxygen Radical Absorbance Capacity
VCAM-1	Vascular Cell Adhesion Molecule-1
ICAM-1	Intercellular Adhesion Molecule-1
HMEC-1	Human Microvascular Endothelial Cell-1
TNF- α	Tumour Necrosis Factor- α
EIA	Cell-Surface Enzyme Immunoassay

References

- Andersen, Ø.M.; Jordheim, M. The anthocyanins. In *Flavonoids: Chemistry, Biochemistry and Applications*; Andersen, Ø.M., Markham, K.R., Eds.; CRC Press: Boca Raton, FL, USA, 2006; pp. 471–551.
- Andersen, Ø.M.; University of Bergen, Norway. Unpublished data. January 2018.
- Kong, J.-M.; Chia, L.-S.; Goh, N.-K.; Chia, T.-F.; Brouillard, R. Analysis and biological activities of anthocyanins. *Phytochemistry* **2003**, *64*, 923–933. [[CrossRef](#)]
- De Pascual-Teresa, S.; Sanchez-Ballesta, M.T. Anthocyanins: From plant to health. *Phytochem. Rev.* **2008**, *7*, 281–299. [[CrossRef](#)]
- Battino, M.; Beekwilder, J.; Denoyes-Rothan, B.; Laimer, M.; McDougall, G.J.; Mezzetti, B. Bioactive compounds in berries relevant to human health. *Nutr. Rev.* **2009**, *67*. [[CrossRef](#)] [[PubMed](#)]
- Andersen, Ø.M.; Jordheim, M. Basic Anthocyanin Chemistry and Dietary Sources. In *Anthocyanins in Health and Disease*; Wallace, T.C., Giusti, M.M., Eds.; Taylor & Francis Inc.: Abingdon, UK; CRC Press: New York, NY, USA, 2013; pp. 13–90.
- Rice-Evans, C.A.; Miller, N.J.; Paganga, G. Structure-antioxidant activity relationships of flavonoids and phenolic acids. *Free Radic. Biol. Med.* **1996**, *20*, 933–956. [[CrossRef](#)]
- Kähkönen, M.P.; Heinonen, M. Antioxidant activity of anthocyanins and their aglycons. *J. Agric. Food Chem.* **2003**, *51*, 628–633. [[CrossRef](#)] [[PubMed](#)]
- Jing, P.; Bomser, J.; Schwartz, S.J.; He, J.; Magnuson, B.A.; Giusti, M.M. Structure-function relationships of anthocyanins from various anthocyanin-rich extracts on the inhibition of colon cancer cell growth. *J. Agric. Food Chem.* **2008**, *56*, 9391–9398. [[CrossRef](#)] [[PubMed](#)]
- Yi, L.; Chen, C.-Y.; Jin, X.; Mi, M.-T.; Yu, B.; Chang, H.; Ling, W.-H.; Zhang, T. Structural requirements of anthocyanins in relation to inhibition of endothelial injury induced by oxidized low-density lipoprotein and correlation with radical scavenging activity. *FEBS Lett.* **2010**, *584*, 583–590. [[CrossRef](#)] [[PubMed](#)]
- Jhin, C.; Hwang, K.T. Prediction of radical scavenging activities of anthocyanins applying adaptive neuro-fuzzy interference system (ANFIS) with quantum chemical descriptors. *Int. J. Mol. Sci.* **2014**, *15*, 14715–14727. [[CrossRef](#)] [[PubMed](#)]
- Ali, M.H.; Almagribi, W.; Al-Rashidi, M.N. Antiradical and reductant activities of anthocyanidins and anthocyanins, structure-activity relationship and synthesis. *Food Chem.* **2016**, *194*, 1275–1282. [[CrossRef](#)] [[PubMed](#)]
- Zhao, C.-L.; Yu, Y.-Q.; Chen, Z.-J.; Wen, G.-S.; Wei, F.-G.; Zheng, Q.; Wang, C.-D.; Xiao, X.-L. Stability-increasing effects of anthocyanin glycosyl acylation. *Food Chem.* **2017**, *214*, 119–128. [[CrossRef](#)] [[PubMed](#)]
- Azevedo, J.; Fernandes, I.; Faria, A.; Oliveira, J.; Fernandes, A.; de Freitas, V.; Mateus, N. Antioxidant properties of anthocyanidins, anthocyanidins 3-glucosides and respective portisins. *Food Chem.* **2010**, *119*, 518–523. [[CrossRef](#)]
- Cassidy, A.; O'Reilly, E.J.; Kay, C.; Sampson, L.; Franz, M.; Forman, J.P.; Curhan, G.; Rimm, E.B. Habitual intake of flavonoid subclasses and incident hypertension in adults. *Am. J. Clin. Nutr.* **2011**, *93*, 338–347. [[CrossRef](#)] [[PubMed](#)]

16. Mink, P.J.; Scrafford, C.G.; Barraj, L.M.; Harnack, L.; Hong, C.P.; Nettleton, J.A.; Jacobs, D.R. Flavonoid intake and cardiovascular disease mortality: A prospective study in postmenopausal women. *Am. J. Clin. Nutr.* **2007**, *85*, 895–909. [[PubMed](#)]
17. Rodriguez-Mateos, A.; Rendeiro, C.; Bergillos-Meca, T.; Tabatabaee, S.; George, T.W.; Heiss, C.; Spencer, J.P.E. Intake and time dependence of blueberry flavonoid-induced improvements in vascular function: A randomized, controlled, double-blind, crossover intervention study with mechanistic insights into biological activity. *Am. J. Clin. Nutr.* **2013**, *98*, 1179–1191. [[CrossRef](#)] [[PubMed](#)]
18. Erlund, I.; Koli, R.; Alftan, G.; Marniemi, J.; Puukka, P.; Mustonen, P.; Mattila, P.; Julia, A. Favorable effects of berry consumption on platelet function, blood pressure, and HDL cholesterol. *Am. J. Clin. Nutr.* **2008**, *87*, 323–331. [[PubMed](#)]
19. Miyazaki, K.; Makino, K.; Iwadata, E.; Deguchi, Y.; Ishikawa, F. Anthocyanins from purple sweet potato ipomoea batatas cultivar Ayamurasaki suppress the development of atherosclerotic lesions and both enhancements of oxidative stress and soluble vascular cell adhesion molecule-1 in Apolipoprotein E-Deficient Mice. *J. Agric. Food Chem.* **2008**, *56*, 11485–11492. [[CrossRef](#)] [[PubMed](#)]
20. Mauray, A.; Milenkovic, D.; Besson, C.; Caccia, N.; Morand, C.; Michel, F.; Mazur, A.; Scalbert, A.; Felgines, C. Atheroprotective effects of bilberry extracts in Apo E-Deficient Mice. *J. Agric. Food Chem.* **2009**, *57*, 11106–11111. [[CrossRef](#)] [[PubMed](#)]
21. Mauray, A.; Felgines, C.; Morand, C.; Mazur, A.; Scalbert, A.; Milenkovic, D. Bilberry anthocyanin-rich extract alters expression of genes related to atherosclerosis development in aorta of apo E-deficient mice. *Nutr. Metab. Cardiovasc. Dis.* **2012**, *22*, 72–80. [[CrossRef](#)] [[PubMed](#)]
22. Libby, P.; Ridker, P.M.; Hansson, G.K. Progress and challenges in translating the biology of atherosclerosis. *Nature* **2011**, *473*, 317–325. [[CrossRef](#)] [[PubMed](#)]
23. Osterud, B.; Bjorklid, E. Role of monocytes in atherogenesis. *Physiol. Rev.* **2003**, *83*, 1069–1112. [[CrossRef](#)] [[PubMed](#)]
24. Kuntz, S.; Asseburg, H.; Dold, S.; Rompp, A.; Frohling, B.; Kunz, C.; Rudloff, S. Inhibition of low-grade inflammation by anthocyanins from grape extract in an in vitro epithelial-endothelial co-culture model. *Food Funct.* **2015**, *6*, 1136–1149. [[CrossRef](#)] [[PubMed](#)]
25. Medda, R.; Lyros, O.; Schmidt, J.L.; Jovanovic, N.; Nie, L.; Link, B.J.; Otterson, M.F.; Stoner, G.D.; Shaker, R.; Rafiee, P. Anti-inflammatory and anti-angiogenic effect of black raspberry extract on human esophageal and intestinal microvascular endothelial cells. *Microvasc. Res.* **2015**, *97*, 167–180. [[CrossRef](#)] [[PubMed](#)]
26. Del Bo, C.; Roursgaard, M.; Porrini, M.; Loft, S.; Moller, P.; Riso, P. Different effects of anthocyanins and phenolic acids from wild blueberry (*Vaccinium angustifolium*) on monocytes adhesion to endothelial cells in a TNF-alpha stimulated proinflammatory environment. *Mol. Nutr. Food Res.* **2016**, *60*, 2355–2366. [[CrossRef](#)] [[PubMed](#)]
27. Niki, E. Antioxidant capacity: Which capacity and how to assess it? *J. Berry Res.* **2011**, *1*, 169–176.
28. Wu, X.; Prior, R.L. Systematic identification and characterization of anthocyanins by HPLC-ESI-MS/MS in common foods in the United States: Fruits and berries. *J. Agric. Food Chem.* **2005**, *53*, 2589–2599. [[CrossRef](#)] [[PubMed](#)]
29. Olivas-Aguirre, F.J.; Rodrigo-García, J.; Martínez-Ruiz, N.D.; Cárdenas-Robles, A.I.; Mendoza-Díaz, S.O.; Álvarez-Parrilla, E.; González-Aguilar, G.A.; de la Rosa, L.A.; Ramos-Jiménez, A.; Wall-Medrano, A. Cyanidin 3-O-glucoside: Physical-chemistry, foodomics and health effects. *Molecules* **2016**, *21*, 1264. [[CrossRef](#)] [[PubMed](#)]
30. Wang, H.; Cao, G.; Prior, R.L. Oxygen radical absorbing capacity of anthocyanins. *J. Agric. Food Chem.* **1997**, *45*, 304–309. [[CrossRef](#)]
31. Czank, C.; Cassidy, A.; Zhang, Q.; Morrison, D.J.; Preston, T.; Kroon, P.A.; Botting, N.P.; Kay, C.D. Human metabolism and elimination of the anthocyanin, cyanidin-3-glucoside: A (13) C-tracer study. *Am. J. Clin. Nutr.* **2013**, *97*, 995–1003. [[CrossRef](#)] [[PubMed](#)]
32. Amin, H.P.; Czank, C.; Raheem, S.; Zhang, Q.Z.; Botting, N.P.; Cassidy, A.; Kay, C.D. Anthocyanins and their physiologically relevant metabolites alter the expression of IL-6 and VCAM-1 in CD40L and oxidized LDL challenged vascular endothelial cells. *Mol. Nutr. Food Res.* **2015**, *59*, 1095–1106. [[CrossRef](#)] [[PubMed](#)]
33. Overall, J.; Bonney, S.A.; Wilson, M.; Beermann, A., III; Grace, M.H.; Esposito, D.; Lila, M.A.; Komarnytsky, S. Metabolic effects of berries with structurally diverse anthocyanins. *Int. J. Mol. Sci.* **2017**, *18*, 422. [[CrossRef](#)] [[PubMed](#)]

34. Esposito, D.; Damsud, T.; Wilson, M.; Grace, M.H.; Strauch, R.; Li, X.; Lila, M.A.; Komarnytsky, S. Blackcurrant anthocyanins attenuate weight gain and improve glucose metabolism in diet-induced obese mice with intact, but not disrupted, gut microbiome. *J. Agric. Food Chem.* **2015**, *63*, 6172–6180. [[CrossRef](#)] [[PubMed](#)]
35. Tani, T.; Nishikawa, S.; Kato, M.; Tsuda, T. Delphinidin 3-rutinoside-rich blackcurrant extract ameliorates glucose tolerance by increasing the release of glucagon-like peptide-1 secretion. *Food Sci. Nutr.* **2017**, *5*, 929–933. [[CrossRef](#)] [[PubMed](#)]
36. Azuma, K.; Ohyama, A.; Ippoushi, K.; Ichiyanagi, T.; Takeuchi, A.; Saito, T.; Fukuoka, H. Structures and antioxidant activity of anthocyanins in many accessions of eggplant and its related species. *J. Agric. Food Chem.* **2008**, *56*, 10154–10159. [[CrossRef](#)] [[PubMed](#)]
37. Passamonti, S.; Vrhovsek, U.; Mattivi, F. The interaction of anthocyanins with bilitranslocase. *Biochem. Biophys. Res. Commun.* **2002**, *296*, 631–636. [[CrossRef](#)]
38. Kurilich, A.; Clevidence, B.A.; Britz, S.J.; Simon, P.W.; Novotny, J.A. Plasma and urine responses are lower for acylated vs. non-acylated anthocyanins from raw and cooked purple carrots. *J. Agric. Food Chem.* **2005**, *53*, 6537–6542. [[CrossRef](#)] [[PubMed](#)]
39. Gonzali, S.; Mazzucato, A.; Perata, P. Purple as a tomato: Towards high anthocyanin tomatoes. *Trends Plant Sci.* **2009**, *14*, 237–241. [[CrossRef](#)] [[PubMed](#)]
40. Bakowska-Barczak, A. Acylated anthocyanins as stable, natural food colorants—A review. *Pol. J. Food Nutr. Sci.* **2005**, *14/55*, 107–116.
41. Yi, L.; Chen, C.Y.; Jin, X.; Zhang, T.; Zhou, Y.; Zhang, Q.Y.; Zhu, J.D.; Mi, M.T. Differential suppression of intracellular reactive oxygen species-mediated signaling pathway in vascular endothelial cells by several subclasses of flavonoids. *Biochimie* **2012**, *94*, 2035–2044. [[CrossRef](#)] [[PubMed](#)]
42. Speciale, A.; Canali, R.; Chirafisi, J.; Saija, A.; Virgili, F.; Cimino, F. Cyanidin-3-O-glucoside protection against TNF-alpha-induced endothelial dysfunction: Involvement of nuclear factor-kappa B signaling. *J. Agric. Food Chem.* **2010**, *58*, 12048–12054. [[CrossRef](#)] [[PubMed](#)]
43. Krga, I.; Monfoulet, L.E.; Konic-Ristic, A.; Mercier, S.; Glibetic, M.; Morand, C.; Milenkovic, D. Anthocyanins and their gut metabolites reduce the adhesion of monocyte to TNF alpha-activated endothelial cells at physiologically relevant concentrations. *Arch. Biochem. Biophys.* **2016**, *599*, 51–59. [[CrossRef](#)] [[PubMed](#)]
44. Gerardi, C.; Frassinetti, S.; Caltavuturo, L.; Leone, A.; Lecci, R.; Calabriso, N.; Carluccio, M.A.; Blando, F.; Mita, G. Anti-proliferative, anti-inflammatory and anti-mutagenic activities of a *Prunus mahaleb* L. anthocyanin-rich fruit extract. *J. Funct. Food* **2016**, *27*, 537–548. [[CrossRef](#)]
45. Blando, F.; Albano, C.; Liu, Y.Z.; Nicoletti, I.; Corradini, D.; Tommasi, N.; Gerardi, C.; Mita, G.; Kitts, D.D. Polyphenolic composition and antioxidant activity of the under-utilised *Prunus mahaleb* L. fruit. *J. Sci. Food Agric.* **2016**, *96*, 2641–2649. [[CrossRef](#)] [[PubMed](#)]
46. Frøytlog, C.; Slimestad, R.; Andersen, Ø.M. Combination of chromatographic techniques for the preparative isolation of anthocyanins—Applied on blackcurrant (*Ribes nigrum*) fruits. *J. Chromatogr. A* **1998**, *825*, 89–95. [[CrossRef](#)]
47. Glässgen, W.E.; Wray, V.; Strack, D.; Metzger, J.W.; Seitz, H.U. Anthocyanins from cell suspension cultures of *Daucus carota*. *Phytochemistry* **1992**, *31*, 1593–1601. [[CrossRef](#)]
48. Andersen, Ø.M.; Opheim, S.; Aksnes, D.W.; Frøystein, N.Å. Structure of petanin, an acylated anthocyanin isolated from *Solanum tuberosum*, using homo- and hetero-nuclear two-dimensional nuclear magnetic resonance techniques. *Phytochem. Anal.* **1991**, *2*, 230–236. [[CrossRef](#)]
49. Slimestad, R.; Aaberg, A.; Andersen, Ø.M. Acylated anthocyanins from petunia flowers. *Phytochemistry* **1999**, *50*, 1081–1086. [[CrossRef](#)]
50. Chandra, A.; Rana, J.; Li, Y. Separation, identification, quantification and method validation of anthocyanins in botanical raw materials by HPLC and HPLC/MS. *J. Agric. Food Chem.* **2001**, *49*, 3515–3521. [[CrossRef](#)] [[PubMed](#)]
51. Gerardi, C.; Tommasi, N.; Albano, C.; Pinthus, E.; Rescio, L.; Blando, F.; Mita, G. *Prunus mahaleb* L. fruit extracts: A novel source for natural pigments. *Eur. Food Res. Technol.* **2015**, *241*, 683–695. [[CrossRef](#)]
52. Scoditti, E.; Calabriso, N.; Massaro, M.; Pellegrino, M.; Storelli, C.; Martines, G.; De Caterina, R.; Carluccio, M.A. Mediterranean diet polyphenols reduce inflammatory angiogenesis through MMP-9 and COX-2 inhibition in human vascular endothelial cells: A potentially protective mechanism in atherosclerotic vascular disease and cancer. *Arch. Biochem. Biophys.* **2012**, *527*, 81–89. [[CrossRef](#)] [[PubMed](#)]

53. Carluccio, M.A.; Siculella, L.; Ancora, M.A.; Massaro, M.; Scoditti, E.; Storelli, C.; Visioli, F.; Distanto, A.; De Caterina, R. Olive oil and red wine antioxidant polyphenols inhibit endothelial activation—Antiatherogenic properties of Mediterranean diet phytochemicals. *Arterioscler. Thromb. Vasc. Biol.* **2003**, *23*, 622–629. [[CrossRef](#)] [[PubMed](#)]



© 2018 by the authors. Licensee MDPI, Basel, Switzerland. This article is an open access article distributed under the terms and conditions of the Creative Commons Attribution (CC BY) license (<http://creativecommons.org/licenses/by/4.0/>).



Graphic design: Communication Division, UIB / Print: Skjipes Kommunikasjon AS



uib.no

ISBN: 9788230843376 (print)
9788230868010 (PDF)